Studies on Photofunctional Acene-Based Materials Using Optically and/or Thermally Convertible Precursor Method

Tatsuya Aotake

2015

Laboratory for Photofunctional Organic Chemistry
Graduate School of Materials Science
Nara Institute of Science and Technology

Contents

Abbreviations

PMMA	Polymethylmethacrylate
XRD	X-ray diffraction
ITO	Indium tin oxide
PEDOT:PSS	Poly(3,4-ethylenedioxythiophene) polystyrene sulfonate
BCP	Bathociproine
$PC_{61}BM$	[6,6]-Phenyl-C_{61}-buthric acid methyl ester
$PC_{71}BM$	[6,6]-Phenyl-C_{71}-buthric acid methyl ester
THF	Tetrahydrofuran
TFAA	Trifluoroacetic anhydride
DIPEA	*N*,*N*-Diisopropylethylamine
DMSO	Dimethyl sulfoxide
TMS	Tetramethylsilane
Fc	Ferrocene
LED	Light emitting diode
NMR	Nuclear magnetic resonance
TLC	Thin-layer chromatography
MALDI	Matrix assisted laser desorption ionization
TOF	Time-of-flight
FAB	Fast atom bombardment
HOMO	Highest occupied molecular orbital
LUMO	Lowest unoccupied molecular orbital
TFA	Trifluoroacetic acid
DDQ	2,3-Dichloro-5,6-dicyano-1,4-benzoquinone
NBS	*N*-Bromosucinimide
ESR	Electron spin resonance
SOMO	Singly occupied molecular orbital

Chapter 1

General Introduction

In this chapter, general introductions of α-diketone type acene precursors including properties, history and applications are described.

1-1 History of Thermally and Photochemically Convertible Acene Precursors

Acene is one type of polycyclic aromatic hydrocarbons (PAHs) and multi-benzene rings are fused linearly.[1] Typical and isolated acenes are anthracene, naphthacene, pentacene, and hexacene[2] (Figure 1-1). Worthinesses of acene compound are light emitting characteristics and good semiconducting properties. Pentacene has been especially studied as an organic semiconductor material such as organic field-effect transistor (OFET)[3] and organic photovoltaic cell (OPV).[4] The single-crystal pentacene shows high hole mobility over 5 cm^2/Vs.[5] The OPV with fullerene as an n-type semiconductor also shows power conversion efficiency (PCE) of 2.7%[6]. Since pentacene is insoluble in common organic solvents, those devices were generally fabricated by vacuum deposition process. On another front, from the viewpoint of manufacture on a large scale, device fabrication technology in the solution process is required, however, pentacene isn't suitable for device fabrication in solution processing because the solubility is terribly poor.

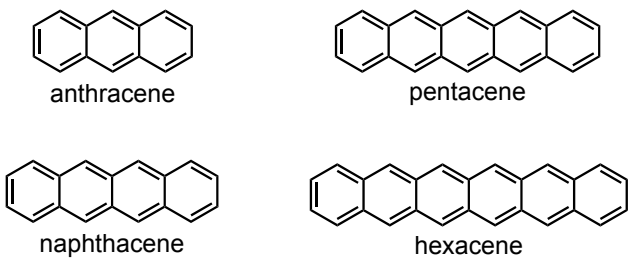

Figure 1-1. Typical and isolated acenes.

To solve this problem, two approaches have been proposed. The first approach is the introduction of substituents at 6,13-positions of pentacene (Figure 1-2).[7] 6,13-Bis(triisopropylsilylethynyl) pentacene (**1**) has been reported by Anthony and co-workers in 2001 to show good solubility and performances of organic semiconductor devices.[8] The hole mobility (μ_h) of 11 cm^2/Vs as the highest performance has been reported using fluid-flow-enhanced crystal growth method by Bao and co-workers in 2013.[9] Since the stability of acene is greatly improved, introduction of substituent is also applied to the synthesis of new acenes which are difficult to isolate such as large acenes[10] and pentacene dimers.[11]

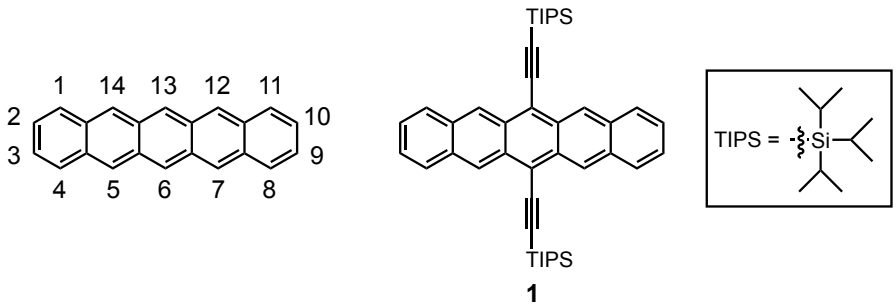

1

Figure 1-2. The numberings of pentacene and the structure of pentacene derivative **1**.

The second approach is the thermally- or photochemically convertible precursor method (Figure 1-3).[12] The first report on the pentacene precursor is **2** by Müllen and co-workers in 1996.[13] The precursor **2** can be converted to pentacene with removing tetrachlorobenzene by heating at 140 ºC. The authors have succeeded to fabricate OFETs by solution process with $\mu_h = 9 \times 10^{-3}$ cm^2/Vs. In 2002, Afzali and co-workers have synthesized *N*-sulfinylacetamide adduct **3** in 1 step by the Diels-Alder reaction with pentacene.[14] The retro Diels-Alder reaction proceeds at 200 ºC for 1.5 min or 130 ºC for 25 min. The device showed the highest hole mobility (0.89 cm^2/Vs) among the solution processed pentacene devices with the precursor methods. In 2004, Afzali and co-workers have also prepared a similar pentacene precursor **4**.[15] In addition, retro Diels-Alder reaction type precursors (**5**–**9**) have been widely reported between 2003 to 2004.[16–18] In 2005, Yamada, Uno, Ono and co-workers have reported an α-diketone type precursor of pentacene (**6,13-PDK)** as the first photoconversion type precursor.[19] **6,13-PDK** can be converted to pentacene with removing two carbon monoxide (CO) molecules upon photoirradiation. As will be described later in this chapter, the precursor method is useful to synthesize new acenes and fabricates organic devices by solution process. In 2007, Chow and co-workers have reported a soluble monoketone type precursor **10** which releases a CO molecule by thermal- or photochemical activation. The OFET showed the hole mobility of 8.8×10^{-3} cm^2/Vs.[20] The monoketone type precursor method can be applied to synthesis of acene derivatives,[21] especially, the first isolation of hexacene was achieved by this precursor method.[2] The thermally convertible precursor **11** also has been prepared by Chow and co-workers. The hole mobility of 0.38 cm^2/Vs has been reported.[22]

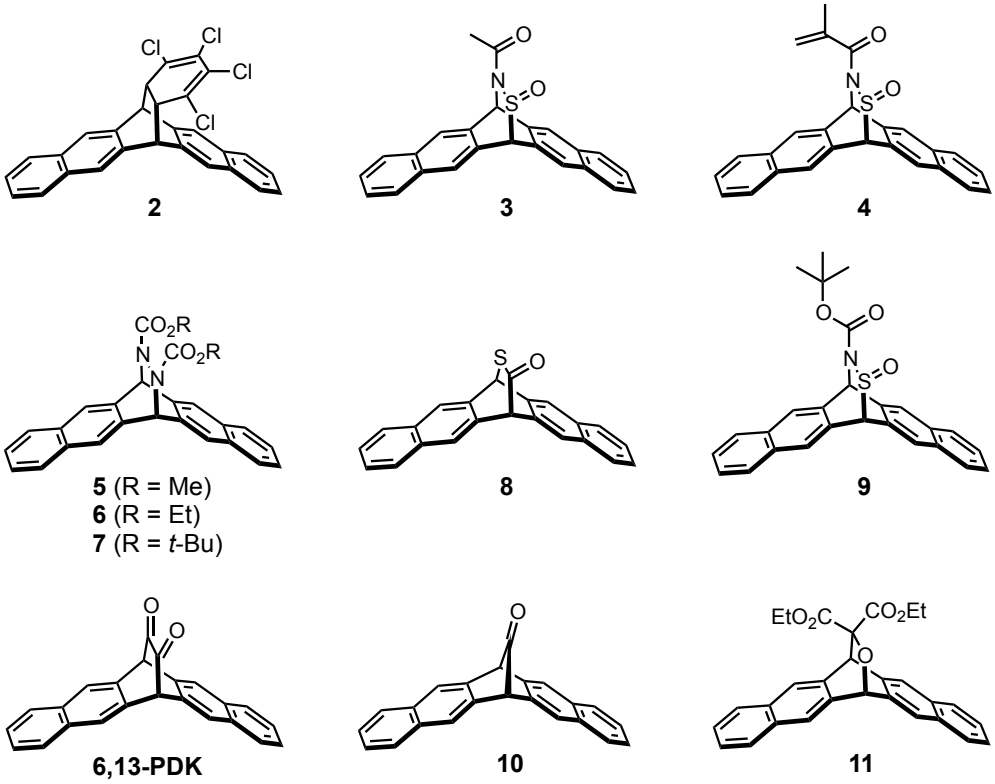

Figure 1-3. Thermally- or optically convertible precursors of pentacene.

1-2 Applications of α-Diketone Type Precursors

In this section, characteristics and applications of α-diketone type photoprecursors are described. As described in section 1-1, pentacene can be generated from α-diketone type photoprecursor (**6,13-PDK**) upon photoirradiation. Strating, Zwanenberg and co-workers have reported the first example for acene compound in 1969.[23,24] The photoprecursor of anthracene (**ADK**) is converted to anthracene with removing two CO molecules. The reaction is called "Strating-Zwanenberg reaction" (Figure 1-4).

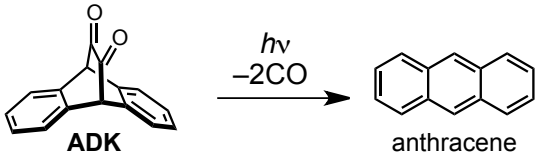

Figure 1-4. Strating-Zwanenberg reaction from **ADK** to anthracene.

This photoprecursor method for other acene materials is applicable in other field. The examples of the application are mainly classified into two types, as follows: 1) synthetic tool of unstable acene materials such as large acenes and terminal substituted pentacenes, 2) device fabrication tool of organic semiconducting acene materials toward solution processable OPV and OFET.

(1) Synthetic Tool

The precursor method is one of the most convenient tool to synthesize the insoluble and instable large acenes.[24] Since the large acene compounds and their intermediates are insoluble to common organic solvents and unstable to oxidation, the synthesis has been difficult in the general synthetic methods. However, photoprecursor method can improve the problems, and decarbonylation proceeds quantitatively upon photoirradiation. Neckers and co-workers have synthesized hexacene[25] and heptacene[26] in PMMA by the decarbonylation. The generations of the acenes were confirmed by UV-vis absorption spectra and mass spectra. Bettinger and co-worker have succeeded to study the absorption characteristics of the generated large acenes in 2009.[27]

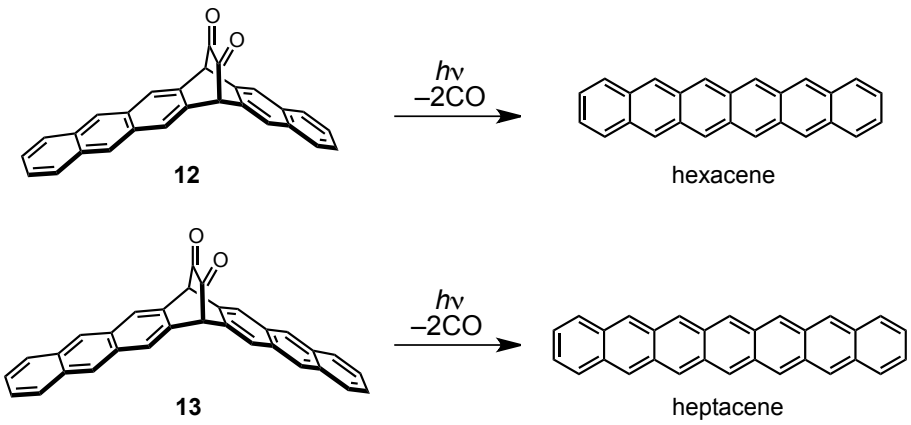

Figure 1-5. Photochemical synthesis of hexacene and heptacene.

Tönshoff and Bettinger have also prepared the precursors (**14** and **15**) of octacene and nonacene.[28] The photoconversions of **14** and **15** were monitored in solid argon at 30 K under matrix-isolation conditions.

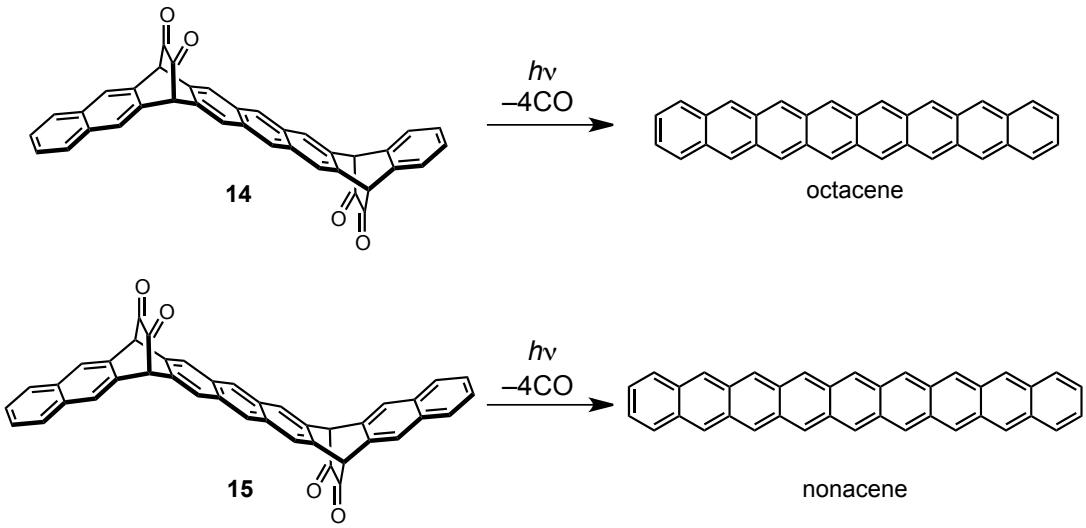

Figure 1-6. Photochemical synthesis of octacene and nonacene.

For the purpose to improve the semiconducting characteristics, many reports related to 6,13-substituted pentacene have been published with synthetic root using 6,13-pentacenequinone (**16**) as a starting material.

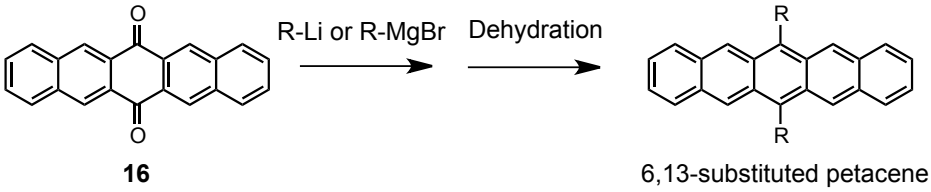

Figure 1-7. Typical synthesis of 6,13-substituted pentacene.

On the other hand, the synthesis of terminal substituted pentacene is also difficult due to instability and insolubility of intermediates. The α-diketone type photoprecursor method can overcome these problems. The examples are shown in Figure 1-8. In 2008 and 2009, Neckers and co-workers have reported the photoprecursors (**17**–**21**) of 2,3,9,10-tetrasubstituted pentacenes (**22**–**26**).[29] These synthetic route can prepare tetra-aryl substituted pentacenes using tetrabromo intermediate as a key compound. Bettinger and co-workers have synthesized terminal push-pull substituted pentacenes (**31**–**34**).[30] The photoprecursor of 2,3,9,10-tetraethylester substituted pentacene (**35**) and the corresponding pentacene (**36**) have been synthesized by Lin and co-woekers.[31] The homo-elongation method can be prepared for synthesis of photoconvertible large acene precursors from the precursor **35**. Yamada and co-workers have synthesized 2,3,9,10-tetraalkylated pentacenes (**40**–**42**) as OFET materials.[32]

The authors have also reported 1,4,8,11-tetrasubstituted pentacene using the precursor method.[33]

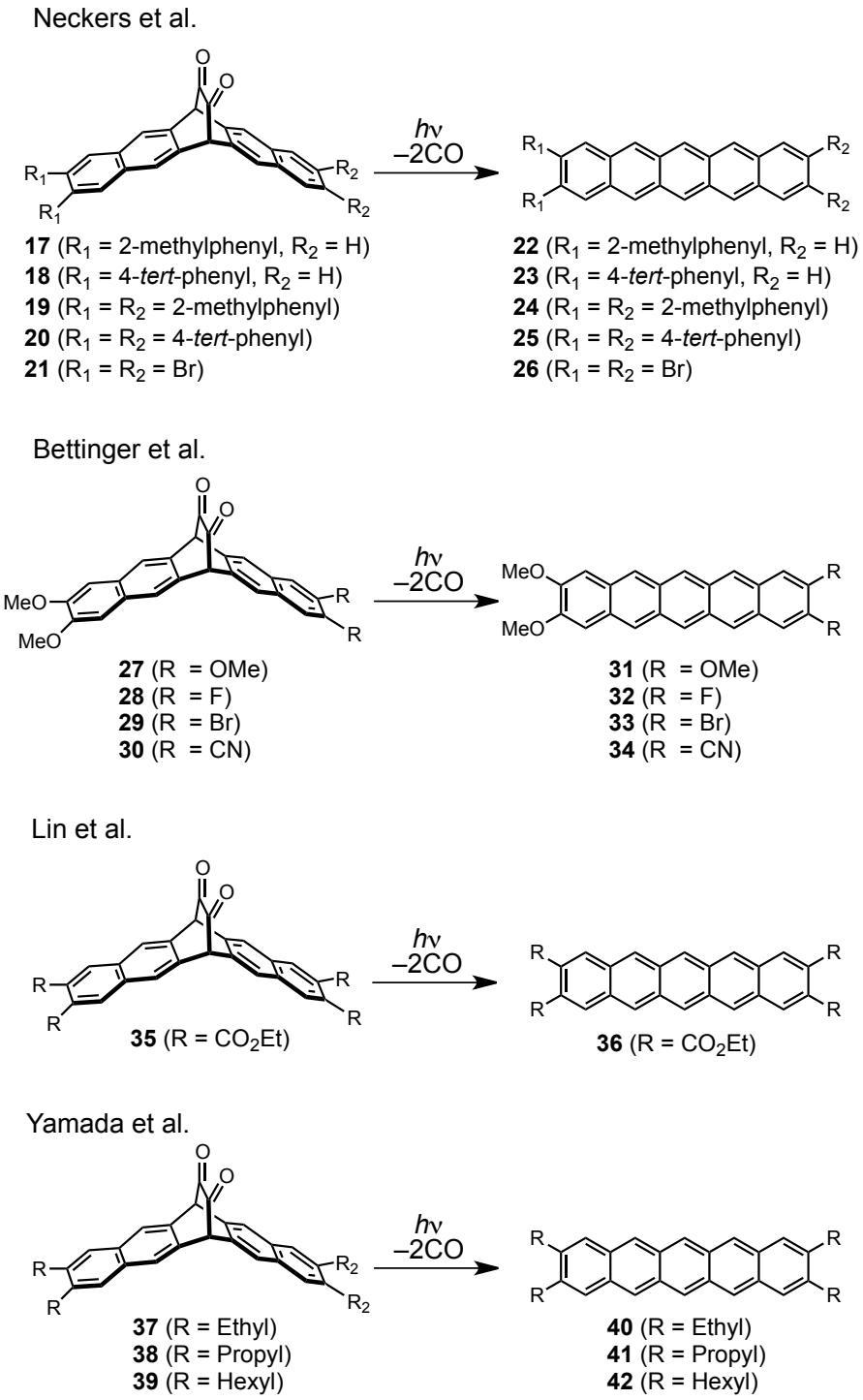

Figure 1-8. Photogenerations of terminal 2,3,9,10-tetrasubstituted pentacenes.

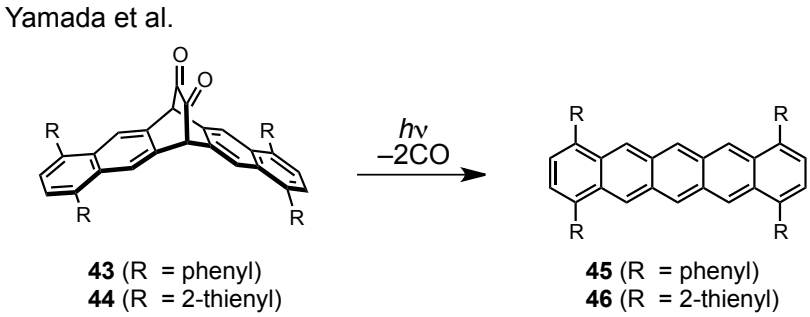

Figure 1-9. Photogeneration of terminal 1,4,8,11-tetrasubstituted pentacenes.

(2) Device Fabrication Tool for Solution Process

The photoprecursor method is not only useful for synthesis of unstable acenes, but also applied to fabricate organic devices by solution process. As described in section 1-1, pentacene shows good semiconductor characteristic, but the solubility is poor. On the other hand, **6,13-PDK** can be dissolved in toluene (2.3 mg/ml) and quantitatively converted to pentacene upon photoirradiation. The photoconversion also proceeds in film and crystal states.[34] In other words, the pentacene film can be prepared on substrate by solution process with this precursor method. The device fabrication using **6,13-PDK** is shown in Figure 1-10. Yamada, Nakayama and co-workers have reported the fabrication of OFET on Si/SiO_2 substrate by the soluble precursor method. The bottom-gate and top-contact device showed high hole mobility (0.86 cm^2/Vs) and high crystalline morphology similar to vacuum-deposited pentacene film.[35] The precursor method can thus prepare the thin film equivalent to the vacuum-deposition method by solution process. The photoprecursor method of **6,13-PDK** also have been applied to fabricate OPVs.[36] The OPV with fullerene as an n-type semiconductor shows power conversion efficiency (PCE) of 0.47%

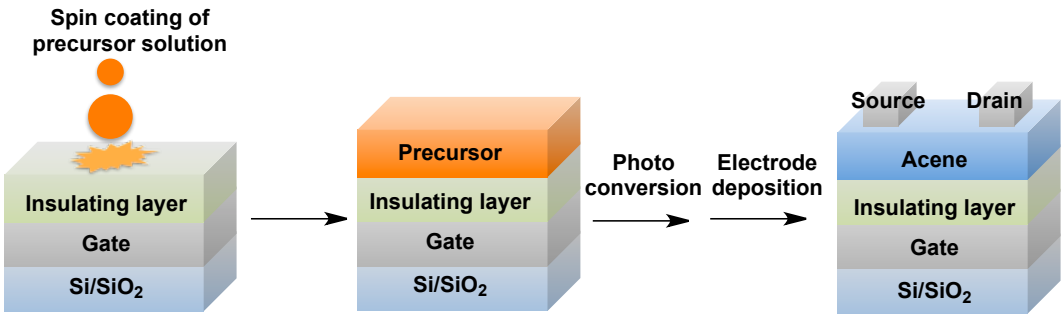

Figure 1-10. The device structure and fabrication process for OFET.

Instead of air-unstable pentacene, anthracene derivatives have been attracted the attention. Yamada, Nakayama and co-workers have applied the precursor method to air-stable anthracene-based semiconductor.[37] The vacuum deposited films of **49** and **50** showed the hole mobility of 0.063 cm^2/Vs and 0.50 cm^2/Vs, respectively.[38] In contrast, solution processed film of **49** and **50** showed 0.047 cm^2/Vs and 2.6×10^{-4} cm^2/Vs, respectively. The career mobility of **49** and **50** obtained by the time resolved microwave conductivity (TRMC) measurement was almost same (0.9 cm^2/Vs and 0.8 cm^2/Vs). While the solution processed film of **49** showed XRD pattern of edge on arrangement similar to vacuum deposited film, the XRD pattern of **50** showed mixed film of edge on and face on arrangements. The results showed the alkyl substituents influence the film structure differently for vacuum deposition and solution process.

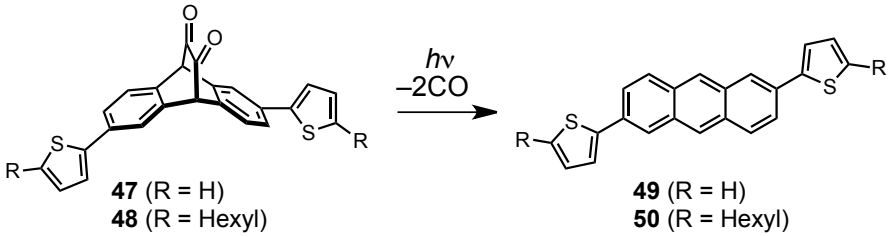

Figure 1-11. Photochemical synthesis of air-stable anthracenes.

The generated anthracene **49** from **47** was also used as p-type semiconductor materials for OPVs. The bulk hetero junction (BHJ) OPV with [6,6]-phenyl-C_{61}-buthric acid methyl ester (**$PC_{61}BM$**) as an n-type semiconductor showed 0.14 % of PCE (updated to 0.68%).[39] The main reason of the low PCE is crystallinity of **49**, the two reagents completely separated in blend film. Meanwhile, the surface morphology was improved by non-symmetric structure **53**, the PCE was slightly improved to 0.16%. The hexyl substituted compound **54** showed higher PCE (1.12%) than **53** since the anthracene was easily mixed with $PC_{61}BM$.[40]

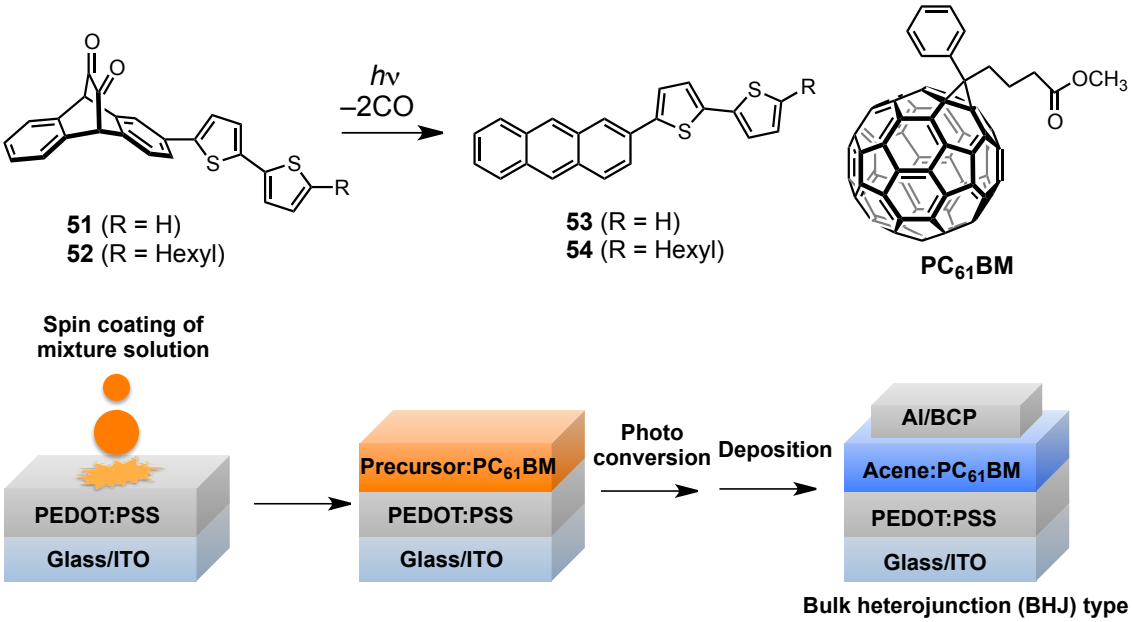

Figure 1-12. The molecular structures of **51**–**54** and **$PC_{61}BM$** and the BHJ junction device structure.

The biggest advantage of the precursor method is dramatic solubility change accompanied with structural change by photoconversion. Anthradithiophene **56**,[41] which is one of thienoacene compounds,[42] is insoluble semiconductor material like pentacene. The precursor **55** can be also converted to **56** on substrate.[43] Since **$PC_{71}BM$** solution can be spin-coated on the insoluble **56** film, the precursor method is useful for fabricating multilayered device. The p-n junction OPV showed 1.54% of PCE, and the value is higher than that of the p-n junction device using pentacene and **$PC_{71}BM$**.

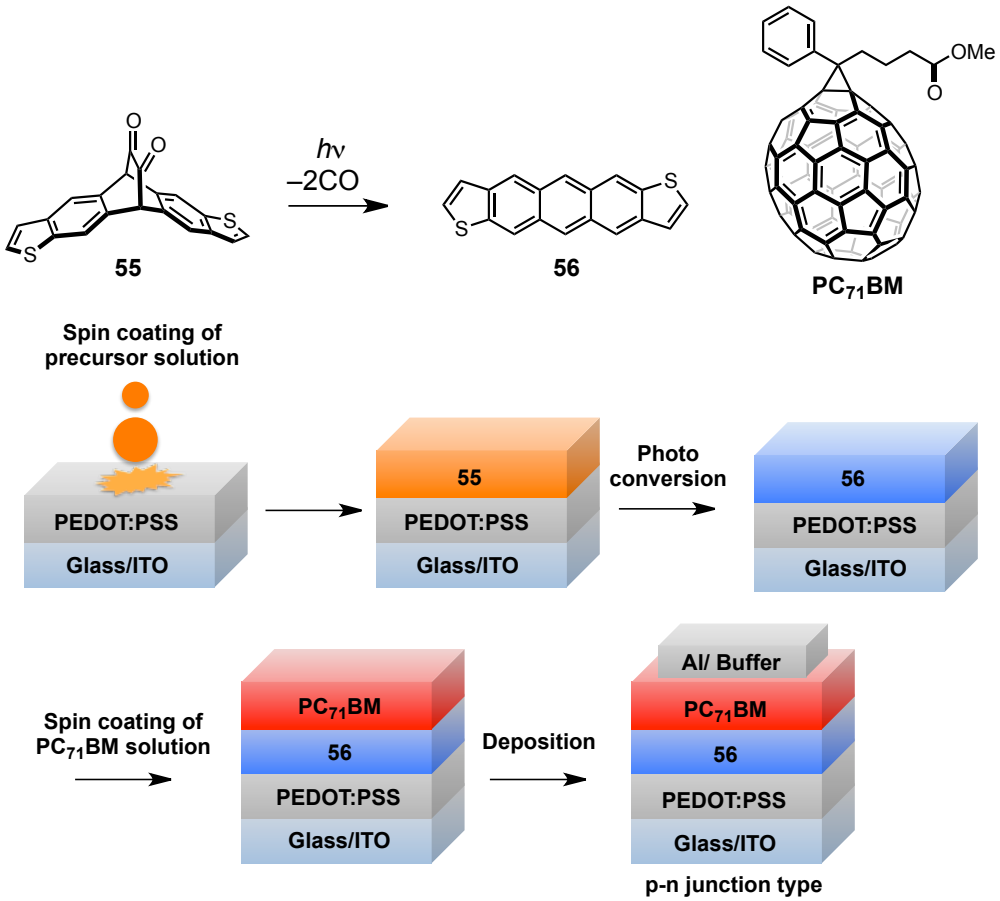

Figure 1-13. The structures of **55**, **56** and **$PC_{71}BM$**, and the p-n junction device structure.

1-3 Overview of This Thesis

As mentioned previously, the photoprecursor has solubilizing property and the mild deprotective reaction is useful for evaluating unstable and insoluble acene compound. The photoprecursor has demonstrated the enormous effect on synthesis and device fabrication, and many reports have been published. Organic device fabrication using photoprecursor method has attracted attention particularly, and further development of the device performance is expected. The existing photoprecursors and acene compounds were used for the fabrication of organic device in the previous research, although, the design and optimization of the molecules according to the purpose have not been performed. Characteristics of photoprecursor method are device fabrication by solution process, the road to practical application will be opened by efficient device fabrication process and high functionality additionally. Therefore, the first subject is molecular design and synthesis for improving and developing of organic electronics materials for solution processable devices. One is the improvement of the photoreaction efficiency of α-diketone type photoprecursor of pentacene and the other is development of new organic electronics materials with ideal energy level and absorption properties toward multilayered OPV.

As described in above section, thin film of pentacene can be prepared from photoprecursor of pentacene (**6,13-PDK**) on substrates. The converted pentacene shows good hole mobility, however, the photoconversion from photoprecursor to pentacene takes a long time because the photoreaction efficiency of the photoprecursor is not high. In order to improve the problem, structural isomer of **6,13-PDK** was designed and synthesized as a new photoprecursor of pentacene. The photoreactivity and characteristic in solid state of the structural isomer are described in Chapter 2.

Photoprecursor approach for multilayer (p-i-n) thin film OPV with solution process is effective to improve the device characteristic. It is not too much to say that the application is the best advantage and the culmination of the precursor method. However, the molecules that match the purpose have not many reported, especially, the development of the p-type semiconducting materials having efficient absorption in visible region for i-layer is needed. To improve the problem, the molecules, which are applicable to multilayer thin film by solution process with improvement of the absorption properties, are designed, synthesized and discussed in Chapter 3.

The second subject is an attempt to apply α-diketone type precursor to latent fluorophore based on the control of the photophysical properties. As described in above sections, α-diketone type

precursor is often used as an optically removable protecting group of unstable compounds and a solubilizing group for improving the solubility of insoluble organic semiconductor. However, there are few reports regarding the other applications, and the study based on different characteristics between α-diketone type photoprecursor and converted acene is expected to widen the utility of the photoprecursor. α-Diketone skeleton is not limited to the photochemical cleavage reaction and exhibits many characteristic properties. The typical properties are n-π* absorption, electron accepting and coordinating properties, etc. On the other hand, converted acene has π-π* absorbing, electron donating properties and fluorescent, consequently, the properties also changes dramatically with the photochemical structural change. For the development of new research areas other than the solubility changes with photoconversion, photoprecursor method is proposed as fluorescence switchable unit in Chapter 4. The three types fluorescence switching mechanisms based on the change of the energetic and electronic properties by photoconversion are described.

As another topic, the successful research at National University of Singapore (Supervisor: Prof. Dr. Jishan Wu) as a part of the International Training Program (ITP) is described in Chapter 5. In general, phenoxyl radical is an unstable species and the isolation is difficult. The unstable radical was stabilized by the two kinds of strategies to isolate the radical compound in this study. The strategies are 1) expanded π-structure for delocalization, and 2) steric protection at the most reactive position. As the steric protection, bicyclo[2,2,2]octadiene (BCOD) was used.

Finally, conclusions of this thesis and future prospects of convertible precursor method are described in Chapter 6.

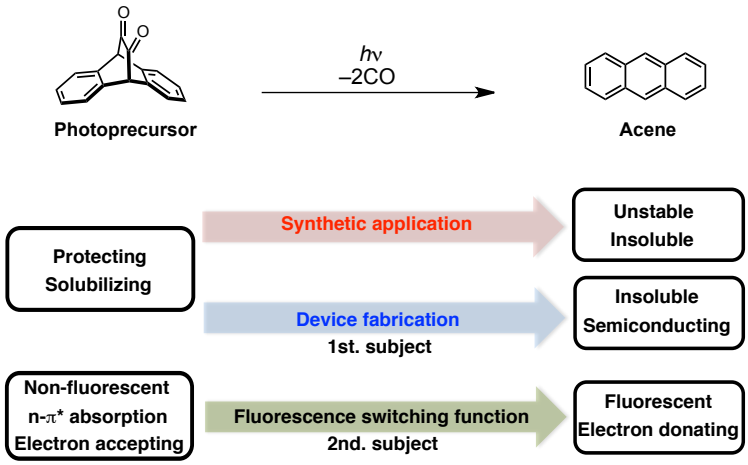

Figure 1-14. Toward "multi-functional tools" in acene chemistry based on changes of the different properties with photoconversion.

1-4 References

(1) Anthony, J. E. *Chem. Rev.* **2006**, *106*, 5028–5048. (b) Anthony, J. E. *Angew. Chem. Int. Ed.* **2008**, *47*, 452–483.

(2) Watanabe, M.; Chang, Y. J.; Liu, S.-W.; Chao, T.-H.; Goto, K.; Islam, M. M.; Yuan, C.-H.; Tao, Y.-T.; Shinmyozu, T.; Chow, T. J. *Nat. Chem.* **2012**, *4*, 574–578.

(3) (a) Knipp, D.; Street, R.A.; Krusor, B.; Apte, R.; Ho, J. *J. Non-Cryst. Solids* **2002**, *299–302*, 1042–1046. (b) Klauk, H.; Halik, M.; Zschieschang, U.; Eder, F.; Schmid, G.; Dehm, C. *App. Phys. Lett.* **2003**, *82*, 4175–4177. (c) Kumaki, D.; Yahiro, M.; Inoue, Y.; Tokito, S. *App. Phys. Lett.* **2007**, *90*, 133511-1–133511-3.

(4) (a) Yo, S.; Domercq, B.; Kippelen, B. *Appl. Phys. Lett.* **2004**, *85*, 5427–5429. (b) Sakai, J.; Taima, T.; Yamanari, T.; Yoshida, Y.; Fujii, A.; Ozaki, M. *Jpn. J. Appl. Phys.* **2010**, *49*, 032301-1–032301-7.

(5) Takeyama, Y.; Ono, S.; Matsumoto, Y. *Appl. Phys. Lett*. **2012**, 083303-1–083303-4.

(6) Yang, J.; Nguyen, T.-Q. *Org. Electron.* **2007**, *8*, 566–574.

(7) (a) Allen, C. F. H.; Bell, A. *J. Am. Chem. Soc*. **1942**, 64, 1253–1260. (b) Maulding, D. R. Roberts, B. G. *J. Org. Chem*. **1969**, *34*, 1734–1736

(8) Anthony, J. E.; Brooks, J. S.; Eaton, D. L.; Parkin, S. R. *J. Am. Chem. Soc*. **2001**, *123*, 9482–948.

(9) Diao, Y.; Tee, B. C.; Giri, G.; Xu, J.; Kim, D. H.; Becerril, H. A.; Stoltenberg, R. M.; Lee, T. H.; Xue, G.; Mannsfeld, S. C.; Bao, Z. *Nat. Mater.* **2013**, *12*, 665–671.

(10) (a) Payne, M. M.; Parkin, S. R.; Anthoxy, J. E. *J. Am. Chem. Soc*. **2005**, *127*, 8028–8029. (b) Purushothaman, B.; Bruzek, M.; Parkin, S. R.; Miller, A.-F.; Anthony, J. E. *Angew. Chem. Int. Ed*. **2011**, *123*, 7151–7155.

(11) (a) Lehnherr, D.; Gao, J.; Hegmann, F. A.; Tykwinski, R. R. *Org. Lett*. **2008**, *10*, 4779–4782. (b) Zhang, X.; Jiang, X.; Luo, J.; Chi, C.; Chen. H.; Wu, J. *Chem. Eur. J.* **2010**, *16*, 464–468.

(12) Watanabe, M.; Chen, K.-Y. Y.; Chang, Y. J.; Chow, T. J. *Acc. Chem. Res.* **2013**, *46*, 1606–1615.

(13) Herwig, P. T.; Müllen, K. *Adv. Mater*. **1999**, *11*, 480–483.

(14) Afzali, A.; Dimitrakopoulos, C.; Breen, T. *J. Am. Chem. Soc.* **2002**, *124*, 8812–8813.

(15) Afzali, A.; Dimitrakopoulos, C. D.; Graham, T. O. *Adv. Mater.* **2003**, *15*, 2066–2069.

(16) Joung, M. J.; Ahn, J. H.; Kang, S. Y.; Baek, K. H.; Ahn, S. D.; Do, L. M.; Kim, C. A.; Kim,

G. H.; You, I. K.; Yoon, S. M.; Suh, K. S. *Bull. Korean. Chem. Soc.* **2003**, *24*, 1862–1864.

(17) Vets, N.; Smet, M.; Dehaen, W. *Tetrahedron Lett.* **2004**, *45*, 7287–7289.

(18) Weidkamp, K.; Afzali, A.; Tromp, R.; Hamers, R. *J. Am. Chem. Soc.* **2004**, *126*, 12740–12741.

(19) (a) Uno, H.; Yamashita, Y.; Kikuchi, M.; Watanabe, H.; Yamada, H.; Okujima, T.; Ogawa, T.; Ono, N. *Tetrahedron Lett.* **2005**, *46*, 1981–1983. (b) Yamada, H.; Yamashita, Y.; Kikuchi, M.; Watanabe, H.; Okujima, T.; Uno, H.; Ogawa, T.; Ohara, K.; Ono, N. *Chem. Eur. J.* **2005**, *11*, 6212–6220.

(20) Chen, K.-Y.; Hsieh, H.-H.; Wu, C.-C.; Hwang, J.-J.; Chow, T. *Chem. Commun.* **2007**, 1065–1067.

(21) (a) Watanabe, M.; Chao, T.-H.; Liu, S.-W.; Chien, C.-T.; Chang, Y.; Yuan, C.-H.; Huang, K.-C.; Chien, S.-H.; Shinmyozu, T.; Chow, T. *J. Mater. Chem.* **2011**, *21*, 11317–11322. (b) Watanabe, M.; Chao, T.-H.; Chien, C.-T.; Liu, S.-W.; Chang, Y.; Chen, K.-Y.; Chow, T. *Tetrahedron Lett.* **2012**, *53*, 2284–2287. (c) Chien, C.-T.; Lin, C.-C.; Watanabe, M.; Lin, Y.-D.; Chao, T.-H.; Chiang, T.; Huang, X.-H.; Wen, Y.-S.; Tu, C.-H.; Sun, C.-H.; Chow, T. *J. Mater. Chem.* **2012**, *22*, 13070–13075. (d) Chien, C.-T.; Chiang, T.-C.; Watanabe, M.; Chao, T.-H.; Chang, Y.; Lin, Y.-D.; Lee, H.-K.; Liu, C.-Y.; Tu, C.-H.; Sun, C.-H.; Chow, T. *Tetrahedron Lett.* **2013**, *54*, 903–906.

(22) (a) Chao, T.-H.; Chang, M.-J.; Watanabe, M.; Luo, M.-H.; Chang, Y.; Fang, T.-C.; Chen, K.-Y.; Chow, T. *Chem. Commun.* **2012**, *48*, 6148–6150. (b) Watanabe, M.; Su, W.-T.; Chen, K.-Y.; Chien, C.-T.; Chao, T.-H.; Chang, Y.; Liu, S.-W.; Chow, T. *Chem. Commun.* **2013**, *49*, 2240–2242.

(23) Strating, J.; Zwanenburg, B.; Wagenaar, A.; Udding, A.C. *Tetrahedron Lett.* **1969**, *10*, 125–128.

(24) Suzuki, M.; Aotake, T.; Yamaguchi, Y.; Noguchi, N.; Nakano, H.; Nakayama, K.; Yamada, H. *J. Photochem. Photobiol. C: Photochem. Reviews* **2014**, *18*, 50–70.

(25) Mondal, R.; Adhikari, R. M.; Shah, B. K.; Neckers, D. C. *Org. Lett.* **2007**, *9*, 2505–2508.

(26) Mondal, R.; Shah, B. K.; Neckers, D. C. *J. Am. Chem. Soc.* **2006**, *128*, 9612–9613.

(27) (a) Bettinger, H. F.; Mondal, R.; Neckers, D. C. *Chem. Commun.* **2007**, 5209–5211. (b) Mondal, R.; Tönshoff, C.; Khon, D.; Neckers, D. C.; Bettinger, H. F. *J. Am. Chem. Soc.* **2009**, *131*, 14281–14289.

(28) Tönshoff, C.; Bettinger, H.F. *Angew. Chem. Int. Ed*. **2010**, *49*, 4125–4128.

(29) Zhan, Y.; Mondal, R.; Neckers, D. C. *J. Org. Chem*. **2008**, *73*, 5506–5513.

(30) Tönshoff, C; Bettinger, *Chem. Eur. J*. **2012**, *18*, 1789–1799.

(31) Lin, C.-H.; Lin, K.-H.; Pal, B.; Tsou, L.-D. *Chem. Commun*. **2009**, 803–805.

(32) Katsuta, S.; Saeki, H.; Tanaka, K.; Murai, Y.; Kuzuhara, D.; Misaki, M.; Aratani, N.; Masuo, S.; Ueda, Y.; Yamada, H. *J. Mater. Chem. C* **2014**, *2*, 986–993.

(33) Katsuta, S.; Yamada, H.; Okujima, T.; Uno, H. *Tetrahedron Lett.* **2010**, *51*, 1397–1400.

(34) Masuo, S.; Tanaka, K.; Oe, M.; Yamada, H. *Phys. Chem. Chem. Phys*. **2014**, *16*, 13483–13488.

(35) (a) Nakayama, K.; Ohashi, C.; Oikawa, Y.; Motoyama, T.; Yamada, H. *J. Mater. Chem. C* **2013**, *1*, 6244–6251. (b) Ohashi, C.; Yamada, H.; Nakayama, K. *Mol. Cryst. Liquid. Cryst.* **2013**. 580, *1*, 103–109.

(36) Motoyama, T.; Kiyota, T.; Yamada, H.; Nakayama, K. *Sol. Energy. Mater. Sol. Cells* **2013**, *114*, 156–160.

(37) Yamada, H.; Ohashi, C.; Aotake, T.; Katsuta, S.; Honsho, Y.; Kawano, H.; Okujima, T.; Uno, H.; Ono, N. Seki, S.; Nakayama, K. *Chem. Commun*. **2012**, *48*, 11136–11138.

(38) Meng, H.; Sun, F.; Goldfinger, M. B.; Jaycox, G. D.; Li, Z.; Marshall, W. J.; Blackman, G. S. *J. Am. Chem. Soc*. **2005**, *127*, 2406–2407.

(39) (a) Motoyama, T.; Sugii, S. Ikeda, S.; Yamaguchi, Y.; Yamada, H.; Nakayama, K. *Jpn. J. Appl. Phys.* **2014**, *53*, 01AB02-1–01AB02-4. (b) Yamagchi, Y.; Suzuki, M.; Motoyama, T.; Sugii, S.; Katagiri, C.; Takahira, K.; Ikeda, S.; Yamada, H.; Nakayama, K. *Sci. Rep.* 4, 7151

(40) Sugii, S. Master thesis, Nara institute of Science and Technology (NAIST), Japan, **2014**.

(41) Laquindanum, J. G.; Katz, H. E.; Lovinger, A. J. *J. Am. Chem. Soc.* **1998**, *120*, 664–672.

(42) Takimiya, K.; Shinamura, S.; Osaka, I.; Miyazaki, E. *Adv. Mater*. **2011**, *23*, 4347–4370.

(43) Yamada, H.; Yamaguchi, Y.; Katoh, R.; Motoyama, T.; Aotake, T.; Kuzuhara, D.; Suzuki, M.; Okujima, T.; Uno, H.; Aratani, N.; Nakayama, K. *Chem. Commun*. **2013**, *49*, 11638–11640.

Chapter 2

Improvement of Photoconversion Efficiency of α-Diketone Type Pentacene Precursor

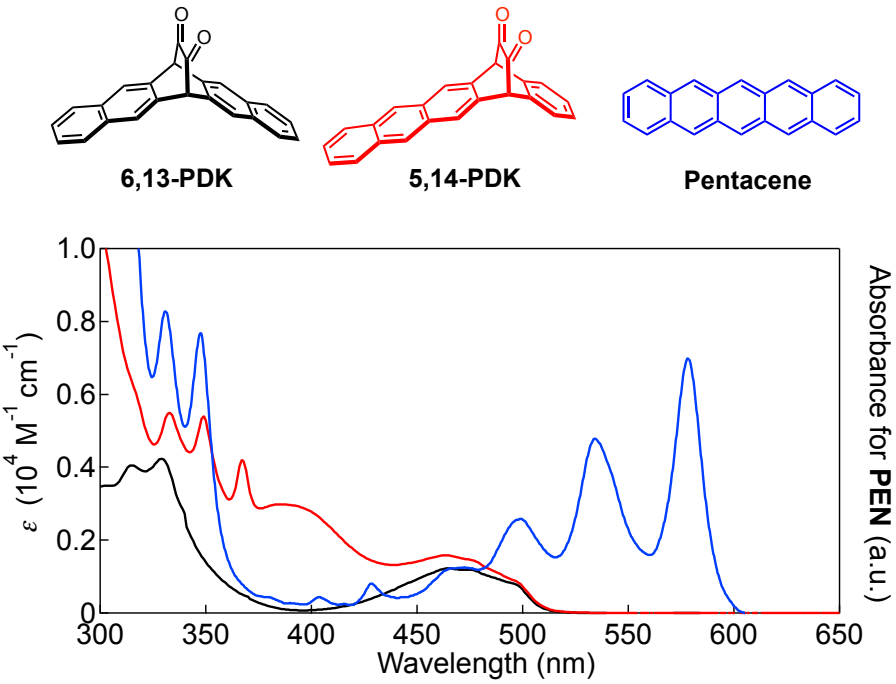

In order to improve the photoconversion efficiency of **6,13-PDK**, α-diketone type precursor of pentacene with anthracene moiety in molecule is studied. In this chapter, synthesis and optical property of **5,14-PDK** is discussed in comparison with **6,13-PDK**.

2-1 Introduction

As described in Chapter 1, the insolubility of pentacene is a problem to be solved for fabrication the organic devices by solution process. To solve the problem, α-diketone type precursor of pentacene (**6,13-PDK**) has been reported as a soluble precursor of pentacene.[1] The precursor can be dissolved in common organic solvent and converted to pentacene in solution or films upon photoirradiation. The UV-vis absorption spectrum of **6,13-PDK** in toluene is shown in Figure 2-1. The absorption band (400–500 nm) of **6,13-PDK** is overlapped with the absorption of pentacene. In addition, since the n-π* transition is forbidden, the molar absorbance coefficient (~1000 M^{-1} cm^{-1}) is smaller than the coefficient of pentacene. The photoconversion efficiency is decreased by the masking effect of absorption of pentacene with the progress of the conversion.

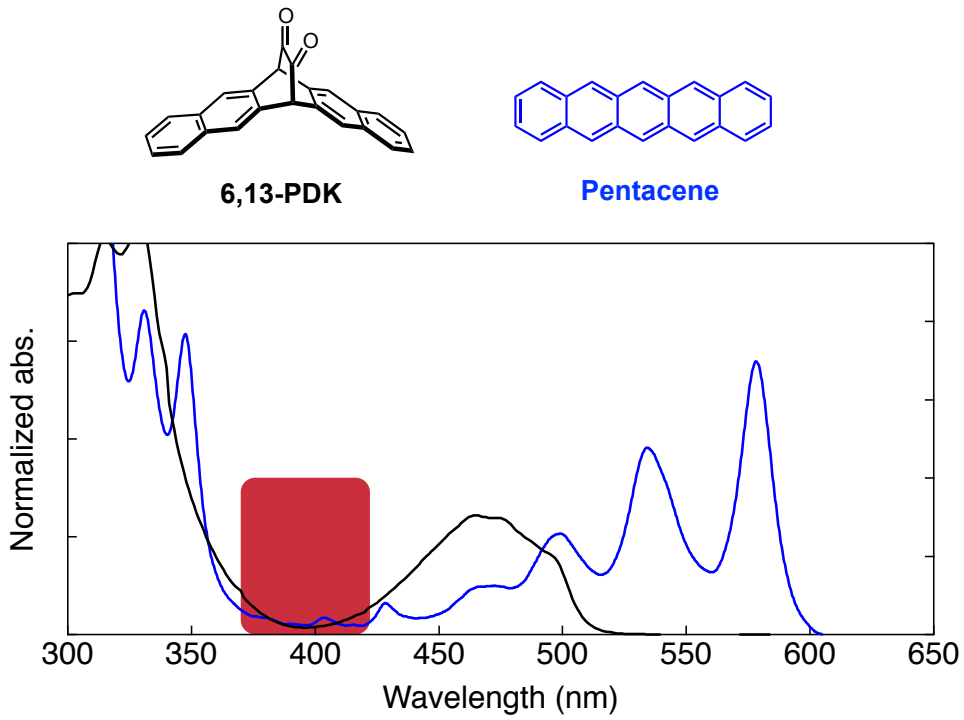

Figure 2-1. UV-vis absorption spectra of **6,13-PDK** and pentacene. Red mark reveals target wavelength.

In order to adjust the absorption wavelength while maintaining the function as photoconvertible precursor, the modification of chromophore is required. It's understood that the α-diketone moiety can't be changed, therefore, the remaining chromophore is only aromatic ring around the bicycle unit. **6,13-PDK** has naphthalenes in the structure and shows absorption at 300–320 nm resulting from π–π* transition of naphthalene moiety. In general, the absorption wavelength red-sift to increase the fused benzene rings, so anthracene is suitable for improving the absorption characteristic around 400 nm. Actually, Prof. Chow et al. have reported 5,14-monoketone type precursor of pentacene (**2-1**) as a structural isomer of 6,13-monoketone type precursor **2-2** (Figure 2-2), and the absorption spectrum shows typical vibrational structure of anthracene around 400 nm.[2]

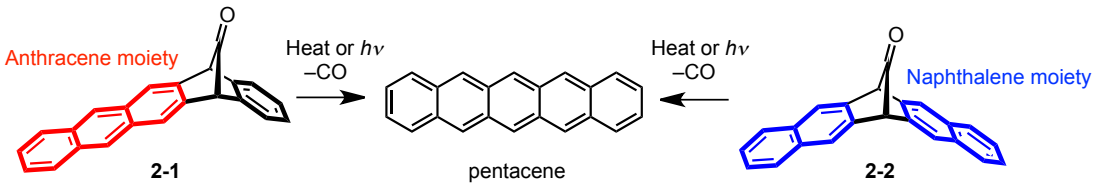

Figure 2-2. Monoketone type precursors of pentacene.

In reference to the result, the author of this thesis designed **5,14-PDK** as a structural isomer of **6,13-PDK** (Figure 2-3). In this chapter, the synthesis, crystal structure, optical properties and photoconversion are discussed.

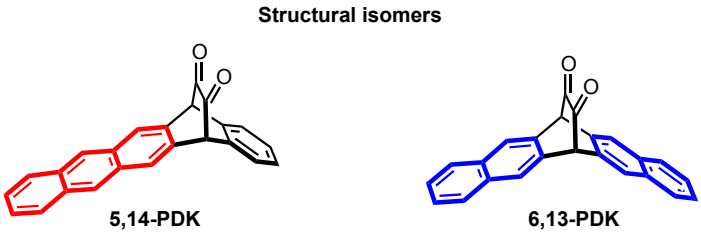

Figure 2-3. Molecular structure of the target compound **5,14-PDK** in this chapter.

2-2 Synthesis of 5,14-Diketopentacene

The synthesis of **5,14-PDK** is shown in Scheme 2-1. Pentacene was reacted with vinylene carbonate in a Diels-Alder reaction to give a mixture of 5,14- (**2-3**) and 6,13- adducts (**2-4**). The compounds were subsequently hydrolyzed to give diols, the mixture was separated by silica gel column chromatography to give the 5,14- (**2-5**) and 6,13- adducts (**2-6**) in 21 and 58%, respectively. Diol **2-5** was oxidized by the Swern reaction to give α-diketone compounds (**5,14-PDK**) in 52% yield.

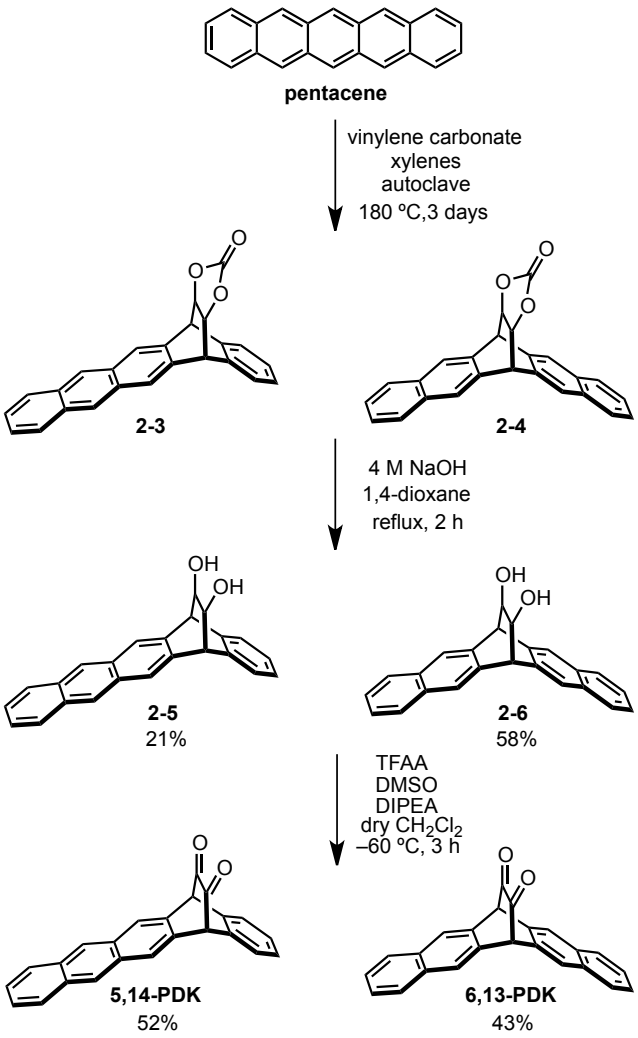

Scheme 2-1. Synthesis of **5,14-PDK** from pentacene.

2-3 Single Crystal Structure of 5,14-Diketopentacene

The recrystallization of **5,14-PDK** from a dichloromethane gave yellow prism crystals suitable for single crystal X-ray diffraction analysis.[3] The angles made by C9-C10-C11 and C16-C17-C18 were 107.6(2) and 106.7(1)º, respectively. The distance between the anthracene–anthracene surfaces is 3.524 Å, which is shorter than that of the naphthalene–naphthalene distance of **6,13-PDK** (3.596 Å). The interaction was not only observed between anthracene moieties, but also between the facing benzene ring. The distance between the surfaces of two benzene moieties was 3.849 Å. In addition, there was a CH–π interaction between hydrogen atoms and the neighboring anthracene moiety. The shortest distance was 2.788 Å. These interactions made the packing structure of **5,14-PDK** rigid and lowered the solubility in common organic solvents. The solubility of **5,14-PDK** in toluene was only 0.44 mg/mL at room temperature, although it was 2.3 mg/mL for **6,13-PDK**.

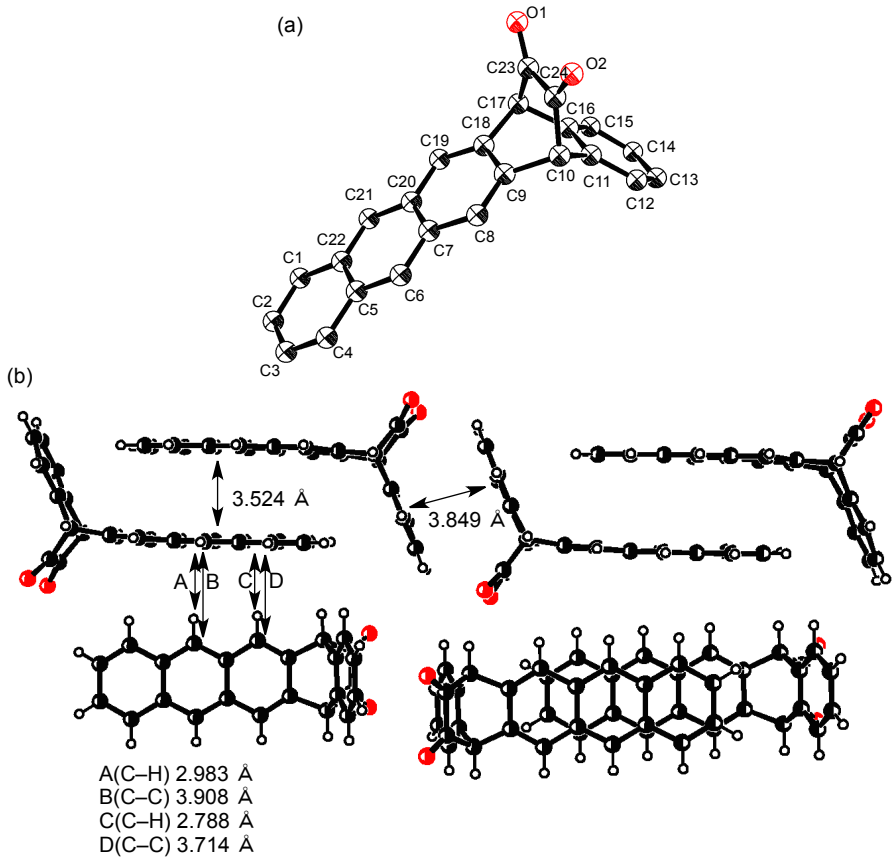

Figure 2-4. (a) ORTEP drawing of the structure of **5,14-PDK** at 25 ºC as determined by single crystal XRD. Hydrogen atoms are omitted for clarity. Ellipsoids are drawn at the 50% probability displacement level. (b) Stacking pattern of neighboring molecules.

2-4 Optical Properties

The UV-vis absorption spectra of **5,14-PDK**, **6,13-PDK** and **2-5** in toluene are shown in Figure 2-5. The UV-vis absorption spectrum of **6,13-PDK** shows an n-π* absorption of the diketone moiety at 466 nm (ε = 1.28 × 10^3 M^{-1} cm^{-1}) and a π-π* absorption at 329 (4.23 × 10^3 M^{-1} cm^{-1}) and 315 nm (4.05 × 10^3 M^{-1} cm^{-1}), while **5,14-PDK** shows a broad peaks at 464 nm (1.58 × 10^3 M^{-1} cm^{-1}), and π–π* absorption at 333 (5.49 × 10^3 M^{-1} cm^{-1}), 349 (5.40 × 10^3 M^{-1} cm^{-1}) and 367 nm (4.20 × 10^3 M^{-1} cm^{-1}). Furthermore, a broad absorption at 386 nm (2.98 × 10^3 M^{-1} cm^{-1}) was observed although a similar peak was not observed for **6,13-PDK**. Compared with the absorption spectrum of **2-5**, the π-π* absorption is broadened. This means the anthracene moiety of **5,14-PDK** strongly interacts with carbonyl moieties. As a result, the absorption band around 400 nm, which doesn't overlap of absorption with pentacene, increases in comparison with **6,13-PDK**.

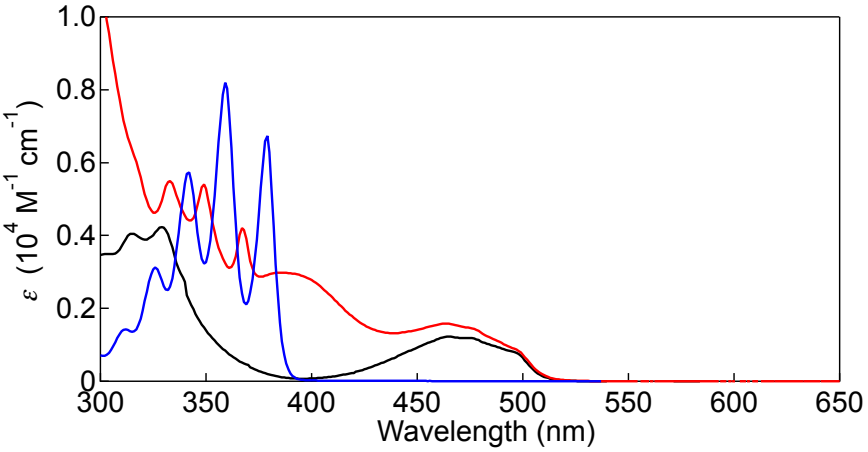

Figure 2-5. UV-vis absorption spectra of **5,14-PDK** (red), **6,13-PDK** (black) and **2-5** (blue) in toluene (blue).

The absorption at 386 nm was characteristic of **5,14-PDK** and was not observed for diol **2-5**. Although the concentration dependence of absorption spectra for **5,14-PDK** was measured from 1.79×10^{-1} to 7.39×10^{-3} M, the distinct effect was not observed. These phenomena suggest the characteristic absorption arises from intramolecular interaction. To confirm the solvent effect, the UV-vis absorption spectra were measured in toluene, dichloromethane, acetonitrile and DMF as solvents of different polarity (Figure 2-6). In addition to the π-π* absorptions at 333, 349 and 367 nm, a vibrational peak at 375 nm was observed with shoulders at 400 nm in DMF. In acetonitrile and DMF, similar peaks were observed at 370 and 372 nm, respectively. The broad peaks at 386 nm in toluene showed a clearer vibrational structure than that in other solvents; 382 ($\varepsilon = 1.58 \times 10^3$ M^{-1} cm^{-1}) in dichloromethane, 382 nm (2.55×10^3 M^{-1} cm^{-1}) in DMF and 379 nm (2.75×10^3 M^{-1} cm^{-1}) in acetonitrile with shoulders around 400 nm. The n-π* and π-π* absorption at 333, 349 and 367 nm showed a slight dependence on the solvent. The molecular extinction coefficients of the peaks at 333, 349 and 367 nm were smaller than those in toluene, but the peaks were observed at almost the same wavelength.

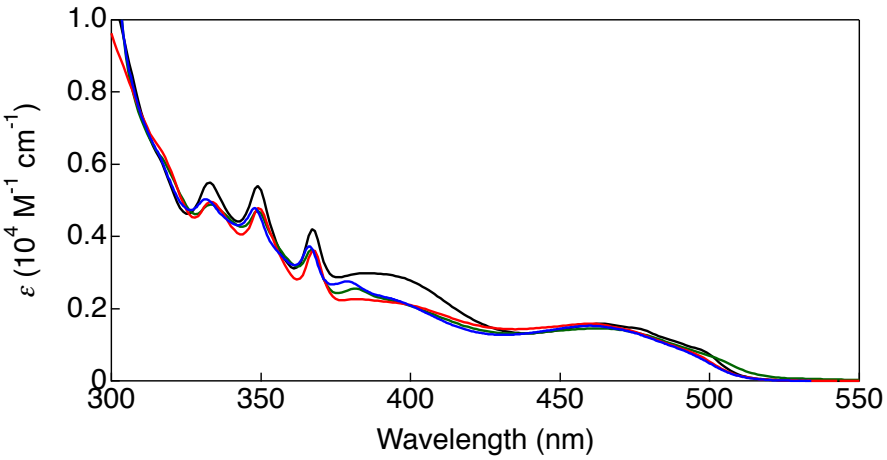

Figure 2-6. Solvent effect on the UV-vis absorption spectra of **5,14-PDK** in toluene (black), dichloromethane (red), acetonitrile (blue) and DMF (green).

Density functional theory (DFT) calculations at the CAM-B3LYP/6-31G(d)//B3LYP/6-31G(d) level were conducted to provide molecular orbital (MO) and time-dependent density functional theory (TD-DFT).[4] The HOMO was localized on the anthracene moiety, the LUMO on the carbonyl π* orbital and the HOMO−1 on the n orbital. TD-DFT calculations showed that the absorption at 456 nm corresponding to an n-π* transition that was mainly composed of the transition from HOMO−1 to LUMO and HOMO−1 to LUMO+1. Also, the absorption at 358 nm was calculated to be transitions from HOMO to LUMO or LUMO+1. The transition is mixed π-π* of anthracene moiety and intramolecular charge transfer from anthracene to diketone moiety.

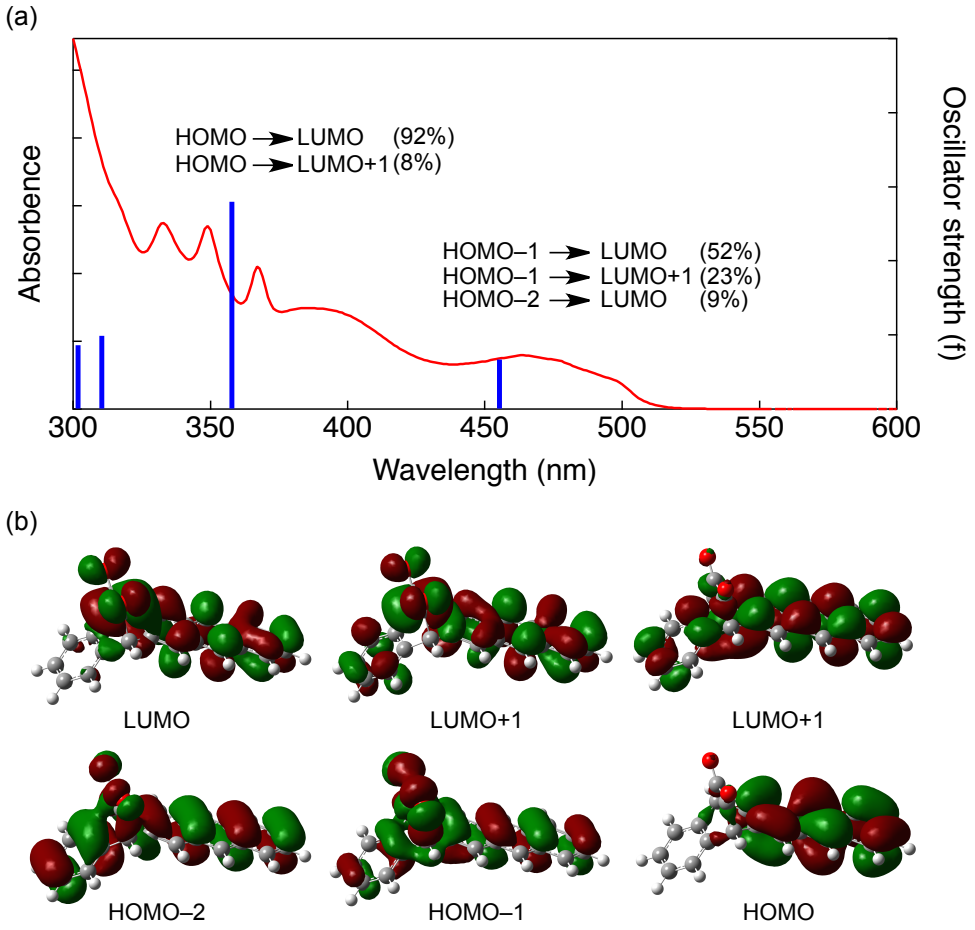

Figure 2-7. (a) UV-vis absorption spectrum (red) and TDDFT calculation (blue) at CAM-B3LYP/6-31G(d) level of **5,14-PDK**; (b) Molecular orbitals by DFT calculations at B3LYP/6-31G (d) level.

2-5 Photoconversion in Solution

The photoreactions of precursors (**5,14-PDK** and **6,13-PDK**) to pentacene were performed using 500 W Xenon lamp with monochromator. Figure 2-8 shows the change in the UV-vis absorption spectra during the photoreaction of **5,14-PDK** in toluene. Firstly, a 1.1×10^{-1} mM solution of **5,14-PDK** was irradiated with light at 405 nm under argon atmosphere. During irradiation, the peaks at 352–484 nm decreased gradually, and new peaks at 495, 530 and 578 nm increased. After the absorption characteristic of pentacene increased for 25 min, a purple solid appeared in the solution. As determined by observing the isosbestic points at 352 and 484 nm, the photoreaction proceeded without byproduct.

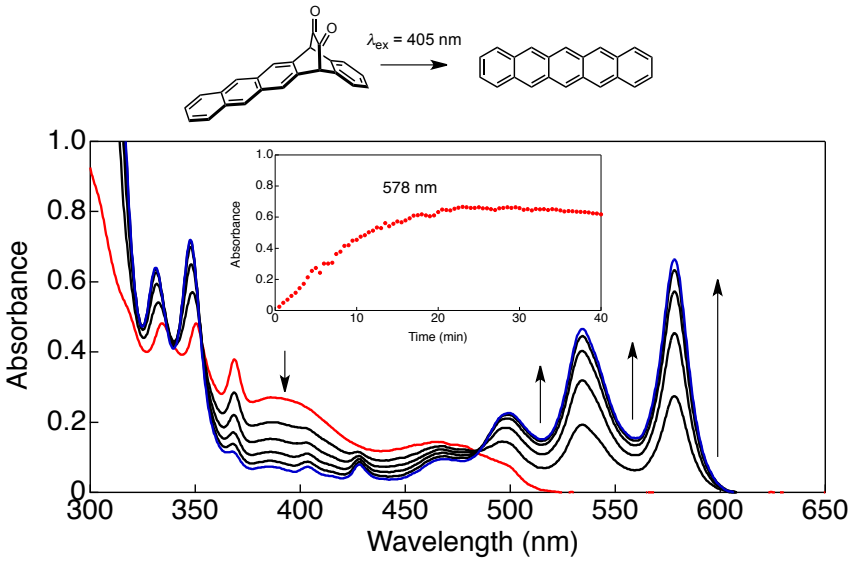

Figure 2-8. Changes in UV-vis absorption spectra and time profiles at 578 nm during photolysis (λ_{ex} = 405 nm) of **5,14-PDK** (1.1×10^{-1} mM) in toluene.

Secondly, solutions of **5,14-PDK** (1.3×10^{-1} mM) and **6,13-PDK** (1.7×10^{-1} mM) in toluene were irradiated with light at 468 nm, as shown in Figure 2-9 and Figure 2-10. Similarly, the absorption spectra changed from the precursor to pentacene with photoirradiation, the photoreaction quantum yields (Φ_R) was measured by using potassium ferrioxalate actinometry. The Φ_R of **5,14-PDK** in toluene were 2.4 (λ_{ex} = 405 nm) and 2.3% (468 nm). The values are about two times as large as that of **6,13-PDK** (1.4%, 468 nm).

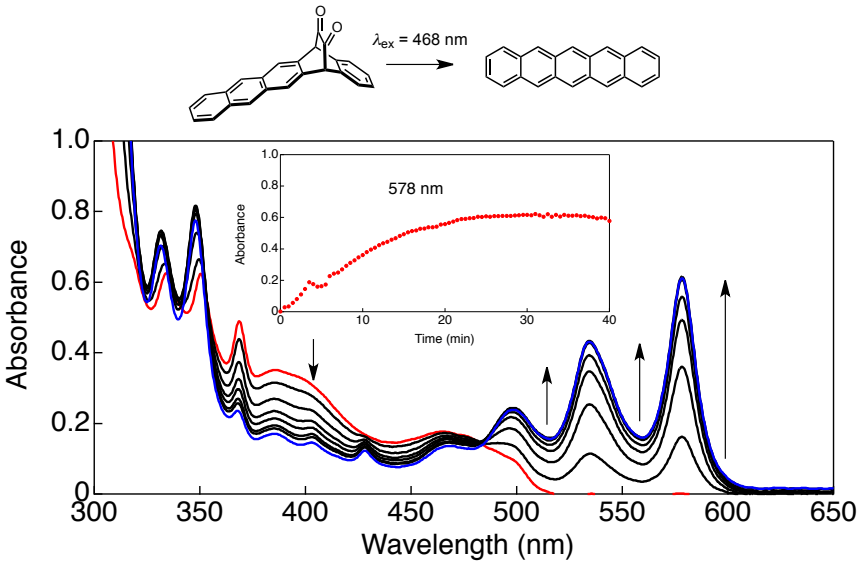

Figure 2-9. Changes in UV-vis absorption spectra and time profiles at 578 nm during photolysis (λ_{ex} = 468 nm) of **5,14-PDK** (1.3×10^{-1} mM) in toluene.

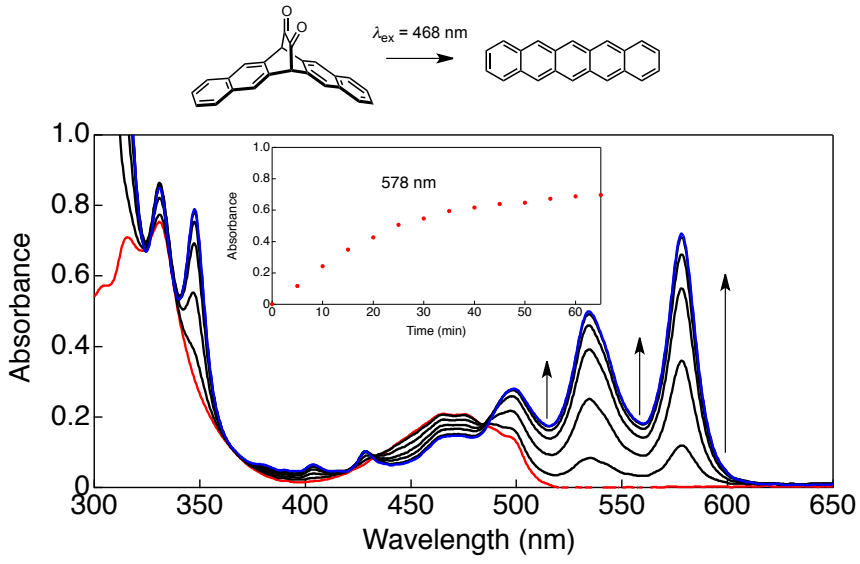

Figure 2-10. Changes in UV-vis absorption spectra and time profiles at 578 nm during photolysis (λ_{ex} = 468 nm) of **6,13-PDK** (1.7×10^{-1} mM) in toluene.

Next, photolysis reactions of **5,14-PDK** and **6,13-PDK** in acetonitrile were performed; the results are shown in Figure 2-11, 12 and 13. In acetonitrile the photoreaction of **5,14-PDK** was slower than that in toluene, and the Φ_R values were 0.28%, which are ten times lower than those in toluene. The Φ_R value of **6,13-PDK** irradiated at 468 nm in acetonitrile was 0.80%; lower than that of 1.4% in toluene. Similar solvent dependent behavior of the reaction on the quantum yield was observed for the α-diketone type precursor of monoanthraporphyrin.[5] Compared with the photoreaction in toluene, the occurrence of rapid photoinduced electron transfer from the singlet excited state porphyrin to the diketone moiety in benzonitrile resulted in a significant decrease in the singlet excited state lifetime, leading to suppression of the photoreaction.

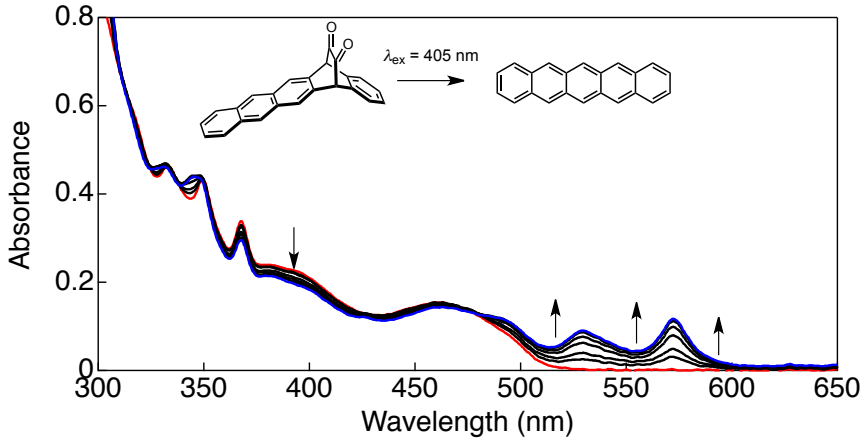

Figure 2-11. Changes in UV-vis absorption spectra during photolysis (λ_{ex} = 405 nm) of **5,14-PDK** in acetonitrile for 15 min.

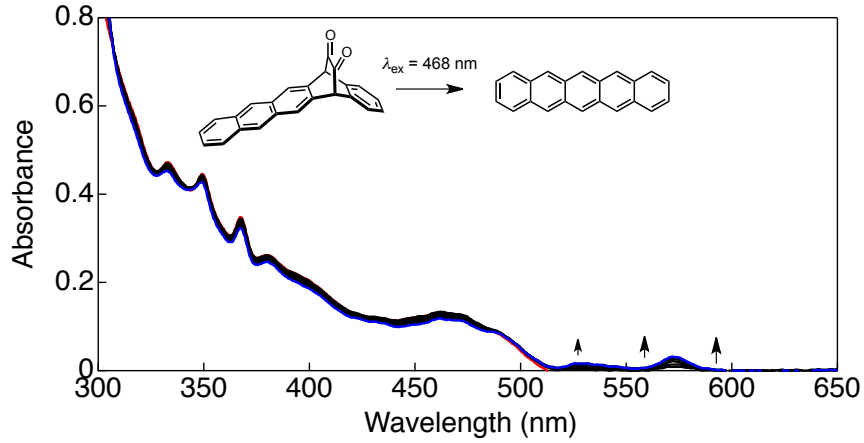

Figure 2-12. Changes in UV-vis absorption spectra during photolysis (λ_{ex} = 468 nm) of **5,14-PDK** in acetonitrile for 15 min.

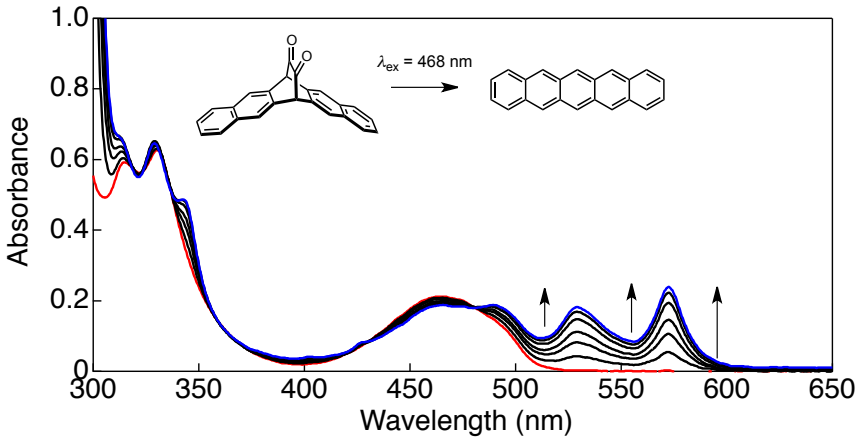

Figure 2-13. Changes in UV-vis absorption spectra during photolysis (λ_{ex} = 468 nm) of **6,13-PDK** in acetonitrile for 15 min.

	Φ_R (%)			
	toluene		acetonitrile	
	405 nm[a]	468 nm[a]	405 nm[a,b]	468 nm[a,b]
5,14-PDK	2.4 ± 1.0	2.3 ± 0.3	0.33 ± 0.13	0.28 ± 0.12
6,13-PDK	-	1.4 ± 0.3	-	0.80 ± 0.10

Table 2-1. Quantum yields of photoreactions of **5,14-PDK** and **6,13-PDK**. [a] Excitation wavelength. [b] The ε value of pentacene in acetonitrile was assumed to be the same as that in toluene.

The electrochemical property of **5,14-PDK** was investigated by cyclic voltammetry (CV) in acetonitrile containing 0.1 M tetrabuthylammonium hexafluorophosphate ($TBAPF_6$) as the supporting electrolyte. The result is shown in Figure 2-14. The one-electron reduction potential ($E_{red}^{1/2}$ vs. Fc/Fc^+) was −1.47 V. The potential was assigned to the reduction of diketone moiety. The oxidation potential was irreversible peak (maximum was at 0.94 V), which corresponds to oxidation of the anthracene moiety.

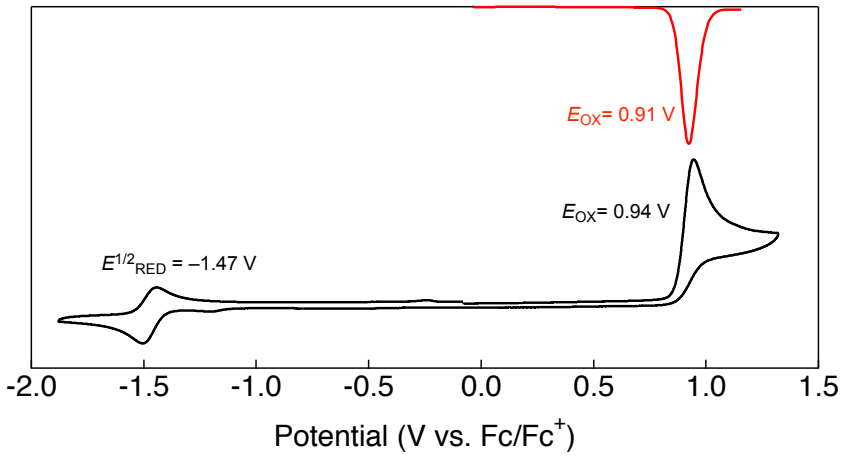

Figure 2-14. Cyclic voltammogram (black) and differential pulse voltmmetry (red) of **5,14-PDK** in acetonitrile. Scan rate 0.1 V s^{-1}. [sample] = 0.1 mM. WE: Glassy carbon, CE: Pt, RE: $Ag/AgNO_3$.

To examine the mechanism of decreasing Φ_R of **5,14-PDK**, the energy level of the charge-separated (CS) state ($Ant^{\bullet+}$–$DK^{\bullet-}$) was determined from the redox potential.[6] The driving force [$-\Delta G_{CR}$] for the intramolecular charge-recombination process from the anion radical of the diketone moiety ($DK^{\bullet-}$) to the cation radical of the anthracene moiety ($Ant^{\bullet+}$) was calculated using Eqs. (1) and (2).

$$-\Delta G_{CR} = [E_{ox}(Ant^{\bullet+}/Ant) - E_{red}(DK/DK^{\bullet-})] + \Delta G_S \quad (1)$$

$$\Delta G_S = e^2/(4\pi\varepsilon_0)[(1/(2R^+) + 1/(2R^-) - 1/R_{cc})(1/\varepsilon_s) - (1/(2R^+) + 1/(2R^-))(1/\varepsilon_r)] \quad (2)$$

Here e is the elementary charge, $E_{ox}(Ant^{\bullet+}/Ant)$ is the oxidation potential of the anthracene moiety in dichloromethane, $E_{red}(DK/DK^{\bullet-})$ is the reduction potential of the diketone moiety in dichloromethane, ε_s and ε_r are the static dielectric constants of the solvents used to estimate the energy level and to measure the redox potentials, respectively, R^+ and R^- are the radii of the

cationic and anionic anthracene and diketone radicals, respectively, and R_{cc} represents the center-to-center distance between the anthracene and diketone moieties. The molecular structures were estimated using the optimized geometries resulting from DFT calculations, and R^+ was determined to be 3.7 Å, while R^- was 1.5 Å for the diketone and the R_{cc} values were 6.2 Å. The driving force for the intramolecular charge separation process [$-\Delta G_{CS}$] from the anthracene unit to the diketone moiety was determined using Eq. (3).

$$-\Delta G_{CS} = \Delta E_{0\text{–}0} - (-\Delta G_{CR}) \qquad (3)$$

Here $\Delta E_{0\text{–}0}$ is the excited singlet state of the diketone moiety (^{1}DK*). The energy levels of ^{1}DK* and ^{3}DK* were calculated from the anthracene diketone already reported. The ^{1}DK* energy level (2.52 eV) was higher than that of the CS state (2.32 eV) in dichloromethane (Figure 2-15). Thus, electron transfer from the anthracene moiety to the diketone moiety occurs, affording the CS state in acetonitrile. This electron transfer is responsible for the lower Φ_R of **5,14-PDK** in acetonitrile. However, the energy level of the CS state in toluene is increased due to the smaller ε value in Eq. (1). Although the Born equation does not give correct values for ΔG_S in nonpolar solvents such as toluene, because of overestimation of the solvent polarity, tentative values of $-\Delta G_{CR}$ were nonetheless estimated. Since the CS energy level was calculated to be 4.05 eV in toluene, the CS level of **5,14-PDK** is higher than the ^{1}DK* level.

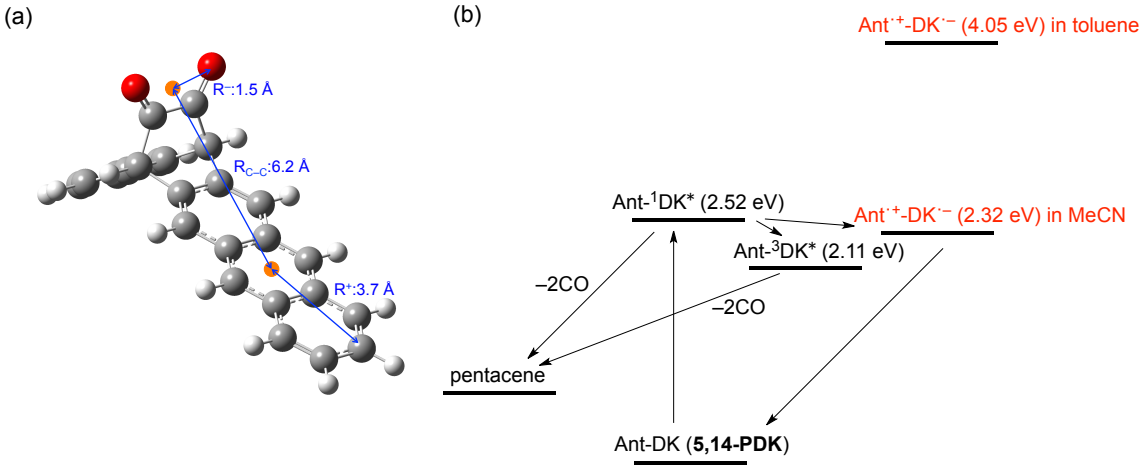

Figure 2-15. (a) Optimized structure by DFT calculation and (b) energy diagram of **5,14-PDK** in solution.

2-6 Photoconversion on Film

The photoconversion reaction was also performed in a thin film. The UV-vis absorption spectra are shown in Figure 2-16 along with photos of the thin film before and after the photoconversion. The yellow film changed to purple after photoirradiation. However, the spectrum of **5,14-PDK** is broad, and the band structures are not clear. **5,14-PDK** has high crystallinity, and crystalline thin film is formed immediately after spin-coating. Therefore, the thin film scattered the light and the correct evaluation is difficult by transmission measurement. The absorption spectrum of pentacene is also broad, but the peaks characteristic for pentacene was observed at around 560 and 610 nm.

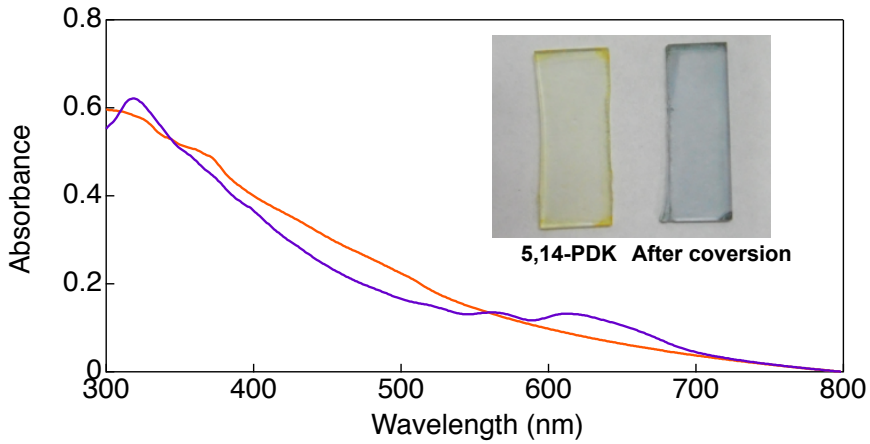

Figure 2-16. UV-vis absorption spectra as film of **5,14-PDK** (orange) and after converted compound (purple).

2-7 Summary

The author of this thesis successfully prepared **5,14-PDK**, which is a photoconvertible precursor of pentacene and a structural isomer of **6,13-PDK**. Compound **5,14-PDK** exhibited a broad absorption at 390 nm and n-π* absorption at 460 nm. Photochemical conversion to pentacene quantitatively proceeded by photoexcitation at the both absorption bands in toluene, with quantum yields (Φ_R) of 2.4 and 2.3%, respectively. The Φ_R is increased about twice of Φ_R of **6,13-PDK**. X-ray single-crystal structure analysis of **5,14-PDK** suggested that has strong π–π interactions and CH-π interaction with neighboring molecules, the solubility of **5,14-PDK** is lower than that of **6,13-PDK**.

2-8 Experimental Section

General Melting points were measured with a Yanaco M-500-D melting point apparatus. ^{1}H NMR and ^{13}C NMR spectra were recorded with JEOL JNM-AL 400 and AL 300 spectrometers at ambient temperature by using tetramethylsilane as an internal standard. FAB mass spectra were measured with a JEOL JMS-MS700 spectrometer. UV/Vis spectra were measured with a JASCO UV/ Vis/NIR spectrophotometer V-570. Elemental analyses were performed with a Yanaco MT-5 elemental analyzer.

Materials: TLC and gravity column chromatography were performed on Art. 5554 (Merck KGaA) plates and silica gel 60N (Kanto Chemical), respectively. Acetonitrile was distilled from P_2O_5 in vacuo. All other solvents and chemicals were reagent-grade quality, obtained commercially, and used without further purification except as noted. For spectral measurements, spectral-grade toluene, dichloromethane, acetonitrile, and DMF were purchased from Nacalai Tesque.

Theoretical Calculations: All DFT calculations were achieved with the Gaussian 09 program package. The geometry was fully optimized at the Becke's three-parameter hybrid functional combined with the Lee–Yang–Parr correlation functional abbreviated as the B3LYP level of density functional theory with 6-31G(d) basis set. Equilibrium geometries were verified by frequency calculations, where no imaginary frequency was found. Based on the B3LYP/6-31G(d)-optimized geometry, TD-DFT calculations were conducted at the CAM-B3LYP/6-31G(d) level of theory.

Electrochemical Measurements: The cyclic voltammetry measurements of investigated compounds were performed with a BAS electrochemical analyzer in deaerated acetonitrile containing nBu_4NPF_6 as a supporting electrolyte at 298 K (100 mV/s^{-1}). The glassy carbon working electrode was polished with BAS polishing alumina suspension and rinsed with acetone before use. The counter electrode was a platinum wire. The measured potentials were recorded with respect to $Ag/AgNO_3$ and normalized to Fc/Fc^{+}.

Photochemical Reactions: The photocleavage reactions were carried out in a quartz UV cell, which was irradiated with monochromatic excitation light through a monochromator (Ritsu MC-10N) from a 500 W xenon lamp (Ushio XB-50102AA-A), and monitored by an OCEAN

OPTICS HR-4000 high-resolution spectrometer system with light source DH-2000-BAL. A standard actionometer ($K_3[Fe(C_2O_4)_3]$) was used for quantum yield determination of the photochemical reactions of **5,14-PDK** and **6,13-PDK** in acetonitrile and toluene.[7] A square quartz cuvette (10 mm i.d.) that contained a deaerated solution (3.0 cm^3) of **5,14-PDK** and **6,13-PDK** was irradiated with monochromatized light (λ = 405 or 468nm) through a monochromator (Ritsu MC-10N) by using a 500 W xenon lamp (Ushio XB-50102AA-A). Under the actinometry experimental conditions, both **5,14-PDK** and **6,13-PDK** absorbed essentially all incident light. The photochemical reaction was monitored by using a JASCO UV/Vis/NIR V-570 spectrophotometer. The quantum yields were determined from the increase in absorbance due to pentacene (578 nm) at the beginning of the reaction.[8]

Photochemical Reactions in Films: Compound **5,14-DK** (10 mg) was dissolved in hot $CHCl_3$ (1 mL), and the solution (100 μL) was spin-coated on glass at 1000 rpm for 20 s. The absorption spectrum of **5,14-DK** in the film was measured. Then the film was irradiated with a 460 W metal halide lamp through a blue filter in a glove box for 90 min, and the absorption spectrum of pentacene was measured.

X-ray Analysis: Single crystals of **5,14-PDK** suitable for X-ray diffraction analysis were obtained by slow diffusion of heptane into a solution of **5,14-PDK** in CH_2Cl_2. The crystals were mounted in Litho Loops (purchased from Protein Wave). The diffraction data was collected at 25 °C with a Rigaku VariMaxRAPID/a imaging plate diffractometer with graphite-monochromated Cu-Kα radiation or with a Rigaku Mercury-8 diffractometer with graphite-monochromated Mo-Kα radiation equipped with a CCD detector. The diffraction data were processed with Crystal structure of the Rigaku program, solved with the SIR-97 program,[9] and refined with the SHELX-97 program.[10]

5,14-Dihydro-15,16-dihydroxy-5,14-ehtanopentacene (2-5)

A mixture of pentacene (1.00 g, 3.60mmon) and vinylene carbonate (0.310 g, 3.64 mmol) in xylenes (68 mL) was heated at 180 ºC in an autoclave for 3 days. After removal of the solvent in vacuo, the residue was washed with ethylacetate to give a mixture of **2-3** and **2-4** (1.29 g). The mixture of carbonate adducts was added to a 4 M aqueous solution of NaOH and 1,4-dioxane (40 mL). The resulting mixture was heated at reflux for 1 h. The reaction mixture was cooled, poured into water, and then extracted with ethylacetate. The combined organic layers were washed with water and dried with Na_2SO_4. After removal of the solvent in vacuo,

the residue was purified by column chromatography on silica gel with ethylacetate /$CHCl_3$ (1:4) to give **2-5** (0.260 g, 21%) as white solid and **2-6** (0.710 g, 58%). Melting Point 275–277 ºC. ^{1}H NMR (400 MHz, $CDCl_3$, TMS): δ = 8.33 (s, 2 H), 7.97–7.95 (m, 2 H), 7.89 (s, 2 H), 7.44–7.72 (m, 2 H), 7.25 (m, 2 H), 4.56 (br., 2 H), 4.23 (br., 2 H), 2.18 (br., 2 H, OH); ^{13}C NMR (100 MHz, $CDCl_3$, TMS): δ = 136.80, 127.88, 127.00, 126.54, 125.70, 125.11, 122.79, 68.81, 51.26; MS (FAB): m/z = 339 $[M + 1]^+$. $C_{24}H_{18}O_2$ (338.41): calcd. C 85.18, H 5.36; found C 85.22, H 5.30.

5,14-Dihydro-5,14-ethanopentacene-15,16-dione (**5,14-PDK**)

Trifluoroacetic anhydride (2.1 mL, 15.1 mmol) was added dropwise to a mixture of dry DMSO (1.0 mL, 14 mmol) and dry CH_2Cl_2 (10 mL) at −60 °C under argon. After stirring for 10 min, **2-3** (0.306 g, 0.905 mmol) dissolved in a mixture of dry DMSO (10 mL) and dry CH_2Cl_2 (7.0 mL) was added dropwise. After stirring for 90 min, *N,N*-diisopropylethylamine (4.5 mL, 26 mmol) was added dropwise to the reaction mixture. The solution was stirred at –60 °C for 60 min and warmed to room temperature. 3 M HCl was added to the mixture for quenching the reaction. The mixture was extracted with CH_2Cl_2, and the combined organic layers were washed with water and brine and dried with Na_2SO_4. After removal of the solvent in *vacuo*, the residue was purified by column chromatography on silica gel with CH_2Cl_2 and recrystallized from toluene to give **5,14-PDK** as yellow crystals (0.157 g, 52 %). Melting Point > 300 °C. ^{1}H NMR (400 MHz, $CDCl_3$, TMS): δ = 8.42 (s, 2 H), 8.07 (s, 2 H), 7.99–8.01 (m, 2 H), 7.48–7.52 (m, 4 H), 7.39–7.41 (m, 2 H), 5.19 (s, 2 H); ^{13}C NMR (75 MHz, $CDCl_3$, TMS): δ = 184.84, 134.90, 132.16, 131.21, 130.95, 129.60, 128.13, 126.50, 126.36, 126.03, 125.45, 60.46; MS (FAB): m/z = 336 $[M + 1]^+$. $C_{24}H_{14}O_2$ (334.37): calcd. C 86.21, H 4.22; found C 86.50, H 4.59.

2-9 References

(1) (a) Uno, H.; Yamashita, Y.; Kikuchi, M.; Watanabe, H.; Yamada, H.; Okujima, T.; Ogawa, T.; Ono, N. *Tetrahedron Lett.* **2005**, *46*, 1981–1983. (b) Yamada, H.; Yamashita, Y.; Kikuchi, M.; Watanabe, H.; Okujima, T.; Uno, H.; Ogawa, T.; Ohara, K.; Ono, N. *Chem. Eur. J.* **2005**, *11*, 6212–6220.

(2) (a) Chen, K.-Y.; Hsieh, H.-H.; Wu, C.-C.; Hwang, J.-J.; Chow, T. *Chem. Commun.* **2007**, 1065–1067. (b) Chuang, T.-H.; Hsieh, H.-H.; Chen, C.-K.; Wu, C.-C.; Lin, C.-C.; Chou, P.-T.; Chao, T.-H.; Chow, T. *Org. Lett.* **2008**, *10*, 2869–2873.

(3) CCDC-854777 (25 °C) contains the supplementary crystallographic data for this paper. These data can be obtained free of change from The Cambridge Crystallographic Data Centre via www.ccdc.cam.ac.uk/data_request/cif.

(4) (*a*) Backe, A. D.; *J. Chem. Phys.* **1993**, *98*, 5648–5652; (*b*) Lee, C.; Yang, W.; Parr, R. G. *Phys. Rev. B*, **1988**, *37*, 785–789. (c) Gaussian 09, Revision **D.01**, Frisch, M. J.; Trucks, G. W.; Schlegel, H. B.; Scuseria, G. E.; Robb, M. A.; Cheeseman, J. R.; Scalmani, G.; Barone, V.; Mennucci, B.; Petersson, G. A.; Nakatsuji, H.; Caricato, M.; Li, X.; Hratchian, H. P.; Izmaylov, A. F.; Bloino, J.; Zheng, G.; Sonnenberg, J. L.; Hada, M.; Ehara, M.; Toyota, K.; Fukuda, R.; Hasegawa, J.; Ishida, M.; Nakajima, T.; Honda, Y.; Kitao, O.; Nakai, H.; Vreven, T.; Montgomery, J. A., Jr.; Peralta, J. E.; Ogliaro, F.; Bearpark, M.; Heyd, J. J.; Brothers, E.; Kudin, K. N.; Staroverov, V. N.; Kobayashi, R.; Normand, J.; Raghavachari, K.; Rendell, A.; Burant, J. C.; Iyengar, S. S.; Tomasi, J.; Cossi, M.; Rega, N.; Millam, M. J.; Klene, M.; Knox, J. E.; Cross, J. B.; Bakken, V.; Adamo, C.; Jaramillo, J.; Gomperts, R.; Stratmann, R. E.; Yazyev, O.; Austin, A. J.; Cammi, R.; Pomelli, C.; Ochterski, J. W.; Martin, R. L.; Morokuma, K.; Zakrzewski, V. G.; Voth, G. A.; Salvador, P.; Dannenberg, J. J.; Dapprich, S.; Daniels, A. D.; Farkas, Ö.; Foresman, J. B.; Ortiz, J. V.; Cioslowski, J.; Fox, D. J. Gaussian, Inc., Wallingford CT, 2009. (b) Becke, A. D. *Phys. Rev. A* **1988**, *38*, 3098–3100; c) Becke, A. D. *J. Chem. Phys.* **1993**, *98*, 5648–5652; d) Lee, C.; Yang, W.; Parr, R. G. *Phys. Rev. B* **1988**, *37*, 785–789.

(5) Yamada, H.; Kuzuhara, D.; Ohkubo, K.; Takahashi, T.; Okujima, T.; Uno, H.; Ono, N.; Fukuzumi, S.; *J. Mater. Chem*. **2010**, *20*, 3011–3024.

(6) Fujitsuka, M; Ito, O.; Imahori, H.; Yamada, K.; Yamada H.; Sakata, Y. *Chem. Lett*., **1999**, *8*, 721–722.

(7) Hatchard, C. G.; Parker, C. A. *Proc. R. Soc. London, Ser. B* **1956**, *235*, 518–536.

(8) Perkampus, H.-H. in UV/Vis Atlas of Organic Compounds, 2nd ed., VCH, Weinheim, **1992**, 652.

(9) Altomare, A.; Burla, M. C.; Camalli, M.; Cascarano, G.; Giacovazzo, C.; Guagliardi, A.; Moliterni, A. G. G.; Polidori, G.; Spagna, R. *J. Appl. Crystallogr*. **1999**, *32*, 115–118.

(10) Sheldrick, G. M. *Acta Crystallogr., Sect. A* **2008**, *64*, 112–122.

Chapter 3

Synthesis of Solution Processable Organic Semiconducting Molecules for OPV Applications

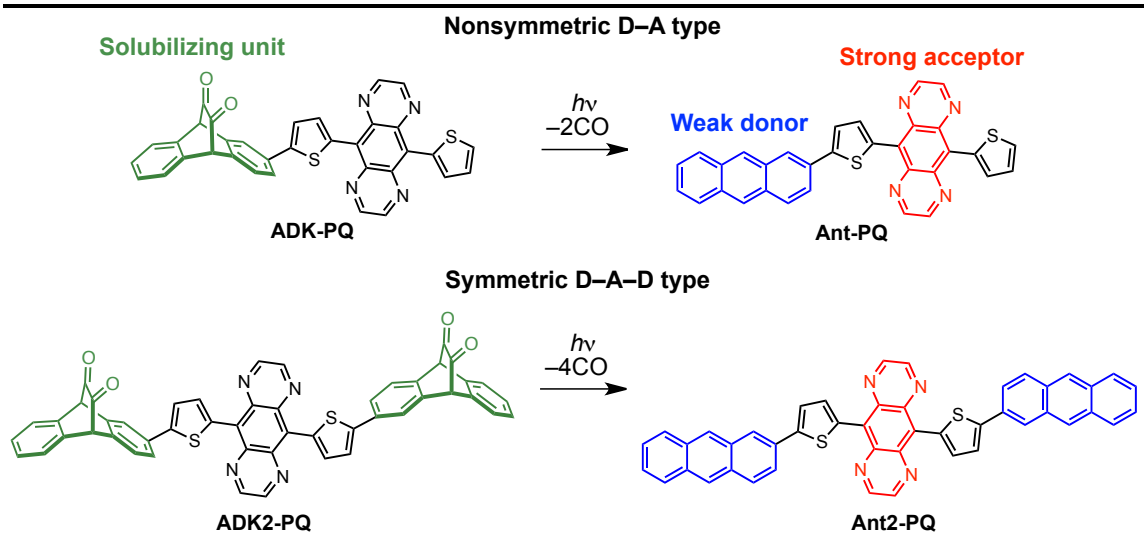

In this Chapter, the synthesis and optical properties of anthracene–pyridino[2,3-*g*]quinoxaline conjugates toward fabricating of organic photovoltaic cell is described.

3-1 Introduction

Organic thin film solar cell, which is one of the organic photovoltaic (OPV), has the attractive characteristics such as lightweight, flexible, and so on.[1] However, organic thin film solar cell has several problems which are low photoconversion efficiency (PCE) and low stability of organic materials. To solve the problems, many researchers have energetically studied organic thin film solar cell in more than 10 years.

The organic semiconducting materials classified into polymer and small molecule. Currently, the PCE of both materials increased to nearly 10%. To the best of the author's knowledge, the maximum PCE reported as an article is 10.31%, where the polymer material (**PTB7-Th**) was used as the p-type semiconductor in the bulk hetero junction film (Figure 3-1).[2] In addition to this example, close PCE of 10% based on polymer-materials have been many reported.[3]

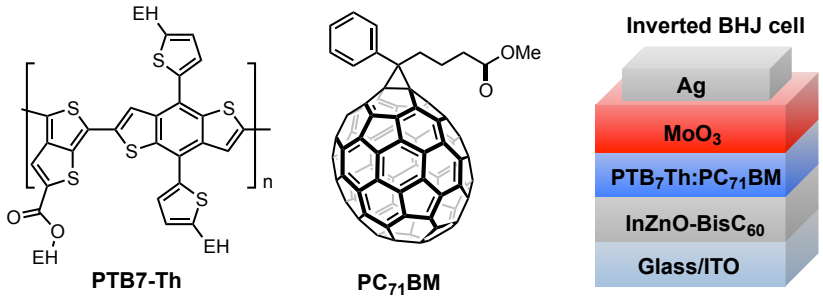

J_{SC}: 17.24 ± 0.05 mA cm^{-2} V_{OC}: 0.80 ± 0.005 V FF: 74.1 ± 0.4% PCE: 10.22 ± 0.09%

ITO/InZnO-BisC$_{60}$ (40 nm)/**PTB7-Th**:**PC$_{71}$BM** (1:1.5 w/w, 100nm)/MoO$_3$ (10 nm)/Ag (100 nm)

Figure 3-1. The example of polymer type OPV which exceeded 10% PCE.

In the case of small molecules, the highest PCE of 9.95 % (average: 9.60%) have been reported by Chen and co-workers in 2014 (Figure 3-2).[4] In the report, the p-type semiconductor based on dialkylthiol-substituted benzodithiophene (**DR3TSBDT**) was used with **PC$_{71}$BM** as n-type semiconductor. Heeger and co-workers have also reported the high PCE solar cell based on small molecules.[5] In the report, **p-DTS(FBTTh$_2$)$_2$** was used as p-type semiconductor, and the BHJ solar cell with **PC$_{71}$BM** shows PCE of 8.94%. Currently, as the trend of molecular design for p-type semiconductor, benzodithiophene (BDT)[6] unit and dithienosilole (DTS)[7] unit are often used. The calculated HOMO levels of BDT and DTS unit are −5.28 and −5.29 eV, respectively.[8] Even if the polymer, the equivalent HOMO level are often observed. The HOMO level of p-type semiconductor can be thus estimated and designed from the unit to form a

molecular structure. The HOMO level of anthracene is calculated as −5.23 eV, therefore, anthracene is also a candidate as the unit to show high V_{oc} in combination with $PC_{71}BM$.

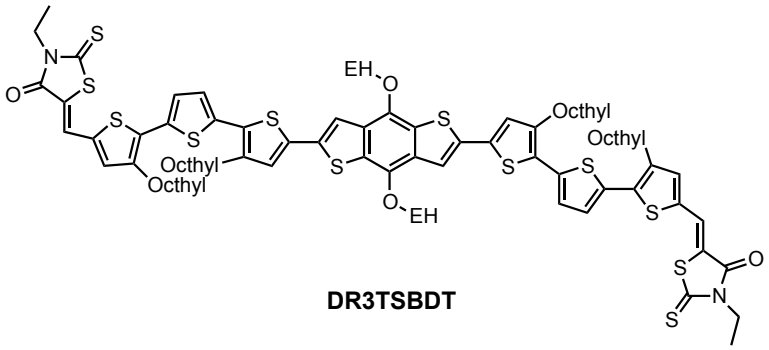

DR3TSBDT

J_{SC}: 14.45 ± 0.18 mA cm^{-2} V_{OC}: 0.91 ± 0.01 V FF: 73.1 ± 0.01% PCE: 9.60 ± 0.35%

ITO/PEDOT:PSS/**DR3TSBDT**:**$PC_{71}BM$**/ETL-1/Al

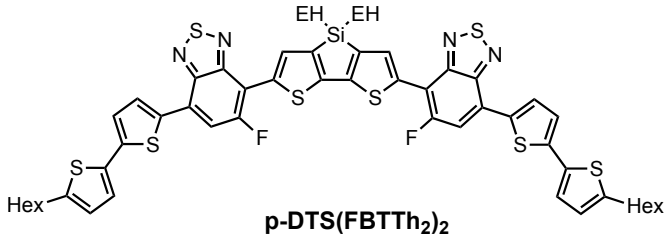

p-DTS(FBTTh$_2$)$_2$

J_{SC}: 15.5 mA cm^{-2} V_{OC}: 0.799 V FF: 72.4% PCE: 8.94%

ITO/PEDOT:PSS/**p-DTS(FBTTh$_2$)$_2$**:**$PC_{71}BM$**/ZnO/Al

Figure 3-2. The molecular structure and device structure of **DR3TSBDT** and **p-DTS(FBTTh$_2$)$_2$**.

As described in Chapter 1, photoprecursor method can be applied to fabricate multi layered organic thin film solar cell (p-n junction and p-i-n junction) by solution process. Recently, Nakayama, Yamada and co-workers have reported the hetero p-i-n junction structure as a new concept of multi layered organic thin film solar cell using photoprecursor method.[9] The organic thin film solar cell used the proper semiconducting materials depending on the role of each layer. The typical example is shown in Figure 3-3. The role of p-layer is to carry holes generated by charge separation at i-layer to electrode, therefore, good hole mobility is required for p-type semiconductor in player. As described in Chapter 1, 2,6-dithienylanthracene (**49**), which is prepared from the photoprecursor **47** on substrate, shows good hole mobility (FET: 4.7×10^{-2} cm^2/Vs) and capable of coating other layer by solution process because of the insolubility of **49**.[10] The most important role of i-layer is the generation of hole and electron by charge separation. However, **49** and n-type semiconductor (**$PC_{71}BM$** in this case) did not mixed well in the blend film since anthracene **49** has high crystallinity, therefore, low charge separation

efficiency is the problem on normal p-i-n device structure of **49** and $PC_{71}BM$. The advantage of photoprecursor method is easy modification of the structure of p-type organic semiconductor. To improve the compatibility to n-type semiconductor, photoprecursor **3-1** was synthesized and anthracene **3-2** was prepared from the photoprecursor on the film of **49** as p-layer. While ethylhexyl substituted anthracene **3-2** shows high compatibility to n-type material, the film is only sparingly soluble during the coating of n-layer. Since the HOMO levels of two p-type semiconductors are almost the same, the charge transferring has not been affected so much. In this way, the PCE was increased to 2.89 % on hetero p-i-n junction device structure. Furthermore, as described in above, the p-type semiconductors based on anthracene shows high V_{oc} (0.91 V).

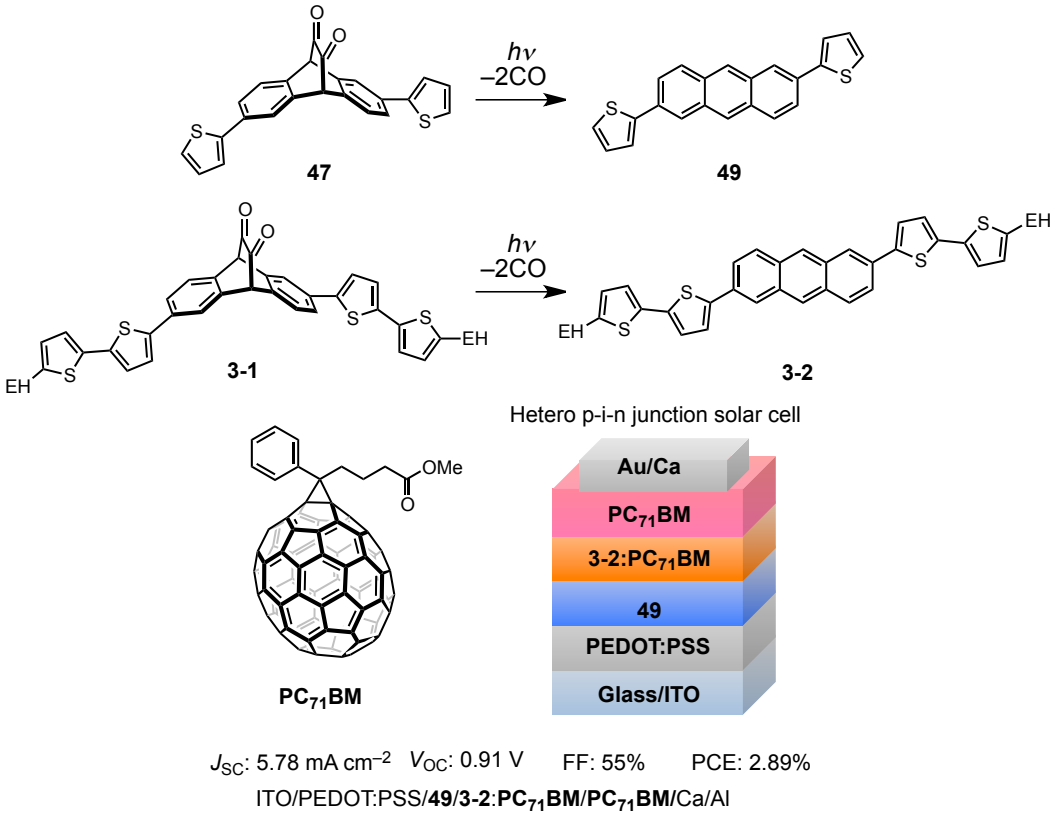

Figure 3-3. Hetero p-i-n junction solar cell based on α-diketone type photoprecursor method.

As the next stage, the improvement of light absorption characteristic in i-layer is required to further increase the PCE. Anthracene **3-2** shows the large absorption in visible area, but the absorption band covers by 500 nm. The absorptions of fullerene derivatives are spread to near IR area, but the absorbance is not so high. Therefore, the materials doesn't effectively absorb the light of over 500 nm, so the PCE will be improved by giving the absorption of long

wavelength area to the anthracene derivative.

To give the long wavelength absorption to anthracene, the author of this thesis selected intramolecular charge transfer (ICT) absorption. The ICT absorption is generated by the weak intramolecular interaction between electron donor and acceptor unit. In fact, the ICT absorption is applied to improve the absorption characteristics of OPV materials.[11] To apply the ICT absorption to the p-type semiconducting materials, the combination of donor and acceptor unit is necessary. From the viewpoint of controlling the solubility by photoconversion, donor unit is limited to anthracene or the derivatives. In addition, anthracene is a weak electron donor unit, so the ICT absorption will be generated by the combination with the electron acceptor.

Lin and co-workers have reported the article about the combinatorial design of the most suitable copolymer materials for bulk hetero junction solar cell.[12] The combination of 780 ways of typical electron donor and acceptor units were calculated and discussed in the article. The premises of the calculation are 65% filling factor (FF), 65% external quantum efficiency (EQE), and n-type semiconductor is $PC_{61}BM$ (LUMO level is –4.3 eV).[13] Additionally, the calculated PCE reflects experimentally proposed results such as the suitable energy gap of LUMO (donor)–LUMO ($PC_{61}BM$) is 0.3 eV, and the suitable HOMO–LUMO energy gap of donor material is 1.2–1.8 eV. The results of cancelation under those premises show pyridino[2,3-*g*]quinoxaline (PQ) is one of the best monomer. PQ is strong electron acceptor unit. In any combinations, the suitable LUMO (donor)-LUMO (**$PC_{61}BM$**) gaps (0.3–0.5 eV) and HOMO–LUMO gaps are calculated. As a result, the compound with PQ as a donor and anthracene as an acceptor was expected to have a potential to give high PCE have been indicated.

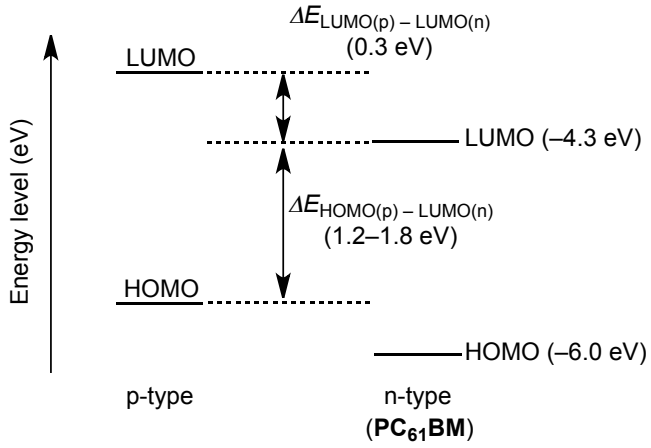

Figure 3-4. The ideal energy diagram with **$PC_{61}BM$** as n-type semiconductor.

Organic thin film solar cell materials including PQ unit have been reported already.[14–17] The molecular structure, device structure and the device performances are shown in Figure 3-5. Most of reported PQ materials are polymers (**3-3**[15], **3-4**[16] and **3-5**[17]), and the copolymer of PQ with indolocarbazole (**3-4**) was observed the highest value of PCE (3.24%). On the other hand, small molecular PQ derivative have been less reported, and the PCE is not so high (**3-6**, Maximum: 1.7%)[17]. However, the open-circuit voltage (V_{oc}) is shown 1.00 V, and the high V_{oc} of PQ derivative is a notable point. In addition, the low LOMO level shows the possibility that PQ derivatives can be used as an n-type semiconductor depending on the molecular design.

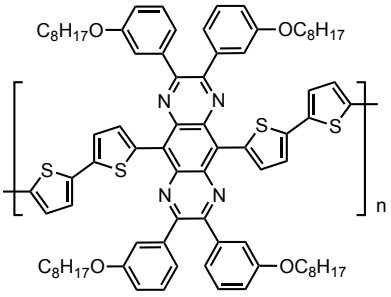

3-3

J_{SC}: 8.7 mA cm^{-2}
V_{OC}: 0.50 V
FF: 54%
PCE: 2.1%

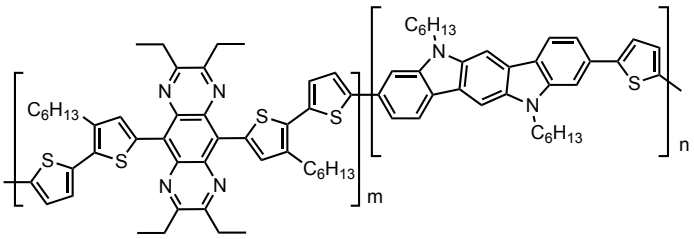

3-4

J_{SC}: 9.55 mA cm^{-2}
V_{OC}: 0.81 V
FF: 43%
PCE: 3.24%

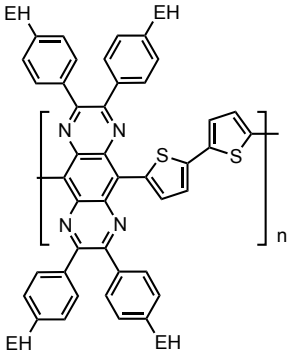

3-5

J_{SC}: 2.2 mA cm^{-2}
V_{OC}: 0.54 V
FF: 63%
PCE: 0.8%

Small molecule type

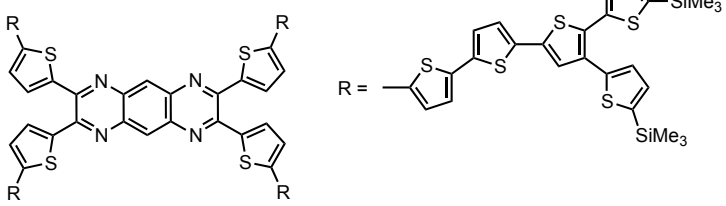

3-6

J_{SC}: 4.9 mA cm^{-2}
V_{OC}: 0.98 V
FF: 32%
PCE: 1.7%

Figure 3-5. The molecular structures and device performances of PQ derivatives with **$PC_{71}BM$**.

3-2 Molecular Design

In view of the above, anthracene–PQ conjugates were designed. The target materials are shown in Figure 3-6. In order to enable fabricate hetero p-i-n junction solar cell, **ADK** is used as a solubilizing unit. Beside, converted anthracene is weak electron donor, and anthracene will contribute to HOMO level of the conjugates. The LUMO levels significantly low by introducing PQ as an electron accepter unit, therefore, it is expected to be conjugate with the ideal energy levels. In this Chapter, the synthesis, thin film fabrication from photoprecursor and the optical properties are described.

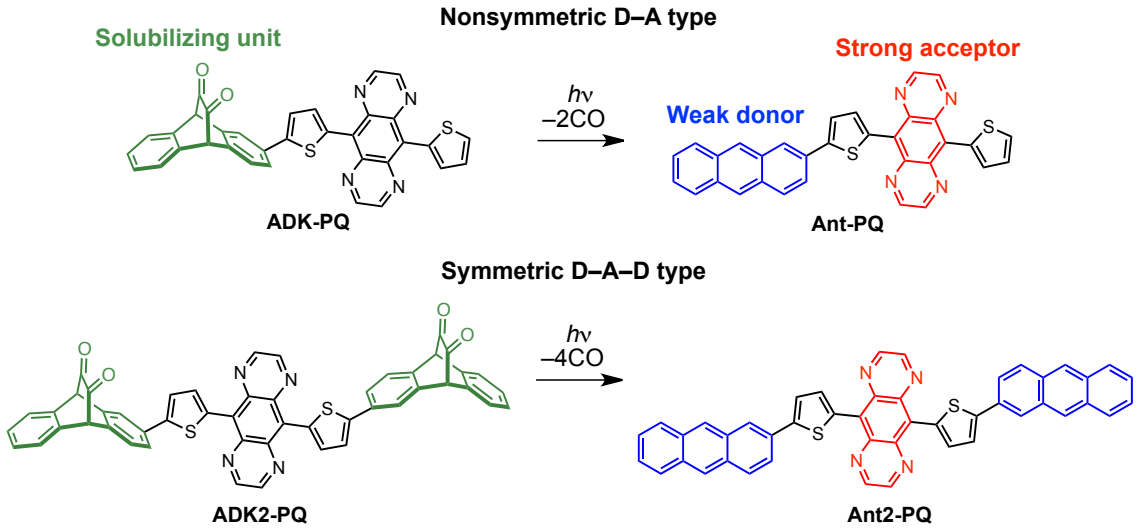

Figure 3-6. The molecular design and target compounds.

3-3 Synthesis

The synthesis of bromo adducts **3-9** and **3-10** is shown in Scheme 3-1. Dibromopyradinoquinoxaline (**3-7**) was prepared according to the literature.[18] Dibromo adduct **3-7** was reacted with 2-tributhystanylthiophene in a Stille coupling to give **3-8** in 38% yield. Bromo adducts **3-9** and **3-10** were synthesized by bromination with NBS in 45% and 48%, respectively.

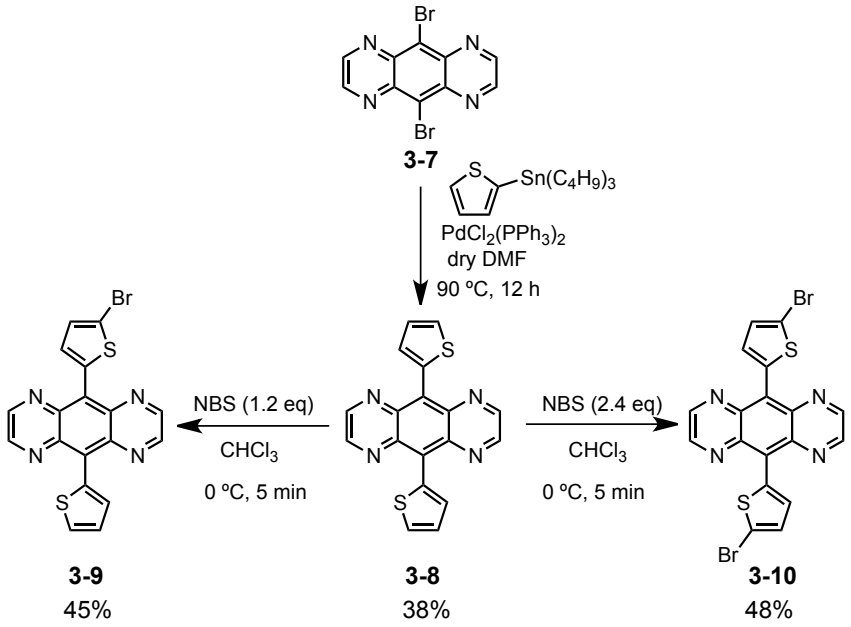

Scheme 3-1. Synthesis of brominated dithienylpyradinoquinoxalines (**3-9** and **3-10**).

Non-symmetric α-diketone precursor (**ADK-PQ**) was prepared as shown in Scheme 3-2. 2-Pinacolateboryl-anthracene **3-11** was reacted with vinylene carbonate in a Diels-Alder reaction to give adduct **3-12** in 70% yield as a mixture of stereoisomers. Compound **3-13** was synthesized with **3-9** in 72% yield in a Suzuki-Miyaura coupling reaction. Compound **3-13** was subsequently hydrolyzed to give diol **3-14** in 68% yield, which was oxidized by the Swern reaction to give **ADK-PQ** in 48% yield.

Symmetric precursor was also synthesized as shown in Scheme 3-3. Compound **3-15** was synthesized with **3-10** and **3-12** in 68% yield in a Suzuki-Miyaura coupling reaction. Compound **3-15** was hydrolyzed to give diol **3-16** in 71% yield, which was oxidized by the Swern reaction to give **ADK2-PQ** in 41% yield.

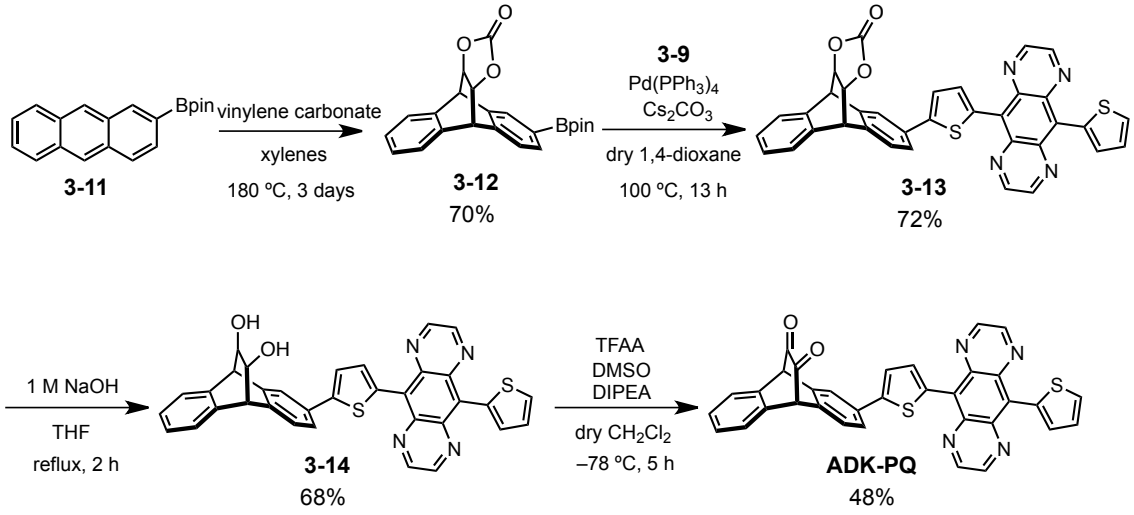

Scheme 3-2. The synthesis route of **ADK-PQ**.

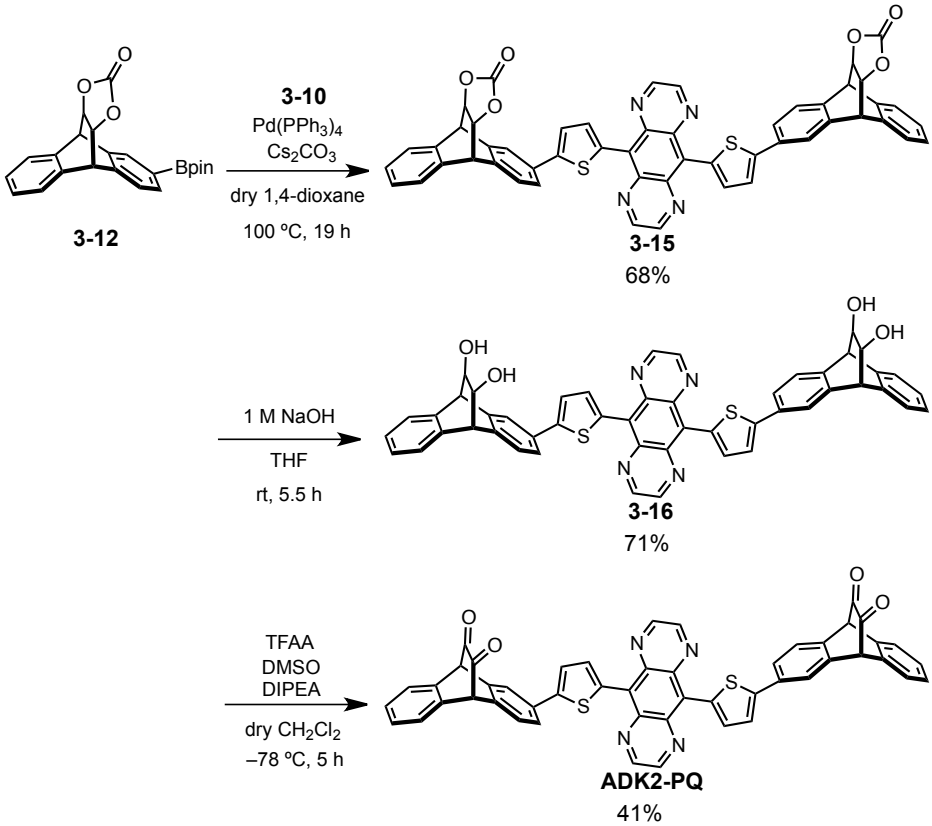

Scheme 5-3. The synthesis route of **ADK2-PQ**.

3-4 Photoconversion in Solution

The photoreaction of **ADK-PQ** was performed using a metal-halide lamp incorporating a UV-cutoff filter under an argon atmosphere. Figure 3-7 shows the changes in ^{1}H NMR spectra during the photoreaction of **ADK-PQ** in $CDCl_3$. The peaks at 5.09 and 5.05 ppm, assigned to H^a and H^b of bridge heads of diketone moiety, are seen to gradually decrease, while the peaks at 8.48 and 8.43 ppm, assigned to the peri position H^c and H^d of anthracene moiety of **Ant-PQ**, increase. After 180 min, the photoreaction was completely proceeds.

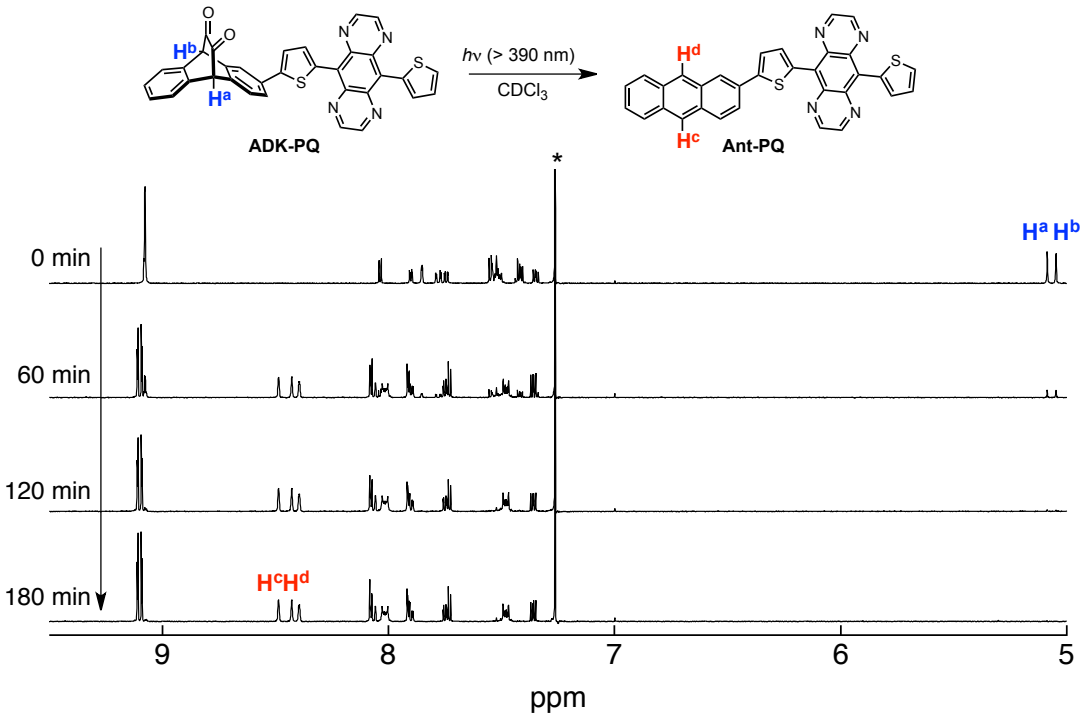

Figure 3-7. Changes in the ^{1}H NMR spectra of **ADK-PQ** during photolysis in $CDCl_3$ under an argon atmosphere. Spectra were acquired at 0, 60, 120 and 180 min. λ_{EX} > 390 nm. The solvent peak is indicated by *.

The same analysis was performed using **ADK2-PQ** in $CDCl_3$ (Figure 3-8). During the photoreaction, the peaks at 5.09 and 5.05 ppm decreased while those at 8.48 and 8.41 increased, indicating the formation of **Ant2-PQ**. Meanwhile the peaks of bridgeheads disappeared after 120 min, the peaks of generated **Ant2-PQ** also decreased because of the low solubility of **Ant2-PQ**.

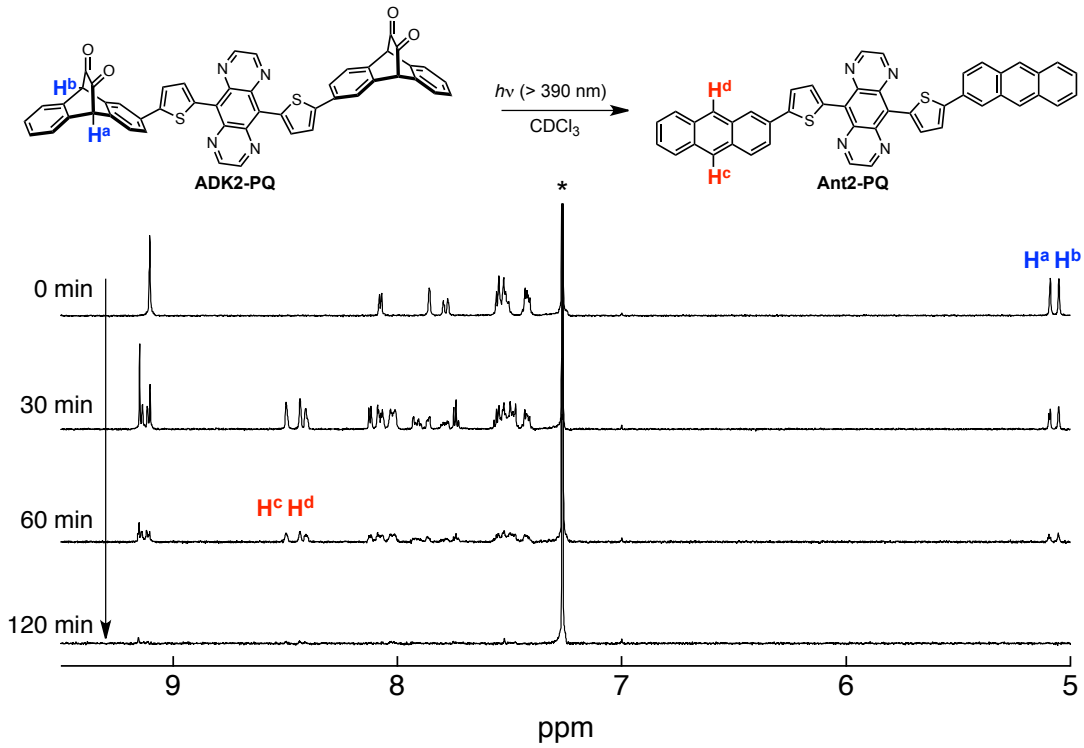

Figure 3-8. Changes in the ^{1}H NMR spectra of **ADK2-PQ** during photolysis in $CDCl_3$ under an argon atmosphere. Spectra were acquired at 0, 30, 60 and 120 min. λ_{EX} > 390 nm. The solvent peak is indicated by *.

3-5 Photoconversion on Film

The progress of photoconversion reaction within films was monitored by UV-vis and IR absorption spectra. The film of **ADK-PQ** was prepared by spin-casting (800 rpm, 30 s) the solution of $CHCl_3$ (200 μl, 10 mg/mL) on glass for UV-vis and ITO for IR absorption spectrum (Figure 3-9). **ADK-PQ** shows broad absorption spectrum, and the peak top is 576 nm. After photoconversion, the peak top of **Ant-PQ** is clearly red-shifted to 613 nm, and the end absorption is 772 nm. Furthermore, the evidence of full conversion from precursor to anthracene moiety was observed by change the IR absorption spectra. Before photoconversion, the peaks of C=O stretching are observed at 1734 and 1750 cm^{-1}. On the other hand, the peaks disappeared after photoconversion.

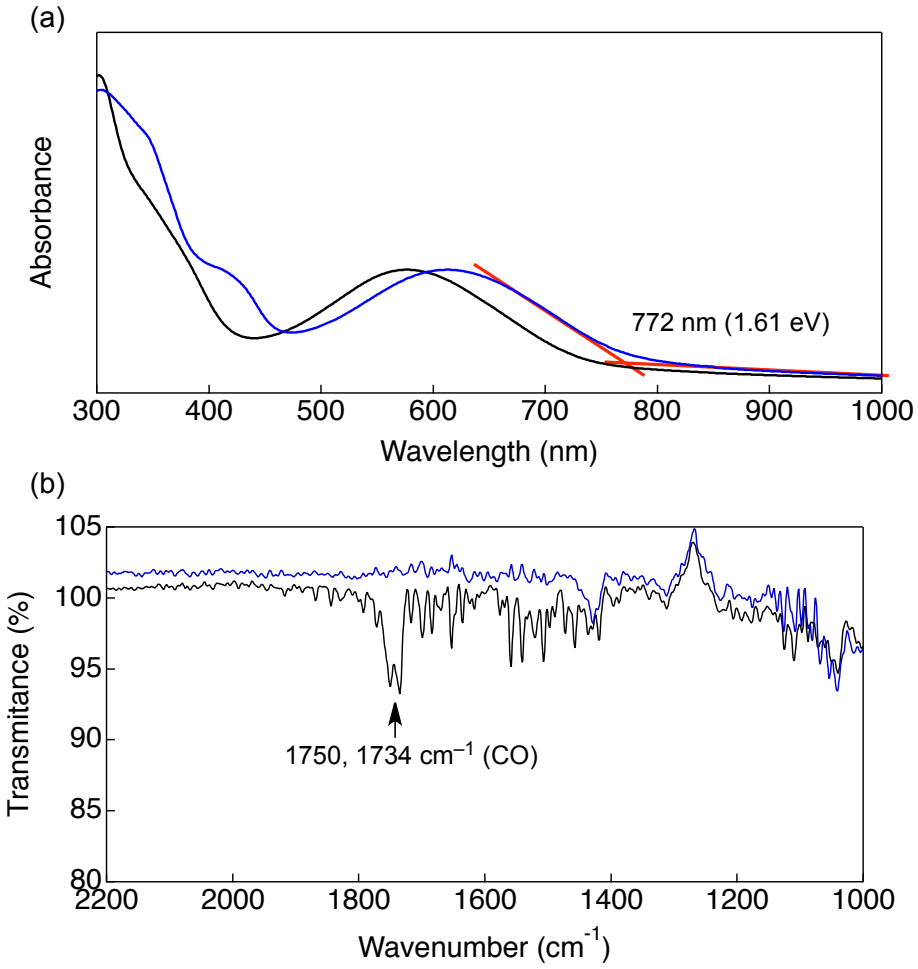

Figure 3-9. Changes of (a) UV-vis absorption spectra and (b) IR absorption spectra. Black line (**ADK-PQ**) and Blue line (**Ant-PQ**), respectively.

The film of **ADK2-PQ** was also prepared by spin casting (800 rpm, 30 s). Since the solubility of **ADK2-PQ** is poor, 10 mg is not soluble in 1 mL of THF or $CHCl_3$. Therefore, the saturated solution was used for preparing the film. **ADK2-PQ** also shows broad absorption spectrum on film, and the peak top is 633 nm. After photoconversion, the peak top is slightly red-shifted to 648 nm and the spectrum spreads to 844 nm. Although not clear change because of low concentration, the disappearance of peaks (1744 and 1753 cm^{-1}) after conversion were checked by IR absorption measurement.

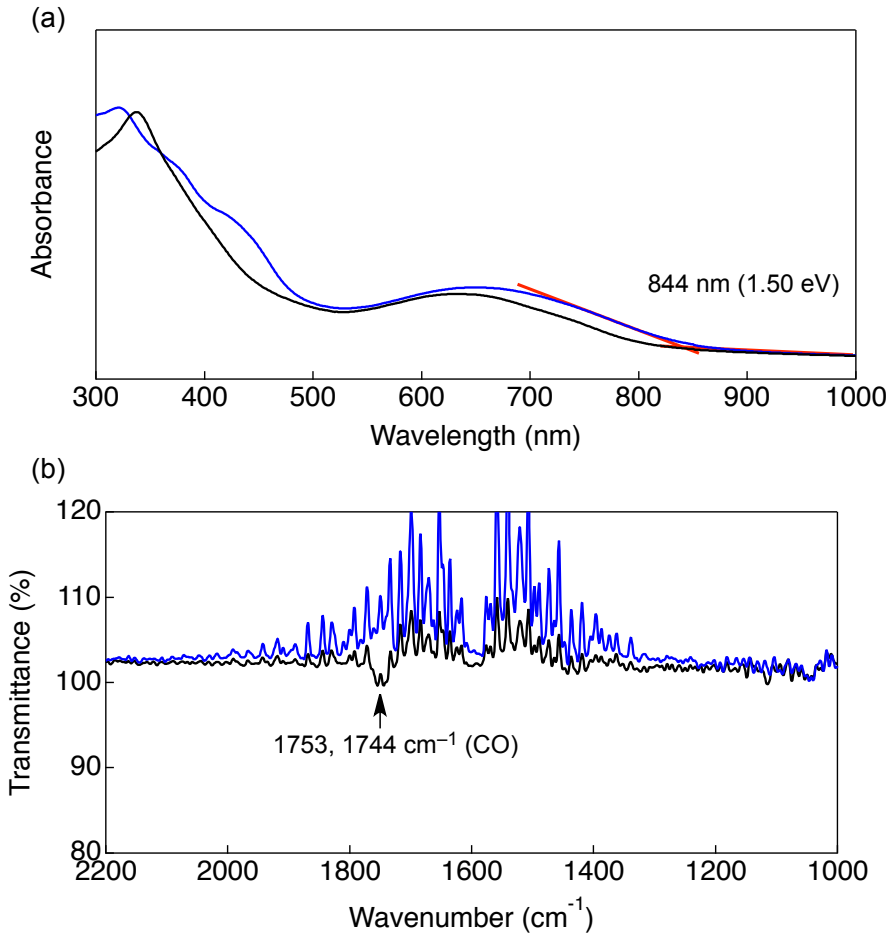

Figure 3-10. Changes of (a) UV-vis absorption spectra and (b) IR absorption spectra. Black line (**ADK2-PQ**) and Blue line (**Ant2-PQ**).

3-6 Computational Calculations

Molecular orbitals (MO) calculation and time-dependent density functional theory (TDDFT) of **Ant-PQ** was performed using the Gaussian 09 program package at the CAM-B3LYP/6-31G(d)//B3LYP/6-31G(d) level.[19] TDDFT calculation indicated the strong strength transition at 573 nm that was composed of the transition from HOMO or HOMO−1 to LUMO. The MOs suggests the broad absorption around 600 nm derive from intramolecular charge transfer (ICT) absorption. **Ant2-PQ** was also calculated at the CAM-B3LYP/6-31G(d)//B3LYP/6-31G(d) level. The result is shown in Figure 3-12. Similar to **Ant-PQ**, ICT transitions from HOMO or HOMO−1 to LUMO are suggested the calculation. The calculated transition energy is 2.0014 eV (619 nm) and agrees the UV-vis absorption spectrum of **Ant2-PQ**.

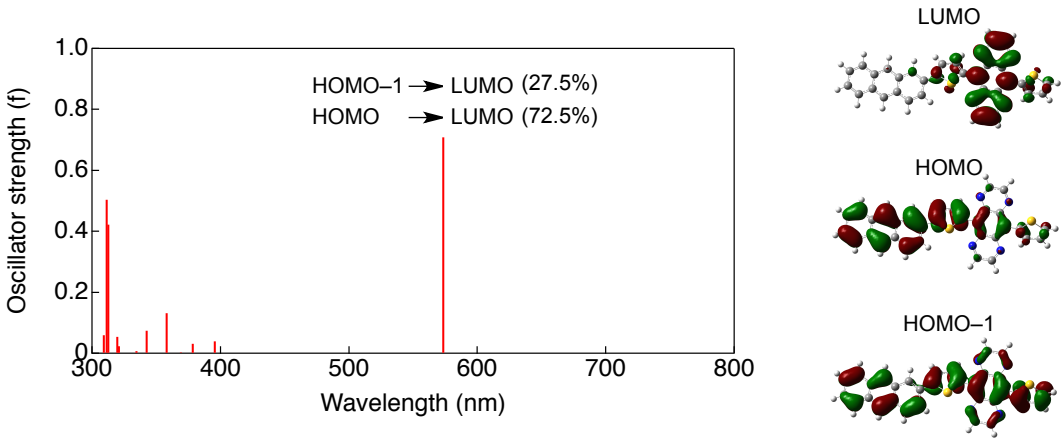

Figure 3-11. MOs and TDDFT calculation of **Ant-PQ** at the CAM-B3LYP/6-31G(d) //B3LYP/6-31G(d) level.

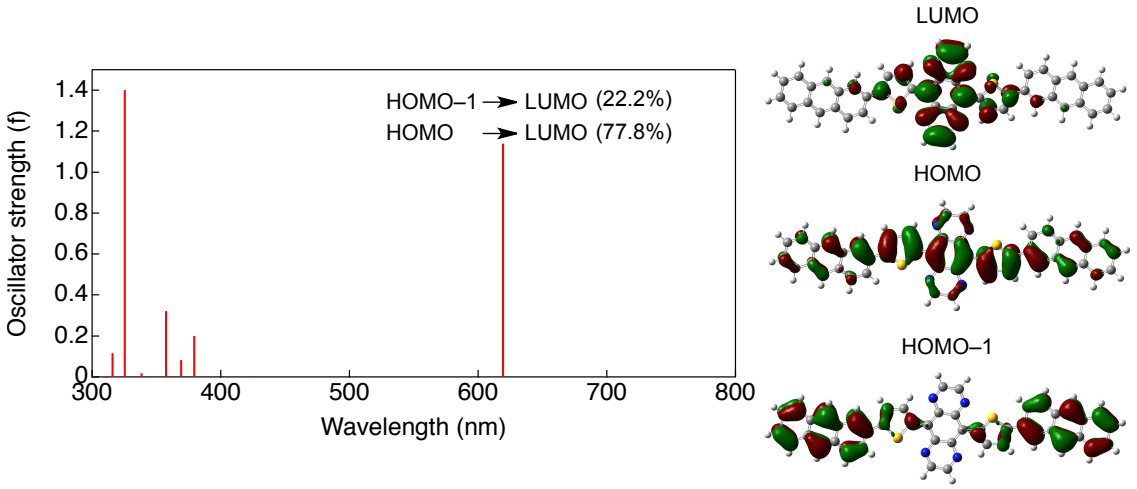

Figure 3-12. MOs and TDDFT calculation of **Ant2-PQ** at the CAM-B3LYP/6-31G(d)//B3LYP/6-31G(d) level.

3-7 Ionization Energy in Film

Ionization energies for the **Ant-PQ** and **Ant2-PQ** in thin film were measured by photo-electron spectroscopy in air. The ionization energy of **Ant-PQ** and **Ant2-PQ** was observed −5.43 and −5.39 eV, respectively. Since the energies are almost the same as the energy of 2,6-dithienyl anthracene **49** (−5.34 eV), the PQ derivatives can be applied to hetero p-i-n junction structure as p-type semiconductor materials for i-layer. In addition, the calculated LUMO energies by optical energy band gap are −3.82 (**Ant-PQ**) and −3.89 eV (**Ant2-PQ**), respectively. As described in introduction, the ideal LUMO level of p-type material is −3.8 ~ −4.0. From these results, it is suggested that anthracene–PQ conjugates has the suitable energy levels.

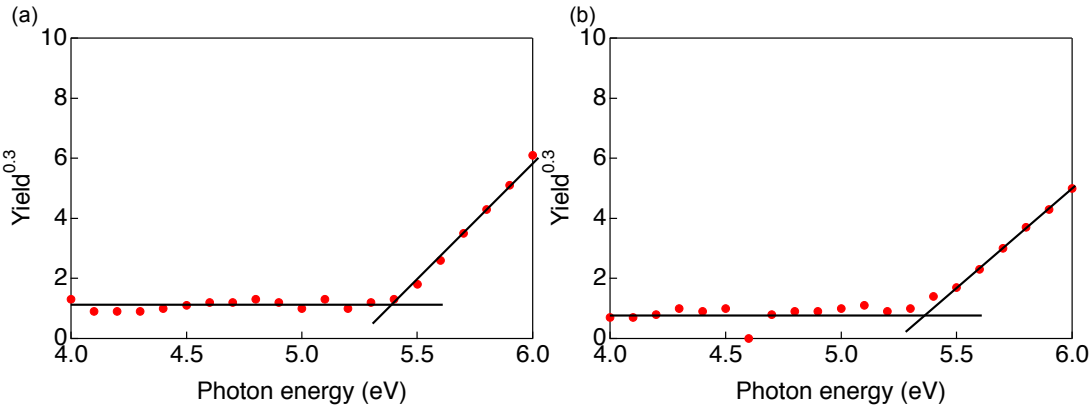

Figure 3-13. Ionization energy of a) **Ant-PQ** and b) **Ant2-PQ** on ITO substrate.

3-8 OPV Fabrication

In order to confirm the OPV performances, solution-processed BHJ devices based on **Ant-PQ** and **$PC_{71}BM$** were fabricated. The results are shown in Figure 3-14 and Table 3-1. After spin-coating of PEDOT:PSS on ITO, solution of a mixture of **ADK-PQ** and **$PC_{71}BM$** in $CHCl_3$ was spin-coated at 800 rpm for 30 s. **ADK-PQ** was converted to **Ant-PQ** with photoirradiation by blue LED at rt for 30 min. Then, Ca (10 nm) and Al (80 nm) were deposited. The device structure described as [ITO/PEDOT:PSS (30 nm)/**Ant-PQ**:**$PC_{71}BM$** x:y (10 mg/mL)/Ca (10 nm)/Al (80 nm)]. In four different conditions of mixing ratio, the best PCE of 0.24% is observed in ratio of 1:3 (J_{sc} = 1.82 mA cm^{-2}; V_{oc} = 0.56 V; FF = 24.1 %). The

maximum IPCE is about 10%, so these values are lower than the expected values. The performance improvement of the device is prospective of FF can be improved, but there may be problems that must be solved fundamentally. The first is protonation at PQ moiety by PEDOT:PSS. PSS is strongly acidic, therefore, the nitrogen atom in PQ moiety might be protonated. The second is close LUMO levels of p-type and n-type semiconductors. As described in introduction, the LUMO levels of the target molecules were designed so that the energy gap between the LUMO levels of the target compound and $PC_{61}BM$ is 0.3. But, the LUMO levels of target compound were lower than the expected level, so the charge separation probably didn't effectively occur. The OPV device of **Ant2-PQ** wasn't fabricated since **ADK2-PQ** doesn't have sufficient solubility for device fabrication.

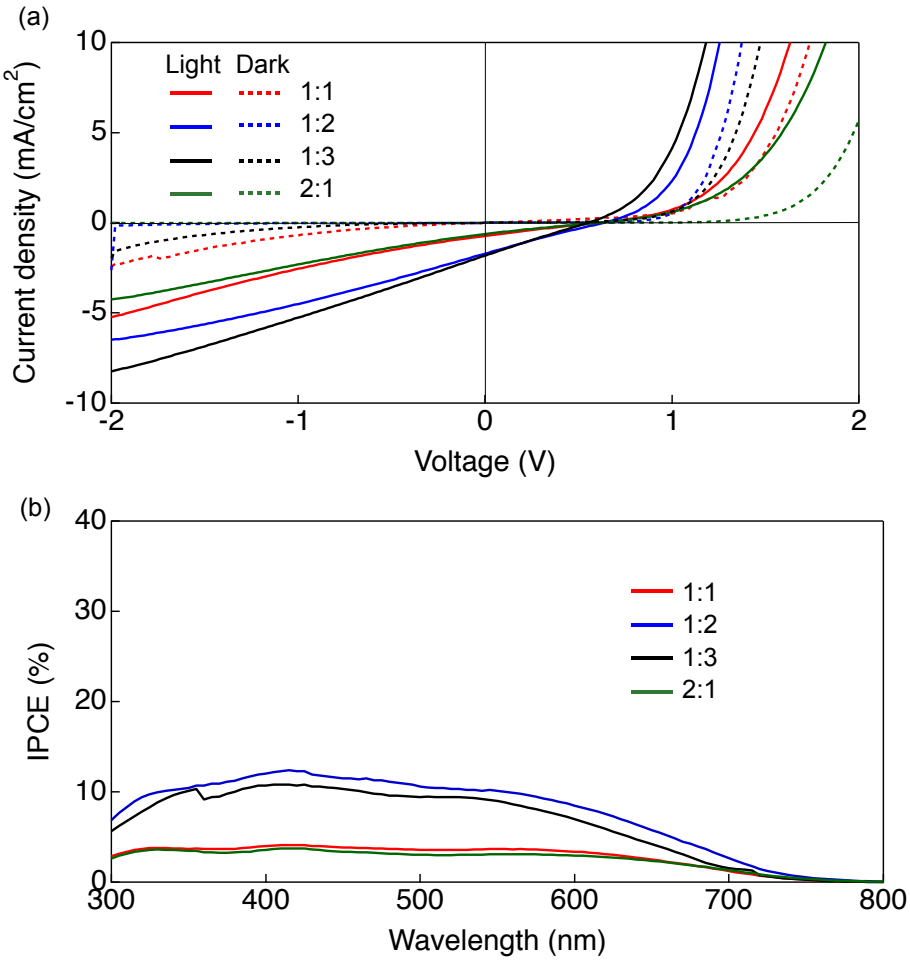

Figure 3-14. (a) *I-V* curves of **Ant-PQ**:**$PC_{71}BM$** devices; (b) IPCE spectra of **Ant-PQ**:**$PC_{71}BM$** devises.

Table 3-1. Performances of BHJ type OPV devices.

x:y	J_{sc} (mA/cm^2)	V_{oc} (V)	FF (%)	PCE (%)	R_S (Ω cm^2)	R_P (Ω cm^2)
1:1	0.72	0.61	23.4	0.10	890	742
1:2	1.75	0.56	23.9	0.24	334	306
1:3	1.82	0.56	24.1	0.24	289	286
2:1	0.63	0.61	22.6	0.09	1048	788

3-9 Summary and Outlooks

In order to increase PCE of multilayered OPV devices, pyridino[2,3-*g*]quinoxaline-anthracene conjugates (**Ant-PQ** and **Ant2-PQ**) were designed based on the ideal energy level of i-layer materials. The synthesis was tried by photoprecursor approach to control the solubility toward preparing the multilayer structure. The reasonable synthetic route of photoprecursor (**ADK-PQ** and **ADK2-PQ**) was established, additionally, the quantitative photoconversions were confirmed by ^{1}H NMR, IR and UV-vis absorption measurements. The HOMO levels of converted structures were sufficient to observe high V_{oc}, and the calculated LUMO levels by optical band gaps were nearly ideal energy level for the LUMO level of $PC_{61}BM$. However, BHJ type OPV using **Ant-PQ** didn't show the expected PCE. The problems such as protonation by PSS and low LUMO level of **Ant-PQ** are considered to be the reason of low efficiency. It seems possible to improve PCE by the modification of the device structure and the molecule structure. The OPV device of **Ant2-PQ** couldn't be fabricated since the solubility of **ADK2-PQ** wasn't enough to be spin-coated. It is future necessary to design and synthesize the molecule structure that can improve the solubility of precursor.

3-10 Experimental Section

Synthesis Commercially available reagents and solvents for syntheses were of reagent grade and used without further purification. TLC and gravity column chromatography were performed on Art. 5554 (Merck KGaA) plates and silica gel 60N (Kanto Chemical), respectively. For spectral measurements, spectral-grade toluene, dichloromethane, methanol and acetonitrile were purchased from Nacalai Tesque. The dichloromethane used for cyclic voltammetry measurements was distilled from CaH_2.

5,10-Di(thiophene-2-yl)pyridino[2,3-*g*]quinoxaline (3-8): In 100 mL 2necks flask, **3-7** (1.252 g, 3.68 mmol), 2-tributhyltin-thiophene (4.16 g, 11.1 mmol), $PdCl_2(PPh_3)_2$ (141 mg) and dry DMF (30 mL) were contained. The mixture was bubbled with Ar gas for 20 min. The mixture was heated at 90 ºC for 12.5 h. After cooling to rt, the compound was dissolved in $CHCl_3$, and filtrated through celite. The organic phase was washed with water and brine. The organic layer was dried over Na_2SO_4 and removed under reduced pressure. The residue was dissolved in small amount of $CHCl_3$ and poured into MeOH. The solvent was decreased under vacuum, the precipitation was filtrated and washed with MeOH. The crude product was purified with silica gel column ($CHCl_3$:ethylacetate = 98:2) and washed with MeOH to give **3-8** dark red powder (488 mg, 38%).^{1}H NMR (400 MHz, $CDCl_3$, TMS): δ = 9.05 (s, 4H), 7.76 (dd, 2H, *J* = 1, 4 Hz), 7.34 (dd, 2H, *J* = 4, 8 Hz); ^{13}C NMR (100 MHz, $CDCl_3$, TMS): δ = 145.69, 139.20, 133.77, 133.21, 132.14, 129.70, 126.67; MS (EI): m/z = 346 $[M]^+$. HR-EI *m/z* = 346.0331 calcd. for $C_{18}H_{10}N_4S_2$ = 346.0347 $[M]^+$

5-(5-Bromothiophene-2-yl)-10-(thiophene-2-yl)pyridino[2,3-*g*]quinoxaline (3-9): **3-8** (487 mg, 1.41 mmol) was dissolved in $CHCl_3$ (240 mL) and heated at 60 ºC for 20 min to dissolve completely. After cooling to 0 ºC, NBS (299 mg, 1.68 mmol) was slowly added to the solution. The solution was stirred for 5 min and quenched with $NaHCO_3$aq. The organic layer was washed with water, brine and dried over Na_2SO_4. The organic solvent was removed under reduced pressure. The crude product was purified with adsorbed silica gel column chromatograph ($CHCl_3$) and filtrated with MeOH to give **3-9** as purple powder.^{1}H NMR (400 MHz, CD_2Cl_2, TMS): δ = 9.04 (s, 4H), 8.06 (d, 1H, *J* = 4 Hz), 7.84 (dd, 1H, *J* = 1, 4 Hz), 7.72 (dd, 1H, *J* = 1, 4 Hz), 7.30 (dd, 1H, *J* = 1, 4 Hz), 7.27 (d, 1H, *J* = 4 Hz); ^{13}C NMR (100 MHz, CD_2Cl_2, TMS): δ =146.14, 145.71, 139.48, 138.78, 136.24, 134.75, 134.38, 133.65,

132.19, 130.49, 129.83, 129.62, 126.75, 118.34; MS (EI): m/z = 423, 425 [M, isotope peaks]$^+$. HR-EI *m/z* = 423.9503 calcd for $C_{18}H_9N_4{}^{79}B_rS_2$ = 423.9452 $[M]^+$

5,10-Di(5-bromothiophene-2-yl)pyridino[2,3-*g*]quinoxaline (3-10): In 500 mL flask, **3-8** (393 mg, 1.13 mmol) was dissolved in $CHCl_3$ (192 mL). NBS (473 mg, 2.66 mmol) was added to the solution at 0 ºC. After stirring for 20 min, the organic layer was washed with water and brine. The organic layer was dried over Na_2SO_4 and removed solvent under reduced pressure. The crude product was purified with silica gel column chromatography ($CHCl_3$), to give **3-10** as red solid (0.271 g, 48%). ^{1}H NMR (400 MHz, CD_2Cl_2, TMS): δ = 9.06 (s, 4H), 8.11 (d, 2H, *J* = 4 Hz), 7.27 (d, 2H, *J* = 4 Hz); ^{13}C NMR (100 MHz, CD_2Cl_2, TMS): The spectrum wasn't measured because of insolubility.; MS (EI): m/z = 501, 503, 505 [M, isotope peaks]$^+$. HR-EI *m/z* = 501.8544 calcd for $C_{18}H_8N_4{}^{79}Br_2S_2$ = 501.8577 $[M]^+$

2-Pinacolateboryl-9,10-dihydro-9,10-ethanoanthracene-*cis*-11,12-diyl carbonate (3-12): A solution of **3-11** (2.01 g, 6.63 mmol) and vinylene carbonate (5.0 mL) in xylenes (35 mL) was mixed at 180 ºC in an autoclave for 3 days. After removal of the solvent in vacuo, the residue was purified by silica gel column chromatography ($CHCl_3$:ethylacetate = 99:1,) and recrystallization from MeOH to give **3-12** as white powder (1.017 g, 70%).
^{1}H NMR (400 MHz, $CDCl_3$, TMS): δ =7.82 (s, 1H), 7.71 (dd, 1H, *J* = 1, 8 Hz), 7.39 (d, *J* = 8 Hz), 7.38–7.32 (m, 3H), 7.22–7.19 (m, 2H); ^{13}C NMR (100 MHz, $CDCl_3$, TMS, Picked up only major peaks because of the mixture of stereoisomers): δ = 154.01, 140.78, 137.03, 136.20, 135.86, 134.41, 131.63, 127.69, 127.60, 126.60, 126.51, 125.05, 84.02, 76.20, 76.11, 47.86, 47.57, 24.81, 24.76; MS (ESI): m/z = 413 $[M + Na]^+$. HR-ESI *m/z* = 413.15401 calcd for $C_{23}H_{23}BNaO_5$ = 413.15362 $[M + Na]^+$

Carbonate adduct (3-13): In 50 mL Schlenck flask, **3-12** (284 mg, 0.728 mmol), **3-9** (245 mg, 0.576 mmol), Cs_2CO_3 (679 mg, 2.08 mmol), dry 1,4-dioxane (20 mL) were contained. The solution was bubbled with Ar gas for 30 min. $Pd(PPh_3)_4$ (30 mg, 2.08 mmol) was added to the solution. The reaction was refluxed for 13 h. After cooling, the solution was poured into water. The product was extracted with $CHCl_3$ and filtrated through celite. The filtration was washed with water, brine and dried over Na_2SO_4. The organic solvent was removed under reduced pressure. The crude product was purified with silica gel column chromatograph ($CHCl_3$) and recrystallized from $CHCl_3$-MeOH to obtain purple solid. (251 mg, 72%) ^{1}H NMR (400 MHz,

CD_2Cl_2, TMS): δ = 9.04–9.02 (m, 4H), 8.03–8.00 (m, 1H), 7.84–7.82 (m, 2H), 7.72–7.64 (m, 2H), 7.53–7.43 (m, 4H), 7.33–7.27 (m, 3H), 4.98–4.95 (m, 2H), 4.82–4.78 (2H, m); ^{13}C NMR (100 MHz, CD_2Cl_2, TMS, Because of isomers are mixed approximately 20 %, large amount of the peak is obtained.): δ = 154.39, 148.10, 147.75, 146.15, 146.12, 145.85, 145.80, 139.59, 139.16, 139.02, 137.99, 137.96, 137.93, 137.53, 136.86, 136.62, 135.40, 134.57, 134.47, 134.24, 134.12, 133.57, 133.47, 131.84, 131.78, 131.59, 129.61, 128.24, 128.20, 128.00, 127.96, 127.37, 126.94, 126.88, 126.72, 126.57, 126.09, 126.02, 125.49, 125.23, 124.30, 123.47, 123.44, 123.33, 76.67, 76.62, 48.12, 47.79, 47.76; MS (Spiral TOF): m/z = 608 $[M]^+$. HR- Spiral TOF *m/z* = 608.09839 calcd for $C_{35}H_{20}N_4O_3S_2$ = 608.09713 $[M]^+$

Diol adduct (3-14): In 2 necks flask (100 mL), **3-13** (220 mg, 0.361 mmol) was dissolved in THF (32 mL). 1 M NaOH (20 mL) was added to the solution. The mixture was refluxed for 2 h. After cooling, the product was extracted with $CHCl_3$ and washed with water, brine and dried over Na_2SO_4. The organic solvent was removed under reduced pressure. The crude product was purified with silica gel column chromatograph ($CHCl_3$→$CHCl_3$:ethylacetate = 85:15) and filtrated with MeOH to obtain **3-14** as purple solid. (143 mg, 68%). ^{1}H NMR (400 MHz, DMSO-d6, TMS, Because of isomers are mixed, the major peaks were picked up.): δ = 9.17–9.16 (m, 4H), 8.09–8.00 (d, 1H, *J* = 4 Hz), 7.92–7.62 (m, 2H), 7.63 (d, 1H, *J* = 4 Hz), 7.55 (m, 1H, *J* = 1, 8 Hz), 7.45 (d, 1H, *J* = 8 Hz), 7.35–7.29 (m, 3H), 7.16–7.13 (m, 2H), 4.71 (m, 2H), 4.49 (d, 1H, *J* = 4 Hz), 4.42 (d, 1H, *J* = 4 Hz), 3.98–3.91 (m, 2H, -OH); ^{13}C NMR (100 MHz, DMSO-d6, TMS): δ = 147.51, 146.47, 146.16, 141.86, 140.66, 139.57, 138.10, 137.72, 135.52, 133.52, 133.43, 132.78, 131.91, 130.30, 130.07, 129.94, 126.30, 126.11, 126.03, 125.59, 125.55, 125.28, 123.35, 122.85, 121.68, 66.79, 51.04, 50.82; MS (Spiral TOF): m/z = 522 $[M–60 (–C_2H_4O_2)]^+$, 582 $[M]^+$. HR- Spiral TOF *m/z* = 582.11770 calcd for $C_{34}H_{22}N_4O_2S_2$ = 582.11787 $[M]^+$

ADK-PQ: In 100 mL flask, dry CH_2Cl_2 (13 mL) and dry DMSO (1.6 mL) was mixed under an argon atmosphere. The solution was cooled to −78 ºC. TFAA (0.7 mL, 5.0 mmol) was slowly added to the solution for 10 min. After stirring for 30 min, **3-14** (203 mg, 0.348 mmol) in dry CH_2Cl_2 (5 mL) and dry-DMSO (4 mL) was slowly added to the solution over 15 min. The solution was stirred for 2 h at −78 ºC and DIPEA (3.2 mL) was added. After stirring for 2 h, the solution was warmed to rt. The reaction was quenched with water and extracted with CH_2Cl_2. The organic layer was washed with 1 M HCl, water and brine, and dried over Na_2SO_4. The

organic solvent was removed under reduced pressure. The product was purified to reprecipitate from CH_2Cl_2-hexane and silica gel column chromatograph (CH_2Cl_2:ethylacetate = 98:2). The product was recrystallized from $CHCl_3$ (amylene added)-hexane to give purple solid. (97 mg, 48%) ^{1}H NMR (400 MHz, $CDCl_3$, TMS): δ = 9.08 (s, 4H, overlapped two singlet peaks), 8.04 (d, 1H, *J* = 4 Hz), 7.90 (d, 1H, *J* = 4 Hz), 7.85 (d, 1H, *J* = 1 Hz), 7.78 (dd, 1H, *J* = 1, 12 Hz), 7.75 (d, 1H, J = 4 Hz), 7.55–7.50 (m, 4H), 7.44–7.41 (m, 2H), 7.35 (m, 1H), 5.09 (s, 1H), 5.05 (s, 1H); ^{13}C NMR (100 MHz, $CDCl_3$, TMS): δ = 183.69, 183.38, 147.11, 145.69, 145.41, 139.20, 138.84, 136.05, 135.62, 135.11, 134.71, 134.67, 134.41, 133.84, 133.72, 133.38, 131.97, 131.19, 129.53, 129.56, 129.53, 127.07, 126.89, 126.68, 126.44, 126.37, 123.77, 123.59, 60.02, 59.71; MS (ESI): *m/z* = 601 $[M + Na]^+$. HR-ESI *m/z* = 601.07656 calcd for $C_{34}H_{18}N_4NaO_2S_2$ = 601.07689 $[M + Na]^+$

Carbonate adduct (3-15): In 100 mL 2necks flask, **3-10** (212 mg, 0.42 mmol), **3-12** (414 mg, 1.06 mmol) and Cs_2CO_3 (931 mg, 2.86 mmol) were dissolved with dry 1,4-dioxane (30 mL). The solution was degassed with Ar bubbling for 40 min. $Pd(PPh_3)_4$ (55 mg, 0.048 mmol) was added to the solution. The reaction mixture was warmed at 100 ºC for 19 h. After cooling, CH_2Cl_2 was added to the solution, and the organic layer was washed with water and brine. The organic layer was dried over Na_2SO_4 and removed solvent under reduced pressure. The crude product was purified with silica gel column chromatography (ethylacetate: CH_2Cl_2 = 1:99), GPC ($CHCl_3$) and reprecipitated from $CHCl_3$-MeOH to give **3-15** as blue solid (0.2474 g, 68%). ^{1}H NMR (400 MHz, $CDCl_3$, TMS): δ = 9.09 (s, 4H), 8.05 (d, 2H, *J* = 4 Hz), 7.78 (d, 2H, *J* = 1 Hz), 7.64 (dd, 2H, *J* = 1, 8 Hz), 7.51 (d, 2H, *J* = 4 Hz), 7.45–7.41 (m, 6H), 7.32–7.29 (m, 3H), 4.96 (m, 4H), 4.78 (dd, 4H, *J* = 4, 16 Hz); ^{13}C NMR (100 MHz, $CDCl_3$, TMS): δ = 154.03, 147.90, 145.31, 138.82, 138.51, 137.02, 136.05, 135.99, 135.25, 134.30, 133.92, 130.93, 127.85, 127.80, 126.70, 126.64, 126.18, 125.37, 123.37, 123.28, 76.20, 76.18, 47.82, 47.47; MS (ESI): m/z = 871 $[M + 1]^+$. HR-ESI *m/z* = 871.16860 calcd for $C_{52}H_{31}N_4O_6S_2$ = 871.16850 $[M + H]^+$

Diol adduct (3-16): Carbonate adduct **3-15** (245 mg, 0.281 mmol) was dissolved in THF (112 ml). 1 M NaOH (48 ml) was added to the solution. The reaction mixture was stirred for 5.5 h. The THF layer was washed with brine (3 times) and dried with Na_2SO_4. After removing the Na_2SO_4 with filtration, the organic solvent was evaporated. The crude product was purified with reprecipitation (THF-MeOH), silica gel column chromatography ($CHCl_3$:ethylacetate = 4:6) and recrystallization from THF-hexane to give diol **3-16** as black blue crystal. Finally, the

compound was heated at 100 ºC for 2 h to remove the including solvents (163 mg, 71%). ^{1}H NMR (400 MHz, DMSO, TMS): δ = 9.19 (s, 4H), 8.11 (d, 2H, *J* = 4 Hz), 7.79 (d, 2H, *J* = 1 Hz), 7.62 (d, 2H, *J* = 4 Hz), 7.55 (dd, 2H, *J* = 4, 8 Hz), 7.44 (d, 2H, *J* = 8 Hz), 7.35–7.30 (m, 4H), 7.16–7.12 (m, 4H), 4.71 (d, 4H, *J* = 4 Hz), 4.48 (d, 4H, *J* = 4 Hz), 4.41 (d, 4H, *J* = 4 Hz), 3.95 (m, 4H, –OH); ^{13}C NMR (100 MHz, DMSO, TMS): δ = 147.56, 146.15, 141.87, 140.68, 139.59, 137.76, 135.59, 132.86, 131.92, 129.56, 126.15, 126.05, 125.61, 125.56, 125.30, 123.36, 122.88, 121.68, 66.80, 51.04, 50.83 ; MS (ESI): *m/z* = 819 $[M + H]^+$. HR-ESI *m/z* = 819.20939 calcd for $C_{50}H_{35}N_4O_4S_2$ = 819.20997 $[M + H]^+$

ADK2-PQ: In 100 mL flask, dry CH_2Cl_2 (16 mL) and dry DMSO (4.0 mL) was mixed under an argon atmosphere. The solution was cooled to −78 ºC. TFAA (1.3 mL, 9.2 mmol) was slowly added to the solution for 10 min. After stirring for 30 min, diol **3-15** (148 mg, 0.181 mmol) in dry CH_2Cl_2 (2.5 mL) and dry DMSO (6.0 mL) was slowly added to the solution over 10 min, and the residue was also dissolved in dry-DMSO (2.0 mL) and added to the solution. The solution was stirred for 2 h at −78 ºC and distilled-DIPEA (3.6 mL) was added. After stirring for 2 h, the solution was warmed to rt. The reaction was quenched with water and extracted with CH_2Cl_2. The organic layer was washed with 1 M HCl, water, $NaHCO_3$aq. and brine, and dried over Na_2SO_4. The organic solvent was removed under reduced pressure. The product was purified to reprecipitate from CH_2Cl_2-hexane, flash silica gel column chromatograph (1st. CH_2Cl_2:ethylacetate = 8:2, 2nd. CH_2Cl_2:ethylacetate = 9.5:0.5→9:1) and heating at 220 ºC for 2 h under vacuum to give **ADK2-PQ** as blue crystal (60 mg, 41%). ^{1}H NMR (400 MHz, $CDCl_3$, TMS): δ = 9.10 (s, 4H), 8.08 (d, 2H, *J* = 4 Hz), 7.86 (d, 2H, *J* = 4 Hz), 7.79 (dd, 2H, *J* = 4, 8 Hz), 7.56–7.50 (m, 8H), 7.42 (m, 4H), 5.09 (s, 2H), 5.05 (s, 5.05); ^{13}C NMR (150 MHz, $CDCl_3$, TMS): δ = 183.69, 183.38, 147.30, 145.43, 138.89, 136.04, 135.66, 135.28, 134.72, 134.67, 134.40, 133.90, 131.05, 129.58, 129.55, 127.09, 126.90, 126.45, 126.39, 123.81, 123.61, 60.04, 59.72; MS (ESI): *m/z* = 833 $[M + Na]^+$. HR-ESI *m/z* = 833.12927 calcd for $C_{50}H_{26}N_4NaO_4S_2$ = 833.12932 $[M + Na]^+$

General: ^{1}H and ^{13}C NMR spectra were recorded with a JEOL JNM-ECX 400 and JEOL JNM-ECA600 spectrometer at ambient temperature by using tetramethylsilane as an internal standard. Mass spectra were measured on a JEOL JMS-700 spectrometer and JEOL spiralTOF JMS-S3000. UV/Vis spectra were measured with a JASCO UV/Vis/NIR spectrophotometer V-570. Ionization energies were measured on a RIKEN KEIKI AC-3. IR spectra were measured

on a JASCO FT/IR 4200 spectrophotometer with RAS PR0410-H.

Photochemical Reactions: The photochemical reactions were carried out in an NMR tube, which irradiated by a metal-halide lamp (Nippon P. I. PCS-UMX375RC, 375 W) through a UV-cutoff filter (390 nm) under an argon atmosphere and monitored by a JNM-ECX 400 spectrometer.

X-ray Crystallographic Analysis: Single-crystal X-ray diffraction data was collected at 90 K with a BRUKER-APEXII X-Ray diffractometer equipped with a large area CCD detector by using graphite monochromated Mo-Kα radiation (λ = 0.71073 Å). The structure was solved by direct method (SHELXS-97) and refined with the SHELX-97 program.[20]

3-11 References

(1) (a) Mishra, A.; Bäuerle, P. *Angew. Chem. Int. Ed*. **2012**, *51*, 2020–2067. (b) Lin, Y.; Li, Y.; Zhan, X. *Chem. Soc. Rev.* **2012**, *41*, 4245–4272.

(2) Liao, S.-H.; Jhuo, H.-J.; Yeh, P.-N.; Cheng, Y.-S.; Li, Y.-L.; Lee, Y.-H.; Sharma, S.; Chen, S.-A. *Sci. Rep.* **2014**, 4: 6813

(3) (a) He, Z.; Zhong, C.; Su, S.; Xu, M.; Wu, H.; Cao, Y. *Nat. Photonics* **2012**, *6*, 591–595. (b) Osaka, I.; Kakara, T.; Takemura, N.; Koganezawa, T.; Takimiya, K. *J. Am. Chem. Soc*. **2013**, *135*, 8834–8837. (c) Kong, J.; Hwang, I.-W.; Lee, K. *Adv. Mater*. **2014**, *26*, 6275–6283.

(4) Kan, B.; Zhang. Q.; Li, M.; Wan, X.; Ni, W.; Long, G; Wang, Y.; Yang, X.; Feng, H.; Chen, Y. *J. Am. Chem. Soc*. **2014**, *136*, 15529–15532.

(5) Kyaw, A. K. K.; Wang, D. H.; Wynands, D.; Zhang, J.; Nguyen, T.-Q.; Bazan, G. C.; Heeger, A. J. *Nano Lett*. **2013**, *13*, 3796–3801.

(6) (a) Liang, Y.; Xu, Z.; Xia, J.; Tsai, S.-T.; Wu, Y.; Li, G.; Ray, C.; Yu, L. *Adv. Mater*. **2010**, *22*, E135–E138. (b) Dou, L.; Gao, J.; Richard, E.; You, J.; Chen, C.-C.; Cha, K. C.; He, Y.; Li, G.; Yang, Y. *J. Am. Chem. Soc*. **2012**, *134*, 10071–10079. (c) Chen, Y.; Wan, X.; Long, G. *Acc. Chem. Res.* **2013**, *46*, 2645–2655.

(7) (a) Zhou, J.; Wan, X.; Liu, Y.; Long, G.; Wang, F.; Li, Z.; Zuo, Y.; Li, C.; Chen, Y. *Chem. Mater*. **2011**, *23*, 4666–4668. (b) Sun, Y.; Welch, G. C.; Leong, W. L.; Takacs, C. J.; Bazan, G. C.; Heeger, A. J. *Nat. Mater*. **2012**, *11*, 44–48.

(8) The energy level was performed using the Gaussian 09 program package at the B3LYP/6-31G(d) level.

(9) Yamagchi, Y.; Suzuki, M.; Motoyama, T.; Sugii, S.; Katagiri, C.; Takahira, K.; Ikeda, S.; Yamada, H.; Nakayama, K. *Sci. Rep.* 4, 7151

(10) (a) Yamada, H.; Ohashi, C.; Aotake, T.; Katsuta, S.; Honsho, Y.; Kawano, H.; Okujima, T.; Uno, H.; Ono, N. Seki, S.; Nakayama, K. *Chem. Commun*. **2012**, *48*, 11136–11138. (b) Motoyama, T.; Sugii, S. Ikeda, S.; Yamaguchi, Y.; Yamada, H.; Nakayama, K. *Jpn. J. Appl. Phys*. **2014**, *53*, 01AB02-1–01AB02-4.

(11) Mühlbacher, D.; Scharber, M.; Morana, M.; Xhu, Z.; Waller, D.; Gaudiana, R.; Brabec, C. *Adv. Mater.* **2006**, *18*, 2884–2889.

(12) Shin, Y.; Liu, J.; Quigley, J. J.; IV,; Luo, H.; Lin, X. *ACS. Nano* **2014**, *8*, 6089–6096.

(13) Scharber, M. C.; Mühlbacher, D.; Koppe, M.; Denk, P.; Waldaul, C.; Heeger, A. J.; Brabec, C. J. *Adv. Mater*. **2006**, *18*, 789–794.

(14) Zhang, F.; Bijleveld, J.; Perzon, E.; Tvingstedt, K.; Barrau, S.; Inganäs, O.; Andersson, M. R. *J. Mater. Chem*. **2008**, *18*, 5468–5474.

(15) Wang, E.; Hoou, L.; Wang, X.; Hellström, S.; Mammo, w.; Zhang, F.; Inganäs, O.; Andersson, M. R. *Org. Lett.* **2010,** *12*, 4470–4473.

(16) Peng, Q.; Liu, X.; Qin, Y.; Xu, J.; Li, M.; Dai, L. *J. Mater. Chem*. **2011**, *21*, 7714–7722.

(17) Schulz, G. L.; Mastalerz, M.; Ma, C.-Q., Wienk, M.; Janssen, R.; Bäuerle, P. *Macromolecules*, **2013**, *46*, 2141–2151.

(18) (a) Harley-Mason, J.; Laird, A. H. *Tetrahedron* **1959**, *7*, 70–76. (b) Ono, K.; Okazaki, Y.; Ohkita, M.; Saito, K.; Yamashita, Y. *Heterocycles*, **2004**, *63*, 2207–2210.

(19) (*a*) Backe, A. D.; *J. Chem. Phys.* **1993**, *98*, 5648–5652; (*b*) Lee, C.; Yang, W.; Parr, R. G. *Phys. Rev. B*, **1988**, *37*, 785–789. (c) Gaussian 09, Revision *D.01*, Frisch, M. J.; Trucks, G. W.; Schlegel, H. B.; Scuseria, G. E.; Robb, M. A.; Cheeseman, J. R.; Scalmani, G.; Barone, V.; Mennucci, B.; Petersson, G. A.; Nakatsuji, H.; Caricato, M.; Li, X.; Hratchian, H. P.; Izmaylov, A. F.; Bloino, J.; Zheng, G.; Sonnenberg, J. L.; Hada, M.; Ehara, M.; Toyota, K.; Fukuda, R.; Hasegawa, J.; Ishida, M.; Nakajima, T.; Honda, Y.; Kitao, O.; Nakai, H.; Vreven, T.; Montgomery, J. A., Jr.; Peralta, J. E.; Ogliaro, F.; Bearpark, M.; Heyd, J. J.; Brothers, E.; Kudin, K. N.; Staroverov, V. N.; Kobayashi, R.; Normand, J.; Raghavachari, K.; Rendell, A.; Burant, J. C.; Iyengar, S. S.; Tomasi, J.; Cossi, M.; Rega, N.; Millam, M. J.; Klene, M.; Knox, J. E.; Cross, J. B.; Bakken, V.; Adamo, C.; Jaramillo, J.; Gomperts, R.; Stratmann, R. E.; Yazyev, O.; Austin, A. J.; Cammi, R.; Pomelli, C.; Ochterski, J. W.; Martin, R. L.;

Morokuma, K.; Zakrzewski, V. G.; Voth, G. A.; Salvador, P.; Dannenberg, J. J.; Dapprich, S.; Daniels, A. D.; Farkas, Ö.; Foresman, J. B.; Ortiz, J. V.; Cioslowski, J.; Fox, D. J. Gaussian, Inc., Wallingford CT, 2009.

(20) Sheldrick, G. M. *Acta Crystallogr., Sect. A* **2008**, *64*, 112–122.

Chapter 4

Synthesis and Physical Properties of Stimuli Induced Fluorescence Switching Materials

---

From Non-Fluorescent Skeleton to Strongly Fluorescent Skeleton

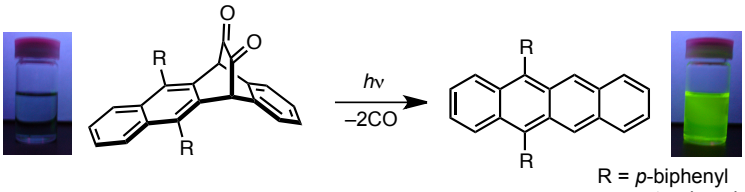

R = *p*-biphenyl
m-terphenyl

Photoactivatable Pyrene Dyes Using Anthracenediketone as an Intramolecular Fluorescence Quencher

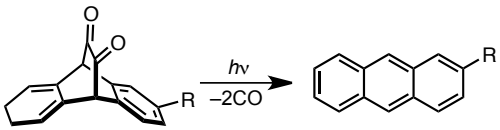

R = 2-pyrene-1-yl
2-pyrene-1-ylethynyl

Thermally and Photochemically Controlable Fluorescent BODIPY Based on Intramolecular Electron Transfer

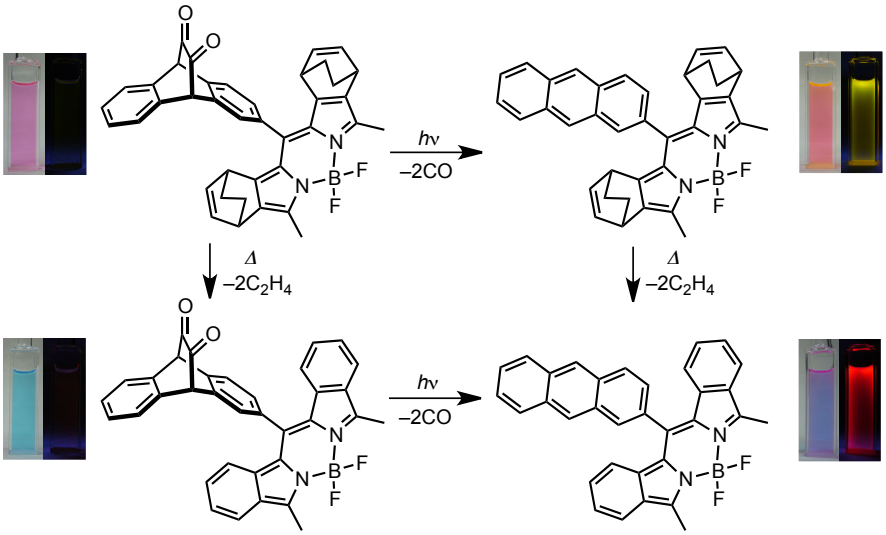

Efficient conversion of non-fluorescent molecule to strongly fluorescent molecule by external stimuli, such as heat or light, has received attention due to their potential application to optical memory media and security system. In this chapter, synthesis and photoswitchable fluorescence properties of α-diketone type precursors are described.

4-1 Introduction

Fluorescence is one of the most useful tools for visualization of molecular scale. A lot of fluorescent structures and the derivatives have been widely reported.[1] The switchable fluorescent molecules, which show dramatic change in fluorescence properties by external stimuli such as ion[2] and pH[3], have been studied as chemical sensor and bioimaging agent.[4] Photoirradiation is one of the external stimuli and can modulate materials at molecular scale.[5] The photoswitchable fluorescent molecule is representative photochromic compound.[6] These molecules are classified into two types. One is photoresponsive molecules, whose skeleton can be changed between non-fluorescent and fluorescent electronic structure (Figure 4-1).[7] Although this type is very simple to control fluorescence property, the reports have been a small number because the molecular design is difficult by two constraints: 1) structural change must proceed effectively by the stimulus, and 2) large difference of fluorescence intensity or wavelength is necessary before and after structural change. As an advantage of this type, the effects of surrounding environment on emission characteristic are small.

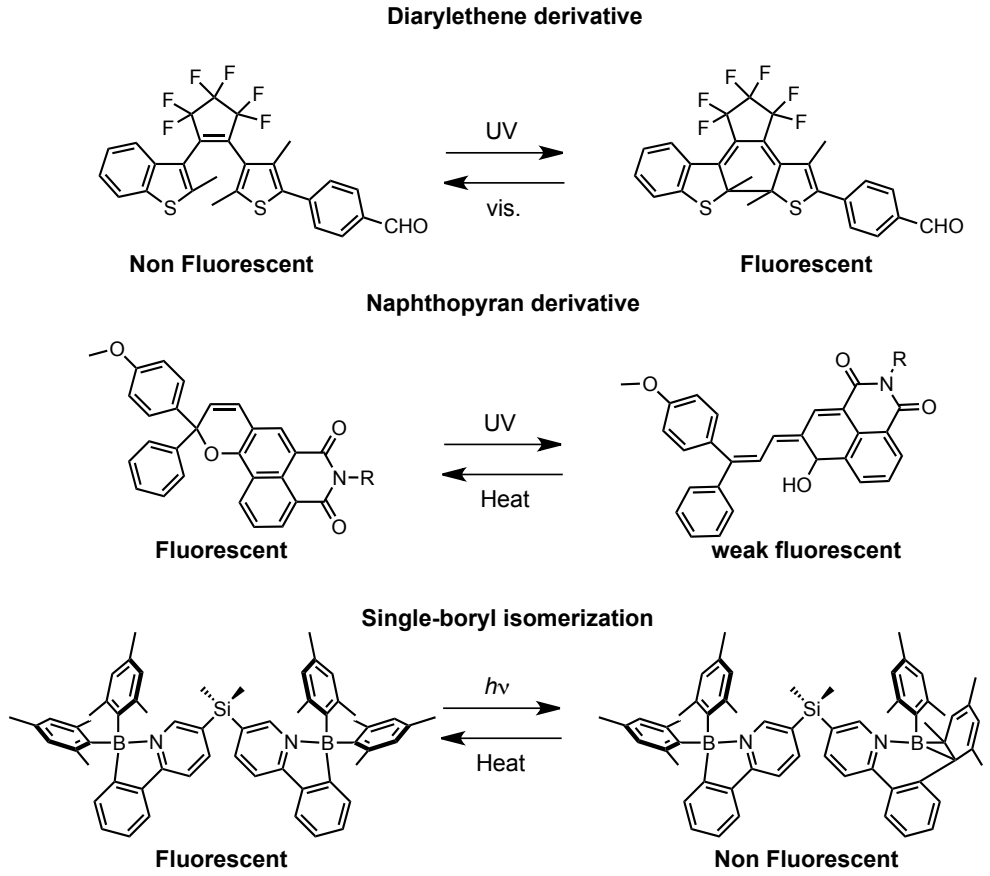

Figure 4-1. Florescence changes based on structural change of photoresponsive unit themselves.

The second type is the combined structure of photo-switching unit and fluorophore unit. The molecules are able to control the fluorescence properties by interaction between the two units. The interaction mechanisms are further classified into energy transfer[8] or electron transfer[9].

A typical example controlled by energy transfer mechanism is shown in Figure 4-2.[10] In this case, fluorescence property is controlled by the absorption wavelength change of the photo-switching units. When photo-switching unit (diarylethene) is the open form, the excited state of photo-switching unit is higher than the excited singlet state of fluorophore. Hence, the fluorescence from fluorophore unit is observed. In contrast, the closed form of switching unit has lower energy of excited state compared to that of fluorophore. The absorption spectrum of closed form completely overlaps the fluorescence spectrum of fluorophore. Therefore, the fluorescence is effectively quenched due to intramolecular energy transfer. As a matter of course, the two structures can be switched by light stimulation.

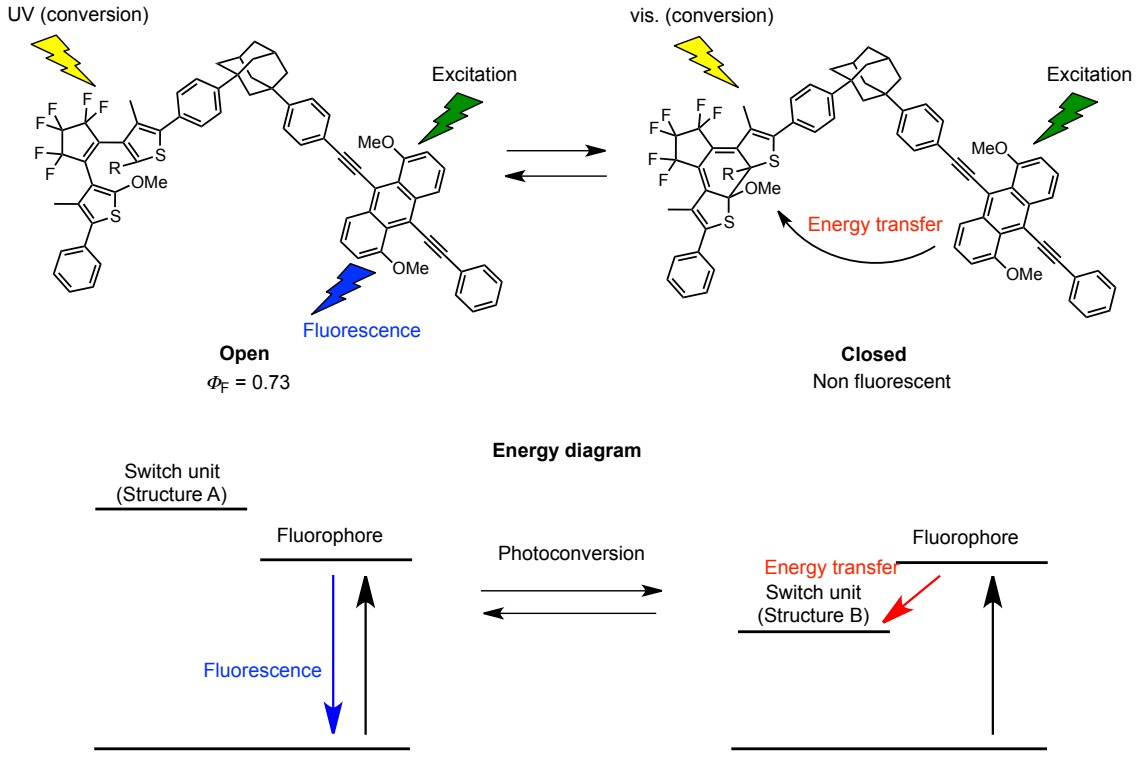

Figure 4-2. The fluorescence change based on intramolecular energy transfer mechanism.

Likewise, the fluorescence quenching system based on intramolecular electron transfer is one of the strategies. Typical examples are shown in Figure 4-3.[11] In the case of diarylethene (photo-switching)-perylenediimide (fluorophore) conjugate, photo-switching unit is used as an electron accepting unit and fluorophore unit is used as an electron-donating unit. Not surprisingly, the open-close structural change occurs by direct excitation at switch unit. When the switching unit is open form, the molecule shows strong fluorescence derived from fluorophore unit by excitation at 532 nm. On the other hand, closed form structure doesn't show fluorescence because the energy level of charge separated state is lower than the excited singlet state of fluorophore. Therefore, intramolecular electron transfer from fluorophore unit to photo-switching unit is allowed. The difference between two structures is electron-accepting property of the photo-switching unit, and the electron accepting ability of closed form is stronger than that of the open form. Similarly, the combinations of photochromic units and fluorophores have been widely reported. Thus, the molecule needs to be designed on the basis of the redox potentials of two units.

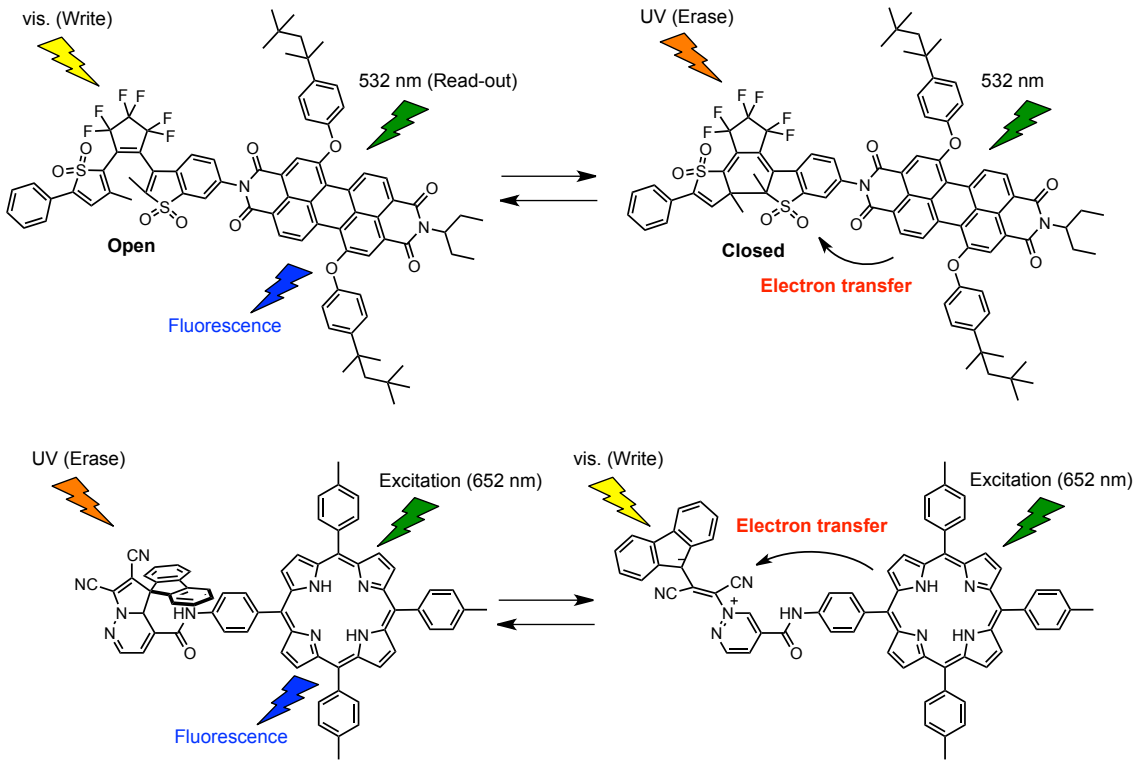

Figure 4-3. The fluorescence change based on intramolecular electron transfer mechanism.

In those studies, photochromic molecule is frequently used as interactive fluorescence switching units from a viewpoint of photoreactivity and reversibility. Those molecules are useful for preparing rewritable information device. However, it is necessary to modify the structure for applying one-way switching. Although quantitatively and irreversible photoconvertible molecule is a big candidate, the report of completely one-way fluorescence switchable materials are much less than the reversible type.[12] Additionally, the high ON-OFF ratio is required. The advantage of o ne-way switching molecule is to maintain the state of structural change permanently. The characteristic is applied to security material and read-only information device. As described in Chapter 1, the photoconversion of α-diketone type precursor proceeds irreversibly and quantitatively by photoactivation. Additionally, the electronic structures of before and after conversion are dramatically changed. From those facts, α-diketone type precursor method is a candidate for a one-way fluorescence switching system. Additionally, the developing as a new application of the precursor method can be expected. In this Chapter, the one-way photoresponsive molecules with the high ON-OFF ratio of fluorescence is studied and discussed.

4-2 Fluorescence Change Based on Structural Change from α-Diketone Type Photoprecursor to Strongly Fluorescent Naphthacene

4-2-1 Molecular Design

Naphthacene (**NAP**) and the derivatives are known as classic fluorescent molecules.[13] **NAP** shows large absorption at 400–500 nm and fluorescence at 500–600 nm with typical vibration structure. The fluorescence quantum yield is moderate 0.12 in toluene. To improve the fluorescence quantum yield, introduction of aryl substituents is often used.[14] As typical examples, the quantum yields of 5,12-diphenylnaphthacene and 5,6,11,12-tetraphenylnaphthacene (rubrene) go up to 0.85 and 0.98 in solution (Figure 4-4).[15]

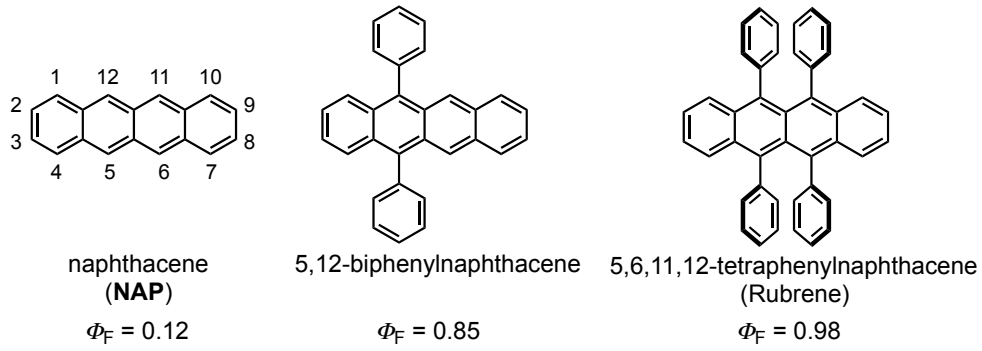

Figure 4-4. Naphthacene (**NAP**) and typical derivatives.

For attaching the photo-switching function to the fluorescent naphthacenes, structural change from non-fluorescent structure by photoinduction is a simple way. As described in Chapter 1, photoprecursor method is useful to prepare acenes by photoactivation. In addition, photoprecursor of anthracene (**ADK**) doesn't show fluorescence since fluorophore isn't present in the molecular structure.[16] 5,12-α-Diketone bridged naphthacene has two chromophores. Naphthalene which shows no absorption in visible region is one, and α-diketone moiety which shows only weak absorbance band at 400–500 nm is the other (Figure 4-5). Since both chromophores show no fluorescence in visible area, 5,12-α-diketone bridged naphthacene is a non-emissive precursor. Consequently, the author of this thesis considered the α-diketone type precursor method could be applied to prepare the photoswitchable fluorescent molecule.

In this content, the synthesis, optical properties and photochemical fluorescence activation are discussed.

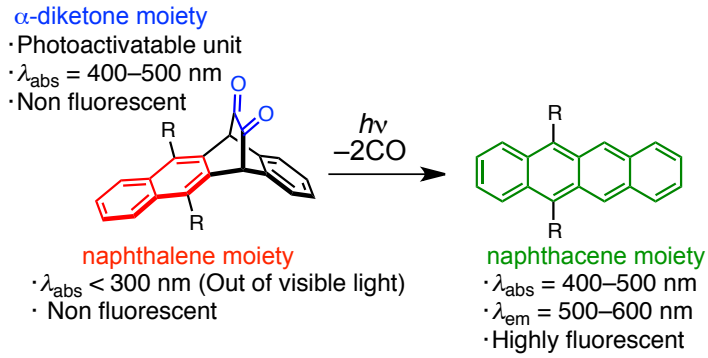

Figure 4-5. Molecular designs for fluorescence control based on structural change of naphthacene and the derivative.

4-2-2 Synthesis of 5,12-Substituted Naphthacene Derivatives

5,12-Substituted naphthacenes **4-3a** and **4-3b** were prepared as shown in Scheme 4-1. 1,1'-Biphenyl-4-yllithium, which was prepared from 4-pheny-bromobenzene and *n*-BuLi, was reacted with 5,12-naphthacenequinone (**4-1**) to afford **4-2a** in 52% yield. The compound **4-2a** was dehydrated with $SnCl_2$ and concd. HCl in refluxing THF to give naphthacene **4-3a** in 95% yield. Similarly **4-2b** was prepared by the reaction **4-1** and 3,5-diphenylphenyllithium, which was prepared from 1-iode-3,4-diphenylbenzene,[17] in 29% yield, and then converted to **4-3b** in 87% yield.

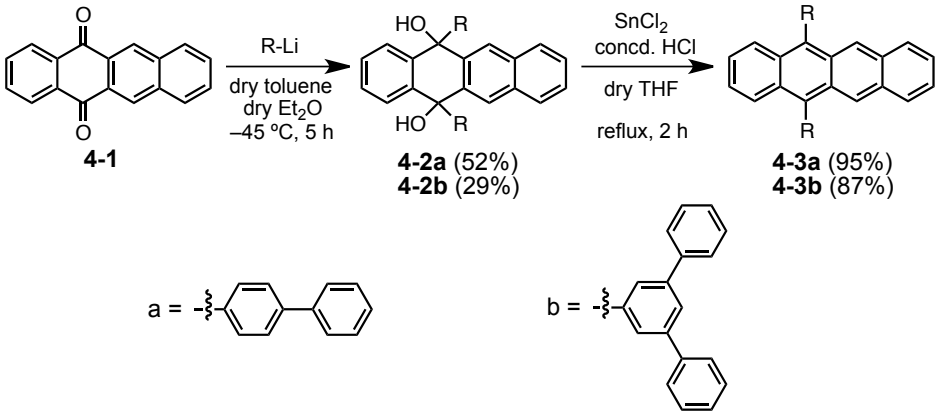

Scheme 4-1. Synthesis of 5,12-substituted naphthacenes (**4-3a** and **4-3b**).

The synthesis of α-diketone type precursors of naphthacenes is shown in Scheme 4-2. Naphthacenes (**NAP**, **4-3a** and **4-3b**) were reacted with vinylene carbonate in a Diels-Alder reaction to give carbonate adducts (**4-4H**, **4-4a** and **4-4b**) as a mixture of stereoisomers. The compounds were subsequently hydrolyzed to give diols (**4-5H**, **4-5a** and **4-5b**), which were oxidized by the Swern reaction to give α-diketone compounds (**4-6H**, **4-6a** and **4-6b**). The solubility of **NAP**, **4-3a** and **4-3b** in toluene were 0.15, 0.81 and 5.2 mg/mL, respectively. On the other hand, solubility of the precursors **4-6H**, **4-6a** and **4-6b** were much improved to 17, 15 and >23 mg/mL, respectively.

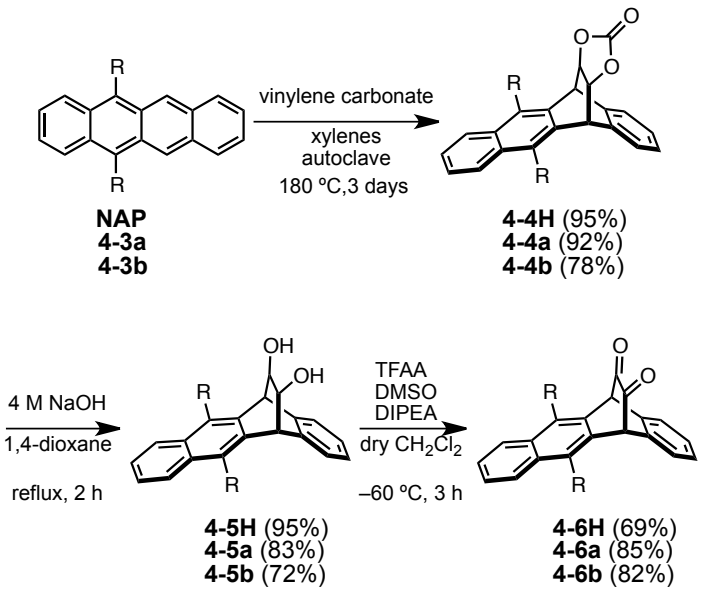

Scheme 4-2. Synthesis of α-diketone type naphthacene precursors (**4-6H**, **4-6a** and **4-6b**).

4-2-3 Optical Properties

The UV-vis absorption and fluorescence spectra of these naphthacenes in toluene are shown in Figure 4-6 and summarized in Table 2-1. The absorption maxima of **4-3a** and **4-3b** in toluene are red-shifted by 20 nm relative to **NAP**. Fluorescence peaks of **4-3a** (511 nm) and **4-3b** (506 nm) are red-shifted by 30 nm and 25 nm compared to **NAP** (481 nm). The absolute fluorescence quantum yields of naphthacenes are 0.67 for **4-3a** and 0.70 for **4-3b**, which are more than 5 times larger than that of **NAP** (Φ_F = 0.12).

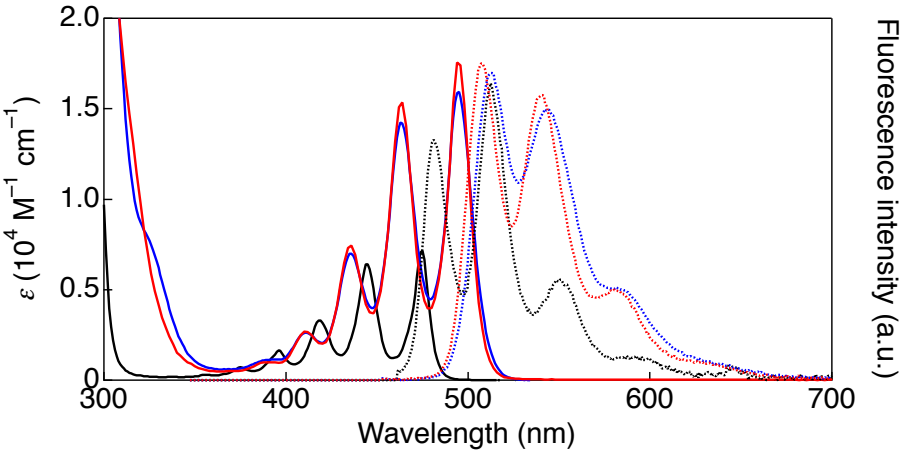

Figure 4-6. UV-vis absorption (solid) and fluorescence (dotted) spectra of **NAP** (black), **4-3a** (blue) and **4-3b** (red) in toluene.

The fluorescence decays and life times (τ_F) of **NAP**, **4-3a** and **4-3b** were measured in toluene excited at 355 nm (Figure 4-7). The τ_F values were evaluated to 3.9 ns (naphthacene), 9.4 ns (**4-3a**) and 9.6 ns (**4-3b**). The τ_F values of **4-3a** and **4-3b** are 2.5 times longer than that of **NAP**, and these phenomena are similar to the relationship between **NAP**, 5,12-diphenylnaphthacene and rubrene. Their fluorescence lifetimes in benzene or toluene were reported as 4.2, 15.2 and 16 ns, respectively.[15]

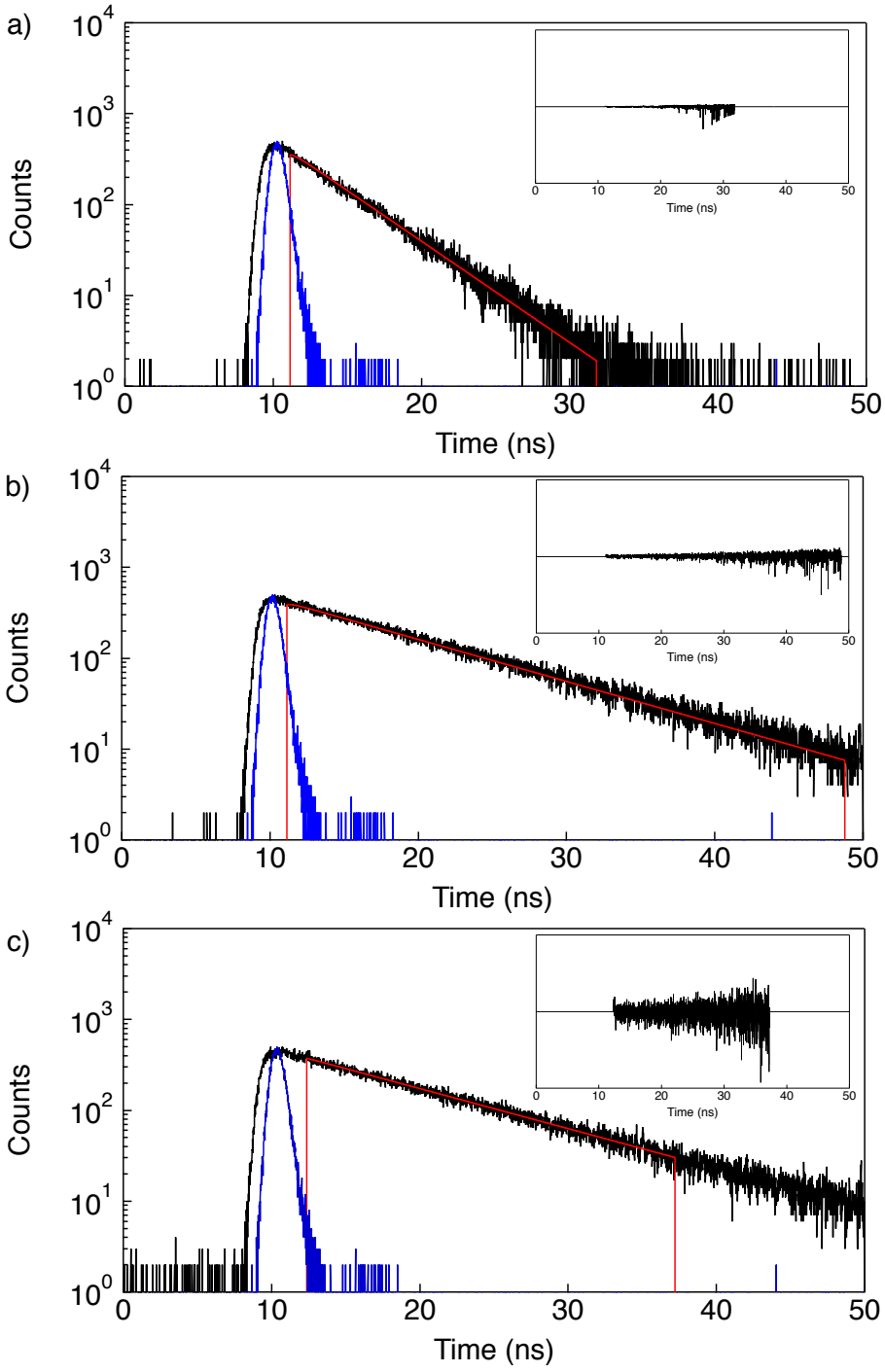

Figure 4-7. Fluorescence decays in toluene by excited at 355 nm. **NAP** at 484 nm (a), **4-3a** at 507 nm (b) and **4-3b** at 508 nm (c).

Table 2-1. UV-vis absorption peaks (λ_{abs}), fluorescence peaks (λ_F), fluorescence quantum yields (Φ_F) and fluorescence lifetimes (τ_F) in toluene.

	λ_{abs} (nm) (logε)	λ_F (nm)[a]	Φ_F[a]	τ_F (ns)[b]
NAP	396 (3.22), 419 (3.52), 445 (3.81), 475 (385)	481, 512, 551	0.12	3.9
4-3a	411 (3.42), 436 (3.84), 463 (4.15), 495 (4.20)	511, 541, 583	0.67	9.4
4-3b	410 (3.43), 436 (3.87), 464 (4.19), 494 (4.24)	506, 539, 589	0.70	9.6

[a]Excitation at 462 nm. [b]Excitation at 355 nm.

The electrochemical properties of the naphthacenes were investigated by cyclic voltammetry (CV) in dichloromethane containing 0.1 M *n*-Bu_4NPF_6 as the supporting electrolyte. The results are shown in Figure 4-8. The oxidation potentials ($E_{ox}^{1/2}$ vs. Fc/Fc^+) of **4-3a** and **4-3b** are 0.44 and 0.47 V respectively and the waveforms are clear reversible. **4-3a** and **4-3b** exhibited reduction peaks at –2.10 and –2.09 V.

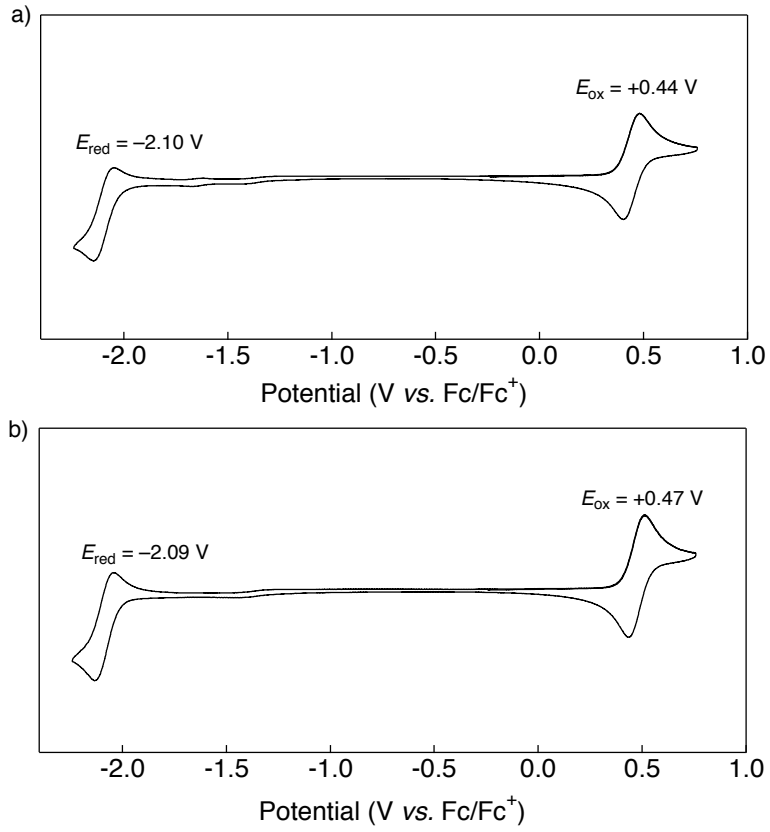

Figure 4-8. Cyclic voltammograms of **4-3a** (a) and **4-3b** (b) in 0.1 M *n*-Bu_4NPF_6 acetonitrile solution. Scan rate 0.1 V s^{-1}. [sample] = 0.1 mM. WE: Glassy carbon, CE: Pt, RE: $Ag/AgNO_3$.

The UV-vis absorption spectra of α-diketone type precursors **4-6H**, **4-6a** and **4-6b** in toluene are shown in Figure 4-9. The absorption spectra show weak n-π* absorption of α-diketone moiety at 400–500 nm. The fluorescence properties were measured in toluene for each precursor. The fluorescence spectrum of **4-6H** wasn't detected by exciting at 468 nm. On the other hand, the Φ_F of **4-6a** and **4-6b** was 0.016 and 0.017, respectively, in the beginning of the measurement, but Φ_Fs increased gradually at every measurement. In addition, the waveforms are similar to the fluorescence spectra of corresponding naphthacenes. These results imply that the precursors immediately reacted to release CO molecules when they were excited for the measurement of fluorescence quantum yield, and fluorescence from the generated acenes were gradually observed depending on the irradiation period.

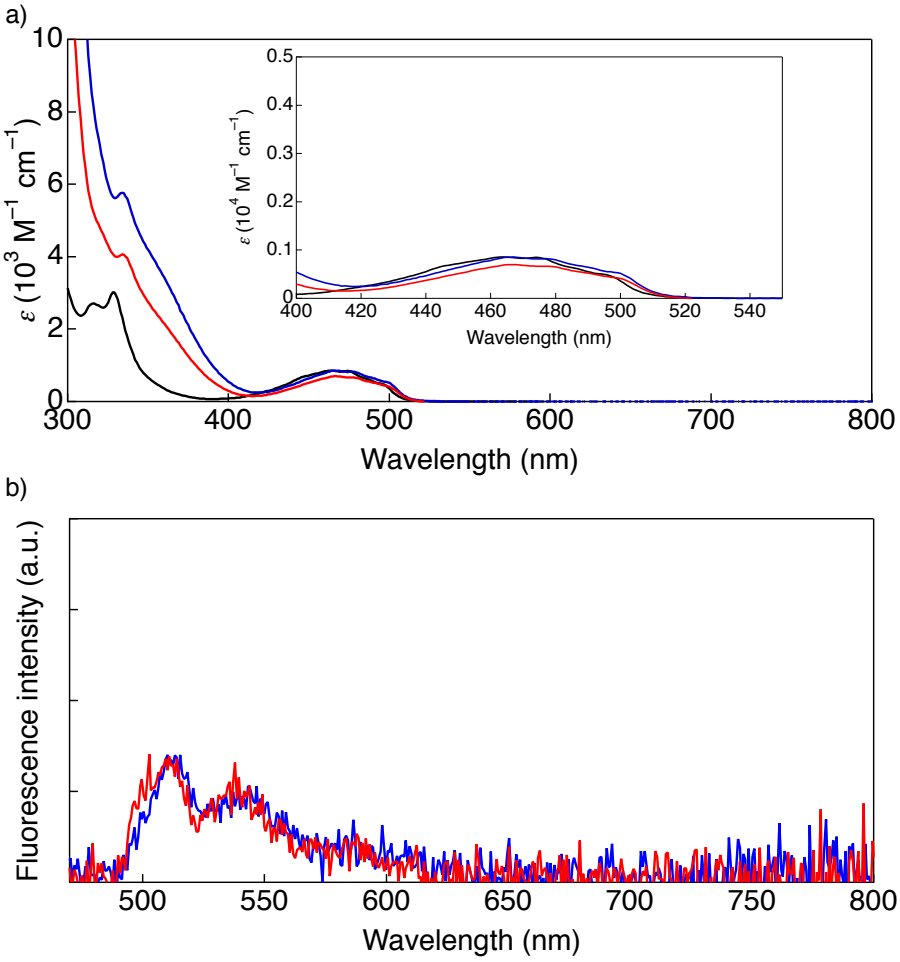

Figure 4-9. UV-vis absorption (a) and fluorescence (b) spectra of **4-6H** (black), **4-6a** (blue) and **4-6b** (red) in toluene.

4-2-4 Photoconversions in Solution

The photoconversions of the precursors to naphthacenes were performed using a blue LED (λ = 470 nm, 25 W/m^2) under a nitrogen atmosphere. Figure 4-10 shows the changes in ^{1}H NMR spectra during the photoconversion of **4-6a** in $CDCl_3$. The singlet peak at 5.16 ppm, assigned to H^a of the diketone moiety, is seen to gradually decrease, while the peaks at 8.41 ppm assigned to the peri protons H^b of **4-3a**, increase. After 15 min, the photoconversion was complete without any evidence of by-products. The same analysis was performed using **4-6b** in $CDCl_3$ (Figure 4-11). During the photoreaction, the peak at 5.25 ppm decreased while those at 8.49 ppm increased, indicating the formation of **4-3b**. These results demonstrate that **4-6a** and **4-6b** were quantitatively converted to the corresponding compounds **4-3a** and **4-3b** upon photoirradiation.

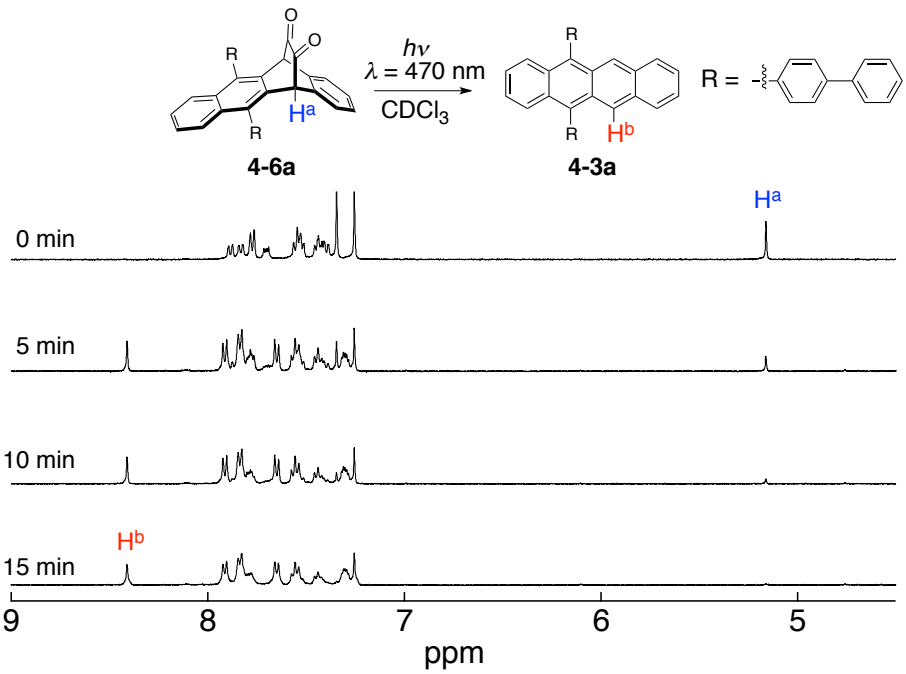

Figure 4-10. Changes in the ^{1}H NMR spectra of **4-6a** during photolysis in $CDCl_3$ under a nitrogen. λ_{ex} = 470 nm.

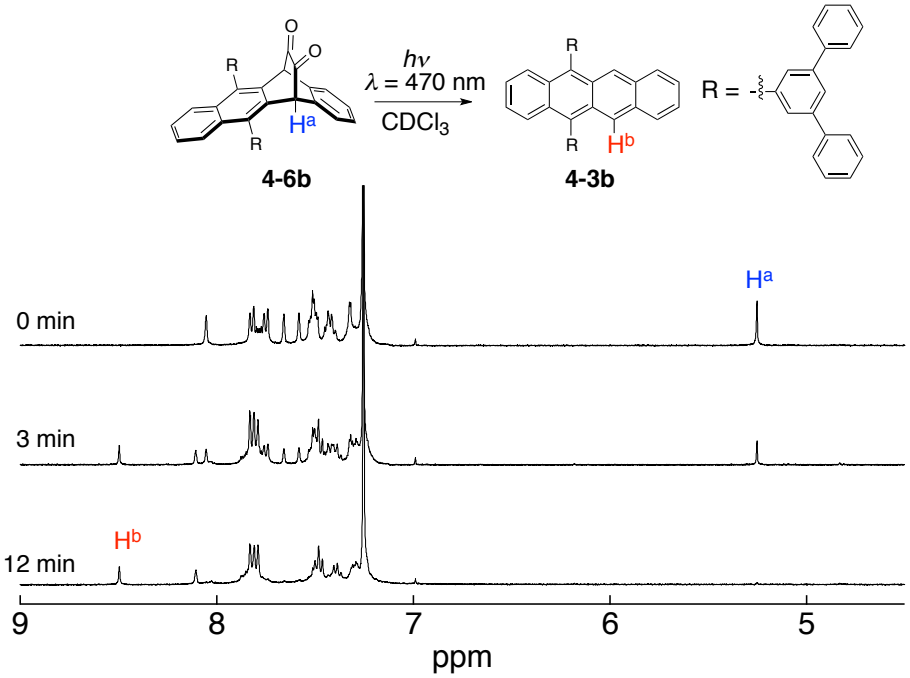

Figure 4-11. Changes in the ^{1}H NMR spectra of **4-6b** during photolysis in $CDCl_3$ under a nitrogen. λ_{ex} = 470 nm.

Figure 4-12 shows the changes in UV-vis absorption spectra during the photoconversion of **4-6H** in toluene under argon atmosphere. **4-6H** was irradiated at λ_{ex} = 468 nm. During irradiation, the broad peak at 460 nm decreased gradually, and new peaks at 395, 418, 444 and 474 nm assigned to naphthacene increased. The absorbance of naphthacene became constant after 40 min irradiation. As determined by observing the isosbestic points at 355 and 485 nm, the photoconversion proceeded quantitatively. Precursor **4-6a** and **4-6b** were converted to the corresponding naphthacenes (**4-3a** and **4-3b**). The changes of UV-vis absorption spectra during the photoconversion in toluene under argon atmosphere are shown in Figure 4-13 and Figure 4-14. Similarly, the absorption spectra changed from the precursor to naphthacenes with the photoconversion.

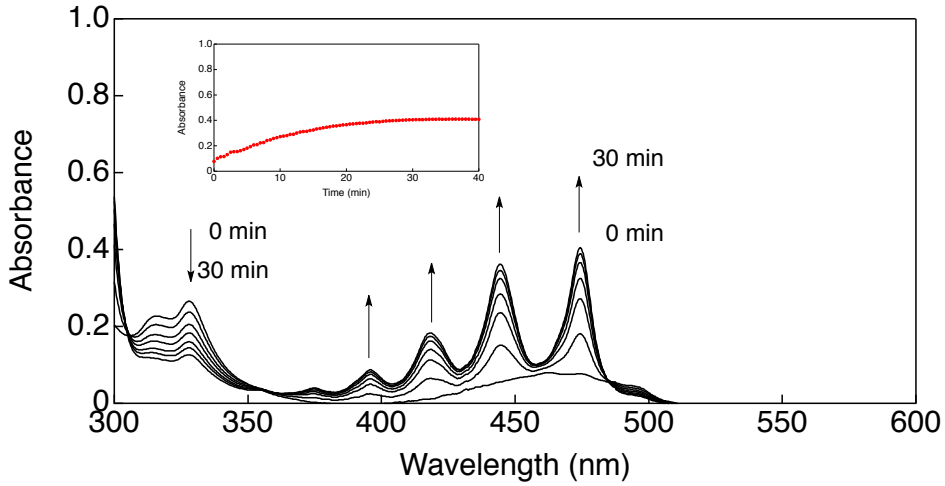

Figure 4-12. Changes in UV-vis absorption spectra and time profiles at 474 nm during photolysis (λ_{ex} = 468 nm) of **4-6H** (9.0×10^{-2} mM) in toluene.

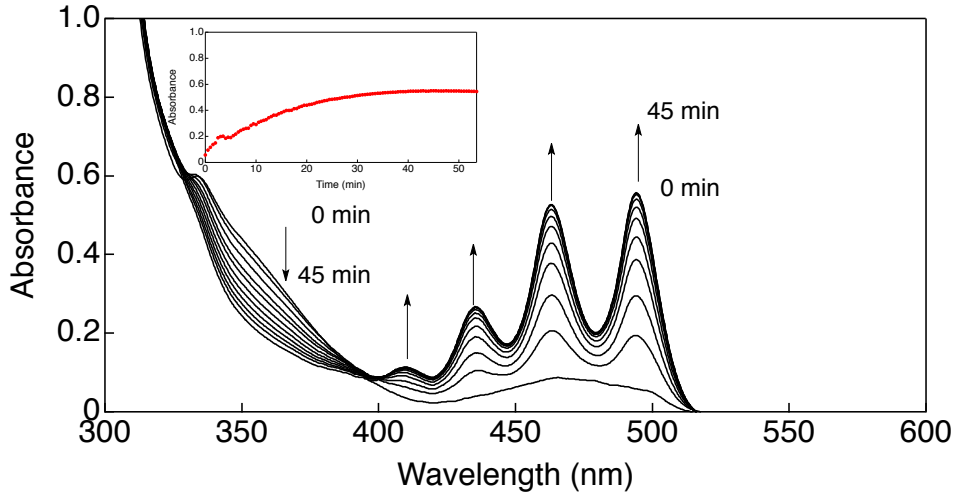

Figure 4-13. Changes in UV-vis absorption spectra and time profiles at 494 nm during photolysis (λ_{ex} = 468 nm) of **4-6a** (1.0×10^{-1} mM) in toluene.

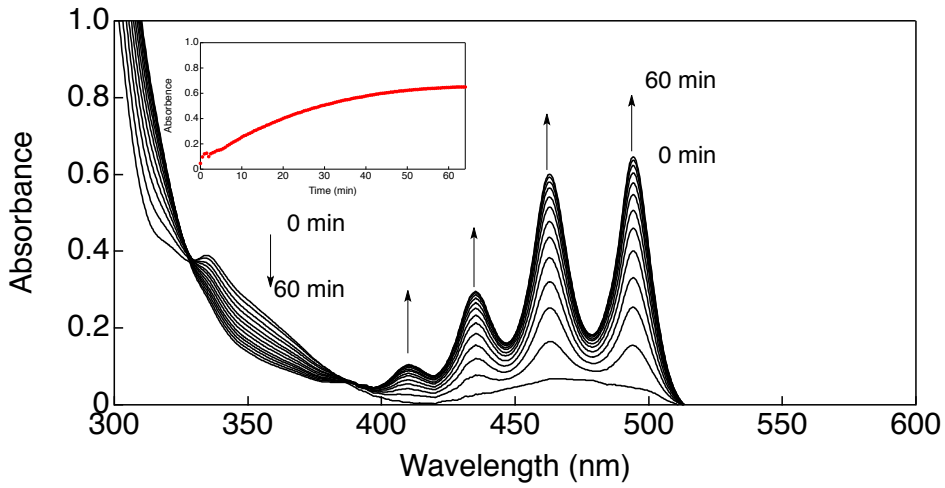

Figure 4-14. Changes in UV-vis absorption spectra and time profiles at 494 nm during photolysis (λ_{ex} = 468 nm) of **4-6b** (1.0×10^{-1} mM) in toluene.

4-2-5 Changes Fluorescence Spectra During Photolysis

The change of the fluorescence spectra of **4-6a** during the conversion is shown in Figure 4-15(a). The colorless fluorescence of the solution gradually changed to light green. Fluorescence intensity of **4-6a** increases significantly with no change of the emission maxima position. After irradiation, the fluorescence intensity stayed constant and the reaction seemed to be finished. The similar change was observed for **4-6b** as shown in Figure 4-15(b).

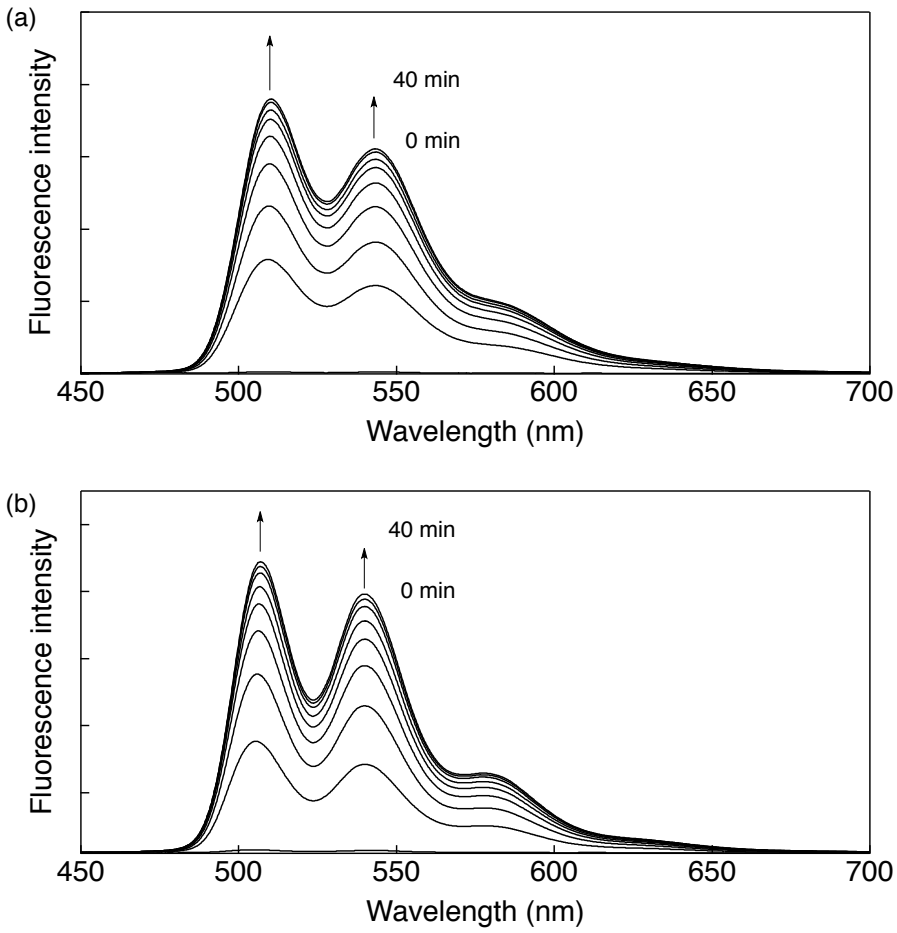

Figure 4-15. Changes in fluorescence spectra of (a) **4-6a** (3.5×10^{-2} mM) and (b) **4-6b** (3.5×10^{-2} mM) in toluene under argon atmosphere (λ_{ex} = 468 nm).

4-2-6 Photoconversions in PMMA Film

The conversion reaction was also performed in a PMMA film. The UV-vis absorption spectra of before and after photoirradiation were shown in Figure 4-16(a). Before irradiation, a typical n–π* absorption was observed at 470 nm. After irradiation, the peaks at 435, 463 and 494 nm appeared, similar to those in toluene solution. The fluorescence spectrum indicates **4-3a** is dispersed in the PMMA film without stacking. Similar result was obtained for the photoconversion from **4-6b** to **4-3b** in PMMA film (Figure 4-16(b)). Although the fluorescence spectra aren't detected in PMMA before photoconversion, the films show orange emission after conversions. The Φ_F of **4-3a** and **4-3b** were 0.33 and 0.34, respectively, in the PMMA film.

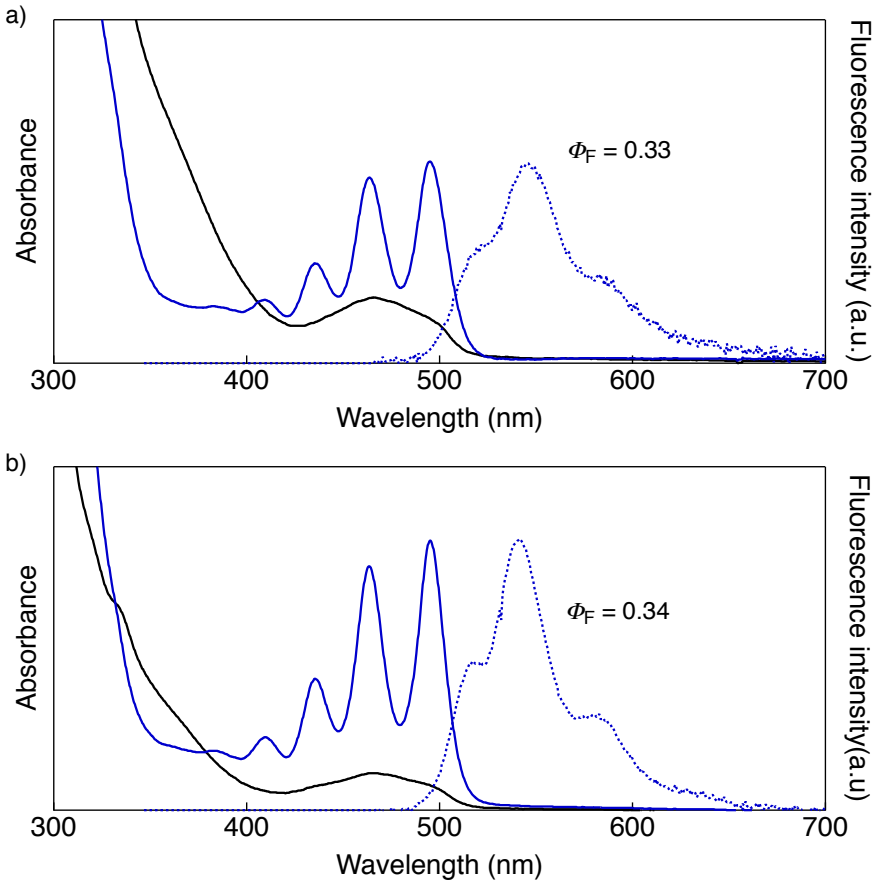

Figure 4-16. (a) UV-vis absorption (solid) and fluorescence (dotted) spectra of **4-6a** (black) and **4-3a** (blue); (b) **4-6b** (black) and **4-3b** (blue) in PMMA.

4-2-7 Short Summary

The photoprecursors of naphthacenes (**4-6a** and **4-6b)** were synthesized and the optical properties were measured. The non-fluorescent precursors were easily converted to the corresponding strongly fluorescent naphthacenes (**4-3a** and **4-3b**) upon photoirradiation in toluene solution. The photoconversions also proceeded in PMMA film and the Φ_Fs increased from non-fluorescence to 0.33 (**4-3a**) and 0.34 (**4-3b**). This result showed the precursor method could be applied to prepare one-way type photoswitchable fluorescent material.

4-2-8 Experimental Section

General ^{1}H NMR and ^{13}C NMR spectra were recorded on JEOL JNM-AL 400 spectrometers at ambient temperature using tetramethylsilane as an internal standard. FAB and TOF mass spectra were measured on a JEOL JMS-700 spectrometer and a Voyager DE Pro (Applied Biosystems). UV-vis spectra were measured on a JASCO UV/VIS/NIR Spectro-photometer V-570. Elemental analyses were performed on a Yanaco MT-5 elemental analyser. Fluorescence quantum yields were measured on Absolute PL Quantum Yield Measurement System (Hamamatsu Photonics C9920-02).

Materials Thin-layer chromatography (TLC) and gravity column chromatography were performed on Art. 5554 (Merck KGaA), and Silica Gel 60N (Kanto Chemical Co.), respectively.

Electrochemical Measurements The cyclic voltammetry measurements of investigated compounds were performed with a BAS electrochemical analyser in deaerated acetonitrile containing nBu$_4$NPF$_6$ as a supporting electrolyte at 298 K (100 mV s^{-1}). The glassy carbon working electrode was polished with BAS polishing alumina suspension and rinsed with acetone before use. The counter electrode was a platinum wire. The measured potentials were recorded with respect to Ag/AgNO$_3$ and normalized to Fc/ Fc$^+$.

Photochemical reactions The photocleavage reactions were carried out in a quartz UV cell which was irradiated by monochromatic excitation light through a monochrometor (Ritsu MC-10N) by a 500 W xenon lamp (Ushio XB-50102AA-A) and monitored by OCEAN

OPTICS high resolution spectrometer system HR-4000 with light source DH-2000-BAL. The changes of fluorescence spectra were monitored by OCEAN OPTICS USB4000FL. The photocleavage reactions were carried out in a NMR tube which irradiated by StockerYale SpecBright™ Blue LED (Peak wavelength : 470 nm; light strength: 25 W/m^2) and monitored by JEOL JNM-AL 400 spectrometer.

Photochemical reactions in film PMMA (470 mg) was dissolved with toluene (10 mL). The solution was stirred overnight and filtrated. Diketone **4-6a** or **4-6b** (5 mg) was dissolved in CH_2Cl_2 (1 mL). PMMA solution (150 μL) and diketone solution (50 μL) were mixed. The mixture solution (5 drops) was dropped on glass substrate (1 cm × 1 cm) and dried under vacuum condition. The substrate was converted upon photo-irradiation for 1 h using a metal-halide lamp (Nippon P. I. PCS-UMX375RC, 375W) over 390 nm under vacuum condition. Steady-state absorption spectra were measured on USB4000 by a light through a monochromator (Ritsu MC-10N) using a 500W Xenon lamp (Ushio XB-50102AA-A). Fluorescence quantum yields were measured on Absolute PL Quantum Yield Measurement System (Hamamatsu Photonics C9920-02).

5,12-Di[(1,1'-biphenyl)-4-yl]-naphthacene-5,12-diol (**4-2a**)

n-BuLi (1.65 M in hexane) (10.0 mL, 16.5 mmol) was added dropwise to a solution of 4-phenyl-bromobenzene (4.56 g, 19.6 mmol) in dry toluene (43.0 mL) and dry diethyl ether (14.0 mL) under a nitrogen atmosphere at –45 ºC. The mixture was allowed to stir for 1 h at –10 ºC. 5,12-naphthacenequinone **4-1** (1.56 g, 6.04 mmol) was added to the reaction mixture over 20 min, and the mixture was stirred for 5 h at room temperature. The excess of *n*-BuLi was quenched by methanol, and the residue was removed by filtration. The solution was concentrated under reduced pressure, the crude product was washed with methanol and filtered to give product **4-2a** as white yellow solid (1.78 g, 52%).

^{1}H NMR (400 MHz, $CDCl_3$) δ 8.48 (s, 2H), 8.09 (dd, J = 7.2 Hz, 3.2 Hz, 2H), 7.98 (dd, J = 7.2 Hz, 3.2 Hz, 2H), 7.58–7.55 (m, 4H), 7.20-7.17 (m, 10H), 6.98 (d, J = 8.4 Hz, 4H), 6.81 (d, J = 8.4 Hz 4H), 2.91 (s, 2H, -OH); ^{13}C NMR (100 MHz, $CDCl_3$, One peak was overlap.) δ 141.70, 141.13, 140.21, 139.67, 139.40, 132.62, 128.35, 127.97, 127.94, 126.93, 126.85, 126.34, 125.96, 125.72, 125.00, 75.78; MS (FAB) *m/z* 556 (M^++1); Anal. Calculated for $C_{42}H_{30}O_2$•1/4H_2O: C, 88.32; H, 5.38. Found: C, 88.26; H, 5.51.

5,12-Di[(1,1':3',1''-terphenyl)-5'-yl]-naphthacene-5,12-diol (**4-2b**)

n-BuLi (1.57 M in hexane) (3.5 mL, 5.5 mmol) was added dropwise to a solution of 1-iode-3,5-diphenylbenzene (1.9 g, 5.3 mmol) in dry toluene (12 mL) and dry diethyl ether (4.1 mL) under a nitrogen atmosphere at −45 ºC. The mixture was allowed to stir for 1 h at −10 ºC. The mixture was added 5,12-naphthacenequinone **4-1** (0.54 g, 2.1 mmol) over 15 min, and the mixture was stirred for 5 h at room temperature. The excess of *n*-BuLi quenched by methanol, and the residue was removed by filtration. After removal of the solvent in *vacuo*, the residue was purified by rinse with methanol and column chromatography on silica gel ($CHCH_3$/hexane = 4/1) to give **4-2b** as white solid (0.43 g, 29%).

^{1}H NMR (400 MHz, $CDCl_3$) δ 8.51 (s, 2H), 8.10 (dd, *J* = 4.4 Hz, 3.2 Hz, 2H), 7.97 (dd, *J* = 4.4 Hz, 3.2 Hz, 2H), 7.55 (m, 4H), 7.16–7.09 (m, 26H), 3.00 (s, 2H, -OH); ^{13}C NMR (100 MHz, $CDCl_3$) δ 144.51, 141.20, 140.88, 140.48, 139.39, 132.72, 128.67, 128.36, 128.29, 128.24, 126.97, 126.30, 126.06, 125.37, 125.26, 125.23, 76.05; MS (FAB) *m/*z 719 (M^++1); HR-FAB *m/z* = 719.2956, calcd for $C_{54}H_{39}O_2$ = 719.8857 (M^++1).

5,12-Di[(1,1'-biphenyl)-4-yl]-naphthacene (**4-3a**)

Dry THF (54.0 mL) was added to a flask containing **4-2a** (1.78 g, 3.14 mmol) and purged with an argon for several minutes. $SnCl_2$ (4.57 g, 24.1 mmol) in *conc*. HCl (18.0 mL) was added dropwise to the solution over 30 min at 40 ºC. The mixture solution was refluxed for 2 h. After the solution was cooled to room temperature, poured into water. After stirred for 30 min, the precipitate was collected by filtration. The residue was washed again by the same operation. The precipitate was filtrated and washed with methanol. The crude product was purified with recrystallization form toluene to give **4-3a** as orange solid (1.58 g, 95%).

^{1}H NMR (400 MHz, $CDCl_3$) δ 8.41 (s, 2H), 7.91 (d, *J* = 5.0 Hz, 4H), 7.85-7.77 (m, 8H), 7.65 (d, *J* = 5.0 Hz, 4H), 7.56 (t, *J* = 7.2 Hz, 4H), 7.44, (t, *J* = 7.2 Hz, 2H), 7.32-7.32 (m, 4H); ^{13}C NMR (100 MHz, $CDCl_3$) δ 140.69, 140.17, 138.12, 136.59, 131.83, 130.88, 129.24, 128.97, 128.79, 128.26, 127.34, 127.06, 127.04, 126.88, 125.57, 125.08, 124.70; MS (MALDI-TOF) *m/z* 532 (M^++1); Anal. Calculated for $C_{42}H_{28}$: C, 94.70; H, 5.30. Found: C, 94.47; H, 5.53.

5,12-Di[(1,1':3',1''-terphenyl)-5'-yl]-naphthacene (**4-3b**)

Dry THF (9.0 mL) was added to a flask containing **4-2b** (0.305 g, 0.424 mmol) and purged with argon for several minutes. $SnCl_2$ (0.614 g, 3.24 mmol) in *conc*. HCl (3.5 mL) was added dropwise to the solution over 8 min at 40 ºC. The mixture solution was refluxed for 2 h. After

the solution was cooled to room temperature, poured into water. After stirred for 30 min, the precipitate was collected by filtration. The residue was washed again by the same operation. The precipitate was filtrated and washed with methanol. The crude product was purified with recrystallization form toluene to give **4-3b** as orange solid (0.253 g, 87%).

^{1}H NMR (400 MHz, $CDCl_3$) δ 8.50 (s, 2H), 8.10 (s, 2H), 7.87–7.79 (m, 16H), 7.48 (t, *J* = 7.2 Hz, 8H), 7.37 (t, *J* = 7.2 Hz, 4H), 7.32–7.29 (m, 4H); ^{13}C NMR (100 MHz, $CDCl_3$) δ 141.73, 140.64, 140.16, 136.74, 130.97, 129.29, 129.08, 128.96, 128.77, 128.32, 127.49, 127.18, 126.91, 125.62, 125.14, 125.03, 124.90; MS (FAB) *m/z* 685 (M^++1); HR-FAB *m/z* = 685.2892, calcd for $C_{54}H_{37}$ = 685.2890 (M^++1).

5,12-Dihydro-5,12-ethanonaphthacene-*cis*-13,14-diyl carbonate (**4-4H**)

A solution of naphthacene (0.50 g, 2.2 mmol) and vinylene carbonate (0.21 mL, 3.3 mmol) in xylene (10 mL) was heated at 180 °C in an autoclave for 3 d. After removal of the solvent in *vacuo*, the residue was rinsed with hexane to give **4-4H** (0.67 g, 95%).

5,12-Di[(1,1'-biphenyl)-4-yl]-6,11-dihydro-6,11-ethanonaphthacene-*cis*-13,14-diyl carbonate (**4-4a**)

A solution of **4-3a** (0.70 g, 1.3 mmol) and vinylene carbonate (0.70 mL, 11 mmol) in xylene (30 mL) was heated at 180 °C in an autoclave for 3 d. After removal of the solvent in *vacuo*, the residue was purified by rinse with hexane and column chromatography on silica gel ($CHCH_3$/hexane = 9/1) to give **4-4a** as white solid (0.75 g, 92%).

^{1}H NMR (400 MHz, CD_2Cl_2, Mixture of stereoisomers) δ 7.92–7.84 (m, 4H), 7.81 (d, *J* = 7.2 Hz, 4H), 7.66-7.54 (m, 8H), 7.46-7.38 (m, 6H), 7.33–7.22 (m, 4H), 5.00 (m, 1H), 4.88 (m, 1H), 4.81 (m, 2H); ^{13}C NMR (100 MHz, $CDCl_3$, Mixture of isomer) δ 153.70, 140.78, 140.58, 140.36, 140.27, 137.92, 136.96, 136.45, 136.30, 136.22, 136.12, 132.22, 131.69, 131.58, 130.99, 130.37, 130.34, 128.82, 128.77, 127.79, 127.75, 127.52, 127.40, 127.35, 127.33, 127.05, 127.01, 126.80, 126.65, 126.59, 126.43, 126.22, 125.87, 125.55, 76.16, 76.07, 45.22, 44.98; MS (FAB) *m/z* 619 (M^++1); Anal. Calculated for $C_{45}H_{30}O_3$•1/2$CHCl_3$: C, 80.55; H, 4.53. Found: C, 80.57; H, 4.56.

5,12-Di[(1,1':3',1''-terphenyl)-5'-yl]-6,11-dihydro-6,11-ethanonaphthacene-*cis*-13,14-diyl carbonate (**4-4b**)

A solution of **4-3b** (0.54 g, 0.79 mmol) and vinylene carbonate (1.0 mL, 16 mmol) in xylene (27

mL) was heated at 180 °C in an autoclave for 3 d. After removal of the solvent in *vacuo*, the residue was purified by rinse with hexane and column chromatography on silica gel ($CHCH_3$/hexane = 9/1) to give **4-4b** as white solid (0.48 g, 78%).

^{1}H NMR (400 MHz, CD_2Cl_2, Mixture of stereoisomers) δ 8.08 (m, 2H), 7.86–7.69 (m, 13H), 7.57–7.40 (m, 16H), 7.32–7.21 (m, 3H), 5.04 (m, 1H), 4.92 (m, 3H); ^{13}C NMR (100 MHz, $CDCl_3$, Mixture of isomer) δ 154.17, 153.68, 142.27, 142.24, 142.06, 141.58, 140.65, 140.50, 140.41, 140.38, 138.64, 138.48, 138.00, 137.23, 136.44, 136.38, 132.34, 131.80, 131.71, 131.20, 128.95, 128.93, 128.87, 128.60, 127.96, 127.82, 127.78, 127.66, 127.59, 127.53, 127.31, 127.29, 127.17, 127.15, 126.79, 126.72, 126.51, 126.14, 126.67, 125.63, 125.15, 76.68, 76.18, 45.42, 45.19.; MS (FAB) *m/z* 770 (M^+); HR-FAB *m/z* = 770.2821, calcd for $C_{57}H_{38}O_3$ = 770.2827 (M^+).

5,12-Dihydro-13,14-dihydroxy-5,12-ethanonaphtacene (**4-5H**)

4-4H (0.56 g, 1.9 mmol) was added to a mixture of 4 M NaOH aq. (5.0 mL) and 1,4-dioxane (20 mL) under a nitrogen atmosphere. The resulting mixture was refluxed for 2 h. The reaction mixture was cooled to room temperature, poured into water and then extracted with $CHCl_3$. The combined organic layer was washed with water and dried over Na_2SO_4. The solvent was removed under reduced pressure to give **4-5H** (0.52 g, 95%).

5,12-Di[(1,1'-biphenyl)-4-yl]-6,11-dihydro-13,14-dihydroxy-6,11-ethanonaphtacene (**4-5a**)

4-4a (0.69 g, 1.2 mmol) was added to a mixture of 4 M NaOH aq. (2.6 mL) and 1,4-dioxane (12 mL) under a nitrogen atmosphere. The resulting mixture was refluxed for 2 h. The reaction mixture was cooled to room temperature, poured into water and then extracted with $CHCl_3$. The combined organic layer was washed with water and dried over Na_2SO_4. The solvent was removed under reduced pressure to give **4-5a** (0.58 g, 83%)

^{1}H NMR (400 MHz, d6-DMSO, Mixture of stereoisomers) δ 7.95–7.85 (m, 8H), 7.74 (m, 1H), 7.59–7.48 (m, 7H), 7.42–7.33 (m, 6H), 7.12–7.09 (m, 4H), 4.87 (m, 1H), 4.64 (m, 1H), 4.39 (m, 1H), 4.29 (m, 1H), 4.06 (m, 1H, -OH), 3.89 (m, 1H, -OH); ^{13}C NMR (100 MHz, d6-DMSO, Mixture of stereoisomers) δ 140.44, 139.72, 139.58, 139.29, 139.24, 128.85, 136.79, 136.65, 135.78, 135.16, 134.91, 133.77, 131.78, 130.78, 130.75, 130.46, 128.95, 128.92, 127.53, 127.42, 126.83, 126.66, 126.60, 126.49, 126.38, 125.82, 125.71, 125.62, 125.08, 124.37, 66.67, 66.59, 49.04, 48.55; MS (FAB) *m/z* 593 (M^++1); Anal. Calculated for $C_{44}H_{32}O_2$: C, 89.16; H, 5.44. Found: C, 89.04; H, 5.49.

5,12-Di[(1,1':3',1''-terphenyl)-5'-yl]-6,11-dihydro-13,14-dihydroxy-6,11-ethanonaphtacene (4-5b)

4-4a (0.97 g, 1.3 mmol) was added to a mixture of 4 M NaOH aq. (3.6 mL) and 1,4-dioxane (17 mL) under a nitrogen atmosphere. The resulting mixture was refluxed for 2 h. The reaction mixture was cooled to room temperature, poured into water and then extracted with $CHCl_3$. The combined organic layer was washed with water and dried over Na_2SO_4. The solvent was removed under reduced pressure to give **4-5b** (0.69 g, 72%)

^{1}H NMR (400 MHz, $CDCl_3$, Mixture of stereoisomers) δ 8.01 (m, 2H), 7.90 (m, 1H), 7.82–7.68 (m, 11H), 7.55–7.34 (m, 17H), 7.24–7.11 (m, 3H), 4.64 (m, 2H), 4.14 (m, 2H), 2.24 (m, 2H, -OH); ^{13}C NMR (100 MHz, $CDCl_3$) δ 141.90, 141.82, 141.55, 141.43, 140.64, 140.50, 140.15, 138.98, 138.57, 136.60, 134.96, 134.93, 133.89, 131.33, 128.83, 128.77, 128.75, 127.87, 127.80, 127.64, 127.53, 127.50, 127.43, 127.41, 127.24, 127.17, 127.06, 126.93, 126.79, 126.51, 126.46, 126.37, 125.73, 125.51, 125.14, 124.79, 124.67, 68.10, 67.88, 48.83, 48.47; MS (FAB) *m/z* 745 (M^++1); Anal. Calculated for $C_{56}H_{40}O_2$•H_2O: C, 88.16; H, 5.55. Found: C, 88.40; H, 5.37.

5,12-Dihydro-5,12-ethanonaphthacene-13,14-dione (4-6H)

Trifluoroacetic anhydride (1.9 mL, 27 mmol) was added dropwise to a mixture of dry DMSO (0.15 mL, 27 mmol) and dry CH_2Cl_2 (18 mL) at −60 °C under an argon. After stirring for 10 min, **4-5H** (0.45 g, 1.6 mmol) dissolved in a mixture of dry DMSO (5.0 mL) was added dropwise. After stirring for 90 min, *N,N*-diisopropylethylamine (9.2 mL, 53 mmol) was added dropwise to the reaction mixture. The solution was stirred at −60 °C for 60 min and warmed to room temperature. 1 M HCl (86 mL) was added to the mixture for quenching the reaction. The mixture was extracted with CH_2Cl_2, and the combined organic layers were washed with water and brine and dried with Na_2SO_4. After removal of the solvent in *vacuo*, the residue was purified by column chromatography on silica gel with CH_2Cl_2 and recrystallized from toluene to give **4-6H** as yellow crystals (0.32 g, 69%). ^{1}H NMR (400 MHz, $CDCl_3$) δ 7.93 (s, 2H), 7.84 (dd, *J* = 6.2 Hz, 3.2 Hz, 2H), 7.53-7.48 (m, 4H), 7.38 (dd, *J* = 6.2 Hz, 3.2 Hz, 2H); ^{13}C NMR (100 MHz, $CDCl_3$) δ 184.33, 134.85, 133.42, 131.62, 129.42, 127.77, 126.90, 126.24, 125.25, 60.26; MS (DI-EI) *m/z* 284 (M^+); Anal. Calculated for $C_{20}H_{12}O_2$: C, 84.49; H, 4.25. Found: C, 84.36; H, 4.45.

5,12-Di[(1,1'-biphenyl)-4-yl]-6,11-dihydro-6,11-ethanonaphthacene-13,14-dione (4-6a)

Trifluoroacetic anhydride (0.30 mL, 2.2 mmol) was added dropwise to a mixture of dry DMSO

(1.9 mL, 2.1 mmol) and dry CH_2Cl_2 (1.5 mL) at −60 °C under argon. After stirring for 10 min, **4-5a** (0.080 g, 0.13 mmol) dissolved in a mixture of dry DMSO (2.8 mL) and dry CH_2Cl_2 (2.8 mL) was added dropwise. After stirring for 90 min, *N,N*-diisopropylethylamine (0.76 mL, 4.4 mmol) was added dropwise to the reaction mixture. The solution was stirred at –60 °C for 60 min and warmed to room temp. 3 M HCl (8 mL) was added to the mixture for quenching the reaction. The mixture was extracted with CH_2Cl_2, and the combined organic layers were washed with water and brine and dried with Na_2SO_4. After removal of the solvent in *vacuo*, the residue was purified by column chromatography on silica gel with CH_2Cl_2 and recrystallized from toluene to give **4-6a** as yellow crystals (0.064 g, 85%). ^{1}H NMR (400 MHz, $CDCl_3$) δ 7.88 (dd, *J* = 8.0, 2.0 Hz, 2H), 7.83 (dd, *J* = 8.0, 2.0 Hz, 2H), 7.77 (d, *J* = 7.2 Hz, 4H), 7.70 (m, 2H), 7.56-7.51 (m, 6H), 7.46-7.38 (m, 6H), 7.35 (s, 4H), 5.16 (s, 2H); ^{13}C NMR (100 MHz, $CDCl_3$) δ 185.29, 140.93, 140.45, 137.11, 135.60, 135.52, 132.56, 131.13, 130.51, 129.74, 129.33, 128.90, 127.70, 127.59, 127.27, 127.13, 126.89, 126.68, 126.19, 58.09; MS (DI-EI) *m/z* 589 (M^++1); Anal. Calculated for $C_{44}H_{28}O_2$: C, 89.77; H, 4.79. Found: C, 89.62; H, 4.81.

5,12-Di[(1,1':3',1''-terphenyl)-5'-yl]-6,11-dihydro-6,11-ethanonaphthacene-13,14-dione (4-6b)

Trifluoroacetic anhydride (1.6 mL, 1.2 mmol) was added dropwise to a mixture of dry DMSO (0.82 mL, 12 mmol) and *dry*-CH_2Cl_2 (8.0 mL) at −60 °C under argon. After stirring for 10 min, **4-5b** (0.33 g, 0.44 mmol) dissolved in a mixture of dry DMSO (12 mL) and dry CH_2Cl_2 (10 mL) was added dropwise. After stirring for 90 min, *N,N*-diisopropylethylamine (3.9 mL, 22 mmol) was added dropwise to the reaction mixture. The solution was stirred at –60 °C for 60 min and warmed to room temp. 3 M HCl (8 mL) was added to the mixture for quenching the reaction. The mixture was extracted with CH_2Cl_2, and the combined organic layers were washed with water and brine and dried with Na_2SO_4. After removal of the solvent in *vacuo*, the residue was purified by column chromatography on silica gel with CH_2Cl_2 and recrystallized from toluene to give **4-6b** as yellow crystals (0.27 g, 0.36 mmol, 82%). ^{1}H NMR (400 MHz, $CDCl_3$) δ 8.05 (s, 2H), 7.83-7.74 (m, 10H), 7.66 (s, 2H), 7.58 (s, 2H), 7.53-7.49 (m, 8H), 7.45-7.42 (m, 4H), 5.25 (s, 2H); ^{13}C NMR (100 MHz, $CDCl_3$) δ 185.17, 142.37, 141.92, 140.36, 140.19, 137.66, 137.23, 135.37, 132.46, 129.76, 129.32, 128.84, 128.25, 127.70, 127.65, 127.38, 127.26, 127.09, 126.84, 126.78, 126.12, 125.63, 58.16; MS (DI-EI) *m/z* 741 (M^++1); Anal. Calculated for $C_{56}H_{34}O_2$: C, 90.78; H, 4.90. Found: C, 90.70; H, 4.90.

4-3 Fluorescence switching of pyrene using α-diketone type precursor as a fluorescence quenching unit

4-3-1 Molecular Design

As described in the previous section, one-way fluorescence control of α-diketone type acene precursor in solution or in film is discussed. Liao and co-workers have synthesized micelle encapsulated α-diketone type precursors of anthracene derivatives as a photoactivatable carbon oxide (CO) releasing material.[18] The precursors of affinity for cells are increased by micelle encapsulation. The precursor allows to deliver to monitored area and generate COs by the photoactivation in physiological conditions. Since the damaged area can be monitored by the fluorescence of converted anthracene, the precursor method is also useful for the research of biological CO function. However, the adjusting of fluorescence wavelength and fluorescence quantum yield is limited because the fluorescence change is derived from the structural change of photoprecursor. In order to develop the fluorescence control using the precursor method, the author of this thesis focused on the combination of α-diketone type photoprecursor of anthracene (**ADK)** and fluorophore unit (Figure 4-17). **ADK** also doesn't show fluorescence since the excited energy is used for the photoreaction.[19] Therefore, **ADK** could behave as an intramolecular fluorescence quenching unit for short wavelength fluorophores. On the other hand, decarbonylated anthracene-fluorophore conjugate doesn't have fluorescence quenching unit in the molecule and will show contrasting fluorescence.

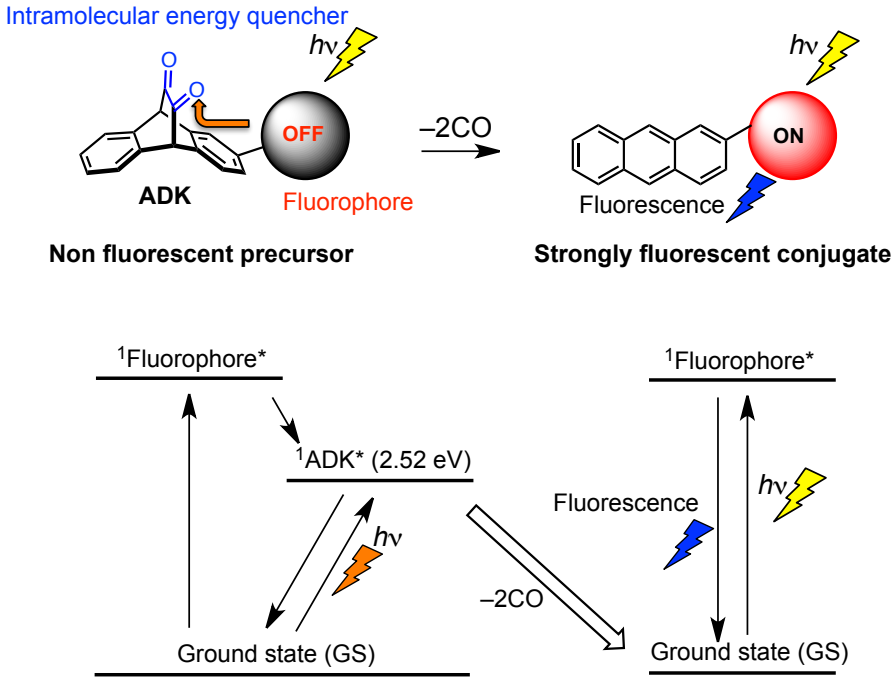

Figure 4-17. Molecular design for fluorescence switching system using α-diketone type photoprecursor as an intramolecular fluorescence quenching unit.

Pyrene is one of the best candidate as a fluorophore for preparing developed photoprecursor method and a versatile blue-fluorophore with high fluorescence quantum yield (Figure 4-18).[20] Compared with the energy level of excited singlet state of **ADK**, the energy level of pyrene is high enough. In addition, pyrene derivatives can be easily synthesized. Aryl-pyrene conjugates are also one of the strongly fluorescent materials. The introductions of substituent to the 1-position of pyrene effectively improve the fluorescence quantum yield, especially, 1-ethynylphenylpyrene shows extremely high quantum yield.[21]

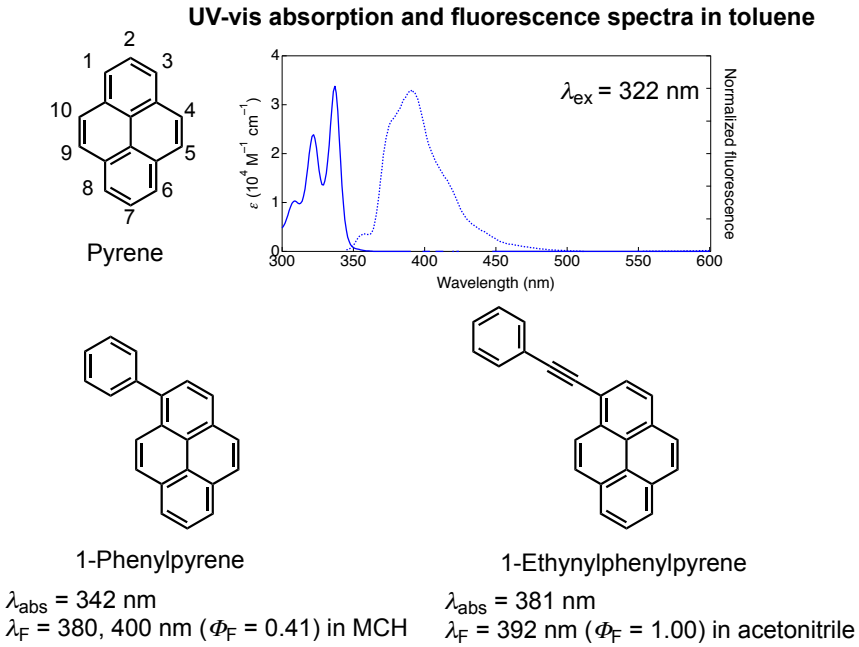

Figure 4-18. Optical properties of pyrene and 1-substituted pyrene.

Consequently, the author of this thesis designed two types of **ADK**-pyrene conjugates (**Py-DK** and **Py-3-DK**) as latent fluorescence molecules (Figure 4-19). In this section, the synthesis, optical properties and photoconversions in solution or film are discussed.

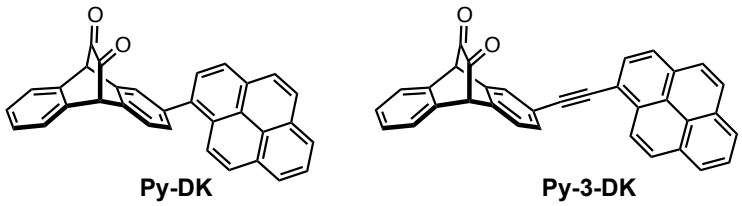

Figure 4-19. Target compounds of photoprecursor-pyrene conjugates.

4-3-2 Synthesis

The synthesis of α-diketone type precursors **Py-DK** and **Py-3-DK** is shown in Schemes 4-3 and 4-4. 2-Bromoanthracene (**4-7**) was reacted with vinylene carbonate by the Diels-Alder reaction to give carbonate adduct (**4-8**) as a mixture of stereoisomers. The compound **4-8** was coupled with pyreneboronic acid by Suzuki-Miyaura coupling to give **4-9** in 51% yield. The compound **4-11** was also obtained with 2-ethynylpyrene by Sonogashira coupling in 34% yield. The compounds were subsequently hydrolyzed to give diols (**4-10** and **4-12**), which was oxidized by the Swern reaction to give α-diketone compounds (**Py-DK** and **Py-3-DK**).

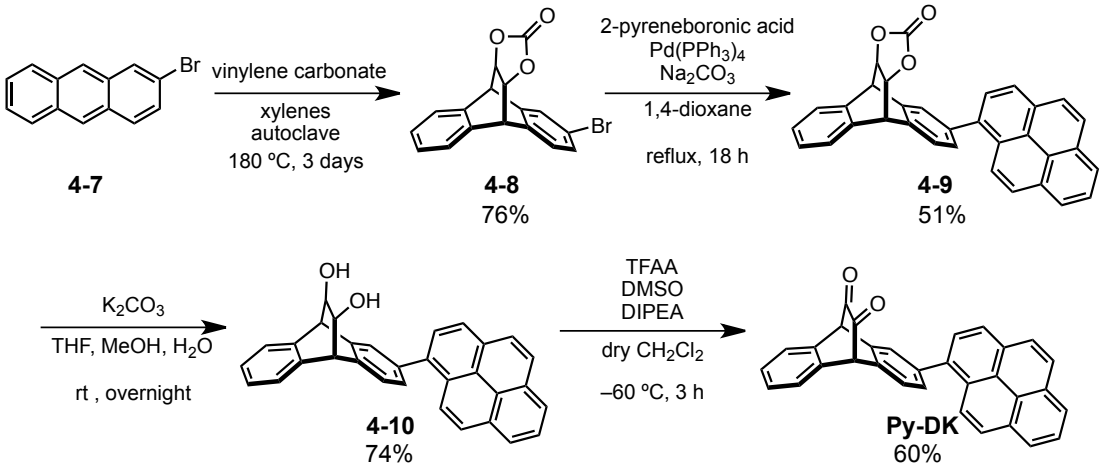

Scheme 4-3. Synthesis route of **Py-DK**.

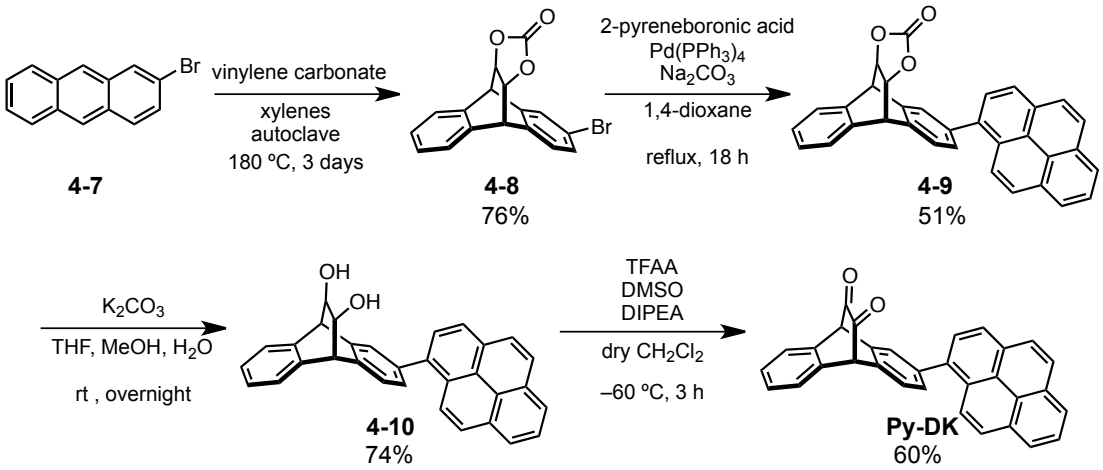

Scheme 4-4. Synthesis route of **Py-3-DK**.

4-3-3 Optical Properties of Precursors

UV-vis absorption spectra

The UV-vis absorption spectrum of α-diketone type precursor **Py-DK** in toluene is shown in Figure 4-20. The absorption spectrum shows two major bands at 461 nm (ε = 7.40 × 10^2 M^{-1} cm^{-1}) and 348 nm (ε = 2.71 × 10^4 M^{-1} cm^{-1}). Molecular orbitals (MO) and time-dependent density functional theory (TDDFT) calculation was performed using the Gaussian 09 program package at the CAM-B3LYP/6-31G(d)//B3LYP-6-31G(d) level of theory.[22] TDDFT calculation indicated the weak transition at 451 nm that was mainly composed of the transition from HOMO−2 to LUMO, which corresponds to n–π* transition at the carbonyl moieties. In addition, the absorption at 461 nm is slightly larger than that of **ADK**, due to the overlap of CT-like absorption from the pyrene moiety to the carbonyl moiety. TDDFT calculation also indicated a transition at 324 nm that is mainly composed of the transition from HOMO to LUMO+1, which corresponds to the π–π* transition at pyrene moiety. The UV-vis absorption spectrum of **Py-3-DK** is shown in Figure 4-21. The absorption spectrum shows broad bands at 462 nm (ε = 1.45 × 10^3 M^{-1} cm^{-1}) and large band at 368 nm (ε = 3.41 × 10^4 M^{-1} cm^{-1}). MO and TDDFT calculation was also performed at the CAM-B3LYP/6-31G(d)//B3LYP-6-31G(d) level of theory. The conjugate of the two chromophores are not completely independent, the electron density delocalized on the whole molecule through ethynyl bridge. The transition at 451 nm that was mainly composed of the transition from HOMO−2 or HOMO−1 to LUMO or LUMO−1, which include n–π* transition at the carbonyl moieties. Similar to **Py-DK**, charge transfer transition from pyrene moiety to carbonyl moiety is suggested in the calculation. Also, the band at assigned 368 nm was calculated to the transitions from HOMO to LUMO or LUMO+1, which correspond to ICT from the pyrene moiety to the carbonyl moiety and the π-π* transition of pyrene moiety.

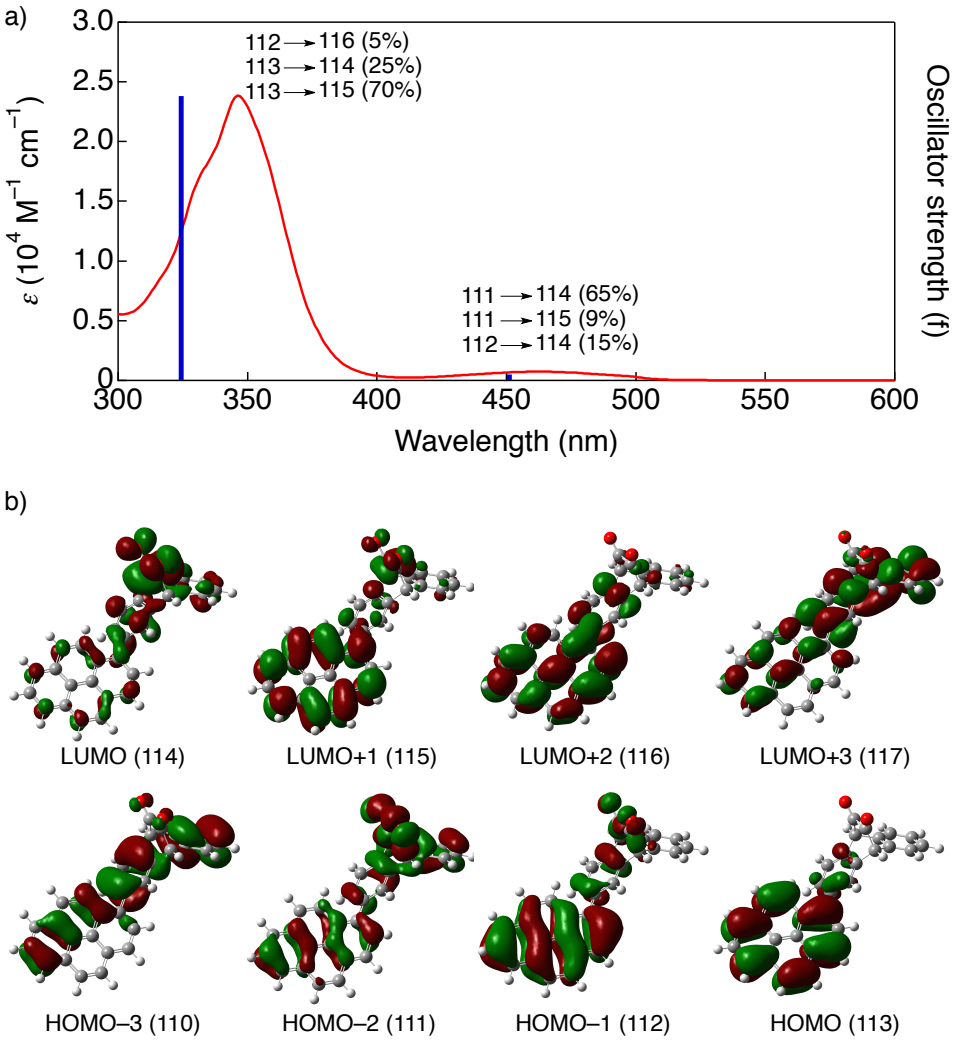

Figure 4-20. (a) UV-vis absorption spectrum (red) and TDDFT calculation (blue) at CAM-B3LYP/6-31G(d) level of **Py-DK**; (b) Molecular orbitals by DFT calculation at B3LYP/6-31G (d) level.

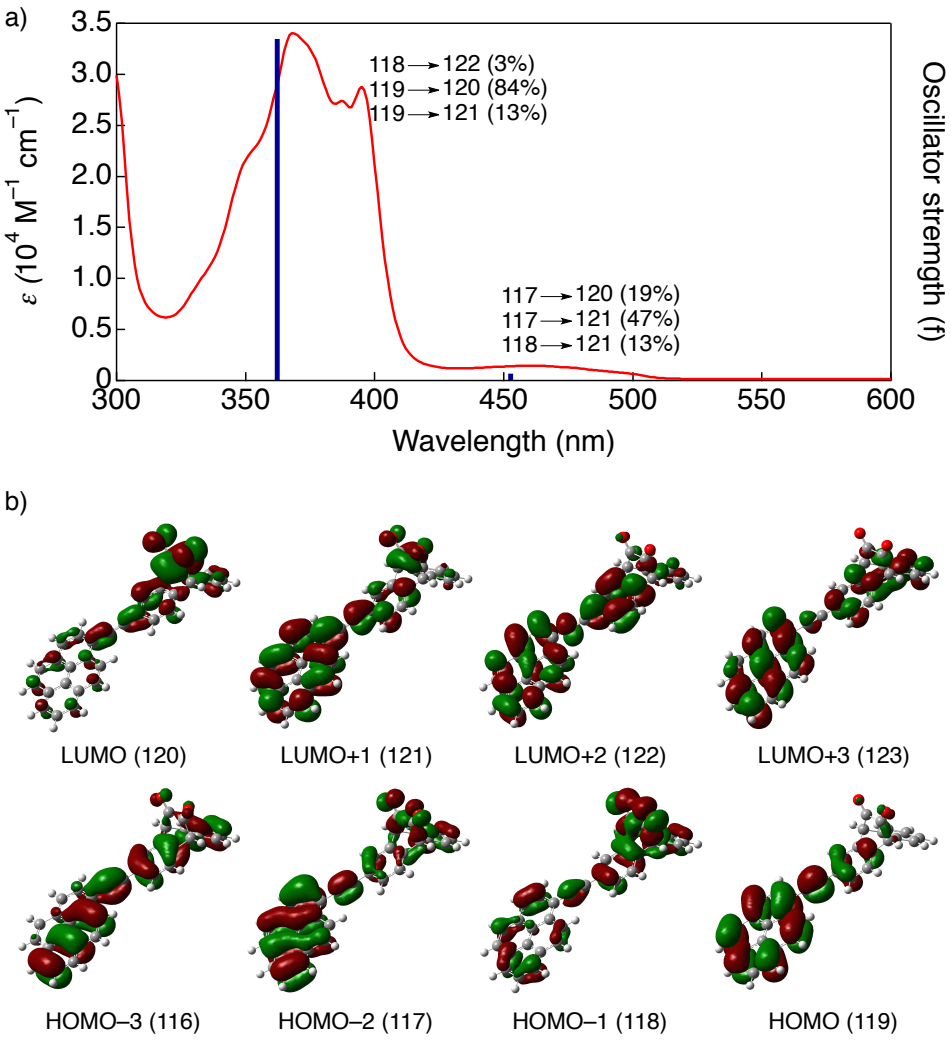

Figure 4-21. (a) UV-vis absorption spectrum (red) and TDDFT calculation (blue) at CAM-B3LYP/6-31G(d) level of **Py-3-DK**; (b) Molecular orbitals by DFT calculation at B3LYP/6-31G (d) level.

The fluorescence properties were measured in toluene for each precursor (Figure 4-22). **Py-DK** and **Py-3-DK** were non-fluorescent with excitation at 460 nm due to the quenching of the excited state of pyrene by the diketone moiety. On the other hand, the Φ_F of **Py-DK** and **Py-3-DK** was 0.029 and 0.061, respectively, in the beginning of the measurement, but Φ_Fs increased gradually at every measurement. These results imply that the precursors immediately reacted to release CO molecules when they were excited for the measurement of fluorescence quantum yield.

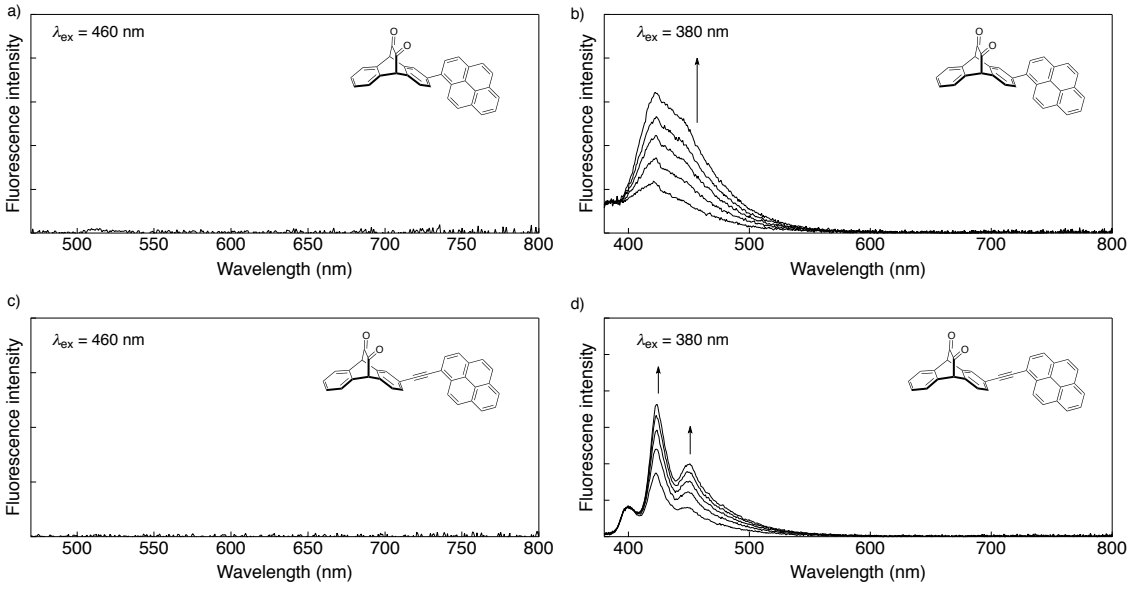

Figure 4-22. Fluorescence spectra of **Py-DK** by excited at (a) λ_{ex} = 460 nm and (b) λ_{ex} = 380 nm; Fluorescence spectra of **Py-3-DK** by excited at (c) λ_{ex} = 460 nm and (b) λ_{ex} = 380 nm.

4-3-3 Photoconversions in Solution

^{1}H NMR spectra

The photoconversion of the precursors to pyrene-anthracene conjugates were performed using a xenon light source through a monochromater (λ = 370 nm) under an argon atmosphere. Figure 4-23 shows the changes in ^{1}H NMR spectra during the photoconversion of **Py-DK** in $CDCl_3$. The singlet peaks at 5.12 and 5.16 ppm, assigned to H^a and $H^{a'}$ of the diketone moiety, gradually decrease, while the peaks at 8.54 and 8.56 ppm, which are assigned to the peri protons H^b and $H^{b'}$ of **Py-Ant**, increase. After 40 min, the photoconversion was complete without any NMR signals of by-products. The same analysis was performed using **Py-3-DK** in $CDCl_3$ (Figure 4-24). During the photoreaction, the peaks at 5.07 and 5.08 ppm decreased while those at 8.76 and 8.79 ppm increased, indicating the formation of **Py-3-Ant**. These results demonstrate that **Py-DK** and **Py-3-DK** were quantitatively converted photochemically to the corresponding aromatic compounds **Py-Ant** and **Py-3-Ant**, respectively.

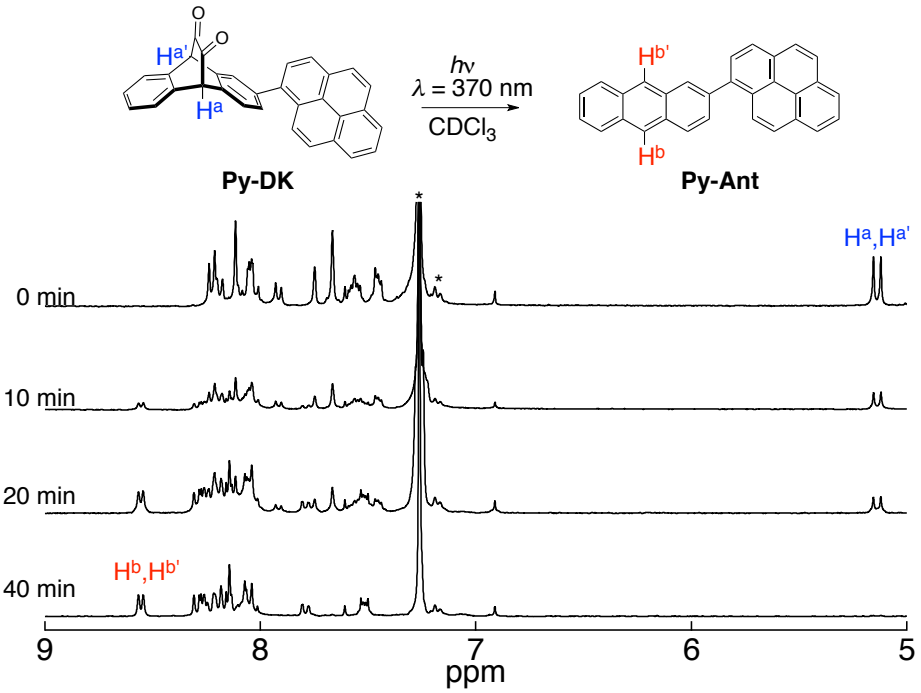

Figure 4-23. Changes in the ^{1}H NMR spectra of **Py-DK** during photolysis in $CDCl_3$ under argon. λ_{ex} = 370 nm. *Solvents.

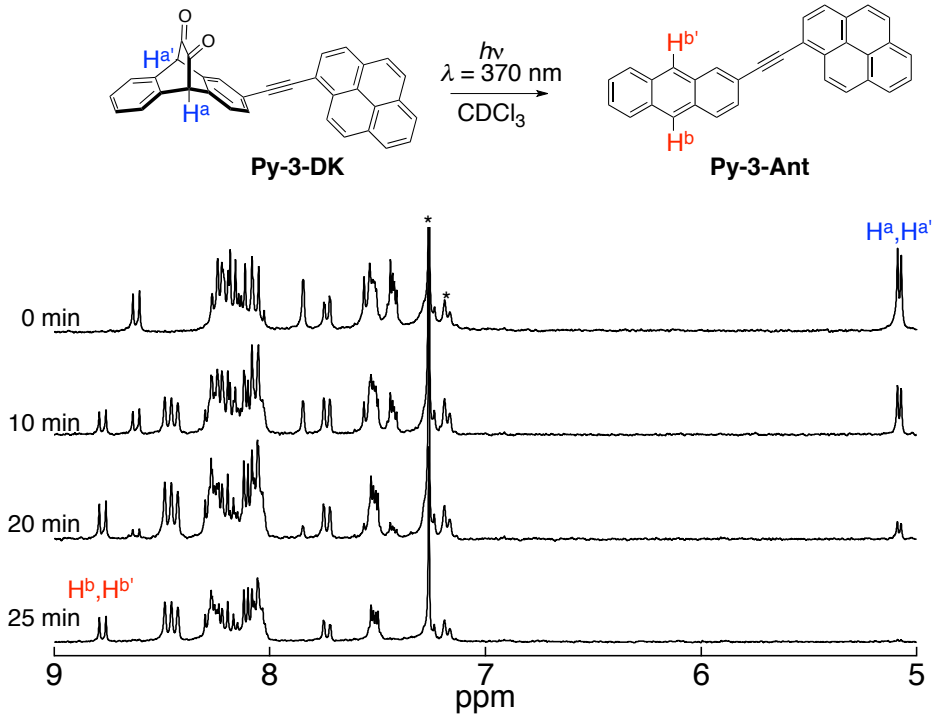

Figure 4-24. Changes in the ^{1}H NMR spectra of **Py-3-DK** during photolysis in $CDCl_3$ under argon. λ_{ex} = 370 nm. *Solvents.

Changes UV-vis absorption and fluorescence spectra

Figure 4-25 shows the changes in UV-vis absorption spectra during the photoconversion of **Py-DK** in toluene under an argon atmosphere. When **Py-DK** was irradiated at 468 nm (1.86 mW/ cm^2), decarbonylation occurred giving the corresponding **Py-Ant**. The relative quantum yield of the photoconversion reaction of **Py-DK** excited at 468 nm was 0.29, compared to the absolute quantum yield of **ADK** (0.37). The photoconversion of **Py-DK** was also performed by excitation at π-π* absorption of pyrene moiety (370 nm, <0.88 mW/cm^2) monitored by the spectral change of the absorption and fluorescence in toluene (Figure 4-26). During the irradiation, the blue fluorescence increased, since **Py-DK** was not fluorescent while **Py-Ant** was strongly fluorescent.

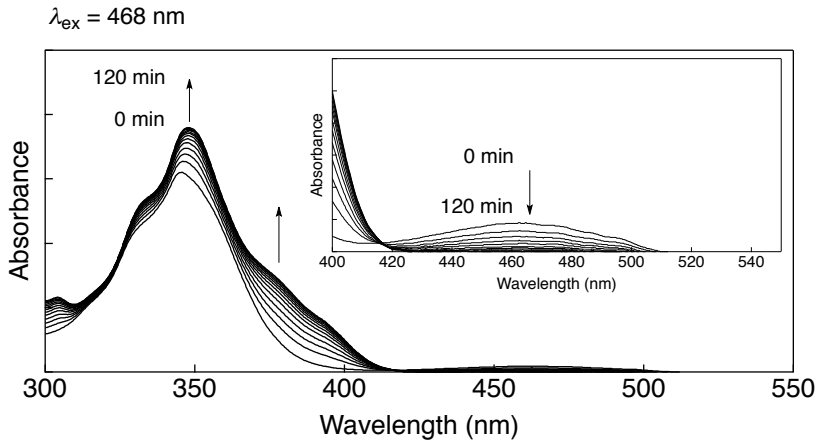

Figure 4-25. Changes in UV-vis absorption spectra during photolysis (λ_{ex} = 468 nm) of **Py-DK** in toluene (4.5×10^{-2} M).

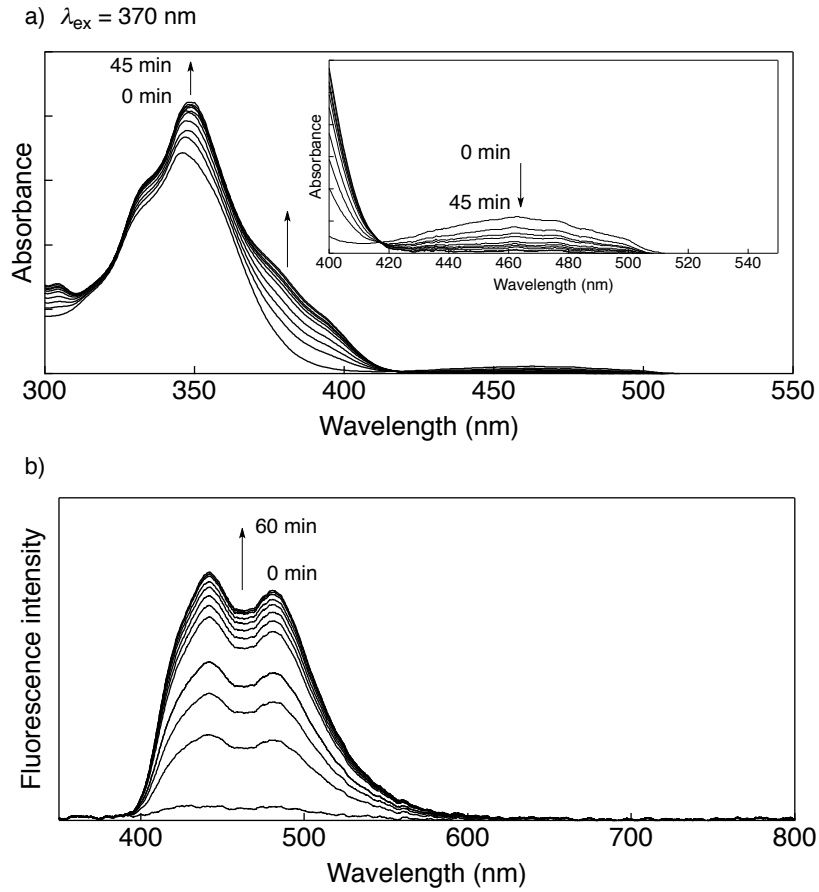

Figure 4-26. Changes in UV-vis absorption spectra (5.6×10^{-2} M) and fluorescence spectra (4.4×10^{-2} M) during photolysis (λ_{ex} = 370 nm) of **Py-DK** in toluene.

The changes of UV-vis absorption spectra of **Py-3-DK** during the photoconversion in toluene under argon atmosphere are shown in Figure 4-27 and Figure 4-28. Similarly, the absorption and fluorescence spectra changed from the precursor to **Py-3-Ant** with photoconversion. The relative quantum yield of the photoconversion reaction of **Py-3-DK** was 0.27 excited at 478 nm.

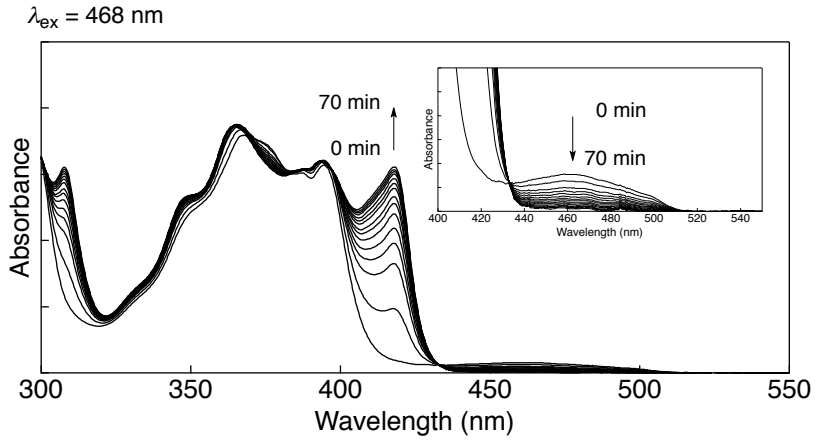

Figure 4-27. Changes in UV-vis absorption spectra during photolysis (λ_{ex} = 468 nm) of **Py-3-DK** in toluene (5.6×10^{-2} M).

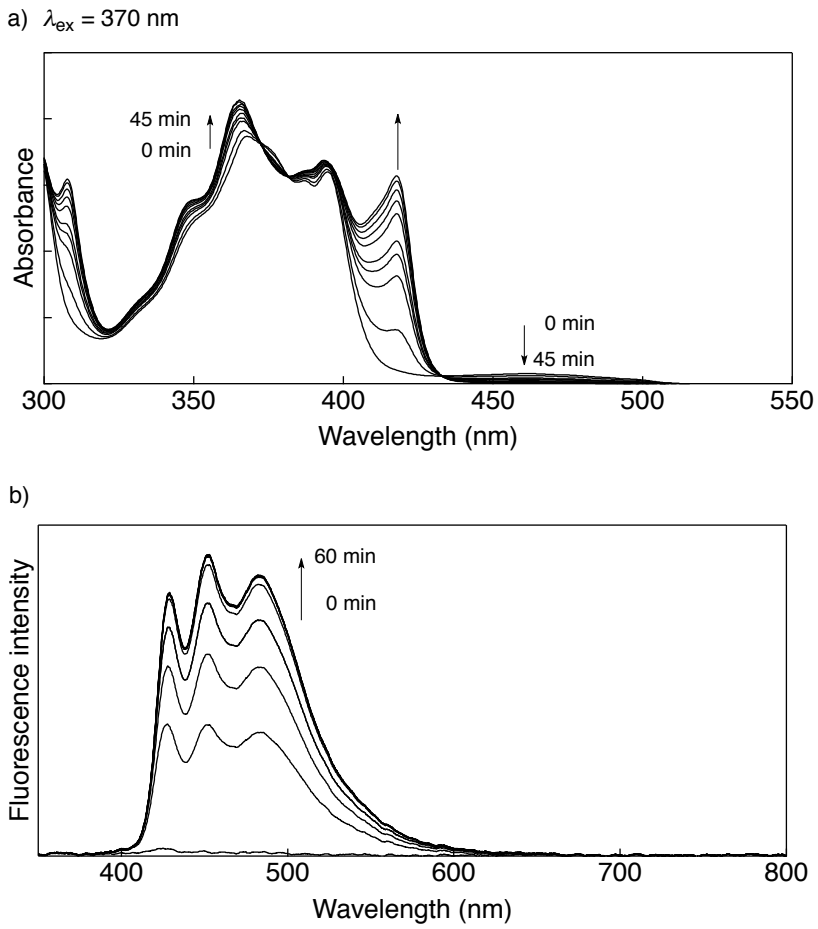

Figure 4-28. Changes in UV-vis absorption spectra (6.0×10^{-2} M) and fluorescence spectra (3.8×10^{-2} M) during photolysis (λ_{ex} = 370 nm) of **Py-3-DK** in toluene.

4-3-4 Optical Properties of converted structures

The UV-vis absorption and fluorescence spectra of **Py-Ant** in toluene, dichloromethane, benzonitrile and DMSO are shown in Figure 4-29 and summarized in Table 4-2. The UV-vis absorption spectrum of **Py-Ant** shows a peak at 349 nm ($\varepsilon = 4.50 \times 10^4$ M^{-1} cm^{-1}) with associated shoulders at both sides in toluene. **Py-Ant** exhibited emission at 443 and 478 nm, with a fluorescence quantum yield (Φ_F) of 0.86. The absorption spectra are almost the same in each solvent, while the fluorescence spectra showed clear solvent effects. The fluorescence peak maxima (λ_F) exhibit changes in response to increasing the solvent polarity. Furthermore, the Φ_Fs were also significantly different: λ_F = 443 nm and 478 nm (Φ_F = 0.86) in toluene, 486 nm (Φ_F = 0.92) in dichloromethane, 486 nm (Φ_F = 0.99) in benzonitrile and 496 nm (Φ_F = 0.91) in DMSO. These results correspond well with the known superposition of a

nonpolar locally excited (LE) and a strongly polar charge transfer (CT) contribution of substituted pyrene compounds. The fluorescence lifetimes (τ_F) of **Py-Ant** were measured by femtosecond laser flash photolysis in each solvent, with excitation at 366 nm (Figure 4-30 and Table 4-2). The τ_Fs were determined to be 4.22 in toluene, 4.26 and 6.71 ns in dichloromethane, 4.79 and 8.78 ns in benzonitrile, and 4.47, 7.69 ns in DMSO. The τ_F values in dichloromethane, benzonitrile and DMSO were calculated using double-exponentials, because the excited state has two components of LE and CT states.[21,23] In non-polar solvent such as toluene, emission from LE state mainly contributes to fluorescence waveform, and the two peak tops are derived from fluorescence at LE state because the fluorescence decay is single-exponential. On the other hand, emission from CT state has an maximum peak at 496 nm in DMSO, then the two components are mixed from LE and CT in polar solvents.

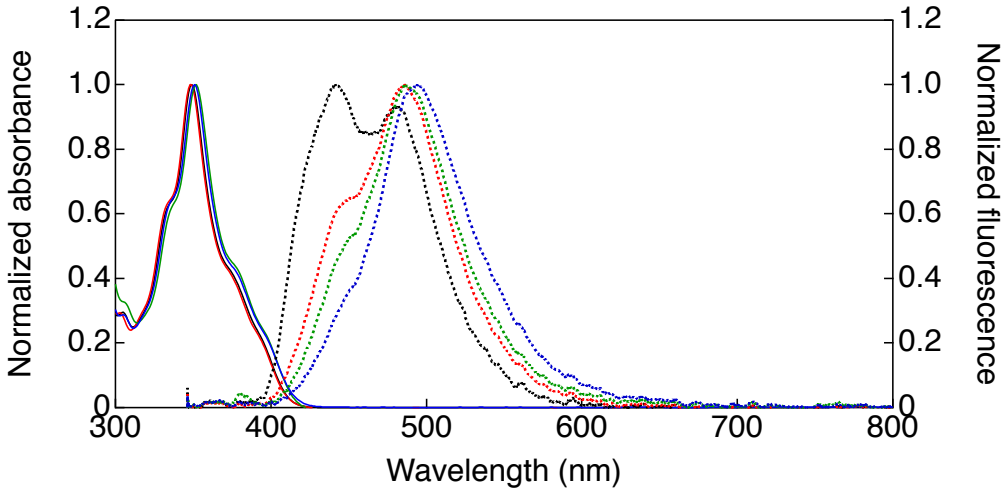

Figure 4-29. Normalized UV-vis absorption (solid) and fluorescence spectra (dotted) of **Py-Ant** in toluene (black), dichloromethane (red), benzonitrile (green) and DMSO (blue).

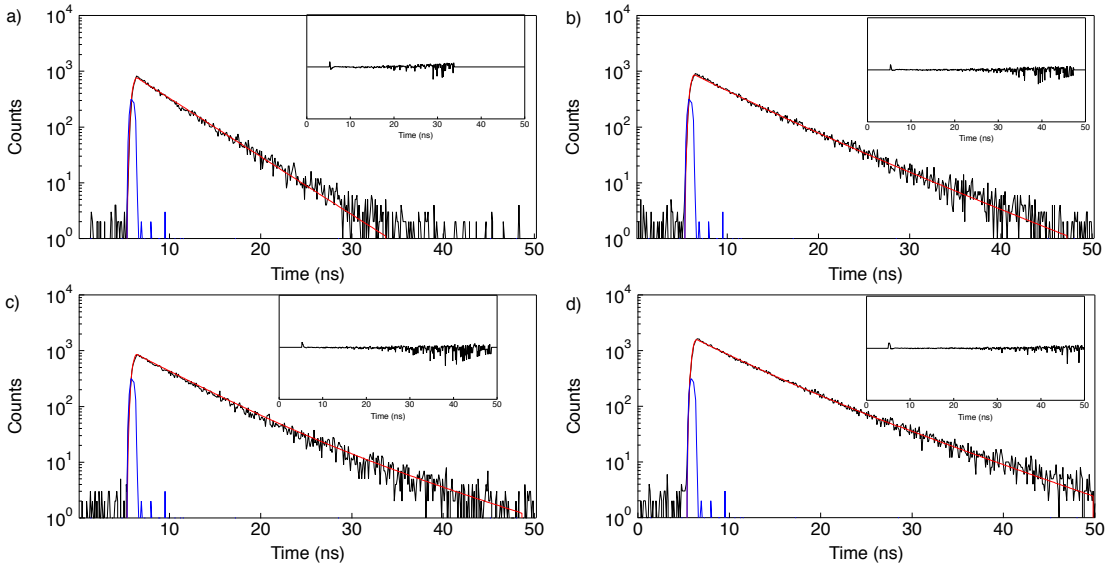

Figure 4-30. Fluorescence decays of **Py-Ant** by excited at 366 nm in (a) toluene, (b) dichloromethane (c) benzonitrile, and (d) DMSO.

A similar tendency was observed for **Py-3-Ant** (Figure 4-31). The UV-vis absorption spectrum of **Py-3-Ant** showed four peaks at 308, 365, 393 and 418 nm in toluene. Due to the triple bonds between pyrene and anthracene moieties the π-conjugation of **Py-3-Ant** expanded more than that of **Py-Ant**, which resulted in a red-shift of the absorption spectra. Fluorescence spectra of **Py-3-Ant** also showed the solvent effects: λ_F = 426, 450 and 482 nm in toluene (Φ_F = 0.90), 485 (Φ_F = 0.92) in dichloromethane, 488 (Φ_F = 0.94) in benzonitrile and 497 (Φ_F = 0.95) in DMSO. The τ_Fs of **Py-3-Ant** were measured in each solvent. The τ_Fs were determined to be 1.98 ns in toluene, 2.85 ns in dichloromethane, 2.96 in benzonitrile, 3.56 and 5.59 ns in DMSO.

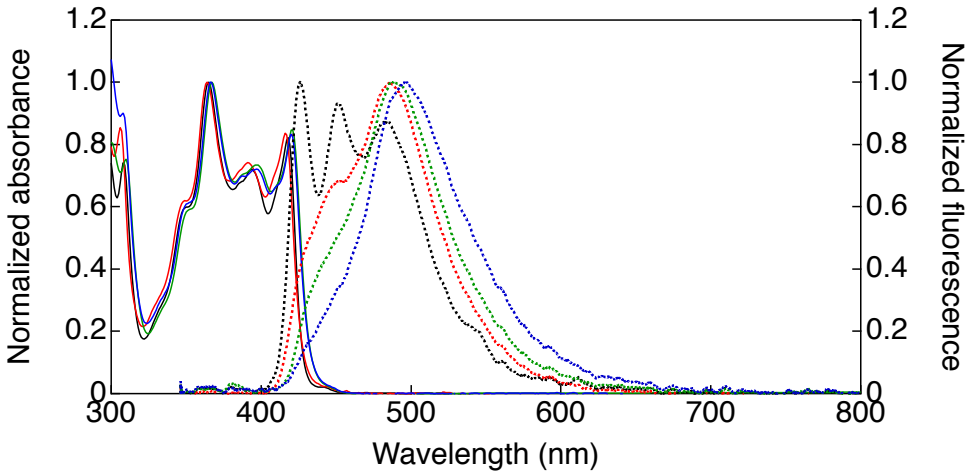

Figure 4-31. Normalized UV-vis absorption (solid) and fluorescence spectra (dotted) of **Py-3-Ant** in toluene (black), dichloromethane (red), benzonitrile (green) and DMSO (bleu).

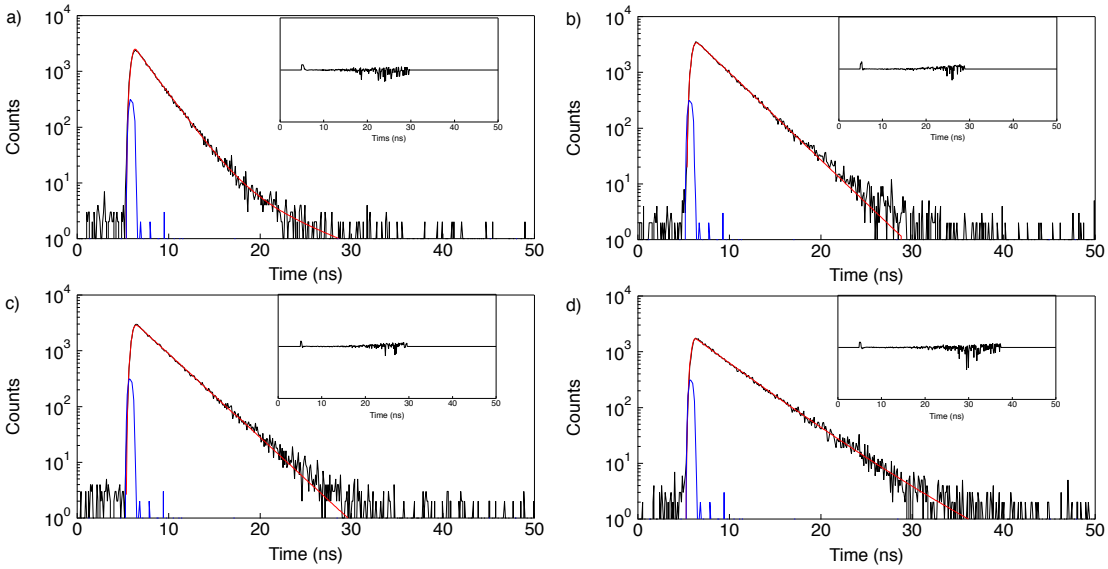

Figure 4-32. Fluorescence decays of **Py-3-Ant** by excited at 366 nm in (a) toluene, (b) dichloromethane (c) benzonitrile, and DMSO (d).

Table 4-2. Absorption and fluorescence peaks (λ_{abs} and λ_F), fluorescence quantum yields (Φ_f) and fluorescence lifetimes (τ_F) of **Py-Ant** and **Py-3-Ant** in various solvents.

Compound	Solvent (ε) [a]	Toluene (2.38)	CH_2Cl_2 (8.93)	PhCN (25.2)	DMSO (46.5)
Py-Ant	λ_{abs}/ nm	349	348	352	351
	λ_F [b]/ nm	443, 478	486	486	496
	Φ_f	0.86	0.92	0.99	0.91
	τ_F [c]/ ns (A)	4.22	4.26 (0.46) 6.71 (0.54)	4.79 (0.85) 8.78 (0.15)	4.47 (0.61) 7.69 (0.39)
	χ^2	1.64	1.33	1.39	1.11
Py-3-Ant	λ_{abs}/nm	308, 365, 393, 418	308, 364, 391, 416	310, 366, 397, 420	308, 367, 397, 421
	λ_F/nm	426, 450, 382	485	488	497
	Φ_f	0.86	0.92	0.94	0.95
	τ_F/ ns (A)	1.98 (0.99) 6.74 (0.01)	2.85	2.96	3.56 (0.92) 5.59 (0.08)
	χ^2	1.68	1.52	1.14	1.40

[a]Dielectric constant. [b]Excited at 380 nm. [c]Excited at 366 nm.

4-3-5 Photoconversions in PMMA film

The photoconversion of **Py-DK** in the PMMA film was performed, as shown in Figure 4-33. After photoirradiation over 390 nm for 10 min, the Φ_F of **Py-Ant** was increased to 0.23. For the **Py-DK** film fluorescence was also observed around 420 nm with Φ_F less than 0.02, which belonged to **Py-Ant** generated during the measurement. This result indicates that **Py-DK** in film is highly sensitive to the light and the photoconversion from **Py-DK** to **Py-Ant** occurred during the measurement.

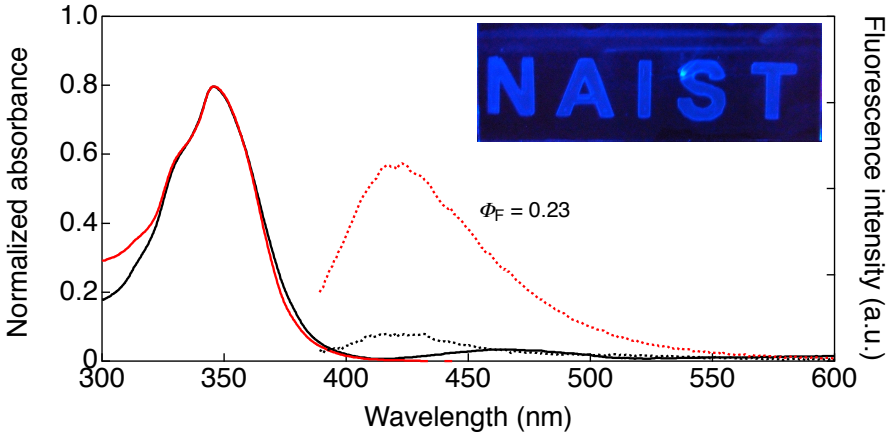

Figure 4-33. UV-vis absorption (solid) and fluorescence (dotted) spectra of **Py-DK** (black) and **Py-Ant** (red) in PMMA

4-3-6 Short Summary

Py-DK and **Py-3-DK** were prepared as latent fluorophores. The emission from pyrene moiety was effectively quenched by α-diketone unit because the excited singlet state of pyrene is higher than that of diketone moiety. The photoconversions of the precursors were monitored by ^{1}H NMR spectra, UV-vis absorption and fluorescence spectra in solution and PMMA film. **Py-Ant** and **Py-3-Ant**, which was obtained by photoconversion, shows high fluorescence quantum yield (Φ_F = 0.86–0.99) in solution. Thus, the highly contrast fluorescence switch of pyrene was succeeded to connect with α-diketone precursor as an intramolecular fluorescence quencher.

4-3-7 Experimental Section

General ^{1}H NMR and ^{13}C NMR spectra were recorded on a JEOL JNM-AL 400 and AL 300 spectrometers at ambient temperature using tetramethylsilane as an internal standard. FAB, EI and ESI mass spectra were measured on a JEOL JMS-700 spectrometer. UV-vis spectra were measured on a JASCO UV/VIS/NIR Spectro-photometer V-570. Steady-state fluorescence spectra were measured on USB4000 (Ocean Optics, Inc.) in the range of 345-1100 nm with an irradiation light through a monochromator (Ritsu MC-10N) using a 500W Xenon lamp (Ushio XB-50102AA-A). Fluorescence quantum yields were measured on an Absolute PL Quantum Yield Measurement System C9920-02. Elemental analyses were performed on a Yanaco MT-5 elemental analyzer.

Materials Thin-layer chromatography (TLC) and gravity column chromatography were performed on Art. 5554 (Merck KGaA), and Silica Gel 60N (Kanto Chemical Co.), respectively. Benzonitrile was distilled from P_2O_5 *in vacuo*. All other solvents and chemicals were reagent grade quality, obtained commercially and used without further purification except as noted. For spectral measurements, spectral grade toluene, dichloromethane and DMSO were purchased from Nacalai tesque Inc.

Photochemical reactions The photocleavage reactions were carried out in a quartz UV cell which was irradiated by monochromatic excitation light through a monochrometor (Ritsu MC-10N) by a 500 W xenon lamp (Ushio XB-50102AA-A) and monitored by an OCEAN OPTICS high resolution spectrometer system HR-4000 with light source DH-2000-BAL.

Measurement of quantum yields of the photoreaction The quantum yield of the photochemical reactions of 9,10-diketoanthracene was determined as 0.37±0.06 with a standard actinometer (potassium ferrioxalate; $K_3[Fe(C_2O_4)_3]$).[25] A square quartz cuvette (10 mm i.d.) which contained a deaerated solution (3.0 cm^3) of 9,10-diketoanthracene was irradiated with monochromatized light of λ = 468 nm by a light through a monochromator (Ritsu MC-10N) using a 500W Xenon lamp (Ushio XB-50102AA-A). Under the conditions of actinometry experiments, the actinometer, 9,10-diketoanthracene absorbed essentially all incident light. The photochemical reaction was monitored using a JASCO UV/VIS/NIR Spectrophotometer V-570. The quantum yields were determined from the increase in absorbance due to the anthracene (378 nm) at the beginning of the reaction. The quantum yield was the average value of 8

measurements. The relative quantum yields of **Py-DK** and **Py-3-DK** were determined based on the quantum yield of 9,10-diketoanthracene.

Photochemical reactions in film PMMA (470 mg) was dissolved with toluene (10 mL). The solution was stirred overnight and filtrated. **Py-DK** or **Py-3-DK** (1 mg) was dissolved in CH_2Cl_2 (200 μL). PMMA solution (200 μL) and diketone solution (10 μL) were mixed. The mixture solution (50 μL) was dropped on glass substrate (1 cm × 1 cm) and dried under vacuum condition. The substrate was converted upon photo-irradiation for 10 min using a metal-halide lamp (Nippon P. I. PCS-UMX375RC, 375W) over 390 nm under vacuum condition. Steady-state absorption spectra were measured on USB4000 by a light through a monochromator (Ritsu MC-10N) using a 500W Xenon lamp (Ushio XB-50102AA-A). Fluorescence quantum yields were measured on Absolute PL Quantum Yield Measurement System (Hamamatsu Photonics C9920-02).

Theoretical calculations All density functional theory calculations were achieved with the Gaussian09[1] program package. The geometry was fully optimized at the Becke's three-parameter hybrid functional combined with the Lee-Yang-Parr correlation functional abbreviated as the B3LYP level of density functional theory with 6-31G(d) basis set. Equilibrium geometries were verified by the frequency calculations, where no imaginary frequency was found. Based on the B3LYP/6-31G(d) optimized geometry, time dependent density functional theory (TDDFT) was conducted at the CAM-B3LYP/6-31G(d) level of theory.

Synthesis

2-brome-9,10-dihydro-9,10-ethanoanthracene-*cis*-11,12-diyl carbonate (4-8)

A solution of 2-bromoanthracene **4-7** (0.72 g, 2.8 mmol) and vinylene carbonate (0.28 mL, 4.4 mmol) in xylenes (12 mL) was heated at 180 °C in an autoclave for 3 days. After removal of the solvent *in vacuo*, the residue was rinsed with hexane to give **4-8** as white crystals (0.73 g, 76%). ^{1}H NMR (400 MHz; $CDCl_3$) [Mixture of isomers] : δ = 7.55 (m, 1H), 7.39-7.37 (m, 3H), 7.28-7.25 (m, 3H), 4.88 (m, 2H), 4.68 (m, 2H); ^{13}C NMR (100 MHz; $CDCl_3$: Mixture of isomers): δ = 153.67, 140.00, 139.83, 136.70, 136.65, 135.37, 134.47, 130.69, 128.76, 127.88, 127.86, 127.30, 126.66, 126.60, 126.58, 121.41, 75.86, 75.79, 75.75, 47.50, 47.38, 47.29; MS (DI-EI) *m*/*z*: 344 [M^+]; Anal. Calcd. for $C_{17}H_{11}BrO_3$•1/6 $CHCl_3$: C, 56.79; H, 3.10.; Found: C,

56.80; H, 3.20.

2-(1-Pyrenyl)-9,10-dihydro-9,10-ethanoanthracene-*cis*-11,12-diyl carbonate (4-9)

The compound **4-8** (0.638 g, 1.86 mmol), pyrene boronic acid (0.586 g, 2.42 mmol), and Na_2CO_3 (3.08 g) were added to 1,4-dioxane (50 mL) and the suspension was degassed by freeze-pump-thaw cycling. Then $Pd(PPh_3)_4$ (0.229 g, 0.198 mmol) was added and the solution was refluxed for 18 h under argon atmosphere, then cooled to room temperature. The solution was poured into aqueous NH_4Cl, filtrated with Celite, and extracted with ethylacetate. The organic layer was washed with water and brine. The organic layer was dried over Na_2SO_4 and the solvent was removed under reduced pressure. The crude product was purified on silica gel column chromatography ($CHCl_3$) and recrystallized from $CHCl_3$/hexane to give **4-9** as white powder (0.441 g, 51%).

^{1}H NMR (400 MHz; $CDCl_3$): δ = 8.21 (d, J = 7.6 Hz, 2H), 8.17 (d, J = 7.6 Hz, 1H), 8.10 (s, 2H), 8.06-7.99 (m, 2H), 7.89 (d, J = 7.6 Hz, 1H), 7.66 (m, 1H), 7.57 (m, 1H), 7.51-7.44 (m, 3H), 7.43-7.30 (m, 2H), 5.05 (m, 2H), 4.83 (m, 2H); ^{13}C NMR (100 MHz; $CDCl_3$) ［Two peaks are lacked.］: δ = 153.95, 140.96, 137.84, 136.54, 136.24, 136.18, 131.38, 130.80, 130.71, 129.97, 128.25, 127.78, 127.43, 127.65, 127.58, 127.43, 127.27, 126.71, 126.64, 126.06, 125.52, 125.24, 124.90, 124.86, 124.80, 124.76, 124.58, 76.33, 76.32, 47.94, 47.65; MS (FAB) m/z: 464 [M^+]; Anal. Calcd. for $C_{33}H_{20}O_3$•$CHCl_3$•1/2 H_2O: C, 68.88; H, 3.74.; Found: C, 68.58; H, 3.77.

2-(1-Pyreno)-9,10-dihydro-11,12-dihydroxy-9,10-ethanoanthracene (4-10)

To a solution of **4-9** (0.250 g, 0.538 mmol) in THF (21 mL), MeOH (20 mL) and water (10 mL), K_2CO_3 (3.60 g) was added. The solution was refluxed for 1 h and cooled to room temperature. The product was extracted with $CHCl_3$ and washed with water and brine and the organic layer was dried over Na_2SO_4. The organic solvent was removed under reduced pressure. The crude product was purified by silica gel column chromatography ($CHCl_3$/ethylacetate =1/1) and recrystallized from $CHCl_3$/hexane to give **4-10** as white powder (0.175 g, 74%).

^{1}H NMR (400 MHz; $CDCl_3$): δ = 8.19 (d, J = 7.6 Hz, 2H), 8.14 (m, 2H), 8.08 (s, 2H), 8.00 (m, 2H), 7.91 (d, J = 7.6 Hz, 1H), 7.58 (m, 1H), 7.51-7.43 (m, 4H), 7.28 (m, 2H), 4.56 (2, 1H), 4.53 (s, 1H), 4.23 (m, 2H), 2.17 (m, 2H, -OH); ^{13}C NMR (100 MHz; $CDCl_3$) ［Two peaks are lacked.］: δ = 139.90, 139.66, 138.69, 138.48, 137.24, 131.32, 130.79, 130.40, 128.88, 128.31, 127.49, 127.31, 127.28, 127.23, 126.76, 126.73, 126.56, 126.49, 125.86, 125.09, 124.96, 124.78, 124.72, 124.67, 124.56, 124.46, 68.21, 68.18, 51.43, 51.14; MS (ESI) m/z: 461 [M+Na];

(HR-ESI-TOF) *m/z* = 461.15170, calcd for $C_{32}H_{22}NaO_2$ = 461.15175 $[M+Na]^+$.

2-(1-Pyreno)-9,10-dihydro-9,10-ethanoanthracene-11,12-dione (**Py-DK**)

Trifluoroacetic anhydride (1.0 mL, 7.09 mmol) was added dropwise to a mixture of dry DMSO (1.0 mL, 14 mmol) and dry CH_2Cl_2 (4.0 mL) at –60 °C under argon. After stirring for 10 min, **4-10** (0.181 g, 0.412 mmol) dissolved in a mixture of dry DMSO (4.0 mL) and dry CH_2Cl_2 (2.0 mL) was added dropwise. After stirring for 120 min, *N,N*-diisopropylethylamine (2.7 mL, 16 mmol) was added dropwise to the reaction mixture. The solution was stirred at –60 °C for 60 min and warmed to room temperature. 1 M HCl was added to the mixture for quenching the reaction. The mixture was extracted with CH_2Cl_2, and the combined organic layers were washed with water and brine and dried with Na_2SO_4. After removal of the solvent in *vacuo*, the residue was purified by column chromatography on silica gel with CH_2Cl_2 and recrystallized from toluene/hexane to give **Py-DK** as yellow powder (0.107 g, 60 %).

^{1}H NMR (400 MHz; $CDCl_3$): δ = 8.21 (d, *J* = 8.0 Hz, 2H), 8.18 (d, *J* = 8.0 Hz, 1H), 8.11 (m, 2H), 8.03 (m, 3H), 7.91 (d, *J* = 8.0 Hz, 1H), 7.74 (s, 1H), 7.65 (m, 2H), 7.55 (m, 2H), 7.44 (m, 2H), 5.15 (s, 1H), 5.11 (s, 1H); ^{13}C NMR (100 MHz; $CDCl_3$): δ = 183.67, 183.47, 142.77, 136.05, 134.97, 134.84, 134.79, 133.62, 131.68, 131.36, 130.88, 130.79, 129.49, 129.46, 128.35, 128.18, 127.85, 127.70, 127.37, 127.26, 126.42, 126.36, 126.23, 126.09, 125.33, 125.01, 124.84, 124.72, 124.65, 124.60, 60.11, 59.84; MS (ESI) m/z: 457 [M+Na]; (HR-ESI-TOF) *m/z* = 457.12038, calcd for $C_{32}H_{18}NaO_2$ = 457.12045 $[M+Na]^+$.

2-(1-Pyreno-ethynyl)-9,10-dihydro-9,10-ethanoanthracene-*cis*-11,12-diyl carbonate (4-11)

The compound **4-8** (0.682 g, 1.99 mmol), 1-ethynylpyrene (0.678 g, 3.00 mmol) and CuI (0.020 mg) were added to a mixture of toluene (10 mL) and Et_3N (10 mL). The solution was bubbled with argon gas for 20 min and dried by freeze-pump-thaw cycling. $Pd(PPh_3)_4$ (0.116 g, 0.100 mmol) was added to the solution. The solution was warmed to 70 °C for 18 h and cooled to rt. The solution was filtered with Celite, washed with $CHCl_3$ and the solvent was removed under reduced pressure. The crude product was purified on silica gel column chromatography (1st. CH_2Cl_2, 2nd. ethylacetate /hexane = 3/7) to give **4-11** as yellow powder (0.331 g, 34%).

^{1}H NMR (300 MHz; $CDCl_3$): δ = 8.64 (d, *J* = 9.0 Hz, 1H), 8.25-8.03 (m, 9H), 7.76 (m, 1H), 7.62 (dd, *J* = 7.7, 1.6 Hz, 1H), 7.47-7.41 (m, 3H), 7.28 (m, 1H), 4.95 (m, 2H), 4.78 (m, 2H); ^{13}C NMR (75 MHz; $CDCl_3$) ［Two peaks are lacked.］: δ = 154.02, 137.29, 136.71, 136.62, 131.93, 131.29, 131.24, 131.10, 131.08, 129.73, 129.62, 128.37, 128.19, 128.04, 127.26, 127.23, 126.78,

126.24, 125.79, 125.74, 125.65, 125.57, 124.54, 124.47, 124.31, 122.94, 117.62, 94.67 88.96, 76.18, 76.11, 47.66, 47.59; MS (FAB) m/z: 488 $[M]^+$; HR-FAB *m/z* = 488.1412, calcd for $C_{35}H_{20}O_3$ = 488.1412 $[M]^+$.

2-(1-Pyreno-ethynyl)-9,10-dihydro-11,12-dihydroxy-9,10-ethanoanthracene carbonate (4-12)

To the solution of compound **4-11** (0.310 g, 0.635 mmol) in a mixture of THF (25 mL), MeOH (25 mL) and water (4 mL), K_2CO_3 (4.03 g) was added. The solution was stirred overnight and quenched with water. The organic solvent was removed under reduced pressure and the product was extracted with ethylacetate. The organic layer was washed with water and brine, and dried over Na_2SO_4. The organic solvent was removed under reduced pressure. The crude product was purified on silica gel column chromatography (ethylacetate / hexane = 1/1) to give **4-12** as yellow powder (0.178 g, 61%). ^{1}H NMR (300 MHz; $CDCl_3$): δ = 8.65 (d, *J* = 9.0 Hz, 1H), 8.24-8.03 (m, 8H), 7.76 (s, 1H), 7.59 (dd, *J* = 7.5 Hz, 1.5 Hz, 1H), 7.44 (d, *J* = 10 Hz, 1H), 7.35 (m, 2H), 7.19 (m, 2H), 4.50 (m, 2H), 4.13 (m, 2H), 2.25 (m, 2H); ^{13}C NMR (75 MHz; $CDCl_3$) ［Three peaks are lacked.］: *δ* = 139.46, 139.30, 138.98, 131.88, 131.24, 131.19, 131.07, 130.20, 129.60, 129.56, 128.31, 128.12, 127.27, 126.98, 126.70, 126.23, 125.60, 125.57, 124.90, 124.53, 124.49, 124.49, 124.32, 121.85, 121.84, 95.15, 88.46, 68.12, 68.03, 51.33, 51.22; MS (FAB) m/z: 462 $[M]^+$; HR-FAB *m/z* = 462.1623, calcd for $C_{34}H_{22}O_2$ = 461.1620 $[M]^+$.

2-(1-Pyreno-ethynyl)-9,10-dihydro-9,10-ethanoanthracene-11,12-dione (Py-3-DK)

Trifluoroacetic anhydride (1.0 mL, 7.09 mmol) was added dropwise to a mixture of dry DMSO (1.0 mL, 14 mmol) and dry CH_2Cl_2 (4.0 mL) at −60 °C under argon. After stirring for 10 min, **4-12** (0.199 g, 0.412 mmol) dissolved in a mixture of dry DMSO (1.0 mL) and dry CH_2Cl_2 (2.0 mL) was added dropwise. After stirring for 120 min, *N,N*-diisopropylethylamine (2.7 mL, 16 mmol) was added dropwise to the reaction mixture. The solution was stirred at –60 °C for 90 min and warmed to room temp. 1 M HCl was added to the mixture for quenching the reaction. The mixture was extracted with CH_2Cl_2, and the combined organic layers were washed with water and brine and dried with Na_2SO_4. After removal of the solvent in *vacuo*, the residue was purified by column chromatography on silica gel with CH_2Cl_2 and recrystallized from toluene/hexane to give **Py-3-DK** as yellow powder (0.039 g, 20 %).

^{1}H NMR (300 MHz; $CDCl_3$): *δ* = 8.62 (d, *J* = 9.1 Hz, 1H), 8.25-8.04 (m, 8H), 7.83 (m, 1H), 7.71 (dd, *J* = 7.5, 1.5 Hz, 1H), 7.54-7.50 (m, 3H), 7.42 (m, 2H), 5.08 (s, 1H), 5.06 (s, 1H); ^{13}C

NMR (75 MHz; $CDCl_3$) ［One peak is lacked.］: δ = 183.42, 183.25, 135.18, 134.70, 134.51,134.45, 132.61, 131.97, 131.51, 131.17, 130.96, 129.61, 129.19, 129.02, 128.53, 128.40, 128.21, 127.20, 126.49, 126.45, 126.41, 126.31, 125.77, 125.27, 124.87, 124.54, 124.42, 124.22, 117.02, 93.86, 90.37, 59.91, 59.78; MS (FAB) m/z: 458 $[M]^+$; HR-FAB *m/z* = 458.1305, calcd for $C_{34}H_{18}O_2$ = 458.1307 $[M]^+$.

4-4 Optically and Thermally Switchable Electronic Structures Based on An Anthracene–BODIPY Conjugate

4-4-1 Molecular Design

As described in 2-3, α-diketone type precursor of anthracene (**ADK**) effectively quenched the excited singlet state of pyrene moiety. The quenching system is only applicable to emissive units having a higher excited state than that of α-diketone unit. In addition, the overlap of the excitation wavelength to trigger the structural change and to monitor the fluorescence is also a problem to be solved. Therefore, the selective excitation of fluorophore was difficult.

As the next approach to the selective excitation of fluorophore, the author of this thesis focused borondipyrromethene (BODIPY) as the dye having absorption and emission over 500 nm or more.[24] Typical BODIPY and the derivatives are shown in Figure 4-34. BODIPY dyes are characterized by large molar absorption coefficients, significant variations in their spectral emission profiles, high fluorescence quantum yields and excellent photostability. An important characteristic of BODIPY is the easy control of absorption and fluorescence wavelength. Various π-extended BODIPYs, such as those generated by aromatic ring fusion, have shown long wavelength fluorescence extending to the near-infrared region.[26] The fluorescence switching of multicolor is possible as long as fluorescence intensity is controlled using BODIPY parents.

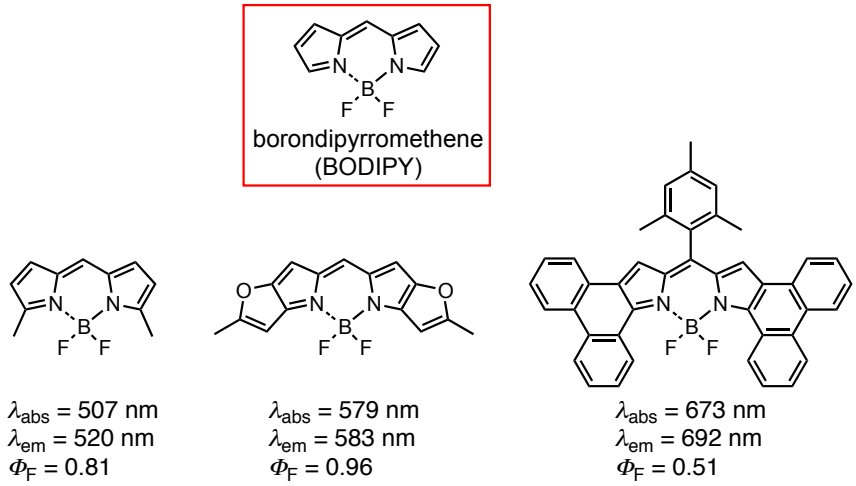

Figure 4-34. Structures of BODIPY and the derivatives.

As described in the beginning of this Chapter, intramolecular electron transfer mechanism is one of strategies for preparing the fluorescence control system. To design the system, the presence of electron donor and electron acceptor unit is essential. Because BODIPY is an electron donor unit and α-diketone unit is an electron accepter unit, the molecule design satisfies the first condition of electron transfer system.[27] Furthermore, in the case of bulky substituent at meso position of BODIPY, the electronic interaction between the two units becomes small by steric hindrance.[28] From these reasons, introduction of α-diketone unit as a photoswitching unit at meso position is the most suitable for mechanism of intramolecular electron transfer.

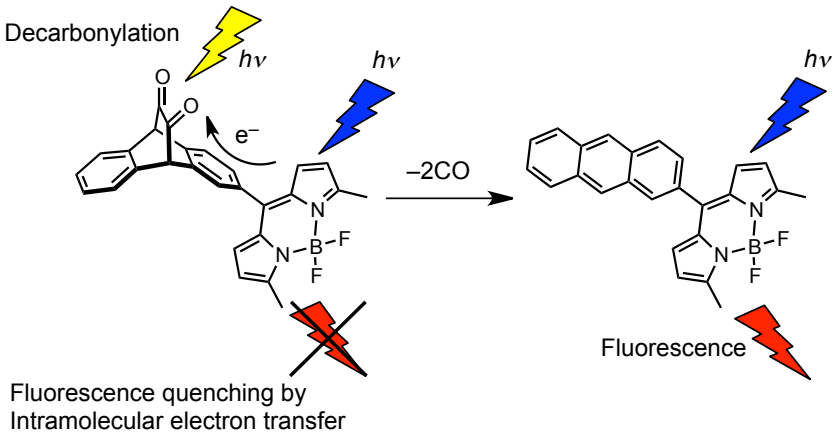

Figure 4-35. The fluorescence quenching mechanism based on BODIPY–photoprecursor conjugate.

Benzo-fused BODIPYs prepared by the retro-Diels-Alder reaction of the corresponding BCOD-fused BODIPYs have been reported by Ono and co-workers.[29] This thermal conversion quantitatively proceeds by heating at 220 °C and leads to dramatic changes in the optical properties of the dye.[30] In other words, BCOD-fused BODIPY is possible to switch the wavelength thermally.

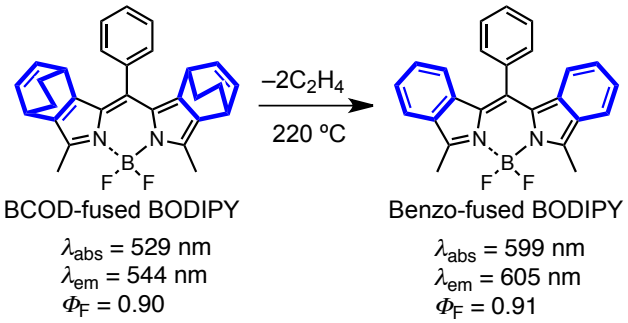

Figure 4-36. Thermal convertible BODIPY.

The author of this thesis designed the optically and thermally switchable electronic structure based on anthracene–BODIPY conjugate (Figure 4-37). In this content, synthesis, optically and/or thermal conversion, optical properties and elucidation of the fluorescence quenching mechanism are discussed.

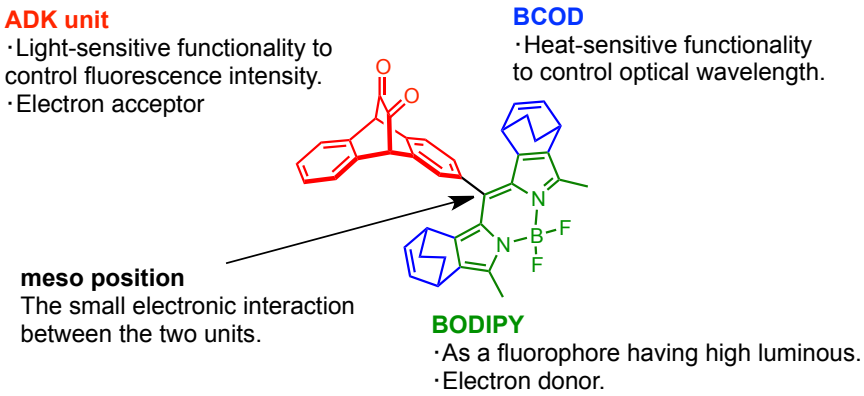

Figure 4-37. Molecular design for optically and thermally fluorescence switchable structure.

4-4-2 Synthesis of BODIPY–Anthracene Precursor Conjugate

BCOD-DK was prepared as shown in Scheme 4-5. Formylanthracene **4-13**[31] was reacted with vinylene carbonate in a Diels–Alder reaction to give adduct **4-14** in 78% yield as a mixture of stereoisomers. Isoindole **4-15** was prepared according to the literature.[29] Compound **4-16** was synthesized in 55% yield through the TFA-catalyzed condensation between **4-14** and **4-15**, followed by oxidation with DDQ and treatment with $BF_3{\cdot}OEt_2$ and *N*,*N*-diisopropylethylamine. Compound **4-16** was subsequently hydrolyzed to give diol **4-17** in 79% yield, which was oxidized by the Swern reaction to give **BCOD-DK** in 30% yield.

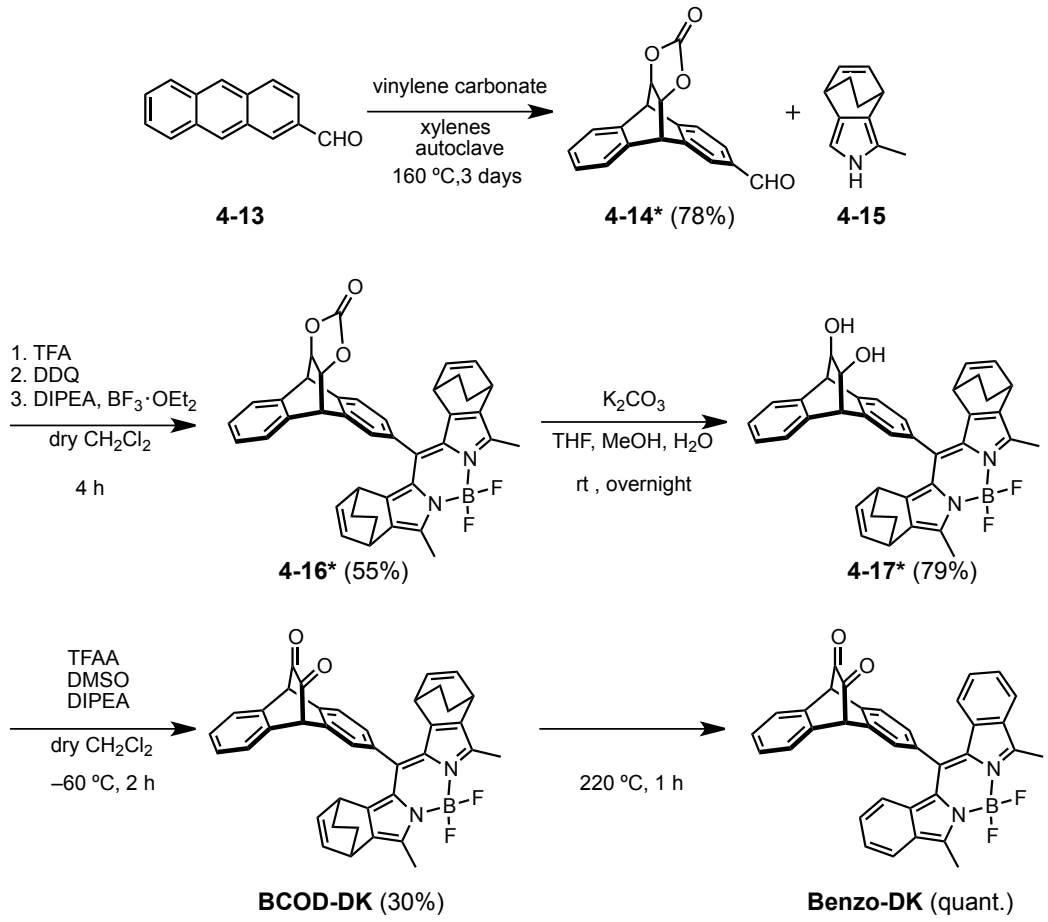

Scheme 4-5. Synthesis of **BCOD-DK** and **Benzo-DK**.

Thermogravimetric analysis of **BCOD-DK** was performed to investigate its thermal conversion properties (Figure 4-38). **BCOD-DK** exhibited mass loss starting at 127 ºC and ending at 208 ºC. This result demonstrates that the BCOD-fused precursor was smoothly converted to the corresponding benzo-fused BODIPY by heating. Based on this experimental information, a bulk sample of **BCOD-DK** was heated at 220 °C to form **Benzo-DK** and the quantitative conversion was confirmed by ^{1}H NMR spectroscopy (Figure 4-39).

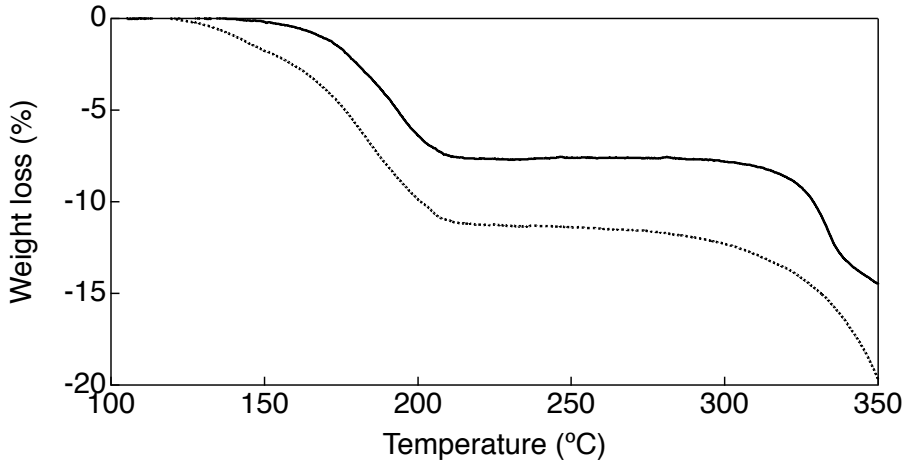

Figure 4-38. Thermogravimetric analysis of **BCOD-DK** (solid line) and **BCOD-Ant** (dotted line). Scan rate: 5 ºC min^{-1}.

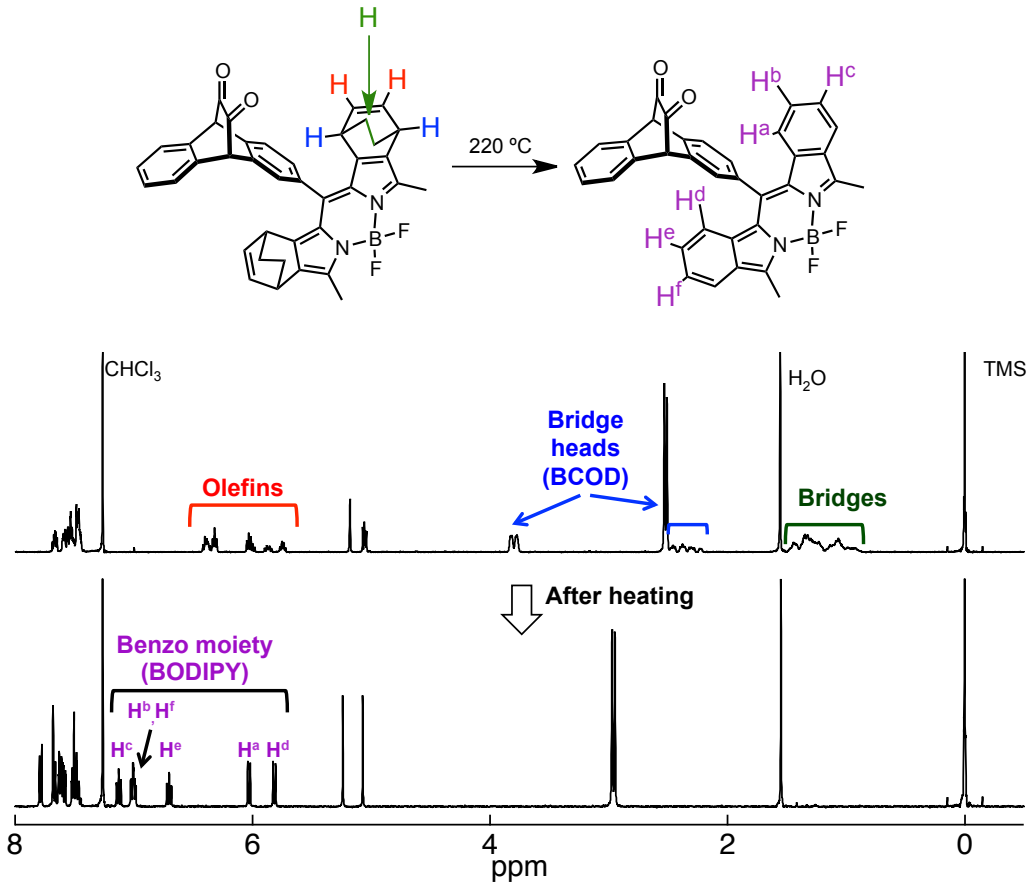

Figure 4-39. The ^{1}H NMR spectral change before and after thermal conversion of **BCOD-DK** in $CDCl_3$.* Solvents and TMS peaks.

4-4-3 Photoconversion in Solution

The photoreaction of the DK moiety to an anthracene moiety was performed using a metal-halide lamp as light source incorporating a UV-cutoff filter under an argon atmosphere. Figure 4-40 shows the changes in ^{1}H NMR spectra during the photoreaction of **BCOD-DK** in $CDCl_3$. The peaks at 5.04–5.18 ppm, which are assigned to H^a and $H^{a'}$ of the diketone moiety, gradually decreased, while the peaks at 8.51–8.60 ppm, corresponding the *peri* protons H^b and $H^{b'}$ of **BCOD-Ant**, increase. After 60 min, the photoreaction was complete without any signal of byproducts.

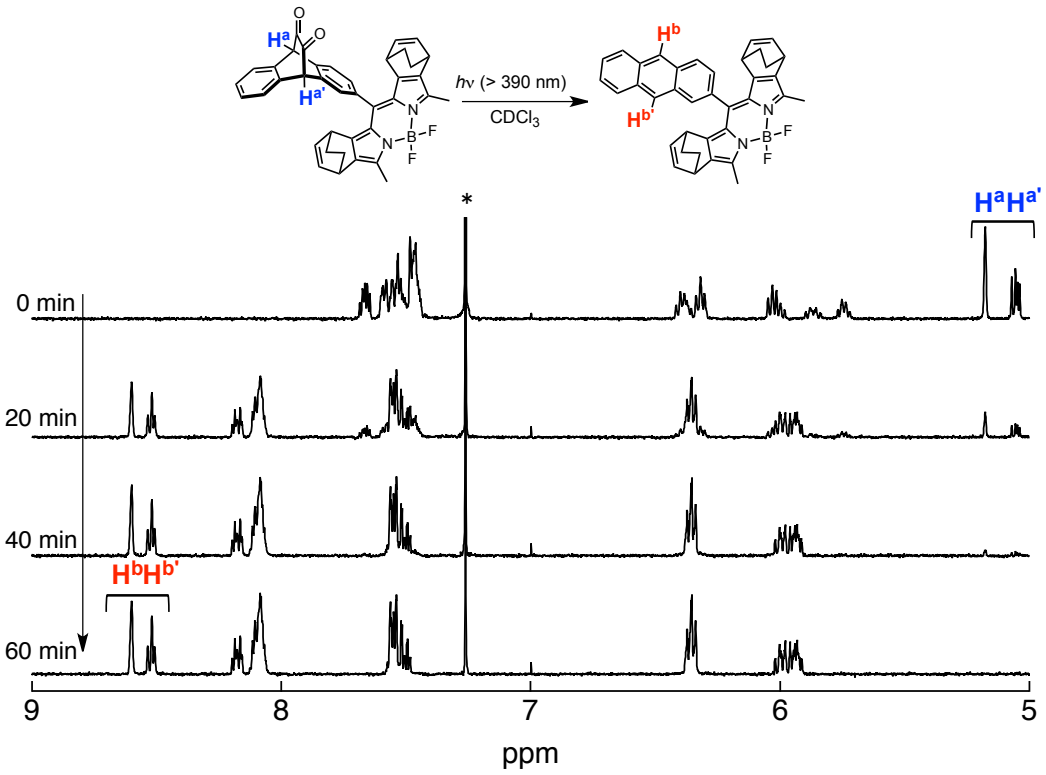

Figure 4-40. Changes in the ^{1}H NMR spectra of **BCOD-DK** during photolysis in $CDCl_3$ under an argon. Spectra were acquired at 0, 20, 40 and 60 min. λ_{EX} > 390 nm. The solvent peak is indicated by *.

The same analysis was performed using **Benzo-DK** in $CDCl_3$ (Figure 4-41). During the photoreaction, the peaks at 5.07 and 5.24 ppm decreased while those at 8.66 and 8.51 ppm increased, indicating the formation of **Benzo-Ant**. These results demonstrate that **BCOD-DK** and **Benzo-DK** were quantitatively converted to the corresponding compounds **BCOD-Ant** and **Benzo-Ant** upon photoirradiation. Finally, a thermogravimetric analysis of **BCOD-Ant** was carried out (Figure 4-38). The mass loss associated with the transition from **BCOD-Ant** to **Benzo-Ant** started at 149 ºC and finished at 207 ºC. Thus we can completely control the four different optical performances of these BODIPYs solely by the application of irradiation and heat.

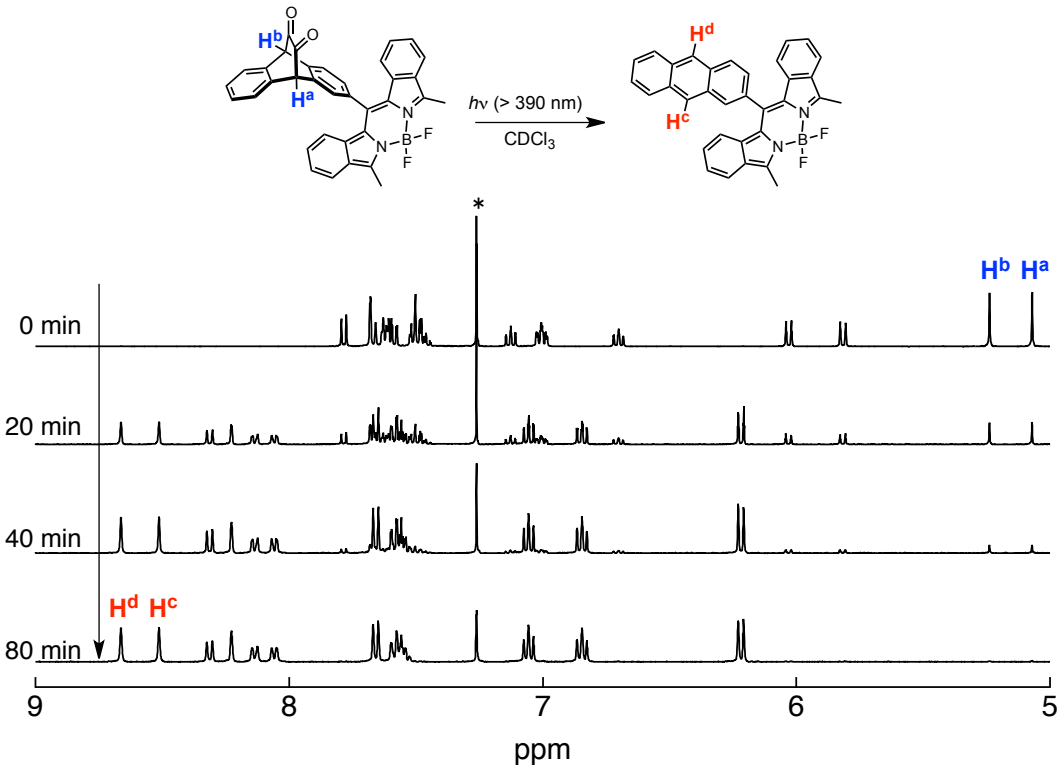

Figure 4-41. Changes in the ^{1}H NMR spectral of **Benzo-DK during photolysis** in $CDCl_3$ under an argon. Spectra were acquired at 0, 20, 40 and 80 min. λ_{EX} > 390 nm. The solvent peak is marked with *.

4-4-4 Single Crystal of BODIPY–Anthracene Precursor Conjugate

The recrystallization of **BCOD-DK** from a dichloromethane–hexane mixture gave prism-shaped orange crystals suitable for single crystal X-ray diffraction analysis. The resulting structure is presented in Figure 4-42. The BCOD unit was treated as a disordered structure of the bicyclo[2,2,2]octadiene moiety. The BODIPY core was found to be substantially planar. Importantly, the dihedral angle between the BODIPY core and the **ADK** unit is 57.9º, while the C5–C24 bond length is 1.487(4) Å. This angle and bond length suggests that the electronic interaction between the two units is rather small, enabling state-to-state electronic and/or excitonic analysis of this compound.

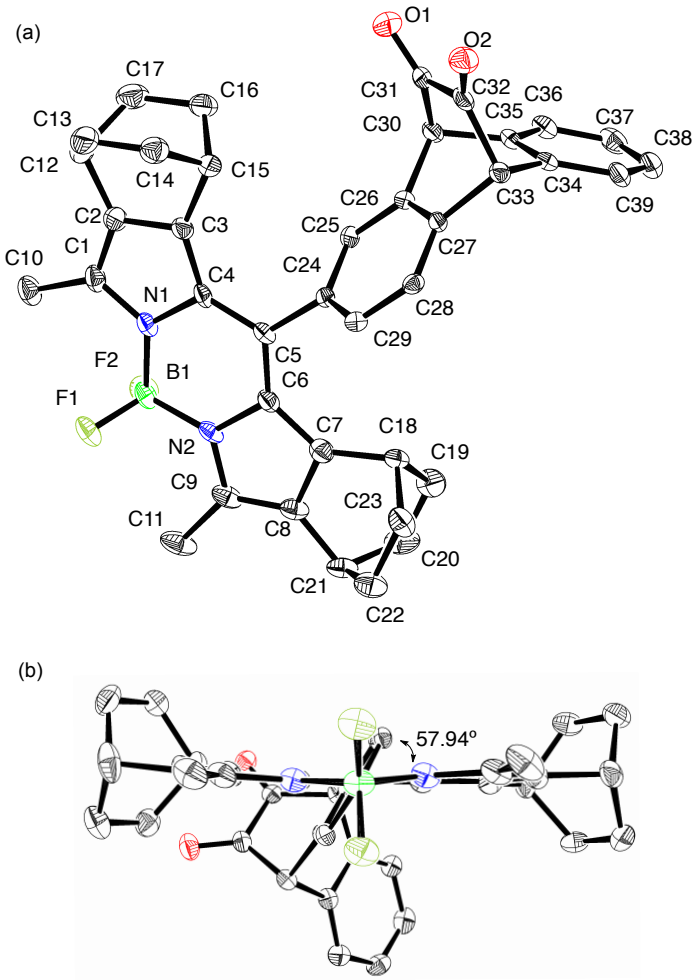

Figure 4-42. ORTEP drawing of the structure of **BCOD-DK** as determined by single crystal XRD. Solvent molecules and hydrogen atoms are omitted for clarity. Ellipsoids are drawn at the 50% probability. Space group $P2_1/c$ a = 12.782(2) Å, b = 22.747(4) Å, c = 10.6677(19) Å, β = 101.419(3)°, Z = 4, R_1 = 0.0587, wR_2 = 0.1350, GOF = 1.025

4-4-5 Steady-State Optical Properties

The UV-vis absorption and fluorescence spectra of these BODIPYs in dichloromethane are shown in Figure 4-43 and summarized in Table 4-3. The UV-vis absorption spectrum of **BCOD-DK** shows a peak at 534 nm with an associated shoulder at 500 nm, while **Benzo-DK** exhibits an absorption peak at 605 nm with a shoulder at 560 nm. The 71 nm red-shift observed in the **Benzo-DK** relative to **BCOD-DK** is caused by the π-expansion of the BODIPY moiety. **BCOD-Ant** and **Benzo-Ant** show UV-vis absorption spectra similar to those of **BCOD-DK** and **Benzo-DK**, respectively, indicating minimal through-bond electronic interactions between the *meso*-anthryl portion of the molecule and the BODIPY framework. The extinction coefficient of the n-π* transition of the diketone moiety is around 1000 M^{-1} cm^{-1}, which is 60 times lower than the value determined from the peak maxima of the BODIPY moieties, and therefore typical n-π* absorption peaks in the vicinity of 460 nm are not observed for **BCOD-DK** and **Benzo-DK**. The fluorescence spectra in dichloromethane showed different trends compared to the absorption spectra. While **BCOD-DK** exhibited only weak emission at 560 nm, with a fluorescence quantum yield (Φ_F) of 0.08, **BCOD-Ant** had a Φ_F of 0.61 at the same wavelength. Similarly, **Benzo-DK** emitted at 624 nm with a low Φ_F of 0.08, while the Φ_F of **Benzo-Ant** was 0.90 at 622 nm. That is, the fluorescence wavelengths are almost the same before and after the photoreaction, while the fluorescence quantum yields are drastically increased upon the photo-induced activation associated with the decarbonylative aromatization.

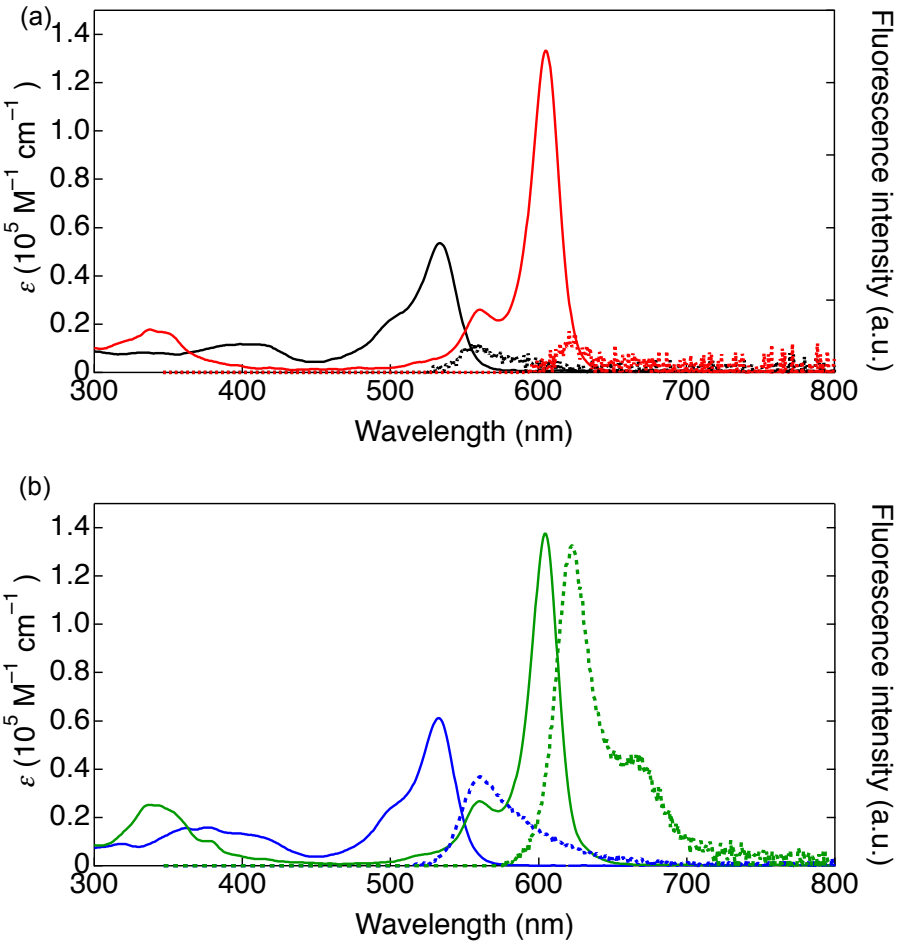

Figure 4-43. UV-vis absorption (solid line) and fluorescence (dotted) spectra of (a) **BCOD-DK** (black) and **Benzo-DK** (red), and (b) **BCOD-Ant** (blue) and **Benzo-Ant** (green) in dichloromethane.

Table 4-3. UV-vis absorption peaks (λ_{abs}), fluorescence peaks (λ_F) and quantum yields (Φ_F) of BODIPY dyes.

	λ_{abs} / nm (log ε)	λ_F / nm (Φ_F)		
	dichloromethane	toluene	dichloromethane	acetonitrile
BCOD-DK	534 (4.73)	560 (0.79) [a]	560 (0.08) [a]	553 (0.08) [a]
Benzo-DK	560 (4.41) 605 (5.13)	623 (0.84) [b]	624 (0.08) [b]	617 (0.08) [b]
BCOD-Ant	534 (4.78)	565 (0.73) [a]	560 (0.61) [a]	556 (0.61) [a]
Benzo-Ant	560 (4.42) 605 (5.12)	626 (0.90) [b]	622 (0.90) [b]	615 (0.83) [b]

[a] Excited at 500 nm. [b] Excited at 562 nm.

The fluorescence properties of BODIPYs were also measured in toluene and acetonitrile (Figure 4-44). The fluorescence spectra of **BCOD-Ant** and **Benzo-Ant** exhibit small blue-shifts in response to increasing the solvent polarity. However, the fluorescence properties of **BCOD-DK** and **Benzo-DK** were dramatically different. The Φ_F values of **BCOD-DK** and **Benzo-DK** were as low as 0.08 in dichloromethane, but increased to 0.79 and 0.84 in non-polar toluene**.** In aprotic, highly polar acetonitrile, the Φ_F values of **BCOD-DK** and **Benzo-DK** were 0.08, as they were in dichloromethane. To confirm the correlation between the fluorescence quantum yields and solvent polarity, the Φ_F values of **BCOD-DK** and **Benzo-DK** were measured in mixtures of toluene and dichloromethane so as to change the solvent polarity systematically. The Φ_F values of **BCOD-DK** and **Benzo-DK** were found to decrease gradually with increasing dichloromethane content in the mixture (Figure 4-45 and Table 4-4). The dielectric constants (ε) of these mixtures were calculated based on the ratios of the two solvents, and the Φ_F values were found to be constant over $\varepsilon =$ 8 for **BCOD-DK** and over $\varepsilon = 5$ for **Benzo-DK**. Thus the Φ_F values in dichloromethane and in acetonitrile were almost the same. This solvent effect appears to result from fluorescence quenching derived from an intramolecular electron transfer process.

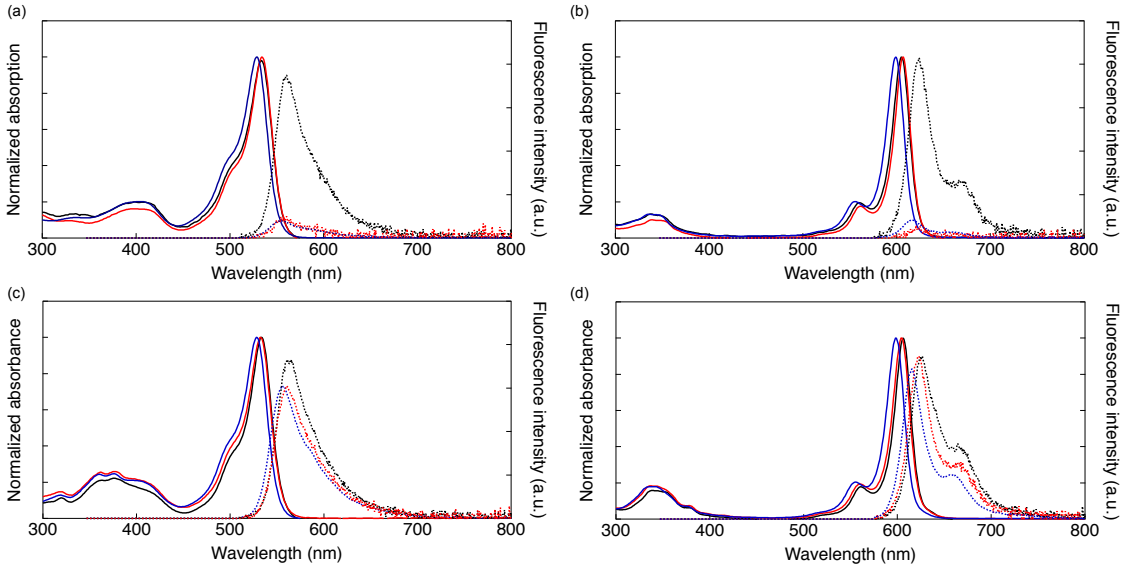

Figure 4-44. UV–vis absorption (solid) and fluorescence (dotted) spectra in toluene (black), dichloromethane (blue) and acetonitrile (red) for (a) **BCOD-DK**, (b) **Benzo-DK**, (c) **BCOD-Ant** and (d) **Benzo-Ant**.

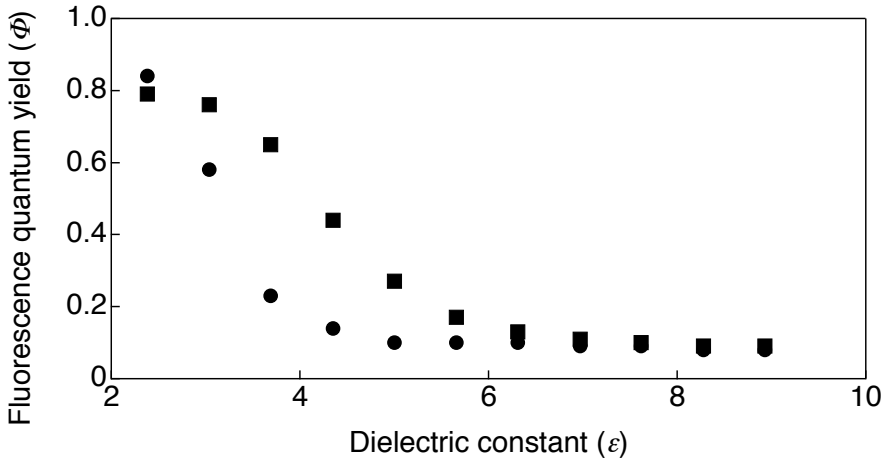

Figure 4-45. The correlation between fluorescence quantum yields (Φ_F) and dielectric constant (ε) for **BCOD-DK** (■) and **Benzo-DK** (●).

Table 4-4. The correlation between fluorescence quantum yields of BODIPY in each solvent.

Solvent (toluene/ CH_2Cl_2)	**BCOD-DK**[a] (Φ_F)	**Benzo-DK**[b] (Φ_F)	dielectric constant (ε)
100/0	0.79	0.84	2.38
90/10	0.76	0.58	3.04
80/20	0.65	0.23	3.69
70/30	0.44	0.14	4.35
60/40	0.27	0.10	5.00
50/50	0.17	0.10	5.66
40/60	0.13	0.10	6.31
30/70	0.11	0.09	6.97
20/80	0.10	0.09	7.62
10/90	0.09	0.08	8.28
0/100	0.08	0.08	8.93
acetonitrile	0.08	0.08	35.9

[a]Excitation at 500 nm. [b]Excitation at 562 nm.

The fluorescence lifetimes (τ_F) of the BODIPYs were measured by femtosecond laser flash photolysis in each solvent, with excitation at 365 nm (Figures 4-46–49 and Table 4-5). The τ_F values of **BCOD-Ant** were determined to be 5.59 ns in toluene, 5.87 ns in dichloromethane, and 5.96 ns in acetonitrile. Due to the solvent relaxation effect, τ_F was increased in more polar solvents. The τ_s values of **Benzo-Ant** showed a similar tendency: 5.68 ns in toluene, 6.29 ns in dichloromethane and 6.41 ns in acetonitrile. The τ_Fs of **BCOD-DK** and **Benzo-DK** in toluene were determined by single-exponential decay, in a manner similar to the analysis of the anthracene adducts, and values of 6.29 and 6.17 ns were found, respectively. The τ_F values of these compounds in dichloromethane and acetonitrile were calculated using double-exponential curves; the lowest τ_s value for **BCOD-DK** was 0.59 ns in both dichloromethane and acetonitrile while **Benzo-DK** had τ_F values of 0.50 ns in dichloromethane and 0.54 ns in acetonitrile. The longest τ_F components for **BCOD-DK** and **Benzo-DK** were 6.35 and 5.46 ns in dichloromethane and 6.71 and 5.63 ns in acetonitrile. These longer lifetimes were attributed to the formation of **BCOD-Ant** and **Benzo-Ant** generated by the irradiation applied during the measurement process.

Table 4-5. Fluorescence lifetimes in each solvent.

Toluene /CH_2Cl_2	**BCOD-DK**[b] τ_F/ns (A) [χ^2]	**Benzo-DK**[c] τ_F/ns (A) [χ^2]	**BCOD-Ant**[b] τ_F/ns (A) [χ^2]	**Benzo-Ant**[c] τ_F/ns (A) [χ^2]	ε
100/0	6.29 [1.44]	6.17 [1.49]	5.59 [1.52]	5.68 [1.36]	2.38
90/10	-	4.65 [1.90]	-	-	3.03
80/20	5.81 [1.40]	-	-	-	3.69
70/30	4.20 [1.46]	-	-	-	4.35
0/100	0.59 (0.79) 6.35 (0.21) [1.36]	0.50 (0.53) 5.46 (0.47) [1.13]	5.87 [1.51]	6.29 [1.51]	8.93
acetonitrile	0.59 (0.92) 6.71 (0.08) [1.36]	0.54 (0.64) 5.63 (0.36) [1.24]	5.96 [1.37]	6.41 [1.59]	35.9

[a]τ_F was measured by excitation at 365 nm. [b]Emission was monitored at 560 nm. [c]Emission was monitored at 624 nm.

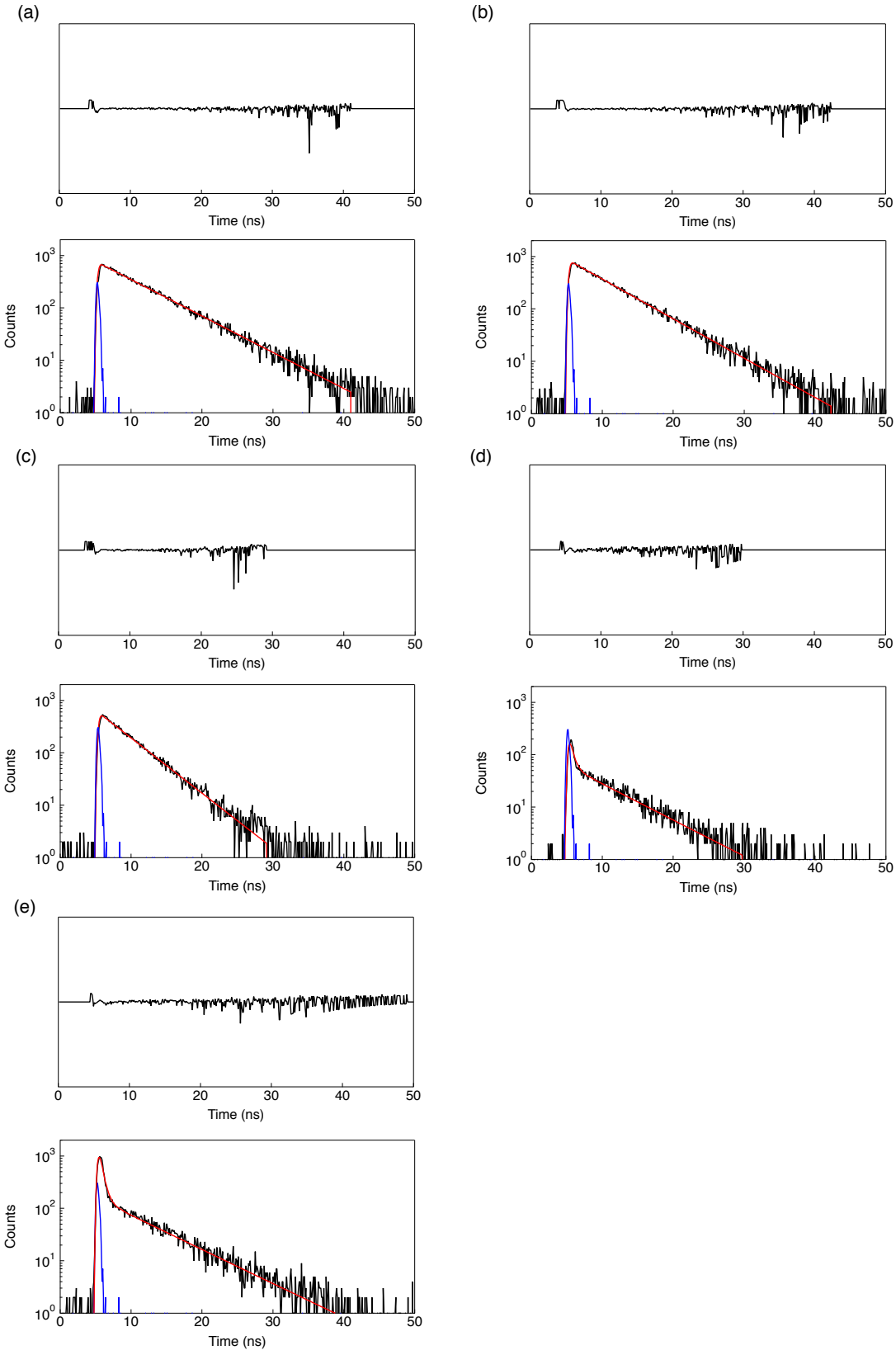

Figure 4-46. Fluorescence decays of **BCOD-DK** in (a) toluene, (b) 20% dichloromethane /toluene, (c) 30% dichloromethane /toluene, (d) dichloromethane and (e) acetonitrile.

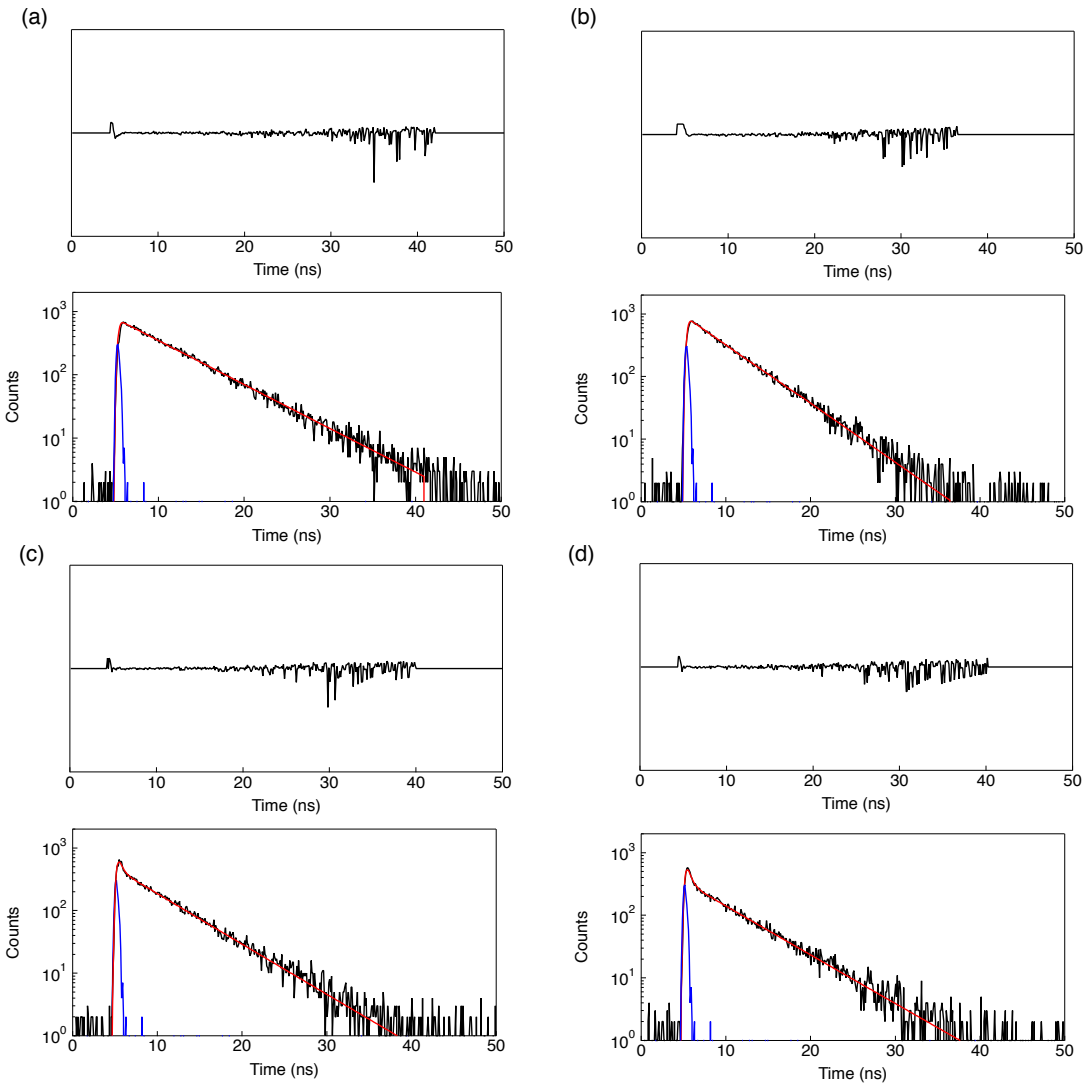

Figure 4-47. Fluorescence decays of **Benzo-DK** in (a) toluene, (b) 10% dichloromethane /toluene, (c) dichloromethane and (d) acetonitrile.

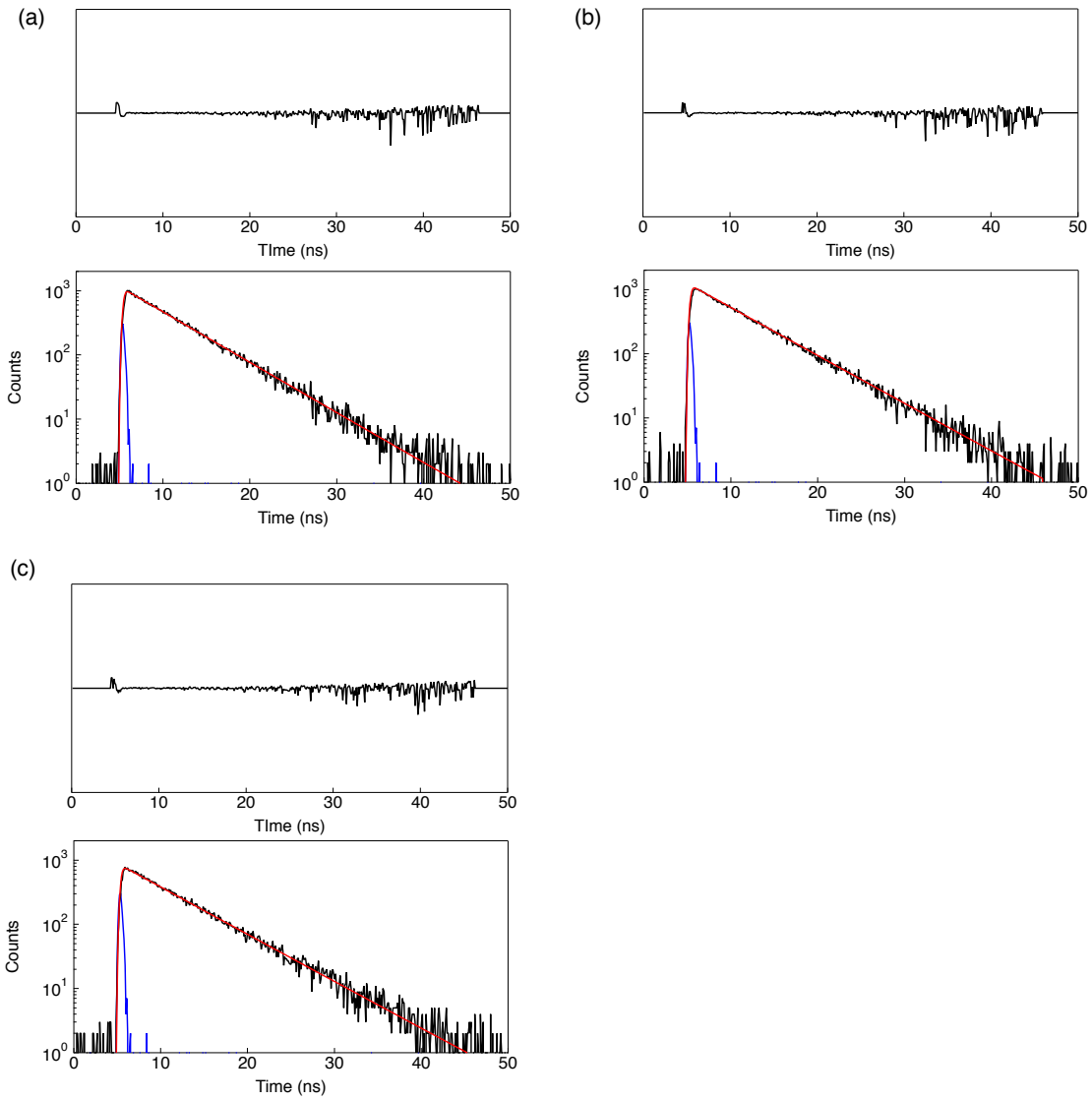

Figure 4-48. Fluorescence decays of **BCOD-Ant** in (a) toluene, (b) dichloromethane and (c) acetonitrile.

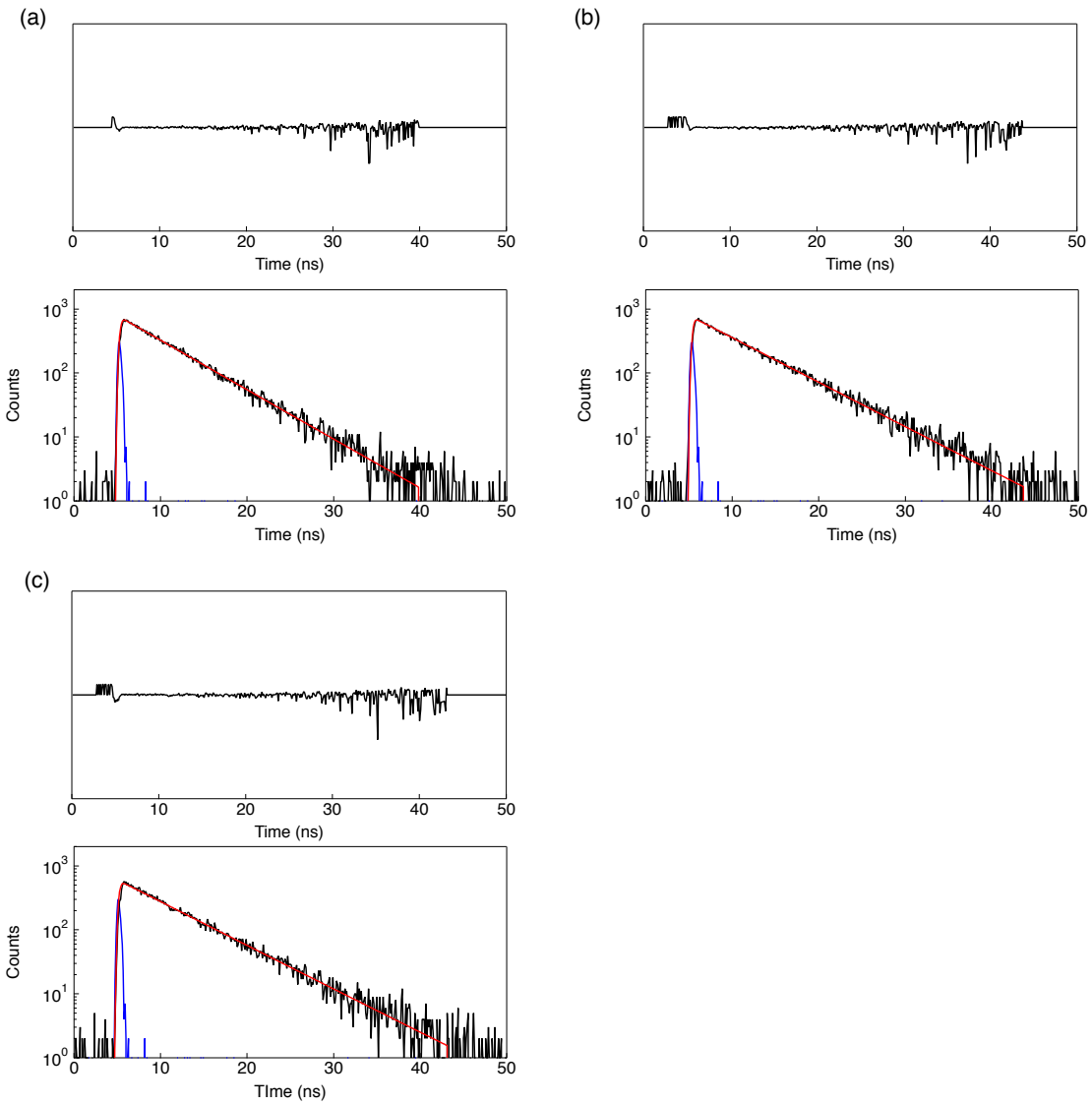

Figure 4-49. Fluorescence decays of **Benzo-Ant** in (a) toluene, (b) dichloromethane and (c) acetonitrile.

4-4-6 Electrochemical Properties

The electrochemical properties of the BODIPY dyes were investigated by cyclic voltammetry (CV) in dichloromethane containing 0.1 M *n*-Bu_4NPF_6 as the supporting electrolyte. The results are summarized in Table 4-6 and Figure 4-50. The one-electron oxidation potentials ($E_{ox}^{1/2}$ *vs.* Fc/Fc^+) of **BCOD-DK**, **Benzo-DK**, **BCOD-Ant** and **Benzo-Ant** were 0.65, 0.32, 0.62 and 0.29 V, respectively. The $E_{ox}^{1/2}$ values of **BCOD-DK** and **BCOD-Ant** were thus similar, with **BCOD-DK** having a slightly higher $E_{ox}^{1/2}$ ($\Delta E_{ox}^{1/2}$ = 0.03 V). The relationship between the **Benzo-DK** and **Benzo-Ant** values was much the same. Thus the first oxidation occurred at the BODIPY moiety and the resulting π-expansion lowered the oxidation potential from 0.65 to 0.32 and from 0.62 to 0.29 V for **BCOD-BODIPY**s and **Benzo-BODIPY**s, respectively. Both **BCOD-Ant** and **Benzo-Ant** exhibited one reduction peak at −1.69 V, whereas **BCOD-DK** and **Benzo-DK** showed two reversible reduction waves, at −1.60 and −1.76 V for **BCOD-DK** and −1.60 and −1.72 V for **Benzo-DK**. Comparing the reduction potentials, the first reduction potentials of **BCOD-DK** and **Benzo-DK** were shifted to the cathode side relative to those of **BCOD-Ant** and **Benzo-Ant**. The first reductions of **BCOD-DK** and **Benzo-DK** were assigned to the reductions of the diketone moieties.

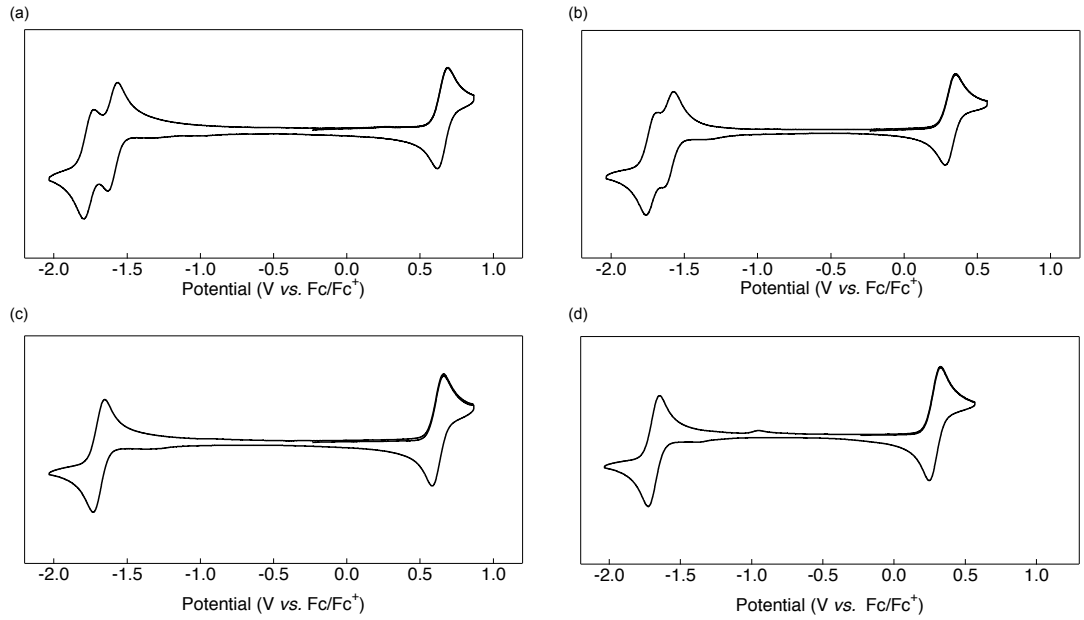

Figure 4-50. Cyclic voltammograms of **BCOD-DK** (a), **Benzo-DK** (b), **BCOD-Ant** (c) and **Benzo-Ant** (d). In 0.1 M *n*-Bu_4NPF_6 in dichloromethane. Scan rate 0.1 V s^{-1}. [BODIPY] = 0.1 mM. WE: Glassy carbon, CE: Pt, RE: $Ag/AgNO_3$.

The redox potentials of **BCOD-DK** and **Benzo-DK** in acetonitrile were also investigated by CV and Differential Pulse Voltammetry (DPV) measurement. The results are summarized in Figure 4-51 and Table 4-6. The oxidation potential of **BCOD-DK** and **Benzo-DK** is 0.69 and 0.34 V, respectively, the oxidation potentials are slightly higher compared with the potential in toluene. On the other hand, the reduction potentials are influenced by the solvation. The reduction potentials of **BCOD-DK** are −1.46 and −1.58 eV, and the reduction potentials of **Benzo-DK** are −1.47 and −1.54 eV. Since the first reduction potential matches to the general reduction potential of α-diketone moiety in acetonitrile, the reduction potentials are totally shifted to positive side.

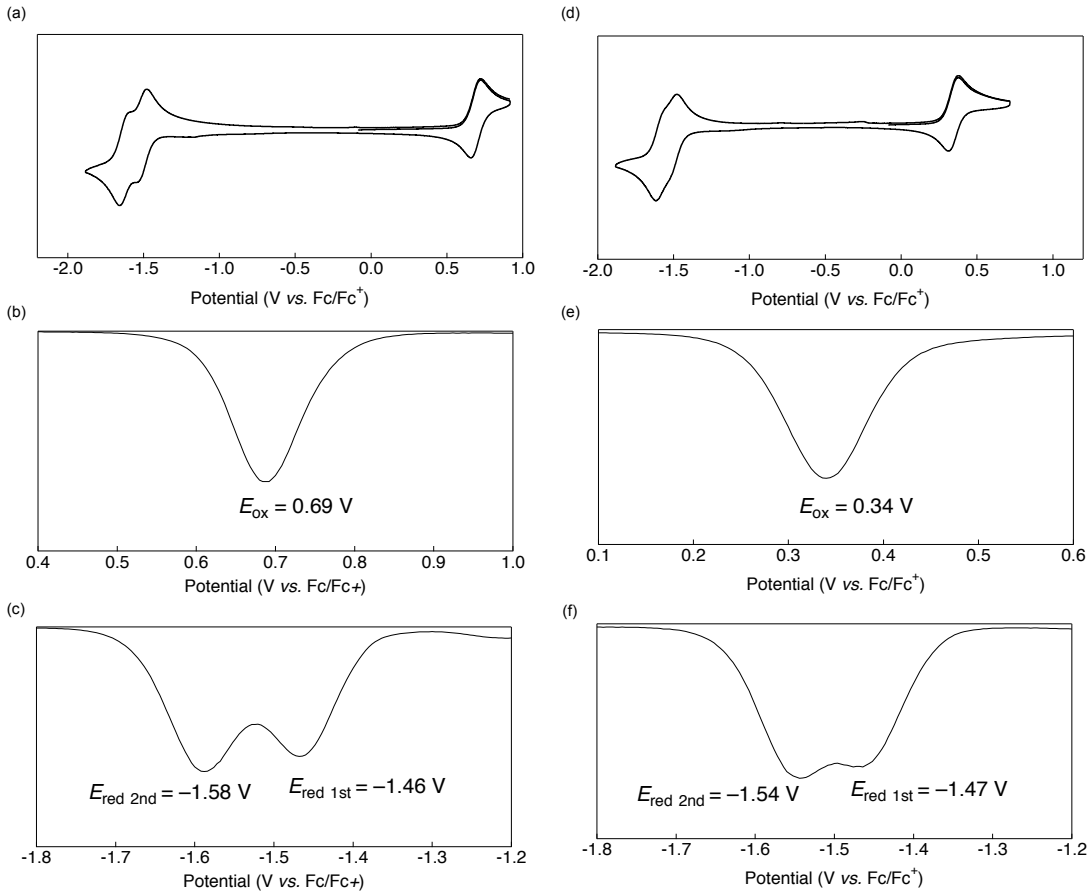

Figure 4-51. Cyclic voltammograms of **BCOD-DK** (a), DPV (0.4 – 1.0 V) of **BCOD-DK** (b), DPV (−1.8 – −1.2 V) of **BCOD-DK** (c), Cyclic voltammograms of **Benzo-DK** (d), DPV (0.1 – 0.6 V) of **Benzo-DK** (e) and DPV (−1.8 – −1.2 V) of **Benzo-DK** (f). In 0.1 M *n*-Bu_4NPF_6 in acetonitrile. Scan rate 0.1 V s^{-1}. [BODIPY] = 0.07 mM (**BCOD-DK**), 0.05 mM (**Benzo-DK**). WE: Glassy carbon, CE: Pt, RE: $Ag/AgNO_3$.

The redox potentials of **BCOD-DK** and **Benzo-DK** in acetonitrile were also investigated by CV and Differential Pulse Voltammetry (DPV) measurement. The results are summarized in Figure 4-51 and Table 4-6. The oxidation potential of **BCOD-DK** and **Benzo-DK** is 0.69 and 0.34 V, respectively, the oxidation potentials are slightly higher compared with the potential in toluene. On the other hand, the reduction potentials are influenced by the solvation. The reduction potentials of **BCOD-DK** are −1.46 and −1.58 eV, and the reduction potentials of **Benzo-DK** are −1.47 and −1.54 eV. Since the first reduction potential matches to the general reduction potential of α-diketone moiety in acetonitrile, the reduction potentials are totally shifted to positive side.

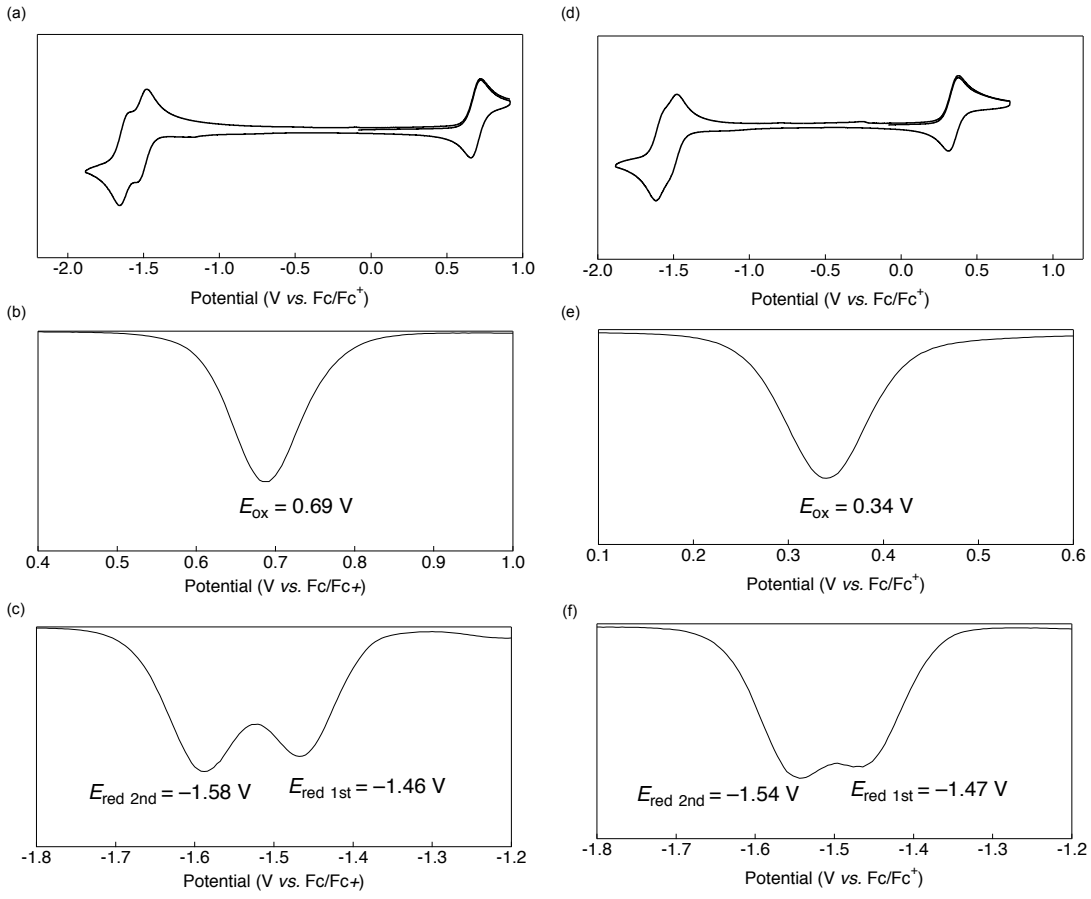

Figure 4-51. Cyclic voltammograms of **BCOD-DK** (a), DPV (0.4 – 1.0 V) of **BCOD-DK** (b), DPV (−1.8 – −1.2 V) of **BCOD-DK** (c), Cyclic voltammograms of **Benzo-DK** (d), DPV (0.1 – 0.6 V) of **Benzo-DK** (e) and DPV (−1.8 – −1.2 V) of **Benzo-DK** (f). In 0.1 M *n*-Bu_4NPF_6 in acetonitrile. Scan rate 0.1 V s^{-1}. [BODIPY] = 0.07 mM (**BCOD-DK**), 0.05 mM (**Benzo-DK**). WE: Glassy carbon, CE: Pt, RE: $Ag/AgNO_3$.

Table 4-6. Summarized redox potential in dichloromethane.

	E_{ox} (V vs. Fc/Fc^+)		E_{RED} (V vs. Fc/Fc^+)	
	CH_2Cl_2	acetonitrile	CH_2Cl_2	acetonitrile
BCOD-DK	0.65	0.69	–1.60, –1.76	–1.46, –1.58
Benzo-DK	0.32	0.34	–1.60, –1.72	–1.47, –1.54
BCOD-Ant	0.62	–	–1.69	–
Benzo-Ant	0.29	–	–1.69	–

4-4-7 Energy Diagrams

To examine the fluorescence quenching mechanism of **BCOD-DK** and **Benzo-DK**, the energy level of the charge-separated (CS) state ($BODIPY^{\bullet+}$–$DK^{\bullet-}$) was determined from the redox potential.[32] The driving force [$-\Delta G_{CR}$] for the intramolecular charge-recombination process from the anion radical of the diketone moiety ($DK^{\bullet-}$) to the cation radical of the BODIPY moiety ($BODIPY^{\bullet+}$) was calculated using Eqs. (1) and (2).

$$-\Delta G_{CR} = [E_{ox}(BOD^{\bullet+}/BOD) - E_{red}(DK/DK^{\bullet-})] + \Delta G_S \quad (1)$$

$$\Delta G_S = e^2/(4\pi\varepsilon_0)[(1/(2R^+) + 1/(2R^-) - 1/R_{cc})(1/\varepsilon_s) - (1/(2R^+) + 1/(2R^-))(1/\varepsilon_r)] \quad (2)$$

Here e is the elementary charge, $E_{ox}(BOD^{\bullet+}/BOD)$ is the oxidation potential of the BODIPY moiety in dichloromethane, $E_{red}(DK/DK^{\bullet-})$ is the reduction potential of the diketone moiety in dichloromethane, ε_s and ε_r are the static dielectric constants of the solvents used to estimate the energy level and to measure the redox potentials, respectively, R^+ and R^- are the radii of the cationic and anionic BODIPY and diketone radicals, respectively, and R_{cc} represents the center-to-center distance between the BODIPY and diketone moieties. The molecular structures were estimated using the optimized geometries resulting from DFT calculations (Figure 4-52), and R^+ was determined to be 3.4 Å in the case of the **BCOD**-fused BODIPY and 5.4 Å (maximum) for the **Benzo**-fused BODIPY, while R was 1.5 Å for the diketone and the R_{cc} values were 7.7 Å for **BCOD-DK** and 7.0 Å for **Benzo-DK**.

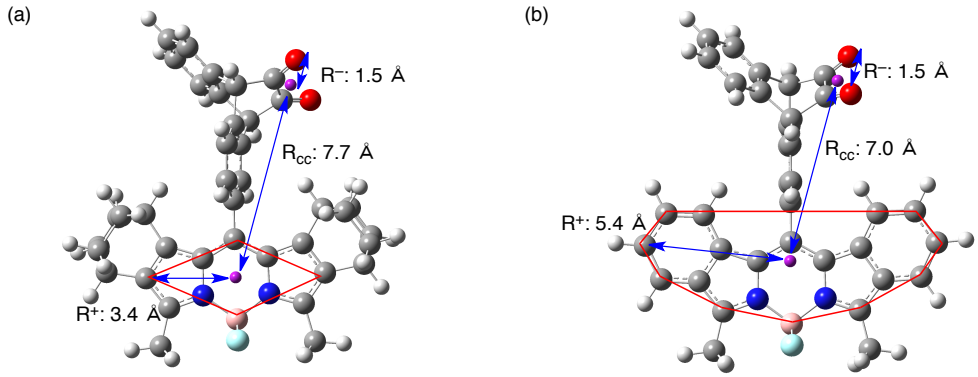

Figure 4-52. Optimized structures of **BCOD-DK** (a) and **Benzo-DK** (b) by DFT calculation of B3LYP/6-31G(d) level.

The driving force for the intramolecular charge separation process [$-\Delta G_{CS}$] from the BODIPY unit to the diketone moiety was determined using Eq. (3).

$$-\Delta G_{CS} = \Delta E_{0\text{–}0}(\text{BODIPY}) - (-\Delta G_{CR}) \qquad (3)$$

Here $\Delta E_{0\text{–}0}$(BODIPY) is the excited singlet state of the BODIPY moiety (^{1}BODIPY*). The ^{1}BODIPY* energy levels were calculated from the absorption and fluorescence spectra of **BCOD-Ant** and **Benzo-Ant**. In the case of **BCOD-DK**, the ^{1}BODIPY* energy level (2.27 eV) was higher than that of the CS state (2.04 eV) in dichloromethane (Figure 4-53). Thus, electron transfer from the BODIPY moiety to the DK moiety occurs, affording the CS state in dichloromethane. This electron transfer is responsible for the lower fluorescence intensity (Φ_F = 0.08) of **BCOD-DK** in dichloromethane. However, the energy level of the CS state in toluene is increased due to the smaller ε value in Eq. (1). Although the Born equation does not give correct values for ΔG_S in nonpolar solvents such as toluene, because of overestimation of the solvent polarity, tentative values of $-\Delta G_{CR}$ were nonetheless estimated. Since the CS energy level was calculated to be 3.60 eV in toluene, the CS level of **BCOD-DK** is higher than the ^{1}BODIPY* level and thus significant fluorescence was observed in toluene.

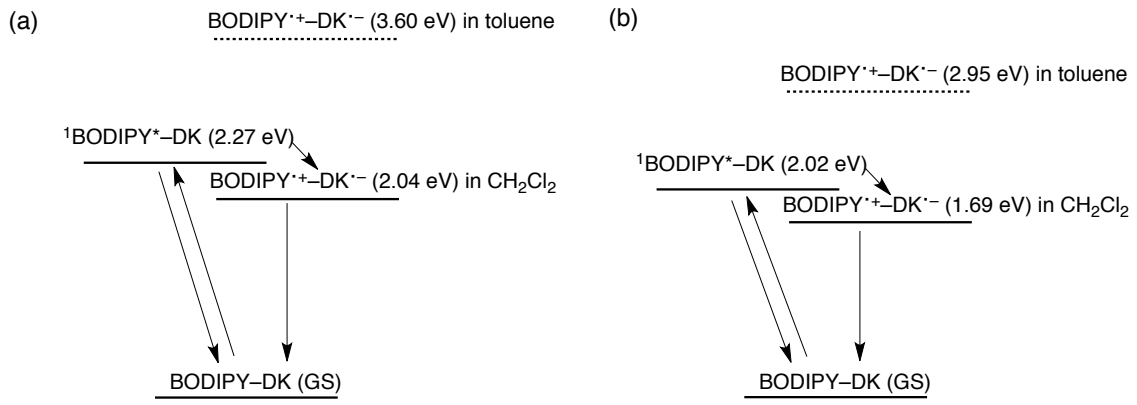

Figure 4-53. Energy diagrams of (a) **BCOD-DK** and (b) **Benzo-DK** in dichloromethane.

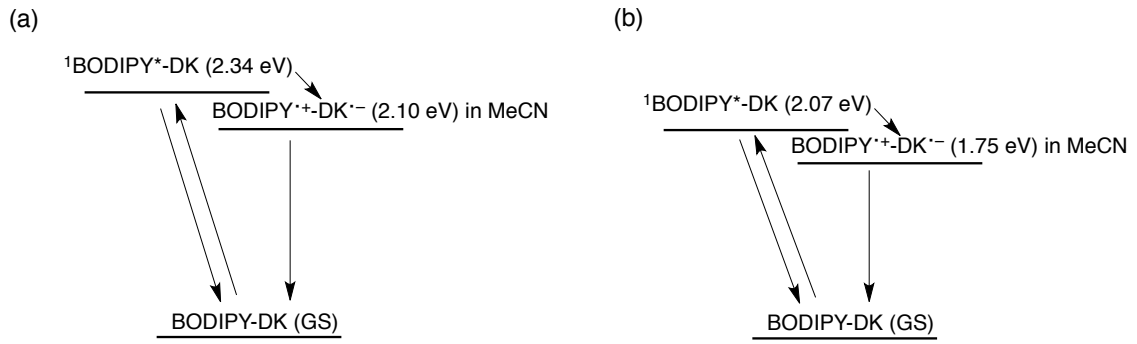

Figure 4-54. Energy diagrams of (a) **BCOD-DK** and (b) **Benzo-DK** in acetonitrile.

Similar phenomena were observed in the case of **Benzo-DK** and for the same reason. The CS energy levels of **Benzo-DK** were estimated to be 1.71 and 3.25 eV in dichloromethane and toluene, respectively, and the value in toluene was again higher than the energy level of the singlet excited state of Benzo-fused BODIPY. Thus, the fluorescence of **Benzo-DK** was not quenched in toluene. In addition, the energy difference between the CS level and singlet excited state for **Benzo-DK** in dichloromethane is larger than the difference in the case of **BCOD-DK**, and therefore fluorescence quenching was more effectively induced by the increase in solvent polarity.

The energy diagrams in acetonitrile are also estimated to consider the reason that almost the same results of fluorescence properties are observed in dichloromethane (Figure 4-54). In the case of **BCOD-DK**, the energy of CS state was calculated as 2.10 eV, and the energy is lower than the ^{1}BODIPY* energy level (2.34 eV) in acetonitrile. The energy gap (ΔE_g) of CS state and ^{1}BODIPY* energy level is 0.24 eV and similar to the ΔE_g in dichloromethane (ΔE_g = 0.23). In the case of **Benzo-DK**, the ^{1}BODIPY* energy level is 2.07 eV and the energy level of CS state

is 1.75 eV. The energy gaps are substantially same value, therefore the large difference in fluorescence properties wasn't observed in dichloromethane and acetonitrile.

Similarly, since the energy of excited singlet state of **ADK** is 2.52 eV, the electron transfer would occur by excitation at α-diketone moiety. Therefore, the photoreaction efficiency could be reduced compared to the efficiency of **ADK**. Additionally, intramolecular energy transfer from α-diketone unit to BODIPY is also possible from the energy diagram when the photoprecursor is excited at the **ADK** unit. The author here in briefly discusses on the kinetics of the competitive reactions, photoreaction on energy transfer. In order to make the mechanism clear, energy transfer efficiency in this system is considered based on the transition dipole moment (TDM) vector.

The rate constant $k_{en}(r)$ of energy transfer is shown as Eq. (4)

$$k_{en}(r) = \Phi_{fD}\kappa^2/\tau_D r^6[9000(\mathrm{In}10)/128\pi^5 N n^4]\, J(\lambda) \qquad (4)$$

Where Φ_{fD} is fluorescence quant yield of donor, κ^2 is direction factor which is determined from relative angle of TDM vectors of excited donor unit and acceptor, τ_D is fluorescence lifetime of donor, r is distance between donor and acceptor unit, N is Avogadro's constant, n is a refractive index of solvent, and $J(\lambda)$ is the overlap integral, respectively.

In this equation, κ^2 and Φ_{fD} affect markedly on energy transfer rate constant. The κ_2 parameters become zero with orthogonal TDM vectors. Each of the TDM vector was evaluated by DFT calculations. The TDM vector of **ADK** is parallel with the long axis of **ADK** unit (Figure 4-45 (d)). While, that of BODIPY is parallel with the long axis of BODIPY unit[33], which is perpendicular to the long axis of the **ADK** unit (Figure 4-45 (d)). Therefore, the two TDM vectors of each unit in BODIPY-DKs are nearly orthogonal, and κ_2 should be closed to zero. In addition, the Φ_{fD} of **ADK** (energy donor) is reported as small as 0.001.[16] For this reason, the $k_{en}(r)$ values of BODIPY-DKs should be small enough compared to the rate constant of photoreaction, which affords the efficient photoconversion of present molecule.

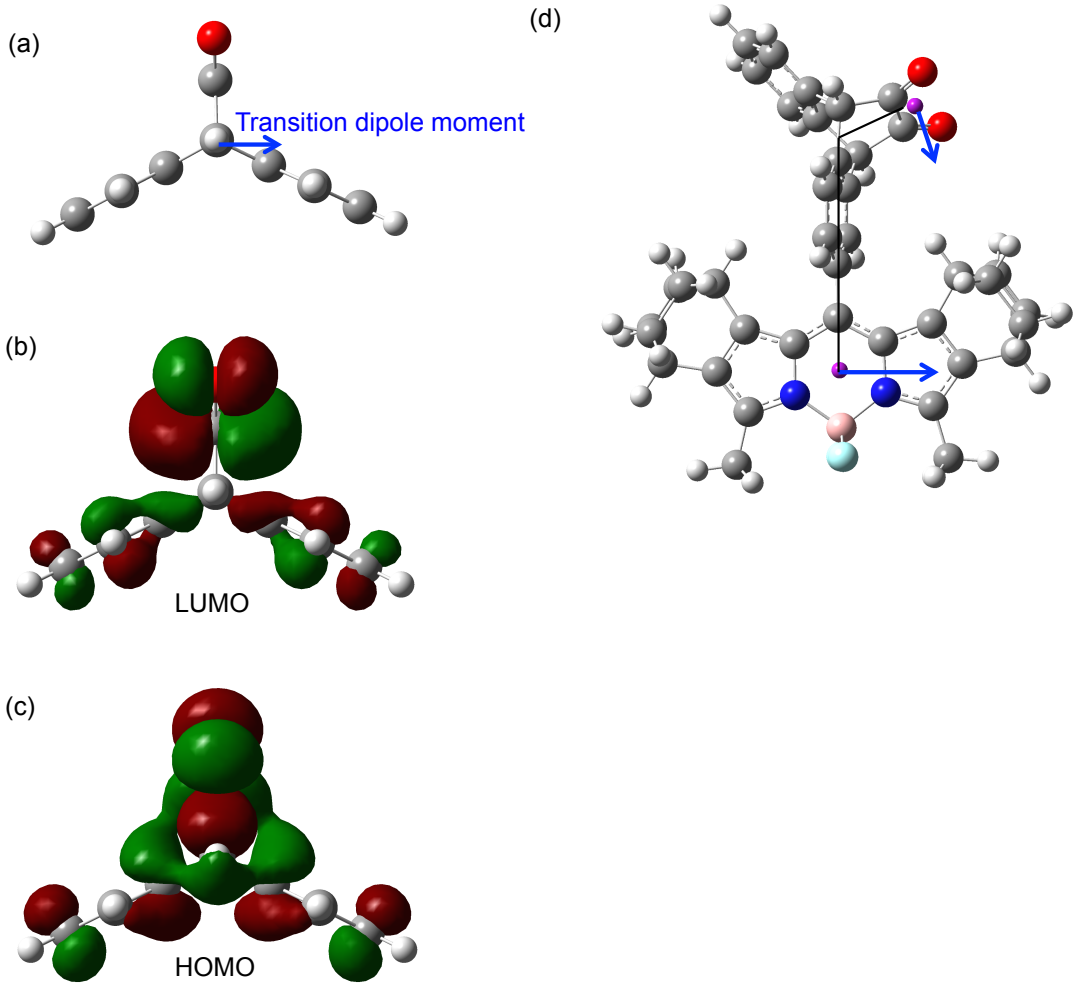

Figure 4-55. TDM vector calculated by TDDFT calculations at the CAM-B3LYP/6-31G(d)//B3LYP/6-31G(d) level (a). Molecular orbital of LUMO for **ADK** (b), Molecular orbital of LUMO for **ADK** (c), TDM vectors for each units.

4-4-8 Transient Absorption Spectroscopy

Femtosecond transient absorption spectra were acquired for each BODIPY in toluene, dichloromethane and acetonitrile (Figures 4-56–59, Table 4-7) to investigate the excited state decay process. When **BCOD-Ant** was irradiated at 500 nm, obvious bleaching of the ground state occurred between 480 and 650 nm, while a new absorption band appeared at approximately 450 nm, corresponding to the BOPIDY excited singlet state.[34] In toluene, decay to the ground state occurred with a lifetime of 6.3 ns. **BCOD-DK** exhibited similar bleaching and a similar decay profile (6.9 ns) in toluene upon irradiation at 450 nm. In contrast, its decay time was reduced to 248 and 351 ps in dichloromethane and acetonitrile, values which agreed

with the **BCOD-DK** fluorescence lifetime. Following irradiation, however, only the singlet excited state of BODIPY was observed and no other transient species, such as the BOPIDY radical cation, were observed.[35] Transient absorption measurements were also performed with **Benzo-Ant** and **Benzo-DK** in each solvent. In both cases, laser irradiation produced bleaching of the ground state of the BODIPY moiety at around 600 nm and generated broad peaks at higher energy wavelengths. The **Benzo-Ant** decay time was 4.8 ns, while those of **Benzo-DK** were 3.6 ns (toluene), 80 ps (dichloromethane) and 101 ps (acetonitrile). This is probably because the back electron transfer from $BODIPY^{\bullet+}$-$DK^{\bullet-}$ is faster than the intramolecular electron transfer from $^{1}BODIPY*$ to DK.

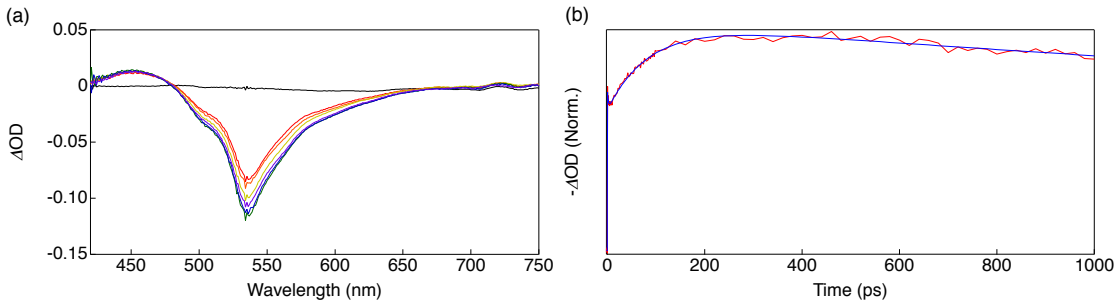

Figure 4-56. Femtosecond transient absorption spectra (a) and kinetic trace recorded at 528 nm (b) of **BCOD-Ant** in toluene: Black line (0 ps), red line (5 ps), orange line (20 ps), yellow line (50 ps), green line (200 ps), blue line (600 ps) and purple line (1000 ps).

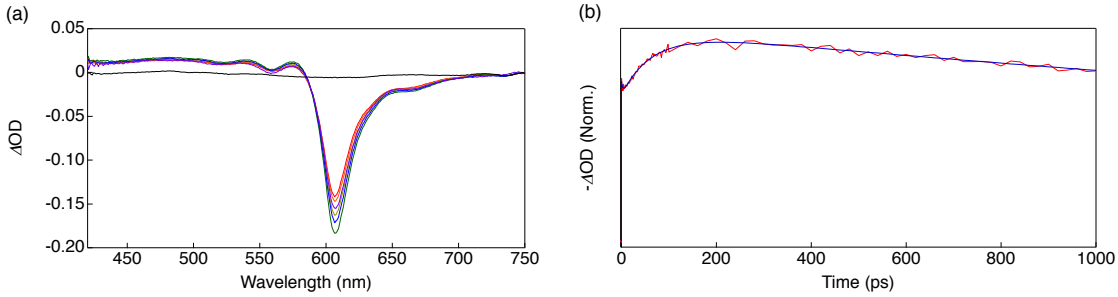

Figure 4-57. Femtosecond transient absorption spectra (a) and kinetic trace recorded at 605 nm (b) of **Benzo-Ant** in toluene (a): Black line (0 ps), red line (5 ps), orange line (20 ps), yellow line (50 ps), green line (200 ps), blue line (600 ps) and purple line (1000 ps).

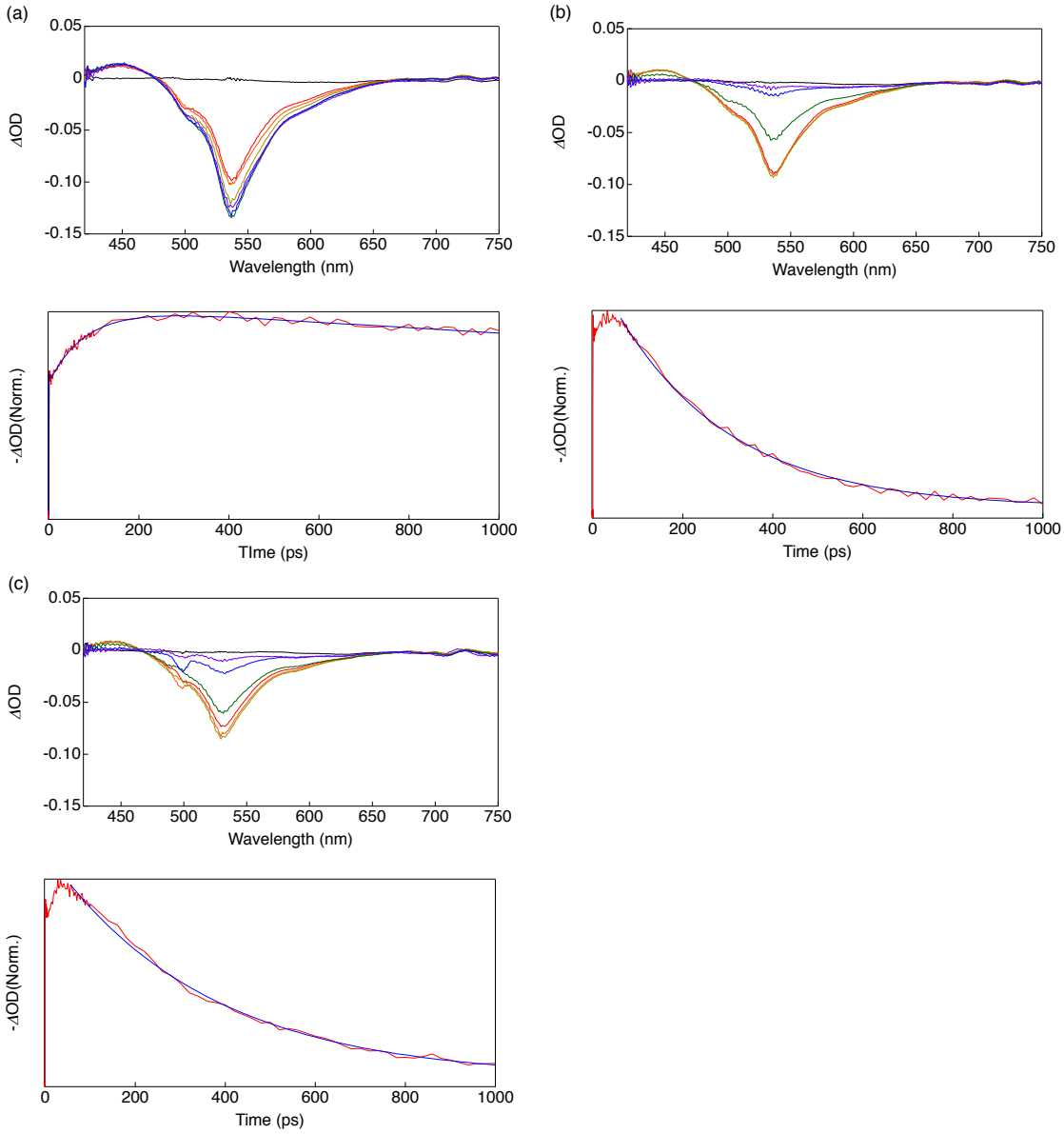

Figure 4-58. Femtosecond transient absorption spectra (top) and kinetic trace recorded at 528 nm (bottom) of **BCOD-DK** in toluene (a), dichloromethane (b) and acetonitrile (c): Black line (0 ps), red line (5 ps), orange line (20 ps), yellow line (50 ps), green line (200 ps), blue line (600 ps) and purple line (1000 ps).

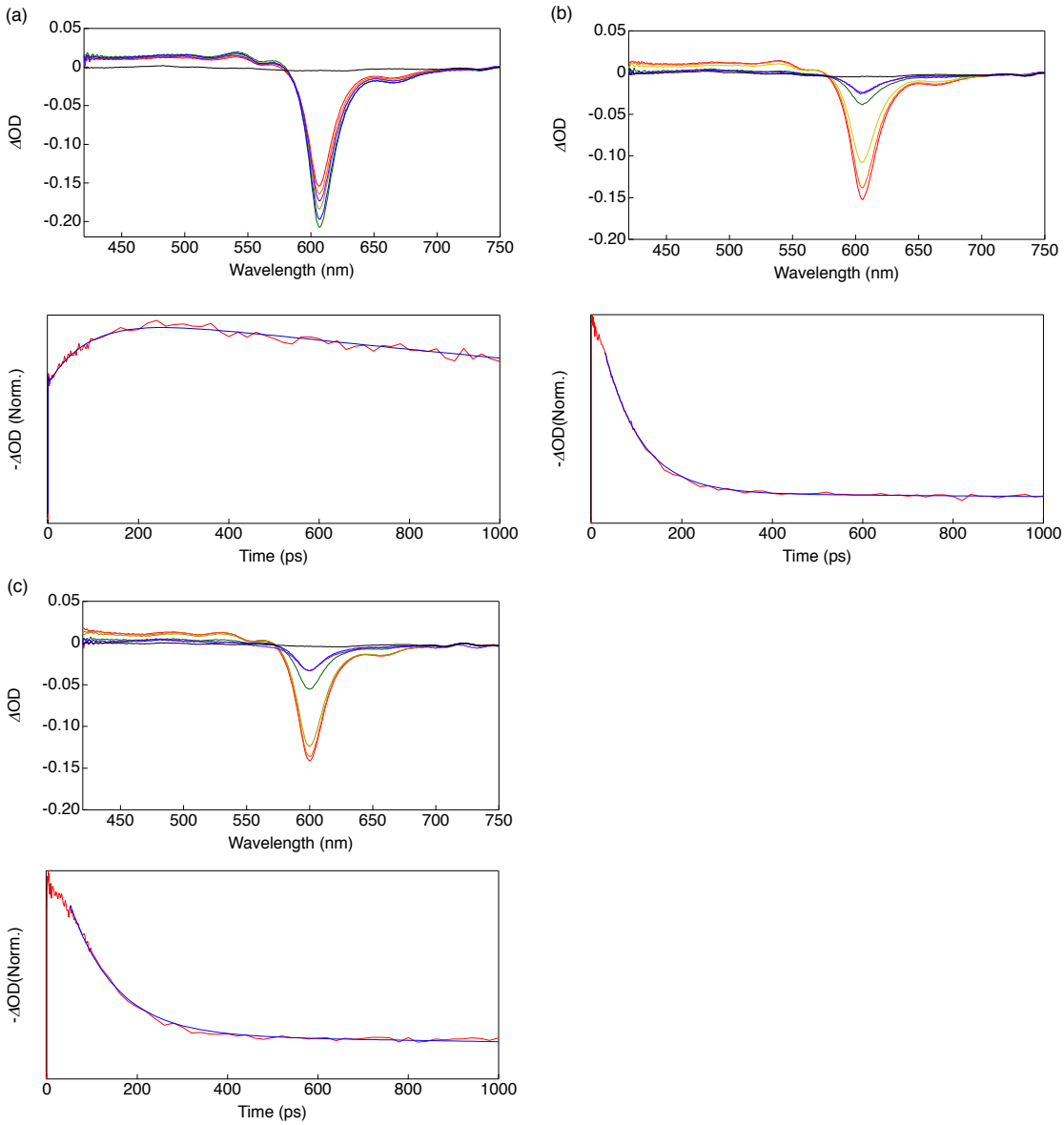

Figure 4-59. Femtosecond transient absorption spectra (top) and kinetic trace recorded at 605 nm (bottom) of **Benzo-DK** in toluene (a), dichloromethane (b) and acetonitrile (c): Black line (0 ps), red line (5 ps), orange line (20 ps), yellow line (50 ps), green line (200 ps), blue line (600 ps) and purple line (1000 ps).

Table 4-7. Summarized results of transient absorption spectra.

	BCOD-Ant		**BCOD-DK**		**Benzo-Ant**		**Benzo-DK**	
toluene	τ / ps	Amp.	τ / ps	Amp.	τ / ps	Amp.	τ / ps	Amp.
	2	0.08	2	0.04	2	0.06	1	0.06
	85	−0.35	84	−0.35	65	−0.29	92	−0.29
	6.3×10^3	0.92	6.9×10^3	0.96	4.8×10^3	0.94	3.6×10^3	0.94
dichloro methane	-		τ / ps	Amp.	-		τ / ps	Amp.
			248	0.90			80	0.90
			6.4×10^3 (fix)	0.10			5.4×10^3 (fix)	0.10
Acetonit rile	-		τ / ps	Amp.	-		τ / ps	Amp.
			351	0.95			101	0.73
			6.7×10^3 (fix)	0.05			6.7×10^3 (fix)	0.26

4-4-9 Short Summary

Photochemical generation of the highly fluorescent BODIPYs, **BCOD-Ant** and **Benzo-Ant**, from the minimally fluorescent BODIPYs **BCOD-DK** and **Benzo-DK** has been successfully achieved. The optical properties of these compounds were observed to change dramatically following the conversion of the DK group to anthracene, while the intrinsic color of each BODIPY in solution was only slightly altered by the photoactivation process. The BODIPYs with the diketone moiety exhibited lower fluorescence quantum yields (Φ_F) in dichloromethane and acetonitrile as compared to the non-polar solvent toluene. The pronounced effect of solvent polarity on Φ_F and fluorescence lifetime suggests that intramolecular electron transfer occurs from the BODIPY moiety to the diketone group.

4-4-10 Experimental Section

Synthesis Commercially available reagents and solvents for syntheses were of reagent grade and used without further purification. TLC and gravity column chromatography were performed on Art. 5554 (Merck KGaA) plates and silica gel 60N (Kanto Chemical), respectively. For spectral measurements, spectral-grade toluene, dichloromethane, methanol and acetonitrile were purchased from Nacalai Tesque. The dichloromethane used for cyclic voltammetry measurements was distilled from CaH_2.

3-Oxo-9,10,11,15-tetrahydro-9,10-epidioxoloanthracene-3-carbaldehyde (4-14): A solution of 2-formylanthracene **4-13** (0.10 g, 0.49 mmol) and vinylene carbonate (0.50 mL, 7.90 mmol) in xylenes (10 mL) was mixed at 160 °C in an autoclave for 3 d. After removal of the solvent in vacuo, the residue was purified by silica gel column chromatography with chloroform and recrystallization from $CHCl_3$-hexane to give **4-14** as white powder. Yield: 78% (0.11 g, 0.38 mmol); ^{1}H NMR ($CDCl_3$, 400 MHz): δ = 9.99 (s, 1H, –CHO), 7.92 (s, 1H), 7.79 (dt, *J* = 4.0, 7.2 Hz, 1H), 7.57 (d, 1H, *J* = 7.8 Hz), 7.42 (m, 2H), 7.30 (m, 2H), 4.95 (t, *J* = 1.6 Hz, 1H), 4.92 (t, *J* = 1.6 Hz, 1H), 4.83 (m, 2H); ^{13}C NMR ($CDCl_3$, 100 MHz, Mixture of stereoisomers): δ = 191.59, 191.33, 153.76, 153.72, 144.44, 143.30, 138.94, 137.62, 136.94, 136.38, 136.02, 135.84, 135.54, 135.00, 130.46, 130.22, 138.30, 128.24, 128.14, 128.09, 127.34, 126.93, 126.86, 126.81, 126.38, 125.91, 125.87, 125.81, 76.00, 75.96, 75.79, 75.66, 48.02, 47.96, 47.63, 47.63; MS (ESI): *m/z*: 315 $[M+Na]^+$; HR-ESI *m/z* = 315.06338 calcd. for $C_{18}H_{12}NaO_4$ = 315.06333 $[M+Na]^+$;

Compound 4-16: To a solution of isoindole **4-15** (0.31 g, 1.9 mmol) and **4-14** (0.265 g, 0.91 mmol) in dry dichloromethane (98 mL) were added six drops of TFA under an argon atmosphere. The mixture was stirred for 3 h in the dark. DDQ (0.45 g, 2.0 mmol) was added, and the mixture was stirred for additional 20 min. After addition of *N*,*N*-diisopropylethylamine (3.0 mL) and $BF_3{\cdot}OEt_2$ (3.0 mL), the mixture was stirred for 30 min. The reaction mixture was poured into water and extracted with dichloromethane. The organic layer was washed with water and brine; dried over sodium sulfate; and concentrated under a reduced pressure. The residue was purified by silica gel column chromatography with chloroform. Recrystallization from chloroform–methanol to give **4-16** as orange powder. Yield: 55% (0.32 g, 0.50 mmol); ^{1}H NMR ($CDCl_3$, 400 MHz, Mixture of stereoisomers): δ = 7.68–7.65 (m, 1H), 7.60–7.43 (m, 6H),

6.41–5.98 (m, 3H), 5.90–5.72 (m, 1H), 5.05–4.78 (m, 2H), 3.83–3.77 (m, 2H), 2.80–2.10 (m, 2H), 2.48 (s, 3H), 2.44 (s, 3H), 1.59–0.86 (m, 8H); ^{13}C NMR (CDCl3, 100 MHz, NMR was measured, however, the sample includes 8 isomers, the number of peaks don't match.) MS (ESI): *m/z*: 660 [M+Na]+; HR-ESI *m/z* = 660.24868 calcd. for $C_{40}H_{33}B_1F_2N_2NaO_3$ = 660.24863 [M+Na]+;

Compound 4-17: To a solution of **4-16** (0.27 g, 0.42 mmol) in THF (16 mL), methanol (16 mL) and water (8.1 mL), potassium carbonate (3.00 g) was added. The solution was stirred for overnight at room temperature. The reaction mixture was quenched with water and extracted with chloroform. The organic layer was washed with water and brine; dried over sodium sulfate; and concentrated under a reduced pressure. The residue was purified by column chromatography on silica gel with (ethyl acetate: chloroform = 1:4) to give **4-17** as orange powder. Yield: 79% (0.20 g, 0.33 mmol); ^{1}H NMR (CD_2Cl_2, 400 MHz, Mixture of stereoisomers): δ = 7.43–7.20 (m, 4H), 7.19–7.06 (m, 3H), 6.37–6.19 (m, 2H), 6.11–5.68 (m, 2H), 4.48–4.35 (m, 2H), 4.08–3.94 (m, 2H), 3.76–3.69 (m, 2H), 2.62–2.20 (m, 8H), 1.41–0.63 (m, 8H); ^{13}C NMR (CD_2Cl_2, 100 MHz, NMR was measured, however, the sample includes 6 isomers, the number of peaks doesn't match.); MS (ESI): *m/z*: 634 $[M+Na]^+$; HR-ESI *m/z* = 634.26933 calcd. for $C_{39}H_{35}B_1F_2N_2NaO_2$ = 634.26937 $[M+Na]^+$;

BCOD-DK: Under an argon atmosphere, dry DMSO (1.0 mL, 14 mmol) and dry dichloromethane (8.5 mL) were cooled to −60 °C. TFAA (0.5 mmol, 3.5 mmol) was added dropwise over 5 min. After the solution was stirred for 10 min, **4-17** (0.15 g, 0.33 mmol) in dry dichloromethane (5.0 mL) was added dropwise over 10 min. After the solution was stirred for 2 h, *N,N*-diisopropylethyamine (2.0 mL, 12 mmol) was added over 5 min. The solution was stirred for 60 min and left to warm up to room temperature. The reaction was quenched with water. The organic layer was washed with water, 1 M HCl and brine; dried over sodium sulfate; and concentrated under a reduced pressure. The residue was purified by silica gel column chromatography with dichloromethane. Recrystallization from dichloromethane–hexane to give **BCOD-DK** as orange powder. Yield: 30% (0.045 g, 0.074 mmol); ^{1}H NMR ($CDCl_3$, 400 MHz, Mixture of stereoisomers): δ = 7.69–7.43 (m, 7H), 6.42–5.72 (m, 2H), 5.18–5.04 (m, 2H), 3.83–3.76 (m, 2H), 2.53 (s, 3H), 2.51 (s, 3H), 2.47–2.10 (m, 2H), 1.44–0.88 (m, 8H); ^{13}C NMR ($CDCl_3$, 100 MHz, NMR was measured, however, the sample includes 3 isomers, the number of

peaks doesn't match.): δ = 183.38, 183.35, 183.29, 183.17, 183.13, 150.36, 150.30, 149.81, 148.50, 148.48, 148.03, 148.00, 147.98, 147.89, 138.73, 138.70, 138.34, 138.25, 138.23, 136.96, 136.93, 136.36, 136.33, 136.28, 136.14, 136.12, 136.09, 136.06, 135.97, 135.95, 135.90, 135.88, 135.36, 135.32, 135.22, 134.52, 134.49, 134.47, 134.43, 134.40, 134.37, 133.69, 133.63, 133.60, 133.54, 133.52, 133.46, 133.39, 130.38, 129.99, 129.86, 129.81, 129.78, 129.76, 129.67, 127.78, 127.41, 127.35, 127.21, 127.16, 127.10, 127.03, 126.61, 126.39, 126.36, 126.32, 126.30, 126.19, 126.12, 126.06, 59.93, 59.89, 59.87, 59.85, 59.82, 35.43, 35.41, 35.35, 35.32, 35.13, 35.10, 35.07, 32.87, 32.79, 32.77, 26.43, 26.36, 26.32, 26.30, 26.27, 25.99, 25.96, 25.89, 25.82, 25.78, 25.72, 12.61, 12.58, 12.56 ppm; MS (ESI): *m/z*: 662 $[M+Na]^+$; HR-ESI *m/z* = 662.26420 calcd for $C_{40}H_{35}B_1F_2N_2NaO_3$ = 662.26428 $[M+Na]^+$;

Benzo-DK: **BCOD-DK** was heated to 220 °C in the solid phase under vacuum for 1 h. After cooling to room temperature, **Benzo-DK** was obtained quantitatively as blue solids. ^{1}H NMR ($CDCl_3$, 400 MHz): δ = 7.78 (d, 1H, J = 7.5 Hz), 7.68–7.57 (m, 5H), 7.53–7.46 (m, 3H), 7.13 (t, J = 6.9 Hz, 1H), 7.00 (m, 2H), 6.70 (t, J = 6.9 MHz, 1H), 6.02 (d, J = 8.4 Hz, 1H), 5.81 (d, J = 8.4 Hz, 1H), 5.24 (s, 1H), 5.07 (s, 1H), 2.97 (s, 3H), 2.95 (s, 3H); ^{13}C NMR ($CDCl_3$, 100 MHz): δ = 183.49, 183.29, 151.50, 150.62, 136.53, 136.46, 136.31, 134.59, 134.52, 133.69, 133.43, 132.85, 130.68, 130.46, 130.25, 129.84, 129.76, 129.40, 128.65, 127.41, 127.39, 126.59, 126.54, 124.52, 124.26, 124.21, 123.72, 122.23, 122.16, 120.60, 120.53, 60.03, 59.84, 12.47, 12.47 ppm; MS (ESI): *m/z*: 606 $[M+Na+MeOH]^+$; HR-ESI *m/z* = 606.20153 calcd for $C_{36}H_{27}B_1F_2N_2NaO_3$ = 606.20168 $[M+Na+MeOH]^+$;

BCOD-Ant: **BCOD-DK** was photo-irradiated over 390 nm under an argon atmosphere and monitored by ^{1}H NMR in an NMR tube. After removal solvent, **BCOD-Ant** was obtained as orange powder. ^{1}H NMR ($CDCl_3$, 400 MHz, Mixture of stereoisomers): δ = 8.60 (s, 1H), 8.52 (t, *J* = 6.0 Hz, 1H), 8.18 (m, 1H), 8.12–8.07 (m, 3H), 7.57–7.49 (m, 3H), 6.36 (m 2H), 6.02–5.92 (m, 2H), 3.82 (m, 2H), 2.69 (m, 2H), 2.56 (s, 6H), 1.40-1.32 (m, 4H), 1.18–1.09 (m, 4H); ^{13}C NMR ($CDCl_3$, 100 MHz): δ = 150.41, 150.33, 150.26, 147.66, 147.64, 147.60, 147.57, 139.05, 138.33, 138.29, 138.24, 135.81, 133.94, 133.88, 132.35, 132.28, 132.26, 132.24, 131.70, 131.59, 131.43, 131.18, 131.15, 131.13, 130.58, 130.53, 130.50, 128.96, 128.63, 128.35, 128.27, 128.24, 128.20, 128.07, 127.54, 127.47, 127.07, 127.02, 126.96, 126.72, 126.58, 126.56, 126.42, 126.13, 126.13, 126.04, 35.42, 35.39, 32.89, 26.50, 26.45, 26.43, 26.38, 25.96, 25.92, 25.87, 25.83,

12.62 ppm (Some peaks lacked because the peaks overlap); MS (ESI): *m/z*: 574 $[M+Na]^+$; HR-ESI *m/z* = 574.24803 calcd. for $C_{37}H_{31}B_1F_2N_2Na$ = 574.24824 $[M+Na]^+$;

Benzo-Ant; **Benzo-DK** was photo-irradiated over 390 nm under an argon atmosphere and monitored by ^1H NMR in an NMR tube. After removal solvent, **Benzo-Ant** was obtained as blue solid. ^1H NMR ($CDCl_3$, 400 MHz): δ = 8.66 (s, 1H), 8.51 (s 1H), 8.32 (d, J = 8.8 Hz, 1H), 8.23 (s, 1H), 8.13 (d, J = 8.4 Hz, 1H), 8.06 (d, J = 8.8 Hz, 1H), 7.66 (d, J = 8.0 Hz, 2H), 7.60–7.52 (m, 3H), 7.05 (t, J = 8.0 Hz, 2H), 6.84 (t, J = 7.6 Hz, 2H), 6.22 (d, J = 8.0 Hz, 2H), 3.00 (s, 6H); ^{13}C NMR ($CDCl_3$, 100 MHz): δ = 150.51, 134.62, 133.84, 132.38, 132.20. 131.68, 131.24, 131.18, 130.56, 129.68, 128.85, 128.64, 128.24, 128.23, 127.16, 126.69, 126.36, 126.10,126.02, 124.84, 123.79, 121.97, 121.24, 12.51; MS (ESI): *m/z*: 518 $[M+Na]^+$; HR-ESI *m/z* = 518.18645 calcd. for $C_{33}H_{23}B_1F_2N_2Na$ = 518.18564 $[M+Na]^+$;

General. ^1H and ^{13}C NMR spectra were recorded with a JEOL JNM-ECX 400 spectrometer at ambient temperature by using tetramethylsilane as an internal standard. Mass spectra were measured on a JEOL JMS-700 spectrometer. UV/Vis spectra were measured with a JASCO UV/Vis/NIR spectrophotometer V-570. Fluorescence quantum yields were measured on an Absolute PL Quantum Yield Measurement System C9920-02. Thermal gravimetric analyses were carried out using an EII nanotechnology DSC/TG-DTA 6200.

Optical Spectroscopy. The fluorescence decays were measured using a C4780 picosecond fluorescence lifetime measurement device (Hamamatsu Photonics). The femtosecond pulse laser, Mira Model 900-F & Pulse Switch, was used and the excitation light wavelength was 365 nm from a Coherent Verdi V-5 Nd:YVO4laser.

Photochemical Reactions. The photochemical reactions were carried out in an NMR tube, which irradiated by a metal-halide lamp (Nippon P. I. PCS-UMX375RC, 375 W) through a UV-cutoff filter (390 nm) under an argon atmosphere and monitored by a JNM-ECX 400 spectrometer.

Cyclic Voltammetry. CV measurements were conducted in a solution of 0.1 M n-Bu_4NPF_6 in dry dichloromethane or acetonitrie with a scan rate of 100 mV/s at room temperature in an

argon-filled cell. A glassy carbon electrode and a Pt wire were used as a working and a counter electrode, respectively. An Ag/Ag^+ electrode was used as a reference electrode, which was normalized with the half-wave potential of ferrocene/ferrocenium$^+$ (Fc/Fc^+) redox couple.

X-ray Crystallographic Analysis. Single-crystal X-ray diffraction data was collected at 90 K with a BRUKER-APEXII X-Ray diffractometer equipped with a large area CCD detector by using graphite monochromated Mo-Kα radiation (λ = 0.71073 Å). The structure was solved by direct method (SHELXS-97) and refined with the SHELX-97 program.[36] Crystallographic data has been deposited at the Cambridge Crystallographic Data Centre (CCDC) under number CCDC-1012964.

Laser Flash Photolysis. Transient absorption spectra were measured by femtosecond pump-probe experiments. Samples were exited at 500 nm or 605 nm by using an optical parametric amplifier (TOPAS, Light Conversion Ltd.) with an amplified mode-locked Ti:Sapphire laser (Spitfire and Tsunami, Spectra-Physics). Excitation intensity was 30 ~ 70 mW with the repetition rate of 0.5 kHz using a chopper (MODEL 3501, New Focus Inc.). Absorption transients were probed by delayed pulses of a femtosecond white-light continuum generated by focusing fundamental laser pulse into a D_2O cell and detected by a polychromator-CCD combination (Spectra Pro-275 and Spec-10, Acton Research Co. and Princeton Instruments). The temporal resolution was 100 fs.

Theoretical calculations

The geometries of **BCOD-DK** and **Benzo-DK** were fully optimized using the density functional theory (DFT). The functional and basis set used in the DFT calculations were the Becke's three-parameter hybrid functional combined with the Lee–Yang–Parr correlation functional (B3LYP) and the 6-31G(d) basis set, respectively.[22] Equilibrium geometries were verified by the frequency calculations, where no imaginary frequency was found. All the calculations were carried out using the Gaussian 09 suite of programs.[22]

4-5 References

(1) (a) Beija, M.; Afonso, C. A. M.; Martinho, J. M. G. *Chem. Soc. Rev.* **2009**, *38*, 2410–2433.

(2) (a) Nola, E. M.; Lippard, S. J. *Chem. Rev.* **2008**, *108*, 3443–3480. (b) Xu, Z.; Yoon, J.; Spring, D. R. *Chem. Soc. Rev.* **2010**, *39*, 1996–2006.

(3) Han, J.; Burgess, K. *Chem. Rev*. **2010**, *110*, 2709–2728.

(4) Carter, K. P.; Young, A. M.; Palmer, A. E. *Chem. Rev.* **2014**, *114*, 4564–4601.

(5) (a) Irie, M.; Fukaminato, T.; Sasaki, T.; Tamai, N.; Kawai, T. *Nature* **2002**, *420*, 759–760. (b) Betzig, E.; Patterson, G. H.; Sougrat, R.; Lindwasser, W. O.; Olenych, S.; Bonifacino, J. S.; Davidson, M. W.; Lippincott-Schwartz, J.; Hess, H. F. *Science* **2006**, *313*, 1642–1645. (c) Bates, M.; Huang, B.; Dempsey, G.; Zhuang, X. *Science* **2007**, *317*, 1749–1753.

(6) Cusido, J.; Deniz, E.; Raymo, F. M. *Eur. J. Org. Chem*. **2009**, 2031–2045.

(7) (a) Takeshita, M.; Irie, M. *Chem. Lett.* **1998**, 1123–1124. (b) Song, L.; Yang, Y.; Zhang, Q.; Tian, H.; Zhu, W. *J. Phys. Chem. B* **2011**, *115*, 14648–14658. (c) Murphy, S. K.; Baik C.; Lu, J.-S.; Wang, S. *Org. Lett*. **2010**, *12*, 5266–5269. (d) Uno, K.; Niikura, H.; Morimoto, M.; Ishibashi, Y.; Miyasaka, H.; Irie, M. *J. Am. Chem. Soc.* **2011**, *133*, 13558–13564.

(8) (a) Osuka, A.; Fujitsuka, D.; Shinmori, H.; Kobatake, S.; Irie, M. *J. Org. Chem*. **2001**, *66*, 3913–3923. (b) Wang, S.; Shen, W.; Feng, Y.; Tian, H. *Chem. Commun*. **2006**, 1497–1499.

(9) (a) Andréasson, J.; Kodis, G.; Terazono, Y.; Liddell, P. A. Nandyopadhyay, S.; Mitchell, R. H.; Moore, T. A.; Gust, D. *J. Am. Chem. Soc.* **2004**, *126*, 15926–15927. (b) Terazono, Y.; Kodis, G.; Andréasson, J.; Jeong, G.; Brune, A.; Hartmann, T.; Dürr, H.; Moore, A. L.; Moore, T. A.; Gust, D. *J. Phys. Chem. B* **2004**, *108*, 1812–1814. (c)

(10) Fukaminato, T.; Sasaki, T.; Kawai, T.; Tamai, N.; Irie, M. *J. Am. Chem. Soc.* **2004**, *126*, 14843–14849.

(11) Fukaminato, T.; Doi, T.; Tamaoki, N.; Okuno, K.; Ishibashi, Y.; Miyasaka, H.; Irie, M. *J. Am. Chem. Soc.* **2011**, *133*, 4984–4990.

(12) (a) Nakagawa, H.; Kawai, S.; Nakashima, T.; Kawai, T. *Org. Lett*. **2009**, *11*, 1475–1478. (b) Thapaliya, E.R.; Captain, B.; Raymo, F. M. *J. Org. Chem.* **2014**, *79*, 3973–3981.

(13) Anthony, J. E. *Chem. Rev.* **2006**, *106*, 5028–5048.

(14) (a) Brown, A. R.; Pomp, A.; De Leeuw, D. M.; Klaassen, D. B. M.; Havinga, E. E.; Herwig, P.; Müllen, K. *J. Appl. Phys.* **1996**, *79*, 2136–2138. (b) Herwig, P. T.; Müllen, K. *Adv. Mater.* **1999**, *11*, 480–483.

(15) (a) Löhmannströben, H.-G. *Appl. Phys. B* **1988**, *47*, 195–199. (b) Burgdorff, C.; Lircher, T.; Löhmannströben, H.-G. *Spectrochim. Acta A.* **1988**, *44*, 1137–1141. (c) Burdett, J. J.; Müller, A. M.; Gosztola, D.; Bardeen, C. J. *J. Chem. Phys.* **2010**, *133*, 144506-1–144506-12.

(16) Mondal, R.; Okhrimenko, A.; Shah, B.; Neckers, D. *J. Phys. Chem. B* **2008**, *112*, 11–15.

(17) Garden, S. J.; Torres, J.; Ferreira, A. A.; Silva, R. B.; Pinto, A. C. *Tetrahedron Lett*. **1997**, *38*, 1501–1504. (b) Heitman, L. H.; Narlawar, R.; de Vries, H.; Willemsen, M. N.;Wolfram, D.;Brussee, J.; IJzerman, A. P. *J. Med. Chem*. **2009**, *52*, 2036–2042.

(18) Peng, P.; Wang, C.; Shi, Z.; Johns, V.; Ma, L.; Oyer, J.; Copik, A.; Igarashi, R.; Liao, Y. *Org. Biomol. Chem.* **2013**, *11*, 6671–6674.

(19) Thapaliya, E.; Swaminathan, S.; Captain, B.; Raymo, F. *J. Am. Chem. Soc.* **2014**, *136*, 13798–13804.

(20) Figueira-Duarteand, T. M.; Müllen, K. *Chem. Rev.* **2011**, *111*, 7260–7314.

(21) (a) Weigel, Q.; Rettig, W.; Dekhtyar, M.; Modrakowski, C.; Beinhoff M.; Schlüter, A. D. *J. Phys. Chem. A* **2003**, *107*, 5941–5947. (b) Yang, S.-W.; Elangovan, A.; Hwang K.-C.; Ho, T.-I. *J. Phys. Chem. B* **2005**, *109*, 16628–16635.

(22) (*a*) Backe, A. D.; *J. Chem. Phys.* **1993**, *98*, 5648–5652; (*b*) Lee, C.; Yang, W.; Parr, R. G. *Phys. Rev. B*, **1988**, *37*, 785–789. (c) Gaussian 09, Revision D.01, Frisch, M. J.; Trucks, G. W.; Schlegel, H. B.; Scuseria, G. E.; Robb, M. A.; Cheeseman, J. R.; Scalmani, G.; Barone, V.; Mennucci, B.; Petersson, G. A.; Nakatsuji, H.; Caricato, M.; Li, X.; Hratchian, H. P.; Izmaylov, A. F.; Bloino, J.; Zheng, G.; Sonnenberg, J. L.; Hada, M.; Ehara, M.; Toyota, K.; Fukuda, R.; Hasegawa, J.; Ishida, M.; Nakajima, T.; Honda, Y.; Kitao, O.; Nakai, H.; Vreven, T.; Montgomery, J. A., Jr.; Peralta, J. E.; Ogliaro, F.; Bearpark, M.; Heyd, J. J.; Brothers, E.; Kudin, K. N.; Staroverov, V. N.; Kobayashi, R.; Normand, J.; Raghavachari, K.; Rendell, A.; Burant, J. C.; Iyengar, S. S.; Tomasi, J.; Cossi, M.; Rega, N.; Millam, M. J.; Klene, M.; Knox, J. E.; Cross, J. B.; Bakken, V.; Adamo, C.; Jaramillo, J.; Gomperts, R.; Stratmann, R. E.; Yazyev, O.; Austin, A. J.; Cammi, R.; Pomelli, C.; Ochterski, J. W.; Martin, R. L.; Morokuma, K.; Zakrzewski, V. G.; Voth, G. A.; Salvador, P.; Dannenberg, J. J.; Dapprich, S.; Daniels, A. D.; Farkas, Ö.; Foresman, J. B.; Ortiz, J. V.; Cioslowski, J.; Fox, D. J. Gaussian, Inc., Wallingford CT, 2009. (b) Becke, A. D. *Phys. Rev. A* **1988**, *38*, 3098–3100; c) Becke, A. D. *J. Chem. Phys.* **1993**, *98*, 5648–5652; d) Lee, C.; Yang, W.; Parr, R. G. *Phys. Rev. B* **1988**, *37*, 785–789.

(23) Baumgarten, M.; Gherghel, L.; Friedrich, J.; Jurczok, M.; Rettig, W. *J. Phys. Chem. A*, **2000**, *104*, 1130–1140.

(24) Hatchard, C. G.; Parker, C. A. *Proc. R. Soc. London, Ser. B* **1956**, *235*, 518–536.

(25) Ulrich, G.; Ziessel, R.; Harriman, A. *Angew. Chem. Int. Ed.* **2008**, *47*, 1184–1201.

(26) (a) Descalzo, A.; Xu, H.-J.; Xue, Z.-L.; Hoffmann, K.; Shen, Z.; Weller, M.; You, X.-Z.; Rurack, K. *Org. Let.* **2008**, *10*, 1581–1584. (b) Umezawa, K.; Nakamura, Y.; Makino, H.; Citterio, D.; Suzuki, K. *J. Am. Chem. Soc.* **2008**, *130*, 1550–1551. (c) Ulrich, G.; Goeb, S.; Nicola, A.; Retailleau, P.; Ziessel, R. *J. Org. Chem.* **2011**, *76*, 4489–4505. (d) Awuah, S.; Polreis, J.; Biradar, V.; You, Y. *Org. Let.* **2011**, *13*, 3884–3887. (e) Zeng, L.; Jiao, C.; Huang, X.; Huang, K.-W.; Chin, W.-S.; Wu, J.*Org. Lett.* **2011**, *13*, 6026–6029. (f) Hayashi, Y.; Obata, N.; Tamaru, M.; Yamaguchi, S.; Matsuo, Y.; Saeki, A.; Seki, S.; Kureishi, Y.; Saito, S.; Yamaguchi, S.; Shinokubo, H. *Org. Lett.* **2012**, *14*, 866–869. (g) Sarma, T.; Panda, P.; Setsune, J. *Chem. Commun.* **2013**,*49*, 9806–9808. (h) Ni, Y.; Zeng, W.; Huang, K.-W.; Wu, J. *Chem. Commun.* **2013**, *49*, 1217–1219.

(27) Yamada, H.; Kuzuhara, D.; Ohkubo, K.; Takahashi, T.; Okujima, T.; Uno, H.; Ono, N.; Fukuzumi, S. *J. Mater. Chem.* **2010**, *20*, 3011–3024.

(28) (a) Kee, H.; Kirmaier, C.; Yu, L.; Thamyongkit, P.; Youngblood, W.; Calder, M.; Ramos, L.; Noll, B.; Bocian, D.; Scheidt, W.; Birge, R.; Lindsey, J.; Holten, D. *J. Phys. Chem. B* **2005**, *109*, 20433–20443. (b) Bahaidarah, E.; Harriman, A.; Stachelek, P.; Rihn, S.; Heyer, E.; Ziessel, R. *Photochem. Photobiol. Sci.* **2014**, *13*, 1397–1401.

(29) (a) Wada, M.; Ito, S.; Uno, H.; Murashima, T.; Ono, N.; Urano, T.; Urano, Y. *Tetrahedron Lett.* **2001**, *42*, 6711–6713. (b) Shen, Z.; Röhr, H.; Rurack, K.; Uno, H.; Spieles, M.; Schulz, B.; Reck, G.; Ono, N. *Chem. Eur. J.* **2004**, *10*, 4853–4871.

(30) (a) Okujima, T.; Tomimori, Y.; Nakamura, J.; Yamada, H.; Uno, H.; Ono, N. *Tetrahedron* **2010**, *66*, 6895–6900. (b) Tomimori, Y.; Okujima, T.; Yano, T., Mori, S.; Ono, N.; Yamada, H.; Uno, H. *Tetrahedron*, **2011**, *67*, 3187–3193. (c) Nakamura, M.; Tahara, H.; Takahashi, K.; Nagata, T.; Uoyama, H.; Kuzuhara, D.; Mori, S.; Okujima, T.; Yamada, H.; Uno, H. *Org. Biomol. Chem*. **2012**, *10*, 6840–6849. (d) Nakamura, M.; Kitatsuka, M.; Takahashi, K.; Nagata, T.; Mori, S.; Kuzuhara, D.; Okujima, T.; Yamada, H.; Nakae, T.; Uno, H. *Org. Biomol. Chem*. **2014**, *12*, 1309–1317.

(31) Dauselt, J.; Zhao, J.; Kind, M.; Binder, R.; Bashir, A.; Terfort, A.; Zharnikov, M. *J. Phys. Chem. C* **2011**, *115*, 2841–2854.

(32) Fujitsuka, M; Ito, O.; Imahori, H.; Yamada, K.; Yamada H.; Sakata, Y. *Chem. Lett*. **1999**, *8*,

721–722.

(33) Bañuelos Prieto, J.; López Arbeloa, F.; Martínez Martínez, V.; López Arbeloa, I. *Chem. Phys.* **2004**, *296*, 13-22.

(34) (a) Harriman, A.; Rostron, J.; Cesario, M.; Ulrich, G.; Ziessel, R. *J. Phys. Chem. A* **2006**, *110*, 7994–8002. (b) Duvanel, G.; Banerji, N.; Vauthey, E. *J. Phys. Chem. A* **2007**, *111*, 5361–5369.

(35) Jones II, G.; Kumar, S.; Klueva, O.; Pacheco, D. *J. Phys. Chem. A* **2003**, *107*, 8429–8434.

(36) Sheldrick, G. M.; *Acta. Cryst.* **2008**, *A64*, 112–122.

4-6 Summary

In this chapter, the one-way photoswitchable molecules with the high ON-OFF ratio of fluorescence were studied as a new application of α-diketone type precursor method. Three different fluorescence switching mechanisms using α-diketone type precursors were described, and the synthesis and photochemical properties were mainly discussed. Firstly, photoswitchable molecules whose skeleton can change from α-diketone type naphthacene precursor with no emission in visible region to highly fluorescent 5,12-aryl substituted naphthacene were described. Although the mechanism is typical fluorescence switching system, the result is a well-meaning research to be presented as a new application of α-diketone type precursor method. As the second system, α-diketone type precursor was used as an intramolecular fluorescence quencher unit of pyrene. The synthesized precursors didn't show fluorescence, meanwhile, photo-converted anthracene-pyrene conjugates show high fluorescence quantum yields (maximum 99%). The fluorescence quenching mechanism of the precursors is considered the intramolecular energy transfer from the excited singlet state of pyrene to diketone. After conversion, since the conjugate has no unit to quench the fluorescence, the fluorescence is observed. Therefore, the fluorescence switching using the precursor method became possible to adjust the fluorescence wavelength by the combination of fluorophore. The third system is fluorescence quenching based on intramolecular electron transfer from BODIPY moiety to α-diketone moiety. In this system, α-diketone unit was used as a photoswitching unit and electron accepter unit. This result clarified α-diketone type precursor can be used for the fluorescent molecules with lower excitation energy than singlet state of α-diketone type precursor. Additionally, stepwise fluorescence switching in optical wavelength and intensity became possible by combining the thermal stimuli responsible unit. As the result, a validity of α-diketone type precursor method for preparation of one-way fluorescence switching material was shown experimentally and new application of the α-diketone type photoprecursor was proposed in this chapter.

Chapter 5

9,9′-Anthryl-Anthroxyl Radicals: Strategic Stabilization for Highly Reactive Phenoxyl Radicals

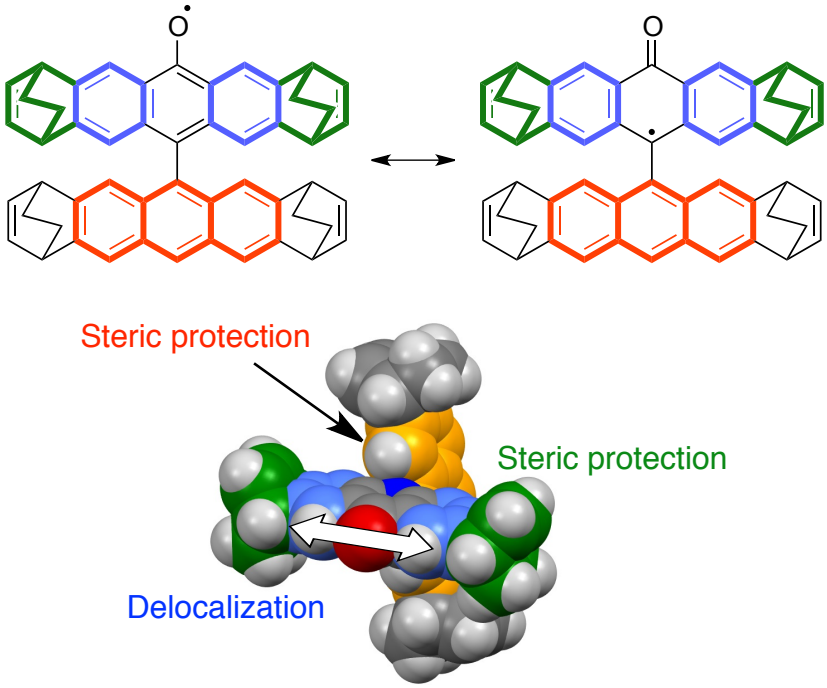

In order to improve the stability of highly reactive phenoxyl radical, 9,9′-anthryl-anthroxyl radicals were designed. In this chapter, synthesis, optical properties and stability of 9,9′-anthryl-anthroxyl radicals are discussed.

5-1 Introduction

Organic radical compounds are known as typically short-lived, highly reactive species for a long time. In 1900, however, Gomberg reported triphenylmethyl radical as a stable species for the first time.[1] Since then the isolation of a variety of radicals has been possible by their electronic stabilization with π-conjugation expansion and by the steric protection with the surrounding substituents (Figure 5-1)[2]. Stable organic radicals show long-wavelength absorption and reversible redox characteristics according to the singly occupied molecular orbital (SOMO). Consequently, they are promising to be applied to organic radical secondary battery[3] and organic electronics[4].

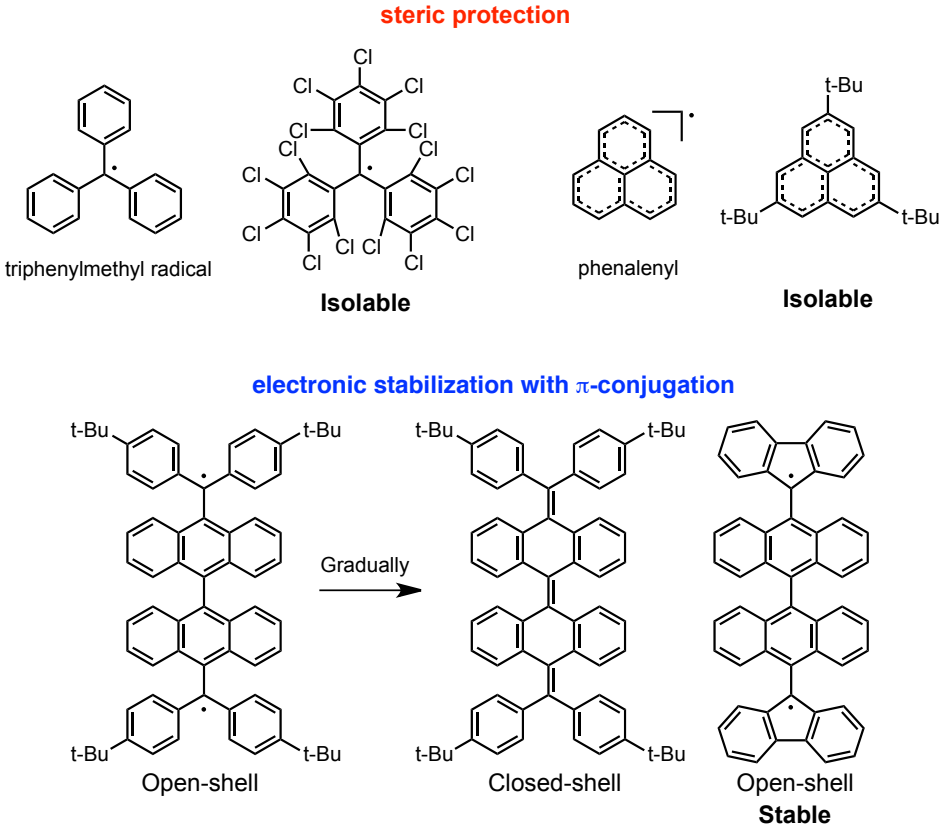

Figure 5-1. Typical examples of stabilized oraganic radical molecules by steric protection and π-delocalization.

Phenoxyl radical,[5] which is one of the highly reactive radicals, is observed in biological processes as tyrosyl radicals related to electron transfer, hydrogen atom transfer and proton coupled electron transfer[6]. The resonance structures of the phenoxyl radical are shown in Scheme 5-1. It formally contains resonance structure and possibly the carbon atom at 4-position is also reactive. The stabilization has been achieved by the bulky ortho-substituents,[7] coordination to metal ions[8] or the π-conjugation expansion[9].

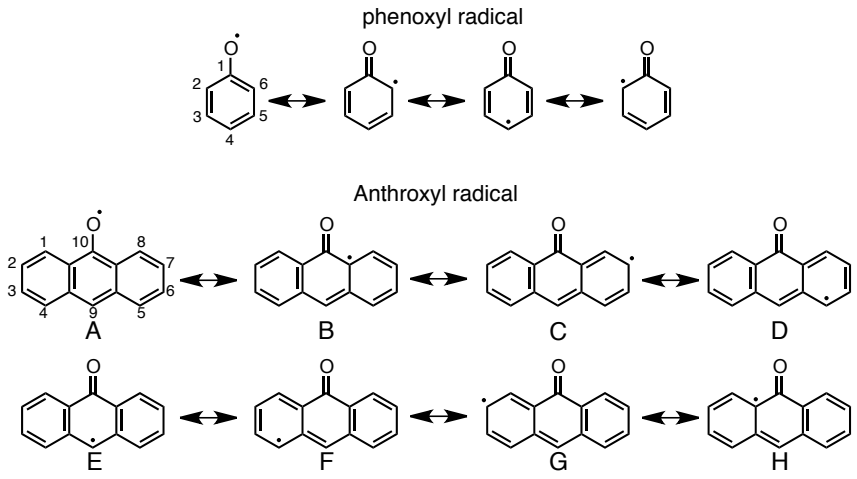

Scheme 5-1. The resonance structures of phenoxyl radical and anthroxyl radical.

During the investigation of creation of molecular graphene nano-ribbons (GNRs)[10], we found the formation of stable anthroxyl radical. The preparation of 9,9′-anthryl-anthr-10-oxy radical (**5-1**), an example of π-expanded phenoxyl radical, was reported by Singer and co-workers in 1971 where **5-1** was obtained by the oxidation of 9,9′-bianthryl by molecular oxygen, but only the hyperfine coupling constants (hfccs) and *g*-value was reported without an ESR spectrum.[11] Yamada and co-workers have recently prepared tetrabicyclo[2.2.2]octadiene(BCOD)-fused 9,9′-bianthryl.[12] Due to the bulky structure of BCOD unit, the BCOD-fused structure should be suitable to stabilize the phenoxyl radical derivatives.

5-2 Molecular Design

The author of this thesis designed more stabilized radical (**5-2**) under ambient conditions in comparison with the radical **5-1** (Figure 5-2). The compound **5-2** has fully taken two kinds of strategies to stabilize the unstable radical (Chart 5-1): 1) phenyl skeleton expands to anthracene, resulting in the gain of two aromatic stabilization energy in resonance structure E, 2) 4′,5′-hydrogen atoms of 9-anthryl group at *peri*-positions steric protect the most reactive carbon atom at 9-position (resonance E, Scheme 1) and BCODs of 2,3,6,7-positions steric protect the peripheral position of anthracene as the bulky substituents.

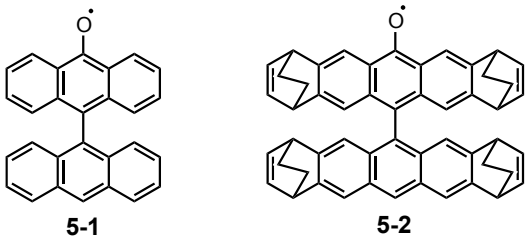

Figure 5-2. The molecule structures of anthryl-anthroxyl radical derivatives.

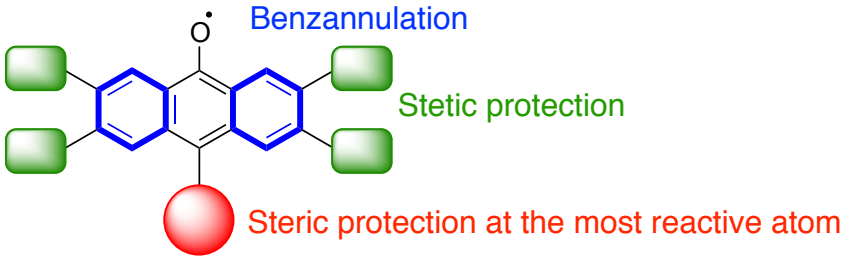

Chart 5-1. The kinds of techniques to stabilize the unstable phenoxyl radical.

In this Chapter, the author of this thesis described the synthesis, identification and optical and electrochemical properties of 9,9'-anthryl-anthr-10-oxy radical derivative **5-2** as a more stabilized radical species under ambient conditions in comparison with the radical **5-1**.

5-3 Synthesis

Synthetic route of **5-1** and **5-2** is shown in Scheme 5-2. Bisanthracene quinones **5-3** and **5-4** were prepared according to the literature.[12,13] Hydride reduction of **5-3** and **5-4** using lithium aluminium hydride (LAH) and 6 N HCl produced monoketones **5-5** and **5-6**, respectively. The monoketones were used in the following reaction without purification because of the instability under ambient conditions. The radicals **5-1** and **5-2** were obtained by the oxidation of monoketones using a pyridine *N*-oxide and $FeSO_4 \cdot 7H_2O$ in 15% and 19% yield in 2 steps, respectively. The products were identified by mass spectrum measurement, single crystal X-ray diffraction analysis and ESR spectroscopy.

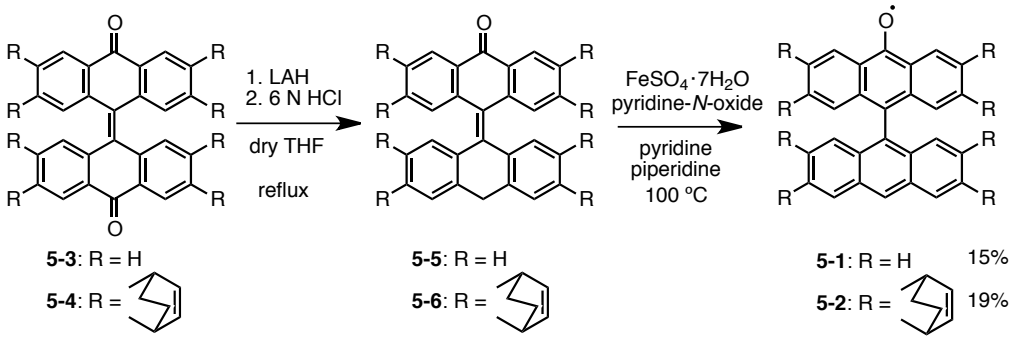

Scheme 5-2. Synthesis of 9,9'-anthryl-anthroxyl radicals.

5-4 Isolation by Single Crystal Structures, ESR Measurements and DFT Calculations

The single crystals were obtained by the diffusion crystallization from chloroform/methanol for **5-1** and toluene/methanol for **5-2**. The radical **5-1** gave two types of crystals (brown needle and brown plate) in one batch. Needle-shaped crystal is the pure crystal of **5-1**, as shown in Figures 5-3. The crystal data was solved as disordered structure due to the position of oxy-radical unit. The dihedral angle between two-anthracene units is 70.1(2)º. The bond length at C8-C8′ is 1.492(3) Å, indicating the single bond.

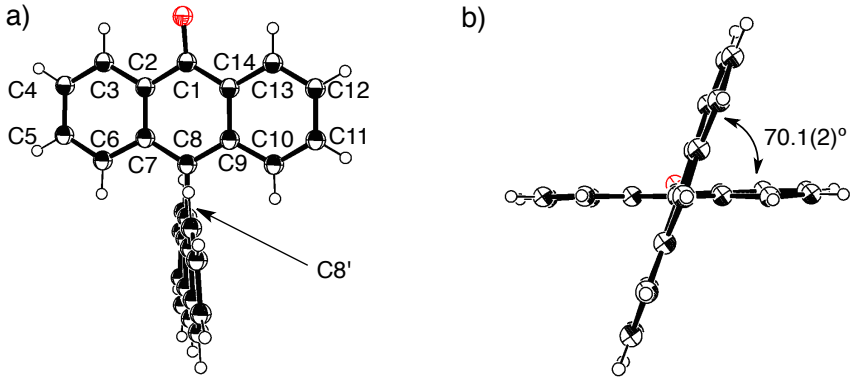

Figure 5-3. Crystal structure of a) top view; and b) side view of **5-1**. Thermal ellipsoids represent 50% probability.

The other crystal with plate-shape contains 10-hydroxy-9,9′-anthyrylanthracene (**5-1-H**) and the radical **5-1** which are paired *via* [O-H···O•] hydrogen bonding (Figures 5-4, 5-5 and 5-6). The bond length of O1-C1 of **5-1-H** is 1.364(3) Å which is conformed as a normal phenoxyl bond. The C-C bond lengths of **5-1-H** are those of typical aromatic C–C bonds and the bond length of C8-C15 for **5-1-H** is 1.496(3) Å. Thus **5-1-H** in the co-crystal is 9,9′-anthryl-10-anthranol. The bond length of O2-C29 of **1** is 1.247(3) Å, which is 0.12 Å shorter than that of O1-C1 of **5-1-H**. The bond lengths of C29-C42, C29-C30, C35-C36, and C36-C37 are 1.457 (3), 1.464(4), 1.425(3), 1.425(7) Å, assigned to single bond characteristics and the central ring next to the O2 is not aromatic. The bond length of C36–C43 for **5-1** is 1.492(3) Å. Thus, the radical **5-1** has the resonance structure as shown in Scheme 5-1. The bond lengths of **5-1** suggest the contribution of resonant structure E in Scheme 5-1 is large. Therefore, the radical spin density should be higher at 9-position and the steric protection of the most reactive carbon atom is effective to stabilize the phenoxyl type radicals.

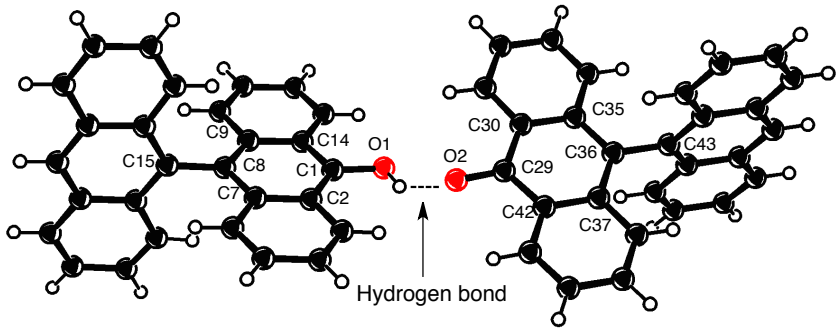

Figure 5-4. Crystal structure of co-crystal with anthroxyl anthracene. Thermal ellipsoids represent 50% probability.

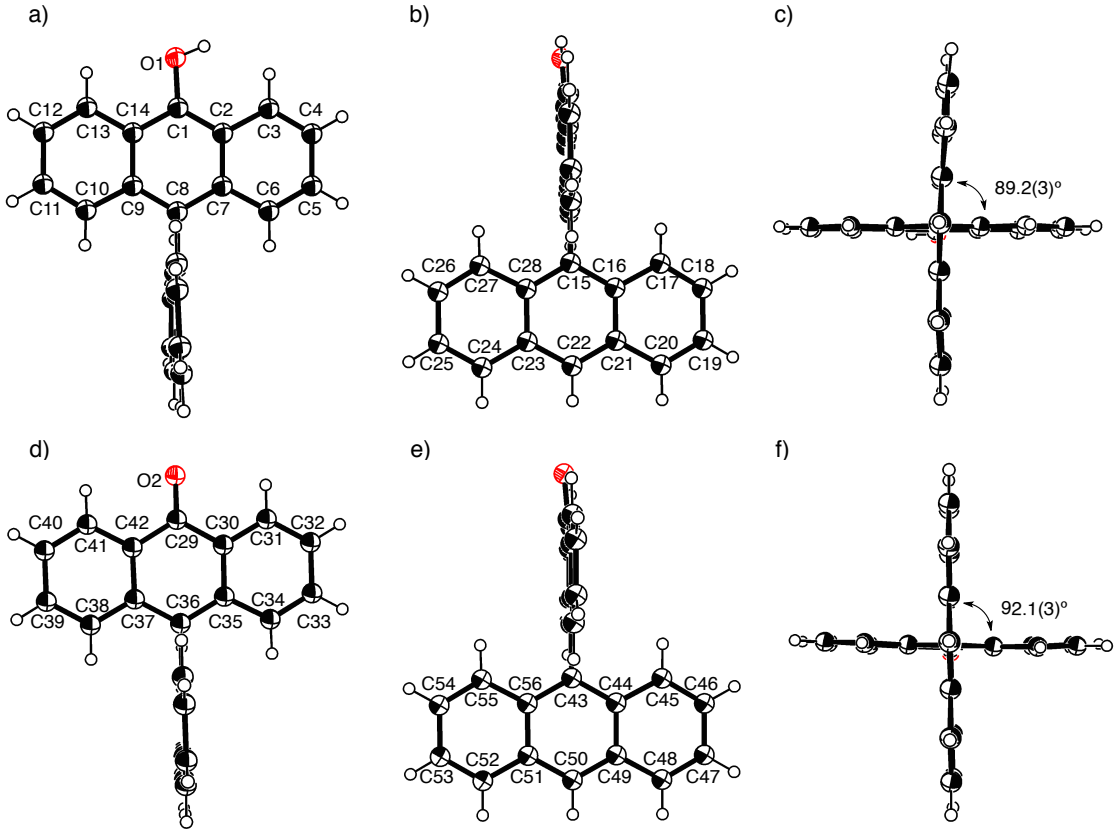

Figure 5-5. The numberings of molecular structures of **5-1-H** (a–c) and **5-1** (d–f) as co-crystal.

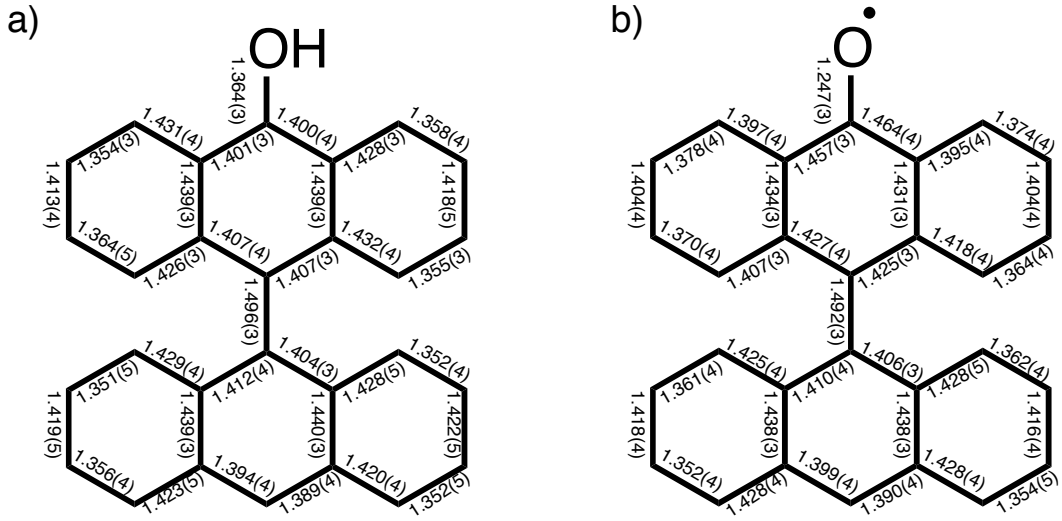

Figure 5-6. The details of bond length of a) **5-1-H** and b) **5-1** in co-crystal.

The crystal structure of **5-2** shows a similar result to the needle-shaped crystal of **5-1** (Figures 5-7). The two anthracenes are cross-shaped and the dihedral angle is 69.2(2)º. The C8-C8′ bond length that connects two anthracene skeletons is 1.498(3) Å.

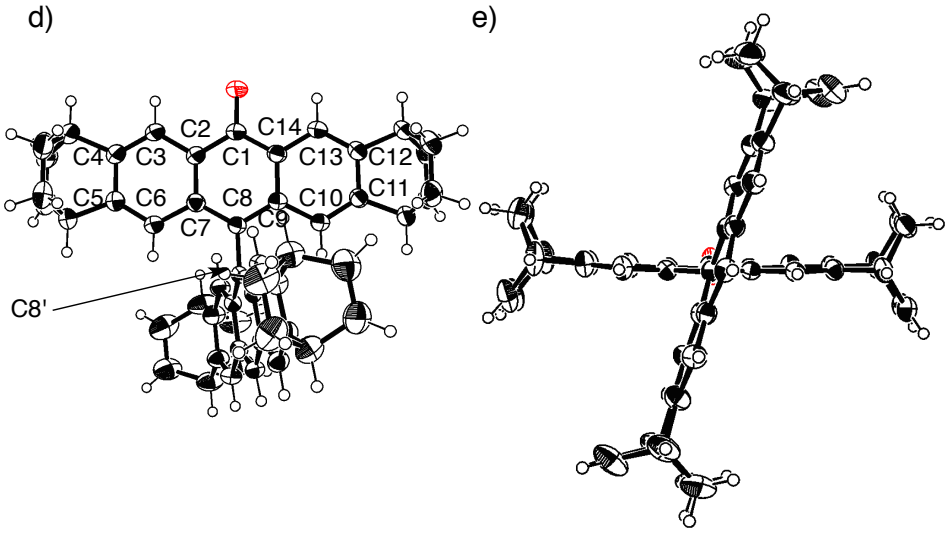

Figure 5-7. Crystal structure of a) top vies; and b) side view of **5-2**.

The electronic structures of **5-1** and **5-2** were investigated by electron spin resonance (ESR) measurement. The ESR spectra of **5-1** and **5-2** in toluene are shown in Figure 5-8 together with the simulation pattern. The signals of **5-1** are attributed to four positions in the anthroxyl skeleton, and the simulated hfccs are 0.90 (2H), 3.28 (2H), 0.90 (2H) and 3.28 G (2H). The *g*-value is 2.0023, which corresponds to a general organic free radical compound. The line width of the ESR spectrum of **5-2** was wider than **5-1** and the spectrum was hardly changed even by varying the temperature. The signals of **5-2** are ascribed to the two positions in the skeleton. The simulated hfccs are 1.00 (2H), 2.80 G (2H) and the *g*-value is 2.0024. According to the spin density calculation (Figures 5-9), both **5-1** and **5-2** have the highest spin densities on the C8 substituted with anthryl or the derivative (For numbering, see Figures 5-5 and 5-7). The anthryl groups are substantially orthogonal to phenoxyl skeleton, contributing as steric protection to the radical. Density functional theory (DFT) calculations at the B3LYP/6-31G(d) level were conducted to provide a further understanding of SOMO.[14] Computed spin densities showed that the unpaired electrons were delocalized on anthroxyl skeleton for each compound (Figure 5-10).

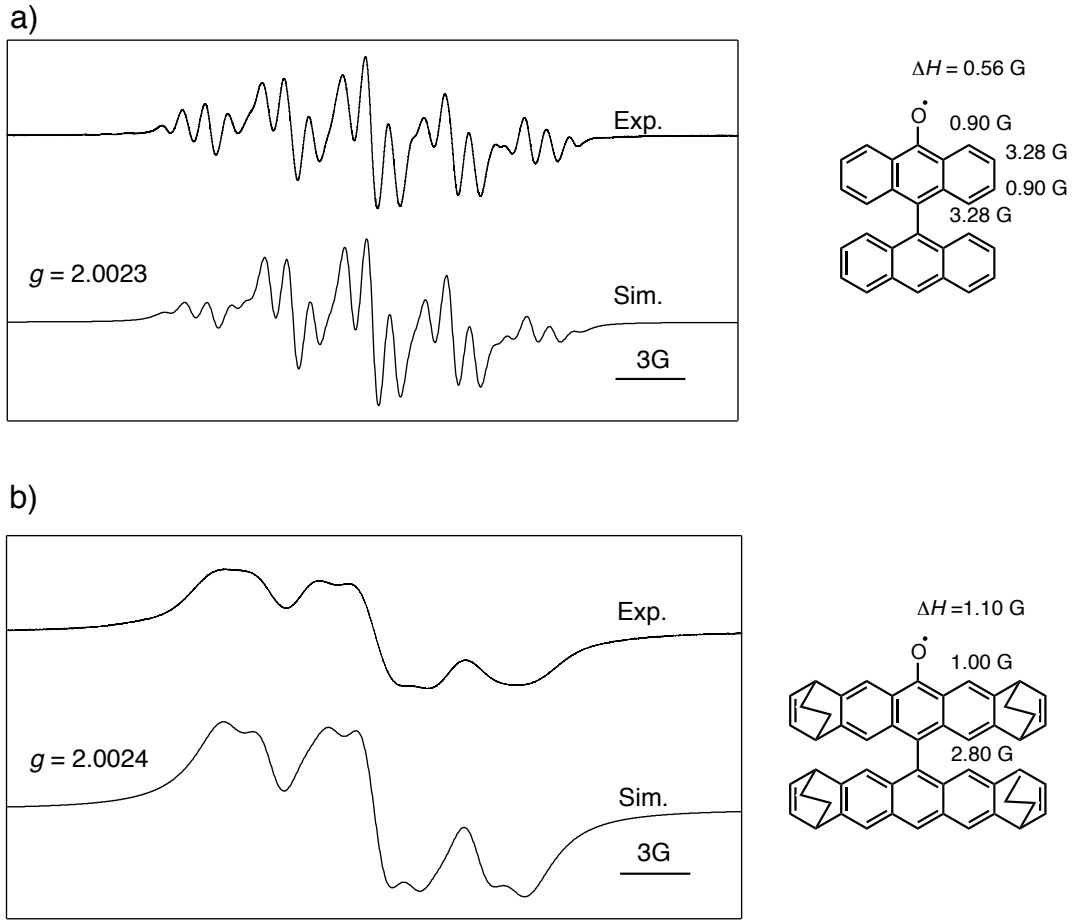

Figure 5-8. ESR spectra and simulation of a) **5-1** in toluene (1.6×10^{-2} mM) at 183 K and b) **5-2** in toluene (2.7×10^{-2} mM) at 183 K.

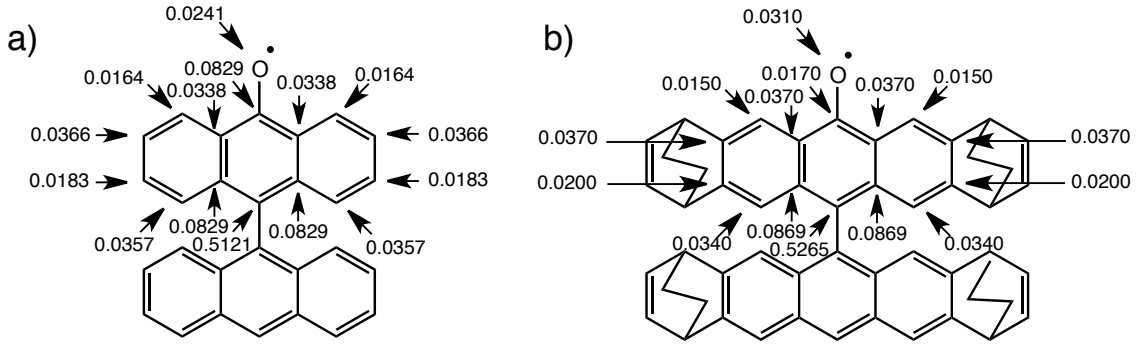

Figure 5-9. Spin density of c) **5-1**; and d) **5-2** computed at the B3LYP/6-31G(d) level.

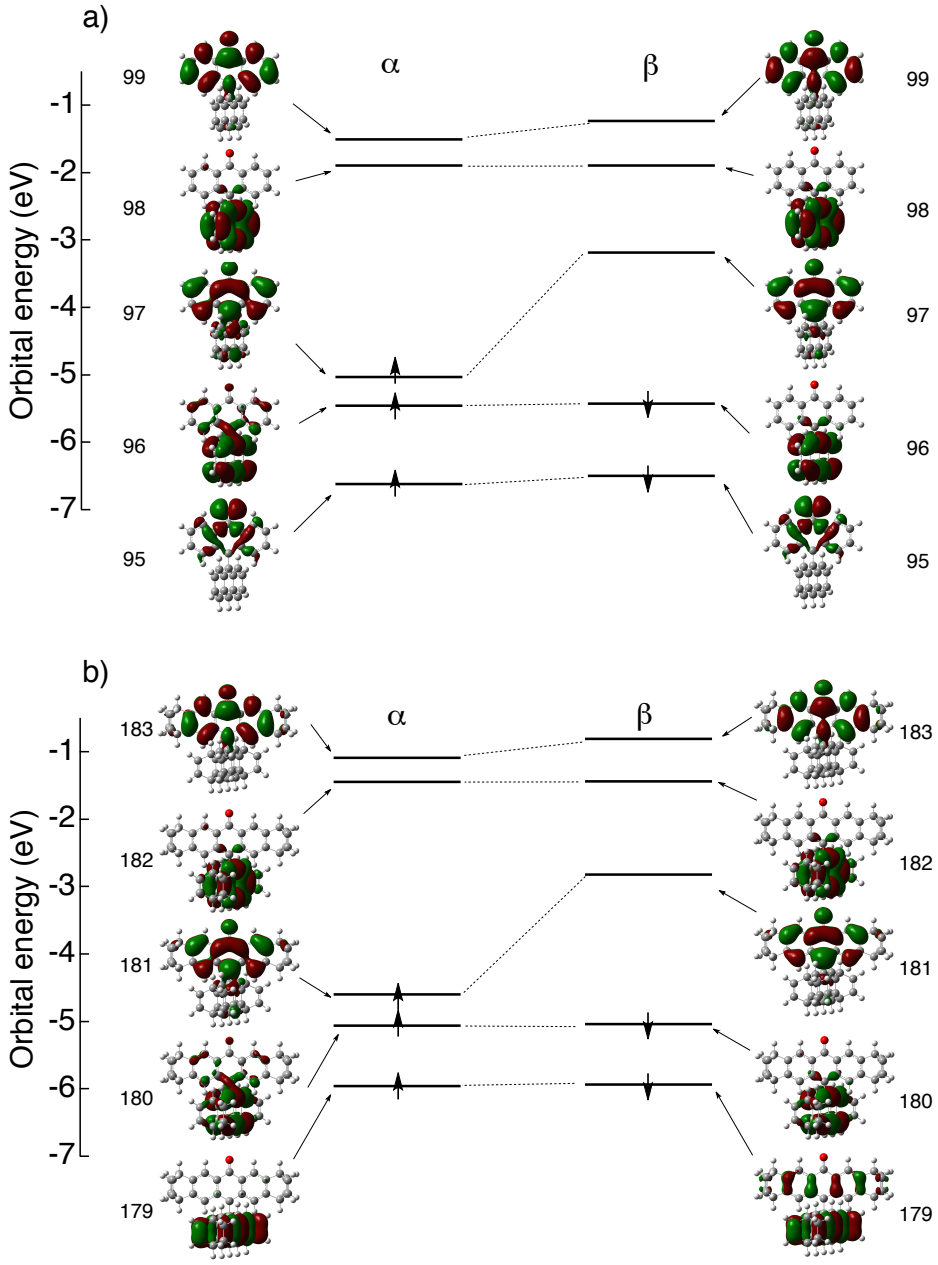

Figure 5-10. Kohn–Sham orbitals of a) **5-1** and b) **5-2** computed at the B3LYP/6-31G(d) level.

5-5 Optical Properties

The UV-vis absorption spectra of **5-1** and **5-2** recorded in toluene are shown in Figures 5-11, 12 and Table 1. Each solution displayed a dark yellow color. The UV-vis absorption spectrum of **5-1** shows the major absorption at 357 (ε = 23,900 $M^{-1}cm^{-1}$) and 387 nm (ε = 12,900 $M^{-1}cm^{-1}$) and the minor absorption broadened to 800 nm with maxima at 413 (ε = 5,590 $M^{-1}cm^{-1}$), 434 (ε = 6,660 $M^{-1}cm^{-1}$), 537 (ε = 1,620 $M^{-1}cm^{-1}$) and 578 nm (ε = 1,830 $M^{-1}cm^{-1}$). Since the UV-vis absorption spectrum of 9,9'-bianthryl is up to 400 nm,[15] the absorption wavelength are red-shifted by the contribution of SOMO, as shown by the TD-DFT calculations (Figures 5-11,12). The BCOD-fused compound **5-2** displays an absorption spectrum with the red-shifted major absorption at 369 (ε = 25,000 $M^{-1}cm^{-1}$) and 384 (ε = 12,800 $M^{-1}cm^{-1}$) nm, and with the minor absorption broader and spread to 800 nm compared to **5-1**. The photo-stability of the radicals in toluene was checked by UV-vis absorption spectral change. The solution was kept under room light under air, and the temporal spectral change was measured, as shown in Figures 5-13. The peak-top (357 nm) of the absorbance of **5-1** is gradually decreased and the half life ($\tau_{1/2}$) is calculated to be 92 h. In contrast, $\tau_{1/2}$ of **5-2** was significantly longer than **5-1** and was estimated as 274 h (11.4 d). The stability was improved about 3 times by inserting the BCOD moieties. These radicals in the solid state hardly degraded under shade conditions and can be easily handled. While many of stable phenoxyl radical derivatives reported often in anaerobic solution state, the examples were isolated as a solid under ambient conditions is small. It is difficult to compare the stability of the other phenoxyl radical derivatives, however, in view of the stability under ambient conditions, these radicals can be classified into a highly stable class.

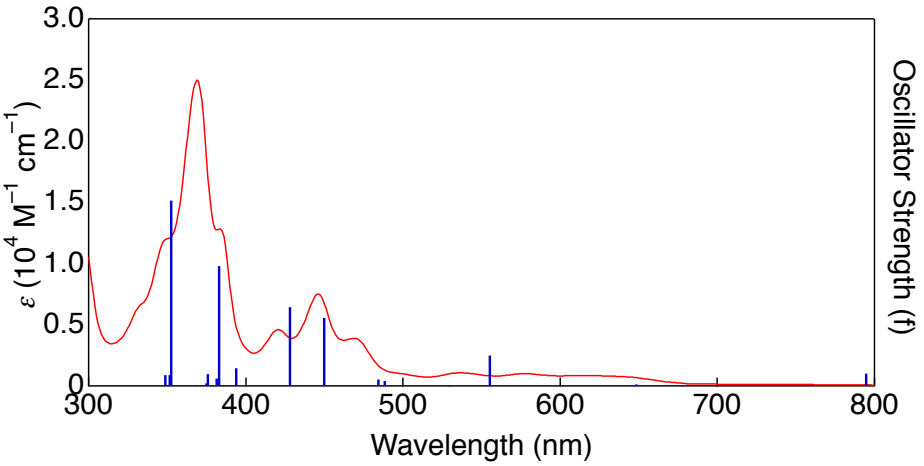

Figure 5-11. UV–vis absorption spectra in toluene (red) and TD-DFT calculation (blue) of **5-1**.

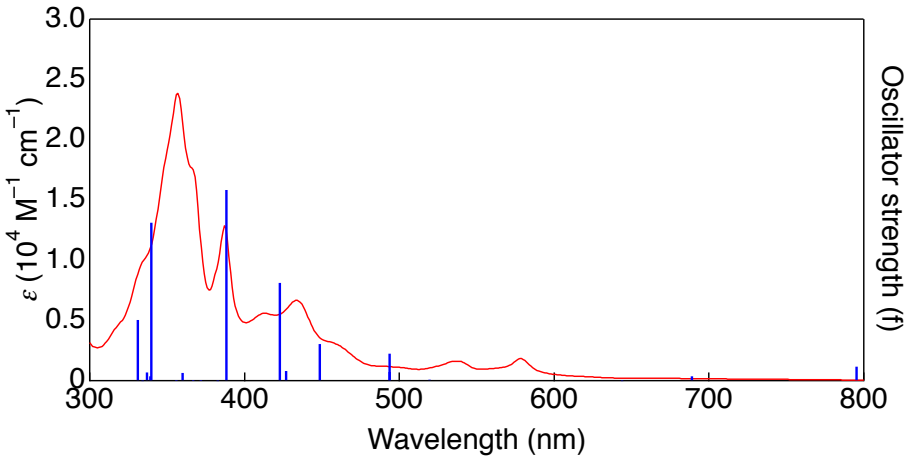

Figure 5-12. UV–vis absorption spectra in toluene (red) and TD-DFT calculation (blue) of **5-2**.

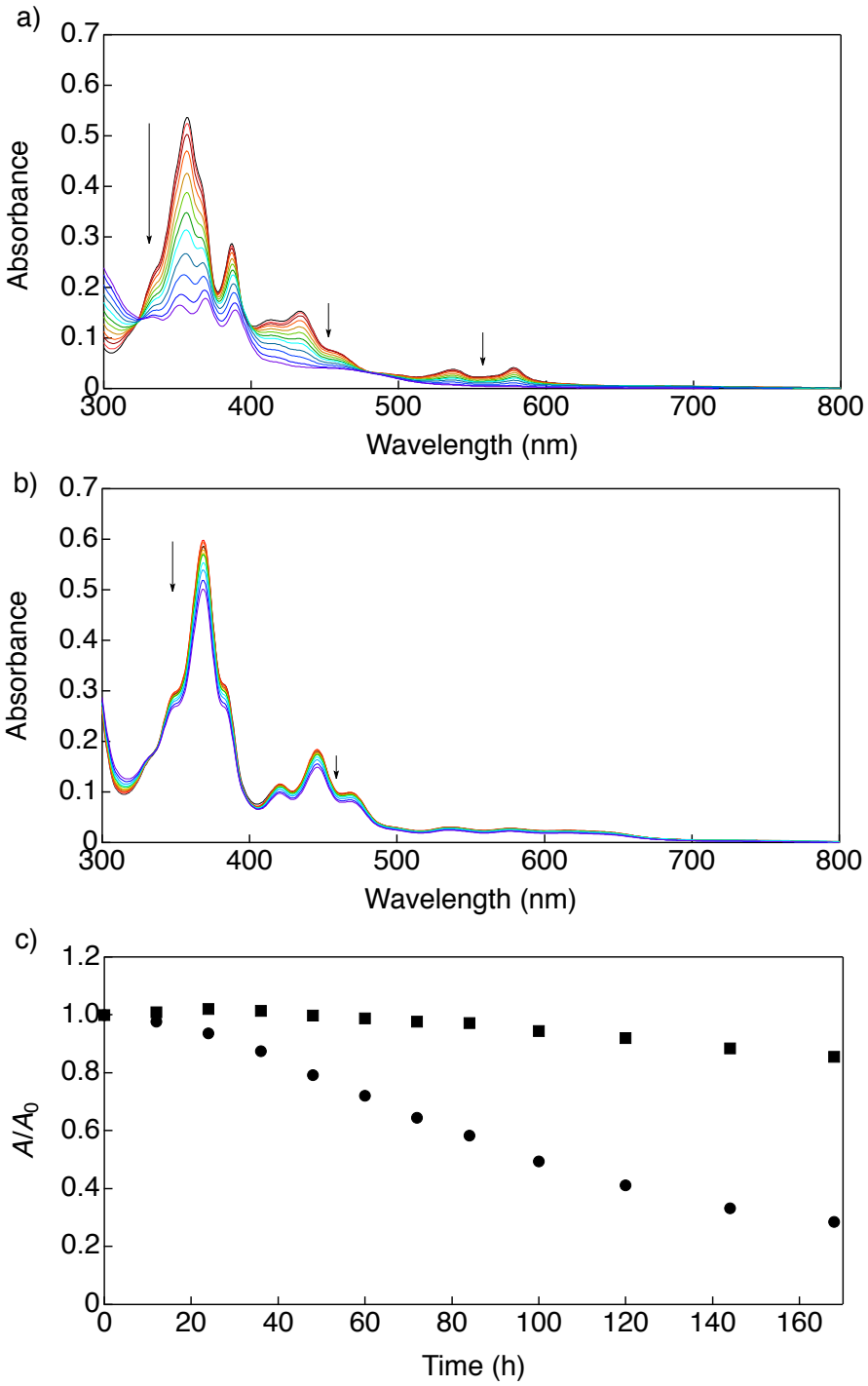

Figure 5-13. c) UV-vis absorption spectra change under ambient conditions a) **5-1** (2.25×10^{-2} mM) and b) **5-2** (2.25×10^{-2} mM). c) Decay profiles of UV-vis absorption spectra a) **5-1** (●, 357 nm) and **5-2** (■, 369 nm).

The electrochemical properties of the radicals were studied by cyclic voltammetry (CV) in dry dichloromethane containing 0.1 M tetra-*n*-buthylammonium hexafluorophosphate (nBu$_4$NPF$_6$) as a supporting electrolyte. The results are summarized in Figure **5-14** and **Table 5-1**. The one-electron reduction potentials ($E_{red}^{1/2}$ *vs*. Fc/Fc$^+$) of **5-1** and **5-2** are at −0.77 V and −0.94 V, respectively. The radical **5-1** shows one oxidation potential at 0.55 V (*vs*. Fc/Fc$^+$), whereas **5-2** shows two reversible oxidation waves at 0.25 and 0.91 V (*vs*. Fc/Fc$^+$). In comparison with **5-1**, the first oxidation and reduction potentials of compound **5-2** are shifted to negative side. It is considered that the SOMO energy level of **5-2** rises by receiving the electric effect of σ–π conjugation of BCOD-units to anthracene moiety.[16] From CV and DFT calculations, stability of **5-2** against electrochemical oxidation is predicted lower than that of **5-1**. The surrounding structures of C8 position of **5-1** and **5-2** are similar in crystals due to the similar angles of two anthryl planes and the similar C8-C8' distances. However, the better stability of **5-2** in solution suggests the restricted rotation freedom on C8-C8′ axis for **5-2** compared to **5-1** owing the BCOD substituents at the edge of anthracene unit, thus restrict the reactivity of C8 to give quinoid structure. Furthermore, the stability of the radical **5-2** in solution was improved owing to the steric hindrance of BCOD-moiety to restrict the rotation around the C8-C8′ axis.

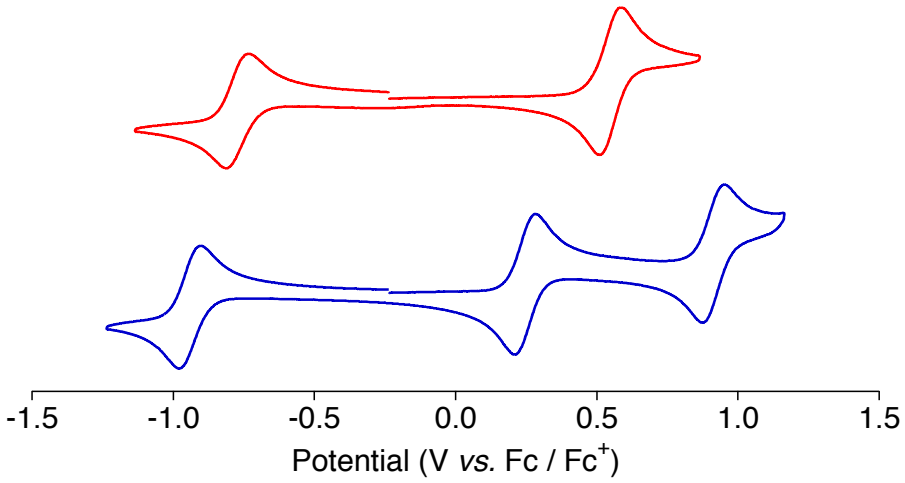

Figure 5-14. Cyclic voltammograms of **5-1** (red) and **5-2** (blue) in dichloromethane with 0.1 M nBu$_4$NPF$_6$, glassy carbon electrode, platinum counter electrode, and an Ag/AgNO$_3$ reference electrode. Scan rate = 100 mV/s.

Table 1. Summary of optical and electrochemical properties of radicals

Compound	λ_{abs} / nm[a]	E_{ox} / V [b]	E_{red} / V [b]
5-1	357, 387, 413, 434, 537, 578	0.55	–0.77
5-2	369, 384, 421, 446, 537, 576, 615	0.25, 0.91	–0.94

[a]In toluene. [b]The values were obtained by cyclic voltammetry. V vs Fc/Fc^+

5-6 Thermal Conversion

The thermal conversion from **5-2** to **5-7** has been tried by retro-Diels–Alder reaction.[12,17] The weight loss in thermogravimetric analysis of 5-2 starts at 200 ºC and ends around 300 ºC, but soon the weight loss started again. The preparation of radical 5-7 was tried by heating by microwave in ethyleneglycol at 300 ºC for 5 min under argon atmosphere. After the quick filtration, the precipitation was suggested to have pentacene dimer unit by APCI-Mass measurement. However, the ESR measurement of **5-7** was not successful at the present because the life-time of the product is much shorter than that of **5-1**.

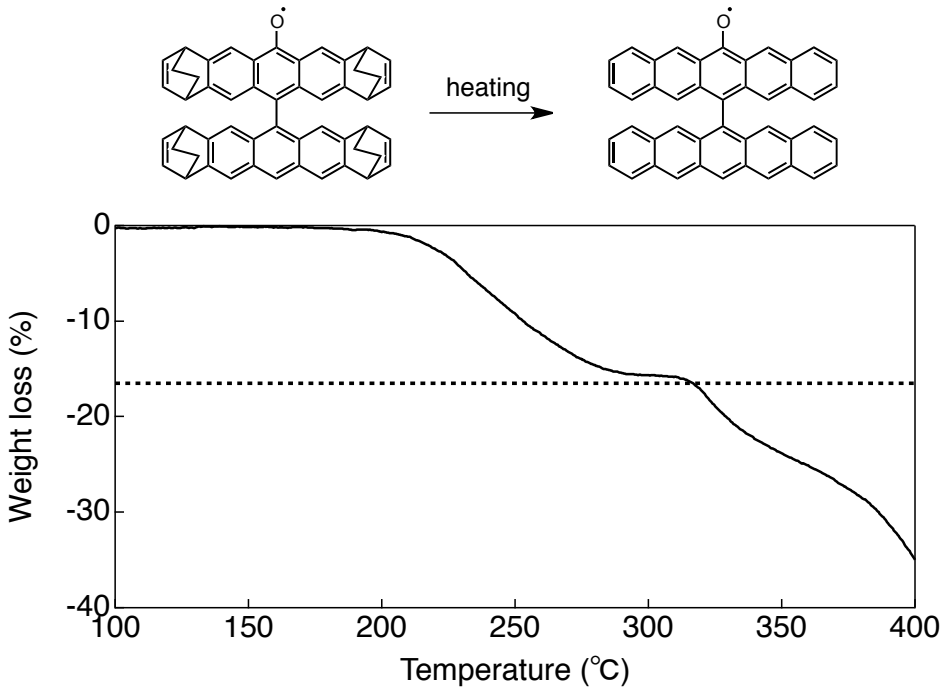

Figure 5-15. Thermogravimetoric analysis of **5-2** (5 ºC/min).

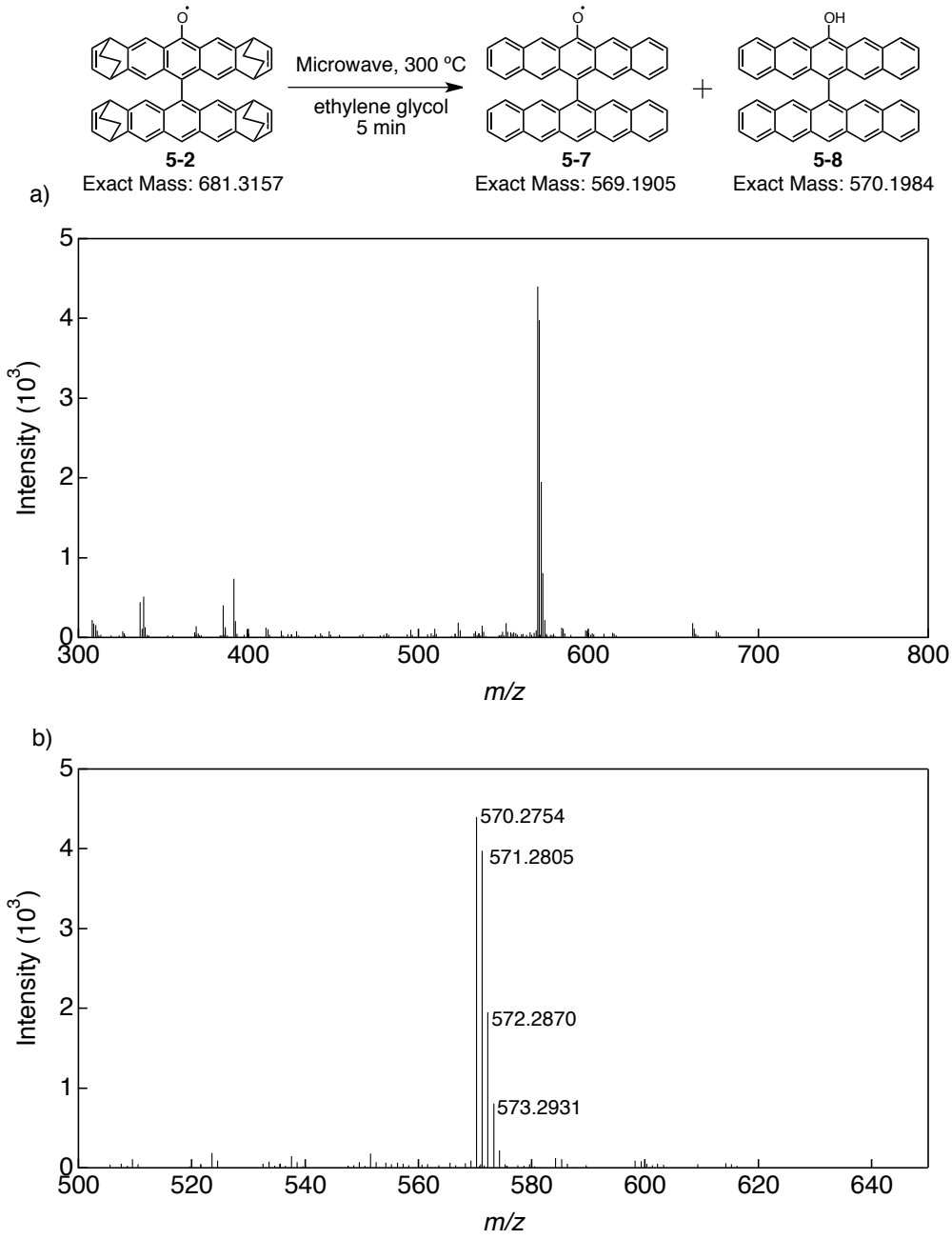

Figure 5-16. APCI-MS spectra (positive) after thermal conversion of **5-2**.

5-8 Summary

The author of this thesis succeeded to stabilize the highly reactive phenoxyl radical by two kinds of strategies. The result of X-ray structural analysis, ESR spectra and DFT calculations suggested the highest spin density of radical **5-1** at 9-position due to the resonance and the stabilization of the phenoxyl radical was achieved by protection of the most reactive position with an anthryl group. The peripheral BCOD-substituents influenced the absorption spectrum to be red-shifted and the energy levels of SOMOs to be raised by σ-π hyperconjugation to encourage the electrochemical oxidation. Furthermore the stability of the radical **5-2** in solution was improved owing to the steric hindrance of BCOD-moiety to restrict the rotation around the C8-C8′ axis.

5-7 Experimental Section

Synthesis and general methods

Commercially available reagents and solvents for syntheses were of reagent grade and used without further purification. TLC and gravity column chromatography were performed on Art. 5554 (Merck KGaA) plates and silica gel 60N (Kanto Chemical), respectively. For spectral measurements, spectral-grade toluene, dichloromethane, methanol and acetonitrile were purchased from Nacalai Tesque. The dichloromethane used for cyclic voltammetry measurements was distilled from CaH_2.

Compound 5-1

LAH (0.53 g, 13.4 mmol) was added slowly to suspension of **5-3** (0.34 g, 0.884 mmol) in dry THF (25 ml) at 0 ºC. After adding, the reaction mixture was refluxed for 2 h. After refluxing, the reaction mixture was cooled to 0 ºC again. 6 N HCl (26 ml) was added to the mixture and refluxed for 1 h again. The precipitate was filtrated off and washed with water and methanol. The product **5-5** was used in the following reaction without purification because of the instability under ambient conditions. Compound **5-5** was dissolved in a mixture of dry pyridine (13 ml) and piperidine (0.80 ml, 8.1 mmol). Pyridine-*N*-oxide (0.70 g, 7.36 mmol) and ferrous sulfate heptahydrate (0.060 g, 0.216 mmmol) were added to the resulting solution, and the reaction mixture was heated to 100 ºC under argon atmosphere for 16 h. After cooling, the

reaction mixture was mixed with 6 N HCl (20 ml). The precipitate was filtrated off and washed with water and methanol. The crude product was purified by chromatography on silica gel with $CHCl_3$ (1st.), $CHCl_3$-hexane (1:2), and $CHCl_3$-hexane (1:3) and gel permeation chromatography ($CHCl_3$) to afford **5-1** as a black solid (0.043 g, 15% in 2 steps). MS (EI): *m/z*: 370 $[M+1]^+$; HR-EI *m/z* = 369.1277, calcd. for $C_{28}H_{17}O$: 369.1279.

Compound 5-2

LAH (0.40 g, 10.5 mmol) was added slowly to suspension of **5-4** (0.40 g, 0.574 mmol) in dry THF (20 ml) at 0 ºC. After adding, the reaction mixture was refluxed for 1 h. After refluxing, the reaction mixture was cooled to 0 ºC again. 6 N HCl (20 ml) was added to the mixture and refluxed for 1 h again. The precipitate was filtrated off and washed with water and methanol. The crude product was purified by chromatography on silica gel with CH_2Cl_2-hexane (4:1) (0.27 g). The product **5-6** was used in the following reaction without more purification because of the instability under ambient conditions. Compound **5-6** (0.27 g) was dissolved in a mixture of dry pyridine (20 ml) and piperidine (0.70 ml, 7.09 mmol). Pyridine-*N*-oxide (0.93 g, 0.978 mmol) and ferrous sulfate heptahydrate (0.074 g, 0.266 mmmol) were added to the resulting solution, and the reaction mixture was heated to 100 ºC under argon atmosphere for 4 h. After cooling, the reaction mixture was mixed with 3 N HCl (20 ml). The precipitate was filtrated off and washed with water and methanol. The crude product was purified by chromatography on silica gel with CH_2Cl_2-hexane (1:1) and recrystallization from CH_2Cl_2–methanol to afford **5-2** as a black solid (0.074 g, 19% in 2 steps). MS (EI): *m/z*: 682 $[M+1]^+$, 653 $[M-28(-C_2H_4)]^+$, 625 $[M-56(-2C_2H_4)]^+$, 597 $[M-84(-3C_2H_4)]^+$, 569 $[M-114(-4C_2H_4)]^+$; HR-EI: *m/z* = 681.3143, calcd. for $C_{52}H_{41}O$: 681.3157.

Compound 5-7

Compound **5-2** (12 mg, 0.0176 mmol) was suspended in ethylene glycol (3 ml). The mixture was bubbled with an argon gas for 20 min. The mixture was heated at 300 ºC for 5 min by microwave. After cooling to room temperature, the precipitate was filtrated and washed with argon bubbled methanol. The product was dissolved in dry toluene and measured by APCI-MS spectrum.

General

EI mass spectra were measured on a JEOL JMS-700 MStation spectrometer. UV-vis spectra were measured on a JASCO UV/VIS/NIR Spectro-photometer V-570. ESR spectra were recorded on a JEOL JES-FA100.

X-ray crystallography

X-ray crystallographic data were recorded at 100 K on a Rigaku R-AXIS RAPID/S using Mo-Kα radiation and at 90 K with a BRUKER-APEXII X-Ray diffractometer equipped with a large area CCD detector by using graphite monochromated Mo-Kα radiation (λ = 0.71073 Å). The diffraction data were processed with Crystal Structure of the Rigaku program, solved with the SIR-97 program and refined with the SHELX-97 program (G. M. Sheldrick, *Acta. Cryst*. 2008, A64, 112–122).

Cyclic voltammetry measurements

CV measurements were conducted in a solution of 0.1 M *n*-Bu_4NPF_6 in dry dichloromethane or acetonitrie with a scan rate of 100 mV/s at room temperature in an argon-filled cell. A glassy carbon electrode and a Pt wire were used as a working and a counter electrode, respectively. An Ag/Ag^+ electrode was used as a reference electrode, which was externally calibrated with the half-wave potential of ferrocene/ferrocenium (Fc/Fc^+) redox couple.

Crystallographic data table

	5-1	co-crystal	**5-2**
Empirical formula	C_{28} H_{17} O	$C_{58.50}$ $H_{37.50}$ $C_{17.50}$ O_2	C_{52} H_{41} O
Formula weight	369.42	1038.26	681.85
Temperature (K)	103(2)	103(2)	103(2)
Crystal system	Orthorhombic	Triclinic	Monoclinic
Space group	*Pbcn*	*P*-1	$P2_1/n$
a [Å]	11.6165(6)	11.5782(3)	10.6594(3)
b [Å]	12.7592(7)	14.3354(5)	21.7535(7)
c [Å]	12.4644(6)	16.4867(5)	16.0991(4)
α [°]	90.00	96.3005(8)	90.00
β [°]	90.00	101.7870(11)	100.1230(10)
γ [°]	90.00	113.7045(8)	90.00
V [Å]	1847.44(17)	2395.88(13)	3674.93(18)
Z	4	2	4
ρcalcd [MgM^{-3}]	1.328	1.439	1.232
μ [mm^{-1}]	0.079	0.488	0.071
F (000)	772	1064	1444
Crystal size[mm^3]	0.20 x 0.02 x 0.01	0.12 x 0.10 x 0.08	0.18 x 0.12 x 0.03
Reflections collected	24374	34238	51609
Independent reflections	1690 [*R*(int) = 0.1079]	8742 [*R*(int) = 0.0539]	6705 [*R*(int) = 0.0515]
parameters	136	667	488
GOF	1.041	1.070	1.017
R_1 [$I > 2\ \sigma(I)$]	0.0606	0.0507	0.0646
R_1 (all data)	01043	0.0793	0.0824
R_2 [$I > 2\ \sigma(I)$]	0.1378	0.1220	0.1708
R_2 (all data)	0.1572	0.1397	0.1832

5-9 References

(1) Gomberg, M. *J. Am. Chem. Soc.* **1900**, *22*, 757–771.

(2) (a) Stable Radicals: Fundamentals and Applied Aspects of Odd-Electron Compounds, ed. R. G. Hicks, John Wiley & Sons, Wiltshire, **2010**. (b) Sun, Z.; Zeng, Z.; Wu, J. *Acc. Chem. Res.* **2014**, *47*, 2582–2591. (c) Tian, Y.; Uchida, K.; Kurata, H.; Hirao, Y.; Nishiuchi, T.; Kubo, T. *J. Am. Chem. Soc.* **2014**, *136*, 12784–12793.

(3) (a) Morita, Y.; Nishida, S.; Murata, T.; Moriguchi, M.; Ueda, A.; Satoh, M.; Arifuku, K.; Sato, K.; Takui, T. *Nat. Mater.* **2011**, *10*, 947–951. (b) Janoschka, T.; Hager, M.; Schubert, U. *Adv. Mater.* **2012**, *24*, 6397–6409.

(4) (a) Wang, Y.; Wang, H.; Liu, Y.; Di, C.; Sun, Y.; Wu, W.; Yu, G.; Zhang, D.; Zhu, D. *J. Am. Chem. Soc.* **2006**,*128*, 13058–13059. (b) Aoki, K.; Akutsu, H.; Yamada, J.; Nakatsuji, S.; Kojima, T.; Yamashita, Y. *Chem. Lett.* **2009**, *38*, 112–113. (c) Tomlinson, E.; Hay, M.; Boudouris, B. *Macromolecules* **2014**, *47*, 6145–6158.

(5) Pummerer, R.; Frankfurter, F. *Chem. Ber.* **1914**, *47*, 1472−1493.

(6) (a) Kreilick, E. W.; Weissman, S. I. *J. Am. Chem. Soc.* **1962**, *84*, 306–307. (b) Krüger, H.-J. *Angew. Chem. Int. Ed.* **1999**, *38*, 627–631. (c) Itoh, S.; Taki, M.; Fukuzumi, S. *Coord. Chem. Rev.* **2000**, *198*, 3–20. (c) Jazdzewski, B. A.; Tolman, W. B.; *Coord. Chem. Rev.* **2000**, *200-202*, 633–685.

(7) (a) Altwicker, E. R. *Chem. Rev.* **1967**, *67*, 475–531. (c) Porter, T. R.; Kaminsky, W.; Mayer, J. M. *J. Org. Chem.* **2014**, *79*, 9451–9454.

(8) (*a*) Sokolowski, A.; Müller, J.; Weyhermüller, T.; Schnepf, R.; Hildebrandt, P.; Hildenbrand, K.; Bothe E.; Wieghardt, K. *J. Am. Chem. Soc.* **1997**, *119*, 8889–8900; (*b*) Philibert, A.; Thomas, F.; Philouze, C.; Hamman, S.; Saint-Aman E.; Pierre, J.-L. *Chem. Eur. J.*, **2003**, *9*, 3803–3812; *(c*) Shimazaki, Y.; Huth, S.; Karasawa, S.; Hirota, S.; Naruta, Y.; Yamaguchi, O. *Inorg. Chem.* **2004**, *43*, 7816–7822.

(9) (*a*) Xie, C.; Lahti. P. M.; George, C. *Org. Lett.* **2000**, *2*, 3417–3420; (*b*) Porter, T. R.; Kaminsky W.; Mayer, J. M. *J. Org. Chem.* **2014**, *79*, 9451–9454.

(10) (a) Cai, J.; Ruffieux, P.; Jaafar, R.; Bieri, M.; Braun, T.; Blankenburg, S.; Muoth, M.; Seitsonen, A.; Saleh, M.; Feng, X.; Müllen, K.; Fasel, R. *Nature* **2010**, *466*, 470–473. (b) Chen, L.; Hernandez, Y.; Feng, X.; Müllen, K. *Angew. Chem. Int. Ed.* **2012**, *51*, 7640–7654. (c) Konishi, A.; Hirao, Y.; Matsumoto, K.; Kurata, H.; Kishi, R.; Shigeta, Y.; Nakano, M.; Tokunaga, K.; Kamada, K.; Kubo, T. *J. Am. Chem. Soc.* **2013**, *135*, 1430–1437.

(11) Singer, L. S.; Lewis, I. C.; Richerzhagen, T.; Vincow, G. *J. Phys. Chem.* **1971**, *75*, 290–

291.

(12) Tanaka, K.; Aratani, N.; Kuzuhara, D.; Sakamoto, S.; Okujima, T.; Ono, N.; Uno, H.; Yamada, H. *RSC Adv.* **2013**, *3*, 15310–15315.

(13) (a) Arabei, S. M.; Pavich, T. A. *J. Appl. Spectrosc.* **2000**, *67*, 236–244; (b) Zhang, X.; Li, J.; Qu, H.; Chi C.; Wu, J. *Org*. *Lett*. **2010**, *12*, 3946–3949.

(14) (a) Backe, A. D.; *J. Chem. Phys.* **1993**, *98*, 5648–5652; (*b*) Lee, C.; Yang, W.; Parr, R. G. *Phys. Rev. B*, **1988**, *37*, 785–789. (c) Gaussian 09, Revision D.01, Frisch, M. J.; Trucks, G. W.; Schlegel, H. B.; Scuseria, G. E.; Robb, M. A.; Cheeseman, J. R.; Scalmani, G.; Barone, V.; Mennucci, B.; Petersson, G. A.; Nakatsuji, H.; Caricato, M.; Li, X.; Hratchian, H. P.; Izmaylov, A. F.; Bloino, J.; Zheng, G.; Sonnenberg, J. L.; Hada, M.; Ehara, M.; Toyota, K.; Fukuda, R.; Hasegawa, J.; Ishida, M.; Nakajima, T.; Honda, Y.; Kitao, O.; Nakai, H.; Vreven, T.; Montgomery, J. A., Jr.; Peralta, J. E.; Ogliaro, F.; Bearpark, M.; Heyd, J. J.; Brothers, E.; Kudin, K. N.; Staroverov, V. N.; Kobayashi, R.; Normand, J.; Raghavachari, K.; Rendell, A.; Burant, J. C.; Iyengar, S. S.; Tomasi, J.; Cossi, M.; Rega, N.; Millam, M. J.; Klene, M.; Knox, J. E.; Cross, J. B.; Bakken, V.; Adamo, C.; Jaramillo, J.; Gomperts, R.; Stratmann, R. E.; Yazyev, O.; Austin, A. J.; Cammi, R.; Pomelli, C.; Ochterski, J. W.; Martin, R. L.; Morokuma, K.; Zakrzewski, V. G.; Voth, G. A.; Salvador, P.; Dannenberg, J. J.; Dapprich, S.; Daniels, A. D.; Farkas, Ö.; Foresman, J. B.; Ortiz, J. V.; Cioslowski, J.; Fox, D. J. Gaussian, Inc., Wallingford CT, **2009**.

(15) Natarajan, P.; Schmittle, M. *J. Org. Chem.* **2013**, *78*, 10383–10394.

(16) (a) Komatsu, K.; Akamatsu, H.; Jinbu, Y.; Okamoto, K. *J. Am. Chem. Soc.* **1988**, *110*, 633–634. (b) Matsuura, A.; Nishinaga, T.; Komatsu, K. *J. Am. Chem. Soc.* **2000**, *122*, 10007–10016.

(17) (a) Ito, S.; Murashima, T.; Ono, N.; Uno, H.; *Chem. Commun.* **1998**, 1661–1662. (b) Yamada, H.; Okujima, T.; Ono, N. *Chem. Commun.* **2008**, 2957–2974.

Chapter 6 Summary and Conclusion

The author of this thesis investigated the photofunctional acene-based materials based on photochemically convertible precursor method. Studies of conventional photoprecursor were method to evaluate the molecule only after structural change. This photoprecursor method has specific advantages such as one-way, quantitative photoreaction. Therefore, the author expected wide variety of the functional materials based on the dramatic characteristic change triggered by the photoconversion for the new application of α-diketone precursor method. As the first subject, the improvements of properties for fabricating the organic electronics by solution process with α-diketone type precursor were studied and described in chapter 2 and chapter 3.

In the Chapter 2, photochemistry and solubility of **5,14-PDK** was described. The conventional **6,13-PDK** can be used for fabricating organic devices by solution process. However, the absorption spectrum of **6,13-PDK** overlaps with absorption spectrum of pentacene, and the photoconversion efficiency is decreased by the masking effect of absorption of pentacene with the progress of the conversion. Therefore, **5,14-PDK** was synthesized for improving the problem. **5,14-PDK** exhibits a broad absorption at the area where pentacene doesn't have absorption. The photoreaction efficiency of **5,14-PDK** significantly improved in comparison with that of **6,13-PDK**.

In the Chapter 3, design, synthesis and optical properties of anthracene–pyridino[2,3-*g*]quinoxaline (PQ) was described for fabricating solution processable OPV device. The photoprecursor of anthracene-PQ conjugates were synthesized and the quantitative photoconversions were confirmed. The converted anthracene-PQ conjugates have ideal energy level and widely absorption spectrum in visible region. However, hetero p-i-n OPV wasn't fabricated because the solubility of **Ant-PQ** (after conversion) and **ADK2-PQ** isn't suitable for the multi layer process. Instead of hetero-p-i-n device structure, BHJ solar cell was fabricated with **$PC_{71}BM$**, however, the PCE is lower than that expected. Protonation of PQ moiety by PEDOT:PSS as a hole transfer layer and close LUMO levels of the two semiconductors are considered as a factor of low PCE. In order to improve the problems, the modification of device structure and molecule structure is required. In addition, to apply to hetero p-i-n junction solar cell, controlling of solubility and LUMO level of PQ derivatives are required.

As the second subject, the new application of photoprecursor method was also studied energetically. The most of α-diketone type precursors were used as a synthetic application of

unstable and insoluble acene compounds and a device fabrication application toward solution process. For these studies, dramatic solubility change is used as one of the characteristic of photoprecursor method. Furthermore, the electronic properties such as light absorbing and electron accepting are also dramatically changed with the structural change from photoprecursor to acene.

In the Chapter 4, the photoprecursor method is applied to switch the fluorescence properties with the electronic structural change, and the three different mechanisms were described. The first type is the simple system which is the structural change from non-fluorescent structure to highly fluorescent structure. The second type is the combined structure of photoprecursor and strongly fluorescent dye. In the system, fluorescence of fluorophore is energetically quenched since the energy was used for structural change of photoprecursor. Although the third system is also the combined structure, the mechanism of fluorescence quenching is intramolecular electron transfer mechanism. In the molecule, photoprecursor was used as an electron acceptor, and fluorophore was used as an electron donor unit. This result clarified α-diketone type precursor can be used for even fluorescent molecules of lower excitation energy than α-diketone moiety. From those results, validity of α-diketone type precursor method for preparation of one-way fluorescence switching material was shown experimentally and new application of the precursor method was proposed in this chapter.

In the Chapter 5, synthesis of 9,9′-anthryl-anthroxyl radical and the derivatives was described. The opportunity of this research is as a part of International Training Program (ITP, JSPS) that NAIST promoted, and this study was conducted at National University of Singapore (NUS) under supervision of Prof. Jishan Wu. The unstable phenoxyl radical was stabilized by expanded π-structure for delocalization and steric protection at the most reactive position.

In this thesis, the author focused on characteristics of α-diketone type photoprecursors such as n-π* absorption and electron accepting properties in addition to control of solubility. α-Diketone type photoprecursor has distinctive natures that can be applied to other research fields. As one example, stretching vibration of carbonyl moiety might be applied to develop security materials detectable with infrared spectroscopic. The stretching vibration is observed strongly in infrared region, and infrared spectroscopic measurement is highly sensitive. Since the photoconversion does not proceed with infrared light irradiation, non-destructive reading of information is possible in photoprecursor method. By the combination of α-diketone unit with chromophores having high molar extinction coefficient, photoconversion at α-diketone does not influence to the UV-vis absorption spectra of the molecules. While the apparent colors are

maintained during the photoconversion, the change of α-diketone unit can be detected with infrared absorption, and security materials with infrared spectroscopy are expected to be developed. As another example, photoprecursor can be used as safe CO source which release CO molecules quantitatively upon visible light irradiation. In organic synthetic chemistry, CO gas is, despite its toxicity, used as a carbon source. CO sources which release CO in reaction vessels are therefore required. Photoprecursors emit two CO molecules quantitatively by visible light irradiation. Furthermore, the CO generation can be monitored with fluorescence of the acenes. Safe CO sources are thus expected taking advantages of present photoprecursor method. The bioactivity of CO and its products after reaction in aqueous environment is also worth for noting. The present molecular systems may thus also be expanded for photo-dynamic therapy and other photo-bio-stimulation systems.

Photoprecursor method is thus not only valuable for researches of synthesis of π-expanded aromatic molecules, organic electronics materials and fluorescent switching materials, but also expected for other application. These researches are considered to be very important for the development of photofunctional materials, and the exploration of new frontiers with α-diketone type photoprecursor method is promising field in future.

List of Publications

1 Synthesis, Structure, and Photochemistry of 5,14-Diketopentacene

Tatsuya Aotake, Shinya Ikeda, Daiki Kuzuhara, Shigeki Mori, Tetsuo Okujima, Hidemitsu Uno, Hiroko Yamada

European Journal of Organic Chemistry, **2012**, 2012(9), 1723–1729

2 Photochemical synthesis of naphthacene and its derivatives for irreversible photo-responsive fluorescent molecules

Tatsuya Aotake, Yuko Yamashita, Tetsuo Okujima, Nobuhiko Shirasawa, Yukari Jo, Shigeo Fujimori, Hidemitsu Uno, Noboru Ono, Hiroko Yamada

Tetrahedron Letters, **2013**, 54(14), 1790–1793

3 *In situ* preparation of highly fluorescent pyrene-dyes from non-luminous precursors upon photoirradiation

Tatsuya Aotake, Hiroshi Tanimoto, Hidekatsu Hotta, Daiki Kuzuhara, Tetsuo Okujima, Hidemitsu Uno, Hiroko Yamada

Chemical Communications, **2013**, 49, 3661–3663

4 An Optically and Thermally Switchable Electronic Structure Based on an Anthracene–BODIPY Conjugate

Tatsuya Aotake, Mitsuharu Suzuki, Kazuaki Tahara, Daiki Kuzuhara, Naoki Aratani, Naoto Tamai, Hiroko Yamada

Chamistry A European Journal, **2015**, *Accepted*.

5 9,9′-Anthryl-Anthroyl Radicals: Strategic Stabilization of Highly Reactive Phenoxyl Radicals

Tatsuya Aotake, Mitsuharu Suzuki, Naoki Aratani, Junpei Yuasa, Daiki Kuzuhara, Hironobu Hayashi, Haruyuki Nakano, Tsuyoshi Kawai, Jishan Wu, Hiroko Yamada

Chemical Communications, **2015**, *Accepted*.

Other Publications

1 FET performance and substitution effect on 2,6-dithienylanthracene devices prepared by photoirradiation of their diketone precursors

Hikoro Yamada, Chika Ohashi, Tatsuya Aotake, Shuhei Katsuta, Yoshihito Honsho, Hiroo Kawano, Tetsuo Okujima, Hidemitsu Uno, Noboru Ono, Shu Seki, Ken-ichi Nakayama

Chemical Communications, **2012**, *48*, 11136–11138

2 Solution-processed anthradithiophene–PCBM p-n junction photovoltaic cells fabricated

by using the photoprecursor method

Hiroko Yamada, Yuji Yamaguchi, Ryuta Katoh, Takao Motoyama, Tatsuya Aotake, Daiki Kuzuhara, Mitsuharu Suzuki, Tetsuo Okujima, Hidemitsu Uno, Naoki Aratani, Ken-ichi Nakayama

Chemical Communications, **2013**, *49*, 11638–11640

3 [Review] Synthesis and photoreactivity of α-diketone-type precursors of acenes and their use in organic-device fabrication

Mitsuharu Suzuki, Tatsuya Aotake, Yuji Yamaguchi, Nao Noguchi, Haruyuki Nakano, Ken-ichi Nakayama, Hiroko Yamada

Journal of Photochemistry and Photobiology C: Photochemistry Reviews, **2014**, *18*, 50–70

Acknowledgements

This thesis deals with the studies accomplished by the author under direction of Prof. Hiroko Yamada at Ehime University and Nara Institute of Science and Technology.

First of all, the author would like to appreciate to Prof. Hiroko Yamada for excellent guidance and constant encouragement throughout this study.

The author also sincerely appreciates to Prof. Naoki Aratani, Dr. Daiki Kuzuhara, Dr. Mitsuharu Suzuki and Dr. Hironobu Hayashi at Nara Institute of Science and Technology for useful advices and encouragements.

The author also thanks to Prof. Hidemitsu Uno, Prof. Tetsuo Okujima and Dr. Shigeki Mori at Ehime University for insightful advises and encouragements.

The author desires to express my appreciation to Prof. Naoto Tamai and Mr. Kazuaki Tahara at Kwansei Gakuin University for transient absorption measurements and discussion. The author desires to express my appreciation to Prof. Ken-ichi Nakayama, Dr. Yuji Yamaguchi and Ms. Chika Ohashi at Yamagata University for OFET and OPV fabrications. The author desires to express my appreciation to Prof. Haruyuki Nakano at Kyusyu University for DFT calculations. The author desires to express my appreciation to Dr. Junpei Yuasa at Nara Institute of Science and Technology for ESR measurements. The author desires to express my appreciation to Prof. Jishan Wu and his group member for helping my research and stay at National University of Singapore. The author desires to express my appreciation to Prof. Tsuyoshi Kawai, Prof. Masakazu Nakamura and Prof. Atsushi Ikeda for their advice as research-adviser. The author greatly appreciates to the current and former group members in Prof. Yamada's laboratory for their generous cooperation. The financial support from JSPS, Research Fellowship of Japan Society for the Promotion of Science for Young Scientists was indispensable, and the author sincerely appreciates. Finally, the author would like to thank his parents, Nobuyuki Aotake and Noriko Aotake for their heartfelt encouragement and continuous assist.

Tatsuya Aotake

DOI: 10.1002/ejoc.201101736

Synthesis, Structure, and Photochemistry of 5,14-Diketopentacene

Tatsuya Aotake,[a] Shinya Ikeda,[b] Daiki Kuzuhara,[b] Shigeki Mori,[c] Tetsuo Okujima,[a] Hidemitsu Uno,[a] and Hiroko Yamada*[b,d]

Keywords: Pentacenes / Photochemistry / Soluble precursors / Ketones / Charge transfer

5,14-α-Diketopentacene, a structural isomer of 6,13-α-diketopentacene, was prepared from pentacene in three steps. In addition to the typical n–π* absorption of the diketone moiety at around 468 nm and the anthracene-like absorption at 333, 349, and 367 nm, a broad absorption was observed at around 386 nm, which could be assigned to an intramolecular charge-transfer absorption from anthracene to the diketone moiety. 5,14-α-Diketopentacene could be converted into pentacene quantitatively by photoirradiation at 405 and 468 nm in toluene with quantum yields of 2.3 and 2.4 %, respectively, and these values are higher than the quantum yield of 1.4 % obtained for 6,13-α-diketopentacene irradiated at 468 nm. The quantum yields in acetonitrile were lowered to 0.33 and 0.28 % with irradiation at 405 and 468 nm. The crystal structure of 5,14-α-diketopentacene showed a CH–π interaction and π–π stacking between neighbouring anthracene and benzene moieties. The lower solubility of 5,14-α-diketopentacene compared with the 6,13-isomer could be explained by this crystal structure.

Introduction

The acenes, which are polycyclic aromatic hydrocarbons composed of linearly combined benzene units, have fascinated organic chemists for more than a century.[1] In particular, pentacene (**PEN**) is currently used for applications in organic electronics, such as organic thin-film transistors (OTFT)[2–6] and organic thin-film photovoltaic cells.[7–10] For the manufacture of low-cost, easy-to-handle, printable devices, the solution processing of semiconducting materials is necessary. However, **PEN** is extremely insoluble in common organic solvents; thus, soluble precursors with thermally or photochemically removable leaving groups have merited increasing attention.[11–13] In this context, the photochemical conversion of an α-diketone precursor into anthracene (**Ant**) with the production of two CO molecules has been known for a long time (Scheme 1).[14] Irradiation of diketone (**DK**) compounds at the n–π* absorption leads to the release of two molecules of CO, and the corresponding acenes can be prepared quantitatively in solutions or in films. This reaction has recently been applied to the photochemical synthesis of **PEN** and larger acenes.[15,16] Such a photochemical method has enabled us to prepare a thin film by a solution process using the 6,13-α-diketone precursor of **PEN** (**6,13-DK**), followed by simultaneous treatment with visible light and mild heating. The thin film thus obtained exhibited top-contact OTFT with a mobility of 0.34 $cm^2 V^{-1} s^{-1}$ and an on–off ratio of 2.0×10^6. These values are comparable with those of devices prepared from thermally convertible precursors.[17] In 2011, we reported the α-diketone precursor of monoanthraporphyrins.[18] Photoirradiation of the Soret band of the porphyrin moiety induced decarbonylation of the connected α-diketone moiety, and monoanthraporphyrin was obtained. To use this mechanism in the **PEN** system, we have designed the 5,14-α-diketone precursor of **PEN** (**5,14-DK**), in which the **Ant**

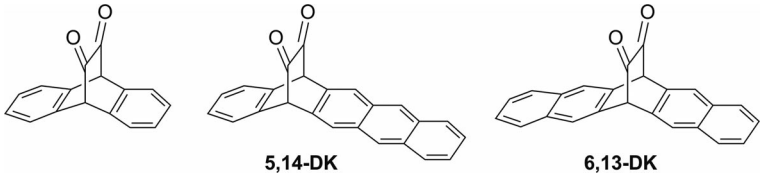

Scheme 1.

[a] Department of Chemistry and Biology, Graduate School of Science and Engineering, Ehime University, Matsuyama 790-8577, Japan
[b] Graduate School of Materials Science, Nara Institute of Science and Technology, Ikoma 630-0192, Japan
Fax: +81-743-72-6041
E-mail: hyamada@ms.naist.jp
[c] Department of Molecular Science, Integrated Center for Sciences, Ehime University, Matsuyama 790-8577, Japan
[d] CREST, JST, Chiyoda-ku 102-0075, Japan
Supporting information for this article is available on the WWW under http://dx.doi.org/10.1002/ejoc.201101736.

moiety has a moderate absorbance separate from the n–π* absorption, and therefore, the useful wavelength for photoconversion from the precursor to **PEN** will be broadened. Herein, we report the synthesis, crystal structures, and photoreactivity of **5,14-DK**.

Results and Discussion

Synthesis

The synthesis of **5,14-DK** is shown in Scheme 2. The Diels–Alder reaction of **PEN** with vinylene carbonate gave a mixture of 5,14 (**1**) and 6,13 adducts (**2**). After deprotection of the diol moieties, the mixture was separated by silica gel column chromatography to give the 5,14 (**5,14-PDO**) and 6,13 adducts (**6,13-PDO**) in 21 and 58%, respectively. Swern oxidation of **5,14-PDO** gave **5,14-DK** in 52% yield. The synthesis of **6,13-DK** has already been reported.[15a,15b]

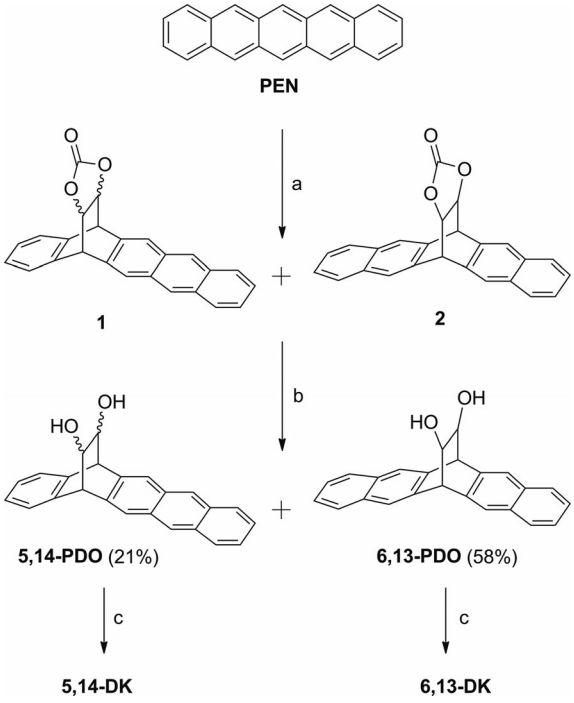

Scheme 2. Reagents and conditions: (i) vinylene carbonate, xylene, autoclave, 180 °C, 3 d; (ii) NaOH aq., dioxane, reflux, 2 h, 21% for **5,14-PDO** and 58% for **6,13-PDO** for 2 steps; (iii) trifluoroacetic anhydride, *N*,*N*-diisopropylethylamine, dry DMSO, dry CH_2Cl_2, –60 °C, 1.5 h, 52% for **5,14-DK** and 43% for **6,13-DK**.

Crystal Structure

An X-ray crystallographic measurement was performed on **5,14-DK** at 25 °C (Figure 1a).[19] The angles made by C(9)–C(10)–C(11) and C(16)–C(17)–C(18) were 107.6(2) and 106.7(1)°, respectively. The stacking pattern of the neighbouring molecules along the *c* axis in the crystal was also examined (Figure 1b). There was π–π overlap between two molecules. The distance between the **Ant** surfaces was 3.524 Å, which is shorter than that of the naphthalene–naphthalene distance of **6,13-DK** (3.596 Å). In general, the **Ant** has a stronger interaction between molecules than naphthalene. In **5,14-DK**, a similar interaction was observed between two molecules. The interaction was not only observed between **Ant** moieties, but also between the facing benzene rings. The distance between the surface of two benzene moieties was 3.849 Å. In addition, there was a CH–π interaction between hydrogen atoms and the neighbouring **Ant** moiety. The shortest contact between the hydrogen atoms and **Ant** surface was 2.767 Å. These interactions made the packing structure of **5,14-DK** rigid and lowered the solubility in common organic solvents. The solubility of **5,14-DK** in toluene was only 0.44 mg mL^{-1} at room temp., although it was 2.3 mg mL^{-1} for **6,13-DK**.

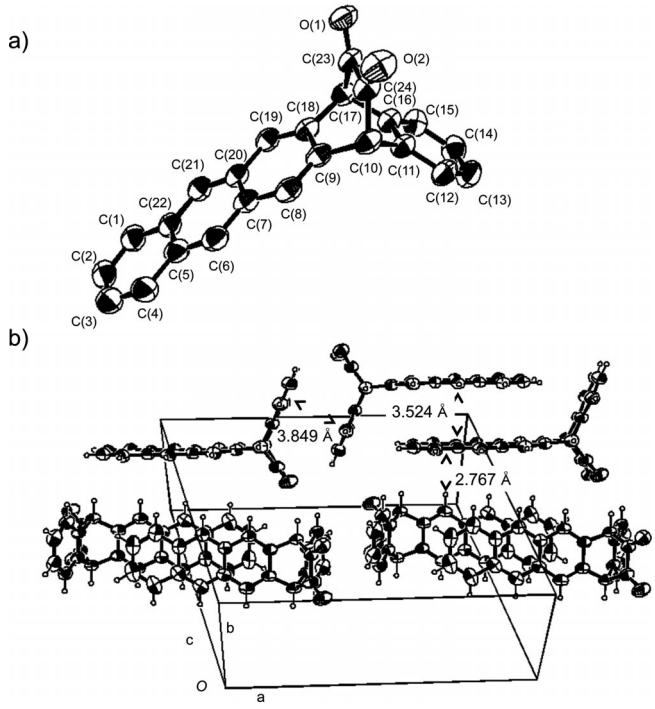

Figure 1. (a) ORTEP drawing of the X-ray structure of **5,14-DK** at 25 °C. Hydrogen atoms are omitted for clarity. Ellipsoids are drawn at the 30% probability displacement level. (b) Stacking pattern of neighbouring molecules.

Absorption Spectra

UV/Vis absorption spectra of **5,14-DK** and **6,13-DK**, along with the reference compounds **5,14-PDO**, **6,13-PDO** and **PEN**, in toluene are shown in Figure 2a. The absorption spectrum of **6,13-DK** showed an n–π* absorption of the **DK** moiety at 466 nm ($\varepsilon = 1.22 \times 10^3$ M^{-1} cm^{-1}) and a π–π* absorption at 329 (4.23×10^3 M^{-1} cm^{-1}) and 315 nm (4.05×10^3 M^{-1} cm^{-1}). The π–π* absorption peaks of **6,13-PDO** were 321 (1.41×10^3 M^{-1} cm^{-1}) and 306 nm (1.22×10^3 M^{-1} cm^{-1}). The π–π* absorption peaks of **6,13-DK** were broader and redshifted by 8 nm relative to those of **6,13-PDO**. For **5,14-DK**, a broad n–π* absorption of the **DK** moiety was observed at 464 nm (1.58×10^3 M^{-1} cm^{-1}), and a π–π* absorption of the **Ant** moiety was observed at

333 (5.49×10^3 M^{-1}cm^{-1}), 349 (5.40×10^3 M^{-1}cm^{-1}), and 367 nm (4.20×10^3 M^{-1}cm^{-1}). Furthermore, a broad absorption at 386 nm (2.98×10^3 M^{-1}cm^{-1}) was observed, although a similar peak was not observed for **6,13-DK**. The edge or broad band reached the n–π* absorption; therefore, the molar extinction coefficient of n–π* absorption of **5,14-DK** was larger than that of **6,13-DK**. Compared with the absorption of **5,14-PDO**, the π–π* absorption of the **Ant** moiety of **5,14-DK** was broadened and redshifted by 7–8 nm; this means the **Ant** moiety of **5,14-DK** strongly interacts with carbonyl moieties.

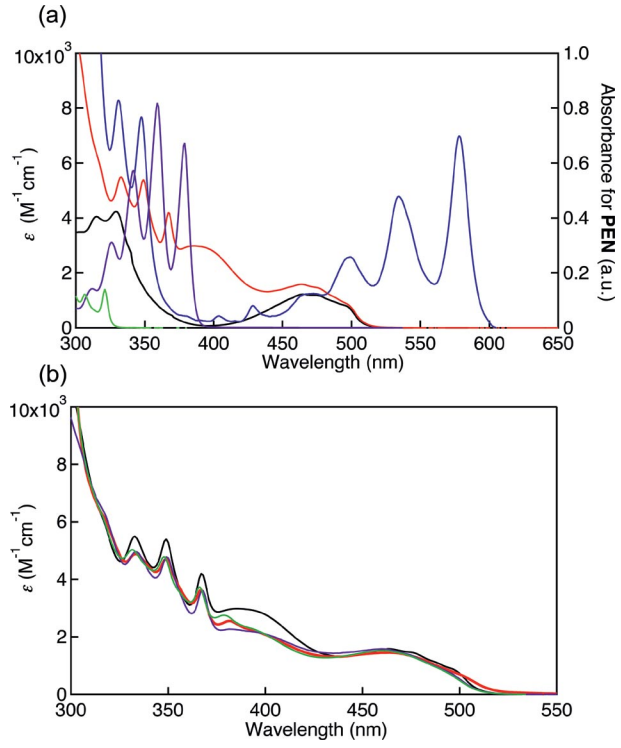

Figure 2. (a) UV/Vis absorption spectra of **5,14-DK** (red), **6,13-DK** (black), **PEN** (blue), **5,14-PDO** (purple), **6,13-PDO** (green) in toluene. (b) Solvent effect of **5,14-DK**. In toluene (black), in dichloromethane (red), in acetonitrile (purple), in DMF (green).

The absorption at 386 nm was characteristic of **5,14-DK** and was not observed for **5,14-PDO**. The absorption spectra of **5,14-DK** were measured from 1.79×10^{-1} to 7.39×10^{-3} mM in toluene, but a dependence on the concentration was not observed. These phenomena suggested that the absorption at 386 nm was an intramolecular charge-transfer (ICT) absorption from the **Ant** moiety to the **DK** moiety. To confirm this hypothesis, the absorption spectra of **5,14-DK** were measured in toluene, dichloromethane, acetonitrile and DMF (Figure 2b). In addition to the π–π* absorptions at 333, 349 and 367 nm, a vibrational peak at 375 nm was observed with shoulders at 400 nm in DMF. In acetonitrile and DMF, similar peaks were observed at 370 and 372 nm, respectively. The broad peak at 386 nm in toluene showed a clearer vibrational structure than that in other solvents; 382 nm (1.58×10^3 M^{-1}cm^{-1}) in dichloromethane, 382 nm (2.55×10^3 M^{-1}cm^{-1}) in DMF and 379 nm (2.75×10^3 M^{-1}cm^{-1}) in acetonitrile with shoulders around 400 nm. The n–π* and π–π* absorptions at 333, 349 and 367 nm showed a slight dependence on the solvent. The molecular extinction coefficients of the peaks at 333, 349 and 367 nm were smaller than those in toluene, but the peaks were observed at almost the same wavelength. On the contrary, with an increase in polarity of the solvents, the peak at 382 nm in dichloromethane was blue-shifted to 379 nm in acetonitrile. Therefore, these peaks were assigned not as the π–π* absorption but as the ICT absorption.

Such an intramolecular interaction was not observed for **6,13-DK**, probably due to the difference in HOMO levels of **Ant** and naphthalene. The energy gap between the HOMO of naphthalene and the LUMO of the **DK** moiety is larger than that between the HOMO of **Ant** and the LUMO of the **DK** moiety. Chow et al. reported 6,13- and 5,14-monocarbonyl **PEN**.[13] In their system, a CT-like absorption was not observed, because the n–π* transition is forbidden in the molecule and the molar extinction coefficient is very small. For **5,14-DK** and **6,13-DK**, the molar extinction coefficients of the n–π* absorption were over 1000, and the n–π* transition became possible to some extent.

Molecular orbital (MO) and time-dependent density functional theory (TD-DFT) calculations were performed for **5,14-DK** by using the Gaussian 09 program package at the B3LYP/6-31G(d)//CAM-B3LYP/6-31G(d) level of theory (Figure 3). The HOMO was localized on the **Ant** moiety, the LUMO on the carbonyl π* orbital and the HOMO-1 on the n orbital. TD-DFT calculations showed that the absorption at 456 nm corresponding to an n–π* transition that was mainly composed of the transition from HOMO-1 to LUMO (Figure S1 in the Supporting Information). Also, the absorption at 358 nm was calculated to be transitions from HOMO to LUMO or LUMO+1, which correspond to ICT from the **Ant** moiety to the **DK** moiety.

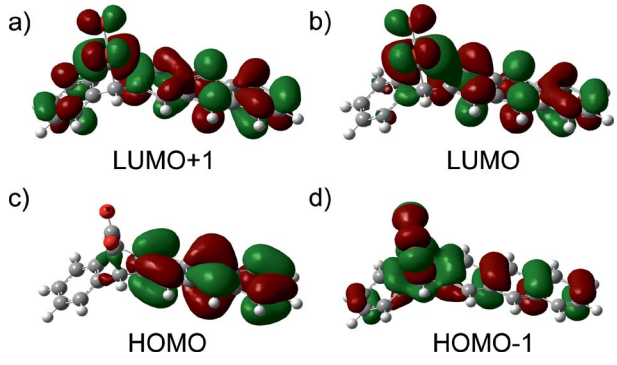

Figure 3. Molecular orbitals of (a) LUMO-1, (b) LUMO, (c) HOMO and (d) HOMO-1 of **5,14-DK** calculated at the B3LYP/6-31G(d)/s/CAM-B3LYP/6-31G(d) level.

Photoreaction

The photolysis reactions of α-diketone **5,14-DK** to **PEN** in argon are shown in Figure 4. Compound **5,14-DK** was irradiated at λ_{ex} = 405 and 468 nm. To monitor the photoreaction process, changes in the UV/Vis absorption spectra were measured every 30 s during photolysis. Firstly, a

1.1×10^{-1} mM solution of **5,14-DK** in toluene under argon was irradiated with light at 405 nm, as shown in Figure 4a. During irradiation, the peaks at 352–484 nm decreased gradually, and new peaks at 495, 530 and 578 nm increased. After the absorptions characteristic of **PEN** increased for 25 min, a purple solid appeared in the solution. As determined by observing the isosbestic points at 352 and 484 nm, the photoreaction proceeded quantitatively.

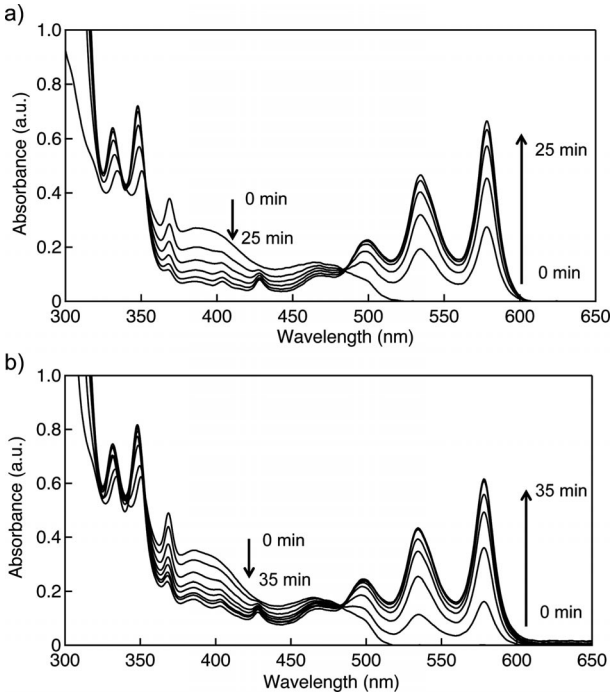

Figure 4. (a) Changes in the absorption spectra during photolysis (λ_{ex} = 405 nm) of **5,14-DK** in toluene. (b) Changes in the absorption spectra during photolysis (λ_{ex} = 468 nm) of **5,14-DK** in toluene.

Secondly, solutions of **5,14-DK** (1.3×10^{-1} mM) and **6,13-DK** (1.7×10^{-1} mM) in toluene under argon were irradiated with light at 468 nm, as shown in Figure 4b and Scheme 3. Similarly, the absorption spectra changed from the α-diketone to **PEN** with photoirradiation. The quantum yield (Φ_r) of the photoreaction of **5,14-DK** was measured by using potassium ferrioxalate actinomerty (Table 1). The Φ_r values of **5,14-DK** in toluene were 2.4 (λ_{ex} = 405 nm) and 2.3% (468 nm). The values are about two times that of **6,13-DK** (1.4%, 468 nm).

Table 1. Quantum yield of photoreactions of **5,14-DK** and **6,13-DK**.

	Φ_r [%] Toluene 405 nm[a]	468 nm[a]	Acetonitrile 405 nm [a,b]	468 nm[a,b]
5,14-DK	2.4 ± 1.0	2.3 ± 0.3	0.33 ± 0.13	0.28 ± 0.12
6,13-DK	–	1.4 ± 0.3	–	0.80 ± 0.10

[a] Excitation wavelength. [b] The ε value of **PEN** in acetonitrile was assumed to be the same as that in toluene.[20]

Next, photolysis reactions of **5,14-DK** and **6,13-DK** in acetonitrile were performed; the results are shown in Figure 5 and Figure S3 in the Supporting Information. In acetonitrile the photoreaction of **5,14-DK** was slower than that in toluene, and the Φ_r values were 0.28% for λ_{ex} = 468 nm and 0.33% for λ_{ex} = 405 nm, which are ten times lower than those in toluene. The Φ_r value of **6,13-DK** irradiated at 468 nm in acetonitrile was 0.80%; lower than that of 1.4% in toluene. Similar solvent-dependent behaviour of the reaction on the quantum yield was observed for the **DK**

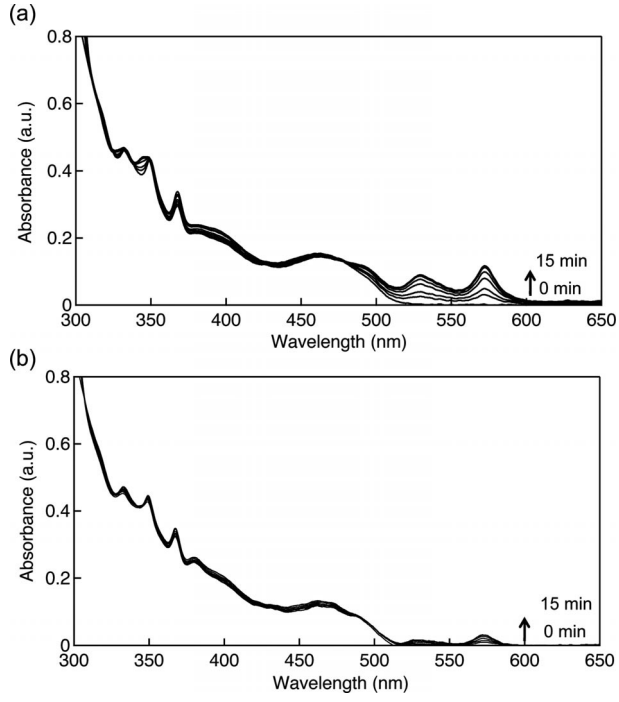

Figure 5. (a) Change in the absorption spectra during photolysis (λ_{ex} = 405 nm) of **5,14-DK** in acetonitrile. (b) Change in the absorption spectra during photolysis (λ_{ex} = 468 nm) of **5,14-DK** in acetonitrile.

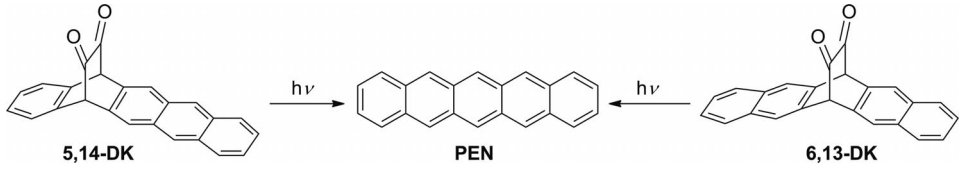

Scheme 3. Photochemical conversion of α-diketone **5,14-DK** and **6,13-DK**.

precursor of monoanthraporphyrin.[18] Compared with the photocleavage reaction in toluene, the occurrence of rapid photoinduced electron transfer from the singlet-excited-state porphyrin to the **DK** moiety in benzonitrile resulted in a significant decrease in the singlet-excited-state lifetime, leading to suppression of the photocleavage reaction.

The photoconversion reaction was also performed in a thin film. The UV spectra before and after photoirradiation are shown in Figure S4 in the Supporting Information along with photos of the thin film. The yellow film changed to purple during photoirradiation. However, the spectrum of **5,14-DK** was broad, and the band structures were not clear, probably due to π–π stacking of the compounds. The absorption spectrum of **PEN** was also broad, but the peaks characteristic for **PEN** were observed at around 560 and 610 nm.[15b]

Electrochemical Properties and Energy Diagrams

The electrochemical properties were measured in deaerated acetonitrile containing tetrabutylammonium hexafluorophosphate ($TBAPF_6$), as shown in Figures S5 and S6 in the Supporting Information. The one-electron reduction peak of **5,14-DK** was observed at –1.47 V (vs. Fc/Fc^+) for the reduction of the **DK** moiety. The oxidation peak was irreversible, and the peak maximum was at 0.94 V (vs. Fc/Fc^+), which corresponds to oxidation of the **Ant** moiety. The energy level of the charge-separated (CS) state (**Ant**$^{\cdot+}$-**DK**$^{\cdot-}$) was determined from the redox potential. The driving forces [$-\Delta G_{ET(CR)}$] for the intramolecular charge-recombination processes from the anion radical of the diketone moiety (**DK**$^{\cdot-}$) to the cation radical of the anthracene moiety (**Ant**$^{\cdot+}$) were calculated by using Equation (1):

$$-\Delta G_{ET(CR)} = e[E_{ox}(\mathbf{Ant}^{\cdot+}/\mathbf{Ant}) - E_{red}(\mathbf{DK}/\mathbf{DK}^{\cdot-})] \quad (1)$$

in which e stands for the elementary charge. On the other hand, the driving forces for the intramolecular charge-separation processes [$-\Delta G_{ET(CS)}$] from **Ant** to the diketone singlet excited state (**^{1}DK***) were determined by using Equation (2):

$$-\Delta G_{ET(CS)} = \Delta E_{0-0} + \Delta G_{ET(CR)} \quad (2)$$

in which ΔE_{0-0} is the singlet excited state of the diketone moiety (**^{1}DK***). The energy levels of **^{1}DK*** and **^{3}DK*** were calculated from the **Ant-DK** compounds already reported.[21] The **^{1}DK*** and ICT [(**Ant-DK**)*] levels were higher than that of the CS state (–2.41 eV). Thus, electron transfer from the **Ant** moiety to the **DK** group may occur, affording the CS state, as shown in the α-diketone precursor of monoanthraporphyrins.[18] The CS state decays mainly to the ground state by radiationless deactivation. However, the CS state in toluene may be higher in energy than that in acetonitrile. Because of this, charge separation of **5,14-DK** is not favourable in toluene, and the quantum yield of the photoreaction is higher than that in acetonitrile (Figure 6).

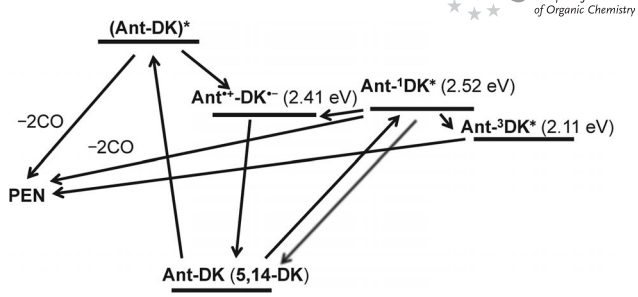

Figure 6. Energy diagram of **5,14-DK** in acetonitrile.

Conclusions

We successfully prepared **5,14-DK**, which is a photoconvertible precursor of **PEN** and a structural isomer of **6,13-DK**. Compound **5,14-DK** exhibited a broad ICT absorption at around 390 nm in addition to an n–π* absorption at 460 nm. Photochemical conversion to **PEN** quantitatively proceeded by photoirradiation at the ICT and n–π* absorptions in toluene, with quantum yields of 2.4 and 2.3%, respectively. However, the photoreaction in acetonitrile was slower, Φ_r = 0.33 (405) and 0.28% (468 nm), probably due to the occurrence of ICT from the **Ant** moiety to the **DK** group. X-ray single-crystal structure analysis of **5,14-DK** suggested that **5,14-DK** has a strong π–π interaction with neighbouring molecules, which lowers the solubility of **5,14-DK** in common organic solvents.

Experimental Section

General: Melting points were measured with a Yanaco M-500-D melting point apparatus. ^{1}H NMR and ^{13}C NMR spectra were recorded with JEOL JNM-AL 400 and AL 300 spectrometers at ambient temperature by using tetramethylsilane as an internal standard. FAB mass spectra were measured with a JEOL JMS-MS700 spectrometer. UV/Vis spectra were measured with a JASCO UV/Vis/NIR spectrophotometer V-570. Elemental analyses were performed with a Yanaco MT-5 elemental analyzer.

Materials: TLC and gravity column chromatography were performed on Art. 5554 (Merck KGaA) plates and silica gel 60N (Kanto Chemical), respectively. Acetonitrile was distilled from P_2O_5 in vacuo. All other solvents and chemicals were reagent-grade quality, obtained commercially, and used without further purification except as noted. For spectral measurements, spectral-grade toluene, dichloromethane, acetonitrile, and DMF were purchased from Nacalai Tesque.

Synthesis of 5,14-Dihydro-15,16-dihydroxy-5,14-ethanopentacene (5,14-PDO): A solution of **PEN** (1.00 g, 3.60 mmol) and vinylene carbonate (0.310 g, 3.64 mmol) in xylene (68 mL) was mixed at 180 °C in an autoclave for 3 d. After removal of the solvent in vacuo, the residue was washed with EtOAc to give a mixture of carbonate compounds (1.29 g). The mixture of carbonate compounds (1.29 g, 3.55 mmol) was added to a 4 M aqueous solution of NaOH and 1,4-dioxane (40 mL). The resulting mixture was heated at reflux for 1 h. The reaction mixture was cooled, poured into water, and then extracted with EtOAc. The combined organic layers were washed with water and dried with Na_2SO_4. After removal of the solvent in vacuo, the residue was purified by column chromatography on silica gel with EtOAc/$CHCl_3$ (1:4) to give **5,14-**

PDO (0.260 g, 0.770 mmol, 21%) as white crystals and 6,13-dihydro-15,16-dihydroxy-6,13-ethanopentacene (**6,13-PDO**; 0.710 g, 2.10 mmol, 58%). **5,14-PDO**: M.p. 275–277 °C. ^{1}H NMR (400 MHz, $CDCl_3$, TMS): δ = 2.18 (br., 2 H, OH), 4.23 (br., 2 H), 4.56 (br., 2 H), 7.25 (m, 2 H), 7.44–7.72 (m, 2 H), 7.89 (s, 2 H), 7.97–7.95 (m, 2 H), 8.33 (s, 2 H) ppm. ^{13}C NMR (100 MHz, $CDCl_3$, TMS): δ = 51.26, 68.81, 122.79, 125.11, 125.70, 126.54, 127.00, 127.88, 136.80 ppm. MS (FAB): *m*/*z* = 339 [M^+ + 1]. $C_{24}H_{18}O_2$ (338.41): calcd. C 85.18, H 5.36; found C 85.22, H 5.30.

Synthesis of 5,14-Dihydro-5,14-ethanopentacene-15,16-dione (5,14-DK): Trifluoroacetic anhydride (2.1 mL, 15.1 mmol) was added dropwise to a mixture of dry DMSO (1.0 mL, 14.0 mmol) and dry CH_2Cl_2 (10 mL) at –60 °C under argon. After stirring for 10 min, **5,14-PDO** (0.306 g, 0.905 mmol) dissolved in a mixture of dry DMSO (10 mL) and dry CH_2Cl_2 (7 mL) was added dropwise. After stirring for 90 min, *N*,*N*-diisopropylethylamine (4.50 mL, 25.8 mmol) was added dropwise to the reaction mixture. The solution was stirred at –60 °C for 60 min and warmed to room temp. before 3 M HCl (50 mL) was added to the mixture. The mixture was extracted with CH_2Cl_2, and the combined organic layers were washed with water and brine and dried with Na_2SO_4. After removal of the solvent in vacuo, the residue was purified by column chromatography on silica gel with CH_2Cl_2 and recrystallized from toluene to give **5,14-DK** as yellow crystals (0.157 g, 0.469 mmol, 52%). M.p. > 300 °C. ^{1}H NMR (400 MHz, $CDCl_3$, TMS): δ = 5.19 (s, 2 H), 7.39–7.41 (m, 2 H), 7.48–7.52 (m, 4 H), 7.99–8.01 (m, 2 H), 8.07 (s, 2 H), 8.42 (s, 2 H) ppm. ^{13}C NMR (75 MHz, $CDCl_3$, TMS): δ = 60.46, 125.45, 126.03, 126.36, 126.50, 128.13, 129.60, 130.95, 131.21, 132.16, 134.90, 184.84 ppm. MS (FAB): *m*/*z* = 336 [M^+ + 1]. $C_{24}H_{14}O_2$ (334.37): calcd. C 86.21, H 4.22; found C 86.50, H 4.59.

Theoretical Calculations: All DFT calculations were achieved with the Gaussian 09[22] program package. The geometry was fully optimized at the Becke's three-parameter hybrid functional combined with the Lee–Yang–Parr correlation functional abbreviated as the B3LYP level of density functional theory with 6-31G(d) basis set. Equilibrium geometries were verified by frequency calculations, where no imaginary frequency was found. Based on the B3LYP/6-31G(d)-optimized geometry, TD-DFT calculations were conducted at the CAM-B3LYP/6-31G(d) level of theory.[23]

Electrochemical Measurements: The cyclic voltammetry measurements of investigated compounds were performed with a BAS electrochemical analyser in deaerated acetonitrile containing nBu$_4$NPF$_6$ as a supporting electrolyte at 298 K (100 mV s^{-1}). The glassy carbon working electrode was polished with BAS polishing alumina suspension and rinsed with acetone before use. The counter electrode was a platinum wire. The measured potentials were recorded with respect to Ag/$AgNO_3$ and normalized to Fc/Fc^+.

Photochemical Reactions: The photocleavage reactions were carried out in a quartz UV cell, which was irradiated with monochromatic excitation light through a monochromator (Ritsu MC-10N) from a 500 W xenon lamp (Ushio XB-50102AA-A), and monitored by an OCEAN OPTICS HR-4000 high-resolution spectrometer system with light source DH-2000-BAL. A standard actionometer ($K_3[Fe(C_2O_4)_3]$)[24] was used for quantum yield determination of the photochemical reactions of **5,14-DK** and **6,13-DK** in acetonitrile and toluene. A square quartz cuvette (10 mm i.d.) that contained a deaerated solution (3.0 cm^3) of **5,14-DK** and **6,13-DK** was irradiated with monochromatized light (λ = 405 or 468 nm) through a monochromator (Ritsu MC-10N) by using a 500 W xenon lamp (Ushio XB-50102AA-A). Under the actinometry experimental conditions, both **5,14-DK** or **6,13-DK** absorbed essentially all incident light. The photochemical reaction was monitored by using a JASCO UV/Vis/NIR V-570 spectrophotometer. The quantum yields were determined from the increase in absorbance due to **PEN** (578 nm) at the beginning of the reaction.

Photochemical Reactions in Films: Compound **5,14-DK** (10 mg) was dissolved in hot $CHCl_3$ (1 mL), and the solution (100 μL) was spin-coated on glass at 1000 rpm for 20 s. The absorption spectrum of **5,14-DK** in the film was measured. Then the film was irradiated with a 460 W metal halide lamp through a blue filter in a glove box for 90 min, and the absorption spectrum of **PEN** was measured.

X-ray Analysis: Single crystals of **5,14-DK** suitable for X-ray diffraction analysis were obtained by slow diffusion of heptane into a solution of **5,14-DK** in CH_2Cl_2. The crystals were mounted in Litho Loops (purchased from Protein Wave). The diffraction data was collected at 25 °C with a Rigaku VariMaxRAPID/a imaging plate diffractometer with graphite-monochromated Cu-K_α radiation or with a Rigaku Mercury-8 diffractometer with graphite-monochromated Mo-K_α radiation equipped with a CCD detector. The diffraction data were processed with CrystalStructure of the Rigaku program, solved with the SIR-97 program,[25] and refined with the SHELX-97 program.[26]

Supporting Information (see footnote on the first page of this article):·TD-DFT calcuration, change in absorption spectra before and after photolysis in film, CV and DPV of **5,14-DK**; change in absorption spectra of **6,13-DK** during photolysis in solution.

Acknowledgments

We thank Prof. Atsushi Wakamiya, Institute of Chemical Research, Kyoto University for his valuable discussion on TD-DFT calculations. This work was partially supported by the Ministry of Education, Culture, Sports, Science and Technology (MEXT), Japan through a Grants-in-Aid (No. 22350083 to H. Y.) and the Green Photonics Project in NAIST sponsored by the Ministry of Education, Culture, Sports, Science and Technology, MEXT, Japan. Leigh McDowel is gratefully acknowledged for proofreading this manuscript.

[1] a) M. Bendikov, F. Wudl, D. F. Perepichka, *Chem. Rev.* **2004**, *104*, 4891–4945; b) J. E. Anthony, *Chem. Rev.* **2006**, *106*, 5028–5048.
[2] D. Knipp, R. A. Street, B. Krusor, R. Apte, J. Ho, *J. Non-Cryst. Solids* **2002**, *299–302*, 1042–1046.
[3] a) H. Klauk, M. Halik, U. Zschieschang, G. Schmid, W. Radlik, W. Weber, *J. Appl. Phys.* **2002**, *92*, 5259–5263; b) H. Klauk, M. Halik, U. Zschieschang, F. Eder, G. Schmid, C. Dehm, *Appl. Phys. Lett.* **2003**, *82*, 4175–4177.
[4] J. A. Nichols, D. J. Gundlach, T. N. Jackson, *Appl. Phys. Lett.* **2003**, *83*, 2366–2368.
[5] M. Kitamura, T. Imada, Y. Arakawa, *Appl. Phys. Lett.* **2003**, *83*, 3410–3412.
[6] D. Kumaki, M. Yahiro, Y. Inoue, S. Tokito, *Appl. Phys. Lett.* **2007**, *90*, 133511-3.
[7] S. Yoo, B. Domercq, B. Kippelen, *Appl. Phys. Lett.* **2004**, *85*, 5427–5429.
[8] J. Yang, T.-Q. Nguyen, *Org. Electron.* **2007**, *8*, 566–574.
[9] J. Sakai, T. Taima, T. Yamanari, Y. Yoshida, A. Fujii, M. Ozaki, *Jpn. J. Appl. Phys.* **2010**, *49*, 032301–7.
[10] K. Nomura, T. Oku, A. Suzuki, K. Kikuchi, G. Kinoshita, *J. Phys. Chem. Solids* **2010**, *71*, 210–213.
[11] a) A. R. Brown, A. Pomp, D. M. de Leeuw, D. B. M. Klaassen, E. E. Havinga, P. Herwig, K. Müllen, *J. Appl. Phys.* **1996**, *79*,

2136–2138; b) P. T. Herwig, K. Müllen, *Adv. Mater.* **1999**, *11*, 480–483.
[12] a) A. Afzali, C. D. Dimitrakopoulos, T. L. Breen, *J. Am. Chem. Soc.* **2002**, *124*, 8812–8813; b) A. Afzali, C. D. Dimitrakopoulos, T. O. Graham, *Adv. Mater.* **2003**, *15*, 2066–2069; c) K. P. Weidkamp, A. Afzali, R. M. Tromp, R. J. Hamers, *J. Am. Chem. Soc.* **2004**, *126*, 12740–12741; d) A. Afzali, C. R. Kagan, G. P. Traub, *Synth. Met.* **2005**, *155*, 490–494; e) D. Zander, N. Hoffmann, K. Lmimouni, S. Lenfant, C. Petit, D. Vuillaume, *Microelectron. Eng.* **2005**, *80*, 394–397; f) T. Akinaga, S. Yasutake, S. Sasaki, O. Sakata, H. Otsuka, A. Takahara, *Chem. Lett.* **2006**, *35*, 1162–1163.
[13] a) K.-Y. Chen, H.-H. Hsieh, C.-C. Wu, J.-J. Hwang, T. J. Chow, *Chem. Commun.* **2007**, *10*, 1065–1067; b) T.-H. Chuang, H.-H. Hsieh, C.-K. Chen, C.-C. Wu, C.-C. Lin, P.-T. Chou, T.-H. Chao, T. J. Chow, *Org. Lett.* **2008**, *10*, 2869–2872.
[14] J. Strating, B. Zwanenburg, A. Wagenaar, A. C. Udding, *Tetrahedron Lett.* **1969**, *10*, 125–128.
[15] a) H. Uno, Y. Yamashita, M. Kikuchi, H. Watanabe, H. Yamada, T. Okujima, T. Ogawa, N. Ono, *Tetrahedron Lett.* **2005**, *46*, 1981–1983; b) H. Yamada, Y. Yamashita, M. Kikuchi, H. Watanabe, T. Okujima, H. Uno, T. Ogawa, K. Ohara, N. Ono, *Chem. Eur. J.* **2005**, *11*, 6212–6220; c) Y. Zhao, R. Mondal, D. C. Neckers, *J. Org. Chem.* **2008**, *73*, 5506–5513; d) S. Katsuta, H. Yamada, T. Okujima, H. Uno, *Tetrahedron Lett.* **2010**, *51*, 1397–1400.
[16] a) R. Mondal, B. K. Shah, D. C. Neckers, *J. Am. Chem. Soc.* **2006**, *128*, 9612–9613; b) R. Mondal, R. M. Adhikari, B. K. Shah, D. C. Neckers, *Org. Lett.* **2007**, *9*, 2505–2508; c) R. Mondal, C. Tönshoff, D. Khon, D. C. Neckers, H. F. Bettinger, *J. Am. Chem. Soc.* **2009**, *131*, 14281–14289; d) C. Tönshoff, H. F. Bettinger, *Angew. Chem. Int. Ed.* **2010**, *49*, 4125–4128.
[17] A. Masumoto, Y. Yamashita, S. Go, T. Kikuchi, H. Yamada, T. Okujima, N. Ono, H. Uno, *Jpn. J. Appl. Phys.* **2009**, *48*, 051505–5.
[18] H. Yamada, D. Kuzuhara, K. Ohkubo, T. Takahashi, T. Okujima, H. Uno, N. Ono, S. Fukuzumi, *J. Mater. Chem.* **2010**, *20*, 3011–3024.
[19] CCDC-854777 (25 °C) contains the supplementary crystallographic data for this paper. These data can be obtained free of change from The Cambridge Crystallographic Data Centre via www.ccdc.cam.ac.uk/data_request/cif.
[20] H-H. Perkampus in *UV/Vis Atlas of Organic Compounds*, 2nd ed., VCH, Weinheim, **1992**, p. 652.
[21] R. Mondal, A. N. Okhrimenko, B. K. Shah, D. C. Neckers, *J. Phys. Chem. B* **2008**, *112*, 11–15.
[22] M. J. Frisch, G. W. Trucks, H. B. Schlegel, G. E. Scuseria, M. A. Robb, J. R. Cheeseman, G. Scalmani, V. Barone, B. Mennucci, G. A. Petersson, H. Nakatsuji, M. Caricato, X. Li, H. P. Hratchian, A. F. Izmaylov, J. Bloino, G. Zheng, J. L. Sonnenberg, M. Hada, M. Ehara, K. Toyota, R. Fukuda, J. Hasegawa, M. Ishida, T. Nakajima, Y. Honda, O. Kitao, H. Nakai, T. Vreven, J. A. Montgomery Jr, J. E. Peralta, F. Ogliaro, M. Bearpark, J. J. Heyd, E. Brothers, K. N. Kudin, V. N. Staroverov, R. Kobayashi, J. Normand, K. Raghavachari, A. Rendell, J. C. Burant, S. S. Iyengar, J. Tomasi, M. Cossi, N. Rega, J. M. Millam, M. Klene, J. E. Knox, J. B. Cross, V. Bakken, C. Adamo, J. Jaramillo, R. Gomperts, R. E. Stratmann, O. Yazyev, A. J. Austin, R. Cammi, C. Pomelli, J. W. Ochterski, R. L. Martin, K. Morokuma, V. G. Zakrzewski, G. A. Voth, P. Salvador, J. J. Dannenberg, S. Dapprich, A. D. Daniels, Ö. Farkas, J. B. Foresman, J. V. Ortiz, J. Cioslowski, D. J. Fox, *Gaussian 09*, Revision A.2, Gaussian, Inc., Wallingford, CT, **2009**.
[23] a) A. D. Becke, *Phys. Rev. A* **1988**, *38*, 3098–3100; b) A. D. Becke, *J. Chem. Phys.* **1993**, *98*, 5648–5652; c) C. Lee, W. Yang, R. G. Parr, *Phys. Rev. B* **1988**, *37*, 785–789.
[24] C. G. Hatchard, C. A. Parker, *Proc. R. Soc. London, Ser. B* **1956**, *235*, 518–536.
[25] A. Altomare, M. C. Burla, M. Camalli, G. Cascarano, C. Giacovazzo, A. Guagliardi, A. G. G. Moliterni, G. Polidori, R. Spagna, *J. Appl. Crystallogr.* **1999**, *32*, 115–118.
[26] G. M. Sheldrick, *Acta Crystallogr., Sect. A* **2008**, *64*, 112–122.

Received: December 2, 2011
Published Online: February 8, 2012

ChemComm

Cite this: *Chem. Commun.*, 2012, **48**, 11136–11138

www.rsc.org/chemcomm

COMMUNICATION

FET performance and substitution effect on 2,6-dithienylanthracene devices prepared by photoirradiation of their diketone precursors†

Hiroko Yamada,*[ab] Chika Ohashi,[c] Tatsuya Aotake,[a] Shuhei Katsuta,[a] Yoshihito Honsho,[d] Hiroo Kawano,[e] Tetsuo Okujima,[e] Hidemitsu Uno,[e] Noboru Ono,[e] Shu Seki*[d] and Ken-ichi Nakayama*[bc]

Received 27th July 2012, Accepted 20th September 2012
DOI: 10.1039/c2cc35439j

Hole mobility was evaluated by top-contact bottom gate field effect transistor and time resolved microwave conductivity measurements in 2,6-dithienylanthracene and hexyl-substituted 2,6-dithienylanthracene films prepared by spin-coating of their α-diketone precursors followed by photoirradiation, revealing enough high potentials for semiconducting films with charge carrier mobilities of 0.8–0.9 cm^2 V^{-1} s^{-1} in the photo-irradiated films.

The replacement of inorganic semiconductors with organic counterparts will decrease manufacturing cost and allow fabrication of devices over large areas or on lightweight, flexible substrates. Especially soluble semiconducting organic inks can be deposited and patterned by a variety of printing techniques, such as ink-jet printing, screen printing, and roll-to-roll technique.[1,2] To attain this goal, many soluble organic electronic materials, polymers or substituted small molecules, have been reported.[3] On the other hand, thermally convertible precursor methods have been developed to utilize intact acenes,[4] phthalocyanines,[5] benzoporphyrins[6] and oligothiophenes[7] by solution processes to take advantage of their good performances.[8] We[9] and others[10] have reported the photoconvertible precursors of pentacene which can be converted to pentacene in solution or film quantitatively. The hole mobility (μ_h) of the top-contact type field-effect transistor (FET) of the pentacene prepared by the spin-coating of the diketone precursor followed by the photoirradiation was 0.56 cm^2 V^{-1} s^{-1},[11] which is comparable with those of deposited pentacene films and amorphous silicon devices.

To overcome the instability of pentacene under air, Meng *et al.* have reported 2,6-dithienylanthracene (**DTAnt**) and hexyl-substituted-2,6-dithienylanthracene (**DHTAnt**) as high performance, stable organic semiconductors.[12] The FET performances of the films prepared by vacuum deposition were 0.063 cm^2 V^{-1} s^{-1} and 0.50 cm^2 V^{-1} s^{-1}, respectively. In 2006 we reported the photoprecursor of **DTAnt** to attain the photoconversion from the precursor under air.[13] Due to the difference of the n–π* absorption band of the precursor (400–500 nm) and the target anthracene compounds (under 400 nm), the photoconversion from the precursor to acenes proceeded similarly under Ar and air. Here we report the FET performance and device structures of **DTAnt** and **DHTAnt** prepared by the solution process of photoconvertible precursors (**1a** and **1b**, Fig. 1). The substituent effects on the photoprecursor methods will also be discussed, by comparing their FET performances with the charge carrier mobilities measured by the time resolved microwave conductivity (TRMC) method.

The synthesis of **1a** and the photoreactivity of **1a** to **DTAnt** in solution and film were reported previously.[13] The precursor (**1b**) was prepared as shown in Fig. S1 (ESI†). The compounds were characterized by ^{1}H- and ^{13}C-NMR and TOF-mass spectra. The diketone precursors were purified by crystallization before the measurement of the FET performance.

The precursors **1a** and **1b** were converted to **DTAnt** and **DHTAnt** in toluene as shown in Fig. 1. The quantum yields of the photoreactions of **1a** and **1b** were 0.32. To make sure there was successful photoconversion of the precursors to acenes in film, UV-vis absorption spectra before and after the photoirradiation of the spun-cast film of **1a** and **1b** were measured, as shown in Fig. 2. Compound **1a** showed the absorption peak at 470 nm (n–π* absorption) and the peak was red-shifted by 4 nm

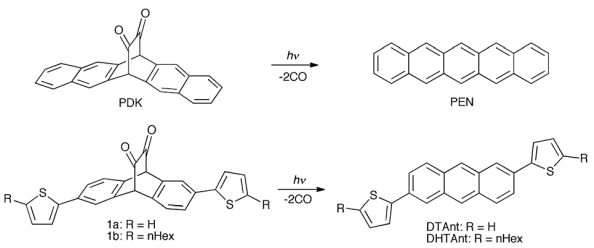

Fig. 1 Photoreaction of precursors to acenes.

[a] *Graduate School of Materials Science, Nara Institute of Science and Technology, Ikoma, 630-0192, Japan. E-mail: hyamada@ms.naist.jp; Fax: +81 743-724-6042*
[b] *CREST, JST, 7 Gobancho, Chiyoda-ku 102-0076, Japan*
[c] *Department of Organic Device Engineering, Graduate School of Science and Engineering, Yamagata University, Yonezawa 992-8510, Japan. E-mail: nakayama@yz.yamagata-u.ac.jp; Fax: +81 238-26-3713*
[d] *Department of Applied Chemistry, Graduate School of Engineering, Osaka University, 2-1, Yamadaoka, Suita, Osaka 565-0871, Japan. E-mail: seki@chem.eng.osaka-u.ac.jp; Fax: +81 6-6879-4586*
[e] *Department of Chemistry and Biology, Graduate School of Science and Engineering, Ehime University, Matsuyama, 790-8577, Japan*
† Electronic supplementary information (ESI) available: Synthetic details, time profiles of photoreaction, AFM image, XRD pattern, IR spectra, ionization potential, FET properties, FP-TRMC properties. See DOI: 10.1039/c2cc35439j

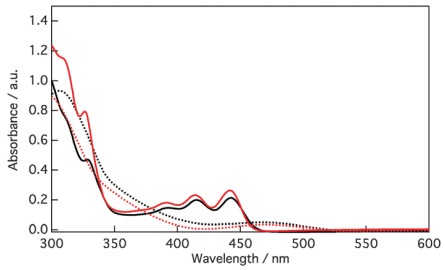

Fig. 2 UV-vis absorption spectra of spun-cast films of **1a** (dotted red line) and **1b** (dotted black line) and of **DTAnt** (solid red line) and **DHTAnt** (solid black line) after photoirradiation of the precursors for 1 h on the glass plates.

from that in toluene. After the photoirradiation for 1 h, the peak of the precursor disappeared and new peaks at 441, 414, and 391 nm corresponding to the anthracene moiety were observed. These peaks were red-shifted by 16–23 nm than those in toluene, due to the π–π interactions between chromophores in the film.

The absorbance of **1b** and **DHTAnt** showed similar phenomena to those of **1a** and **DTAnt**. The conversion of the precursors to acenes in films was also confirmed by IR measurement before and after the photoirradiation of spun-cast films of **1a** and **1b** on glass (Fig. S2, ESI†). The strong peak of C=O stretching observed at 1734 cm^{-1} for the precursor films disappeared after the photoirradiation to show the complete conversion from the precursors to acenes.

Ionization potentials for the **DTAnt** and **DHTAnt** films were obtained to be 5.24 eV for **DTAnt** and 5.01 eV for **DHTAnt** (Fig. S3, ESI†). Bottom-gate, top-contact FET devices were typically prepared as follows. The details of the procedure are given in the ESI.† The surfactant GR650 was spin-coated (20 nm) on the clean SiO_2 (300 nm)/n-doped Si substrate. The chloroform (including 1% trichlorobenzene) solutions of **1a** and **1b** (20 mg mL^{-1}) were spin-coated on the substrates for 60 s at 2000 rpm under an N_2 atmosphere in the dark. The spin-coated film is a solid state film during irradiation because the concentration of trichlorobenzene is only 1%. The substrate was irradiated at 300 mW cm^{-2} for 60 min, then gold source and drain electrodes were deposited (90 nm thickness, L = 50 μm, W = 5.5 mm). The results of the FET performance are shown in Fig. 3 and Fig. S4 (ESI†), and Table 1. The **DTAnt** film prepared from **1a** at rt showed the average μ_h of 0.014 $cm^2\ V^{-1}\ s^{-1}$ and an on/off ratio of 3.2×10^4. When the substrates were annealed at 60 and 80 °C on a hot plate during the photoirradiation, μ_h was improved to 0.029 (the best value was 0.035) and 0.038 (0.047) $cm^2\ V^{-1}\ s^{-1}$ at 60 and 80 °C, respectively, and is comparable with the best FET performance of the vacuum deposited film of **DTAnt** (0.063 $cm^2\ V^{-1}\ s^{-1}$). The **DHTAnt** film prepared from **1b** under similar conditions using $CHCl_3$ as a solvent (Fig. S4, ESI†) showed a μ_h value of 2.6×10^{-4} $cm^2\ V^{-1}\ s^{-1}$ and an on/off ratio of 2.9×10^4 upon annealing at 60 °C. When the annealing was performed at 80 °C, the film shrunk and the FET performance could not be observed. The best μ_h of the vacuum-deposited **DHTAnt** film was 0.50 $cm^2\ V^{-1}\ s^{-1}$, which was 10 times better than that of the vacuum-deposited **DTAnt** film. The results of the vacuum-deposited film showed a sharp contrast to the results of our spun-cast film.

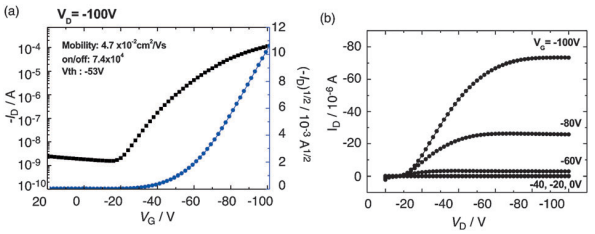

Fig. 3 (a) Transfer characteristics and (b) output characteristics of **DTAnt**-FET prepared by the photoprecursor method from **1a**. Solvent: 1% 1,2,4-trichlorobenzene–$CHCl_3$: irradiated by a high brightness LED area lamp at 300 mW cm^{-2} at 80 °C for 1 h. See the text for details.

Table 1 FET performances of **DTAnt** and **DHTAnt** prepared by the photoprecursor method

Compound	Annealing temp./°C	RMS[a]/ nm	Mobility[b]/ $cm^2\ V^{-1}\ s^{-1}$	On/off	V_{th}/ V
DTAnt	25	5.94	0.014(0.014)	3.2×10^5	−45
	60	11.0	0.035(0.029)	4.5×10^6	−41
	80	25.5	0.047(0.038)	7.4×10^4	−53
DHTAnt	25	1.16	4.1×10^{-5} (2.3×10^{-5})	6.4×10^2	−27
	60	7.94	2.6×10^{-4} (1.9×10^{-4})	2.9×10^4	−21
	80	—	—	—	—

[a] Root mean square granularity values measured by AFM images. [b] The best performance; the values in the brackets are the average performance.

Surface morphologies were observed by AFM for DTAnt and DHTAnt films annealed at 60 °C as shown in Fig. S5 (ESI†) with those of the vacuum deposited films (Fig. S6, ESI†). The Root Mean Square (RMS) granularity values of these films were 11.0 nm and 7.94 nm for **DTAnt** and **DHTAnt**, and grains of **DTAnt** were clearer compared to those of **DHTAnt**. The morphologies of the spun-cast films are similar to that of the vacuum deposited film of **DTAnt**, whereas considerably larger grains were observed for the vacuum deposited film of **DHTAnt**.

To clarify the crystallinity of the film, 2Θ scans of the X-ray diffraction (XRD) of **DTAnt** and **DHTAnt** films were measured in out-of-plane and in-plane modes (Fig. S7, ESI†). The **DTAnt** films showed higher-order diffraction peaks assigned to edge-on alignment to the substrate, which is suitable for FET devices. On the other hand, **DHTAnt** films indicated mixed diffraction patterns of edge-on and flat-on alignments. This is one of the reasons for the lower FET mobility of **DHTAnt**.

In order to confirm the intrinsic carrier mobilities within the **DTAnt** and **DHTAnt** films prepared by the photoconversion of the precursors, flash-photolysis time resolved microwave conductivity (FP-TRMC) measurements, informative of the charge carrier motion in a short distance (<10 nm), were performed for the films of **DTAn** and **DHTAnt**. For comparison, the carrier mobilities of the diketone precursor films (**1a** and **1b**) were also determined (Table 2 and Fig. S7, ESI†). The film of **DTAnt** and **DHTAnt** showed reproducible conductivity transients ($\phi\Sigma\mu$) with maximum values of 2.4×10^{-4} and 1.1×10^{-3} $cm^2\ V^{-1}\ s^{-1}$, respectively, upon excitation with incident laser pulses at 355 nm, and subsequent decays are observed. The observed TRMC signals indicate the generation of mobile charge carriers upon photoexcitation followed by their

Table 2 The charge carrier mobility of acenes and their diketone precursors

	FET mobility/cm^2 V^{-1} s^{-1}		FP-TRMC		
Compounds	Photoprecursor method	Vacuum deposition	$\phi\Sigma\mu/\times 10^{-4}$ cm^2 V^{-1} s^{-1}	$\phi_{max}/\times 10^{-4}$	$\Sigma\mu$/cm^2 V^{-1} s^{-1}
DTAnt	0.038 (0.047)	0.063[12]	2.4	2.6	0.9
1a	—	—	0.43	6.9	0.06
DHTAnt	2.6×10^{-4}	0.50[12]	11	13	0.8
1b	—	—	0.62	23	2×10^{-3}

extinction through trapping and/or recombination events. The photo-carrier generation yields (ϕ) in the thin film of **DTAnt** and **DHTAnt** were determined to be 2.6×10^{-4} and 1.3×10^{-3} by a photo-current integration method. Thus, isotropic charge carrier mobilities ($\Sigma\mu$) were determined to be 0.9 and 0.8 cm^2 V^{-1} s^{-1}, respectively. The $\Sigma\mu$ values of diketone precursors **1a** and **1b** were 0.06 and 2×10^{-3} cm^2 V^{-1} s^{-1}, respectively, which were considerably small. The vacuum deposited films of **DTAnt** and **DHTAnt** showed comparable data to the spun-cast films (Fig. S8, ESI†) with similar kinetic traces of conductivity transients. Based on the observed mobility values of 0.9 and 0.8 cm^2 V^{-1} s^{-1}, the deduced size of the local dislocation of charge carriers is smaller than a few nm,[14] and this strongly suggests that the intra-grain motion of charge carriers is probed predominantly by the TRMC measurement.

The aromatic structures of **DTAnt** and **DHTAnt** are the same and their charge carrier mobilities obtained by FP-TRMC measurements revealed enough high potentials for semiconducting films. The FET performances of **DTAnt** obtained by our photoprecursor method were comparable with that of the vacuum-deposited film, but the hole mobility of **DHTAnt**-FET was much lower than that prepared by vacuum-deposition. These results coincide with the results of XRD patterns; **DTAnt** molecules gave edge-on alignment and **DHTAnt** gave a mixture of edge-on and face-on alignments. Such a difference might be due to the alkyl substituents of **DHTAnt**, disturbing the rearrangement and stacking of the molecules during the photoconversion from the precursor film to the **DHTAnt** film.

The **DTAnt** and **DHTAnt** FET devices were prepared by the spin coating of the diketone precursors, followed by photo-irradiation to convert the precursor films to acene films.

DTAnt showed 0.047 cm^2 V^{-1} s^{-1} hole mobility, comparable with that of the vacuum-deposited film. The **DHTAnt** film did not show the best performance by a solution process, although UV-visible absorption and IR spectra after photo-irradiation showed that photoconversion occurred successfully. Considering the similar intrinsic potential of these materials and the different XRD patterns and AFM images between these materials, the photoconversion method is suitable for the molecules with high crystalline compounds without longer substituents.

The authors thank Ms Mika Yamamura and Ms Yuriko Nishikawa for the measurement of ESI MS. This work was partly supported by Grants-in-Aid (No. 22350083 to H.Y. and K.N.) and the Green Photonics Project in NAIST sponsored by the Ministry of Education, Culture, Sports, Science and Technology, MEXT, Japan.

Notes and references

1 J. E. Anthony, *Angew. Chem., Int. Ed.*, 2008, **47**, 452–483.
2 M. Mas-Torrent and C. Rovira, *Chem. Soc. Rev.*, 2008, **37**, 827–838.
3 A. R. Murphy and J. M. J. Fréchet, *Chem. Rev.*, 2007, **107**, 1066–1096.
4 (*a*) D. Zander, N. Hoffmann, K. Lmimouni, S. Lenfant, C. Petit and D. Vuillaume, *Microelectron. Eng.*, 2005, **80**, 394–397; (*b*) A. Afzali, C. R. Kagan and G. P. Traub, *Synth. Met.*, 2005, **155**, 490–494; (*c*) A. Afzali, C. D. Dimitrakopoulos and T. L. Breen, *J. Am. Chem. Soc.*, 2002, **124**, 8812–8813; (*d*) A. R. Brown, A. Pomp, D. M. de Leeuw, D. B. M. Klaassen, E. E. Havinga, P. Herwig and K. Müllen, *J. Appl. Phys.*, 1996, **79**, 2136–2138; (*e*) P. T. Herwig and K. Müllen, *Adv. Mater.*, 1999, **11**, 480–483; (*f*) M. J. Joung, J. H. Ahn, S. Y. Kang, K. H. Baek, S. D. Ahn, L. M. Do, C. A. Kim, G. H. Kim, I. K. You, S. M. Yoon and K. S. Suh, *Bull. Korean Chem. Soc.*, 2003, **24**, 1862–1864; (*g*) N. Vets, M. Smet and W. Dehaen, *Tetrahedron Lett.*, 2004, **45**, 7287–7289; (*h*) K.-Y. Chen, H.-H. Hsieh, C.-C. Wu, J.-J. Hwang and T. J. Chow, *Chem. Commun.*, 2007, 1065–1067; (*i*) M. Watanabe, Y. J. Chang, S.-W. Liu, T.-H. Chao, K. Goto, M. M. Islam, C.-H. Yuan, Y.-T. Tao, T. Shinmyozu and T. J. Chow, *Nat. Chem.*, 2012, **4**, 574–578.
5 (*a*) A. Hirao, T. Akiyama, T. Okujima, H. Yamada, H. Uno, Y. Sakai, S. Aramaki and N. Ono, *Chem. Commun.*, 2008, 4714–4716; (*b*) T. Akiyama, A. Hirao, T. Okujima, H. Yamada, H. Uno and N. Ono, *Heterocycles*, 2007, **74**, 835–842.
6 (*a*) S. Ito, T. Murashima, H. Uno and N. Ono, *Chem. Commun.*, 1998, 1661–1662; (*b*) S. Aramaki, Y. Sakai and N. Ono, *Appl. Phys. Lett.*, 2004, **84**, 2085–2087; (*c*) T. Okujima, Y. Hashimoto, G. Jin, H. Yamada, H. Uno and N. Ono, *Tetrahedron*, 2008, **64**, 2405–2411.
7 (*a*) A. R. Murphy, J. M. J. Fréchet, P. Chang, J. Lee and V. Subramanian, *J. Am. Chem. Soc.*, 2004, **126**, 1596–1597; (*b*) A. R. Murphy, P. C. Chang, P. VanDyke, J. Liu, J. M. J. Fréchet, V. Subramanian, D. M. DeLongchamp, S. Sambasivan, D. A. Fischer and E. K. Lin, *Chem. Mater.*, 2005, **17**, 6033–6041; (*c*) D. M. DeLongchamp, S. Sambasivan, D. A. Fischer, E. K. Lin, P. Chang, A. R. Murphy, J. M. J. Fréchet and V. Subramanian, *Adv. Mater.*, 2005, **17**, 2340–2344.
8 H. Yamada, T. Okujima and N. Ono, *Chem. Commun.*, 2008, 2957–2974.
9 (*a*) H. Uno, Y. Yamashita, M. Kikuchi, H. Watanabe, H. Yamada, T. Okujima, T. Ogawa and N. Ono, *Tetrahedron Lett.*, 2005, **46**, 1981–1983; (*b*) H. Yamada, Y. Yamashita, M. Kikuchi, H. Watanabe, T. Okujima, H. Uno, T. Ogawa, K. Ohara and N. Ono, *Chem.–Eur. J.*, 2005, **11**, 6212–6220; (*c*) A. Masumoto, Y. Yamashita, S. Go, T. Kikuchi, H. Yamada, T. Okujima, N. Ono and H. Uno, *Jpn. J. Appl. Phys.*, 2009, **48**, 051505; (*d*) T. Aotake, S. Ikeda, D. Kuzuhara, S. Mori, T. Okujima, H. Uno and H. Yamada, *Eur. J. Org. Chem.*, 2012, 1723–1729.
10 T.-H. Chuang, H.-H. Hsieh, C.-K. Chen, C.-C. Wu, C.-C. Lin, P.-T. Chou, T.-H. Chao and T. J. Chow, *Org. Lett.*, 2008, **10**, 2869–2872.
11 K. Nakayama, Y. Oikawa, C. Ohashi, J. Kido and H. Yamada, *MRS Fall Meeting*, Hynes Conbention Center, Boston, 2011.
12 H. Meng, F. Sun, M. B. Goldfinger, G. D. Jaycox, Z. Li, W. J. Marshall and G. S. Blackman, *J. Am. Chem. Soc.*, 2005, **127**, 2406–2407.
13 H. Yamada, E. Kawamura, S. Sakamoto, Y. Yamashita, T. Okujima, H. Uno and N. Ono, *Tetrahedron Lett.*, 2006, **47**, 7501–7504.
14 A. Saeki, Y. Koizumi, T. Aida and S. Seki, *Acc. Chem. Res.*, 2012, **45**, 1193–1202.

ChemComm

RSC Publishing

COMMUNICATION

View Article Online
View Journal | View Issue

In situ preparation of highly fluorescent pyrene-dyes from non-luminous precursors upon photoirradiation†

Cite this: *Chem. Commun.*, 2013, **49**, 3661

Received 31st January 2013,
Accepted 14th March 2013

DOI: 10.1039/c3cc40827b

www.rsc.org/chemcomm

Tatsuya Aotake,[a] Hiroshi Tanimoto,[b] Hidekatsu Hotta,[b] Daiki Kuzuhara,[a] Tetsuo Okujima,[b] Hidemitsu Uno[b] and Hiroko Yamada*[ac]

The non-luminous precursor, 2-(1-pyrenyl)-9,10-dihydro-9,10-ethanoanthracene-11,12-dione, was photochemically converted to highly-fluorescent 2-(1-pyrenyl)anthracene quantitatively in solution and in the PMMA film and the fluorescence quantum yield of the acene in benzonitrile was as high as 0.99.

Fluorescent molecular probes are of great interest due to their versatile applications in chemical, environmental and biological science. Fluorescence is one of the most promising tools for the detection of small amounts of molecules, since fluorescence can even be detected in only one molecule and is applied in various areas such as microanalysis,[1] bioimaging[2] and memory media.[3] Recently an efficient conversion of non-luminous molecules to highly-fluorescent molecules by external stimuli like heat or light has received attention due to their potential for application in optical memory media, fluorescence imaging and super-resolution fluorescence imaging.[4–10] In this context, one-way conversion would be desirable for read-only memory and single-molecule microscopy.

Pyrene is a versatile blue-fluorophore with high fluorescence quantum yields. Aryl-pyrene compounds are one of the highly fluorescent materials,[11] but unfortunately their solubility in common organic solvents is quite low and their purification is difficult. In this regard a photochemical quantitative conversion of 9,10-dihydro-9,10-ethanoanthracene-11,12-dione (**DK**) to anthracene (**Ant**) is a useful one-way reaction in solution or in film (Scheme 1).[12] This reaction has recently been applied to the photochemical synthesis of pentacene[13] and its relatives for the fabrication of FET devices by a solution process,[14] and for the protecting groups, to prepare air-unstable substituted pentacenes[15] and larger acenes.[16] Furthermore we found that the diketone moieties can work as an intramolecular quencher of the fluorophore for the substituted tetracene compounds, resulting in the *in situ* photochemical conversion of a non-fluorescent precursor to a fluorescent compound.[17,18] In connection with these results, this photoconversion will be ideal for the synthesis of highly pure and highly fluorescent aryl-pyrene compounds from soluble and non-luminous precursors. We report here an *in situ* quantitative preparation of highly blue-fluorescent pyrene–anthracene dyes (**PyAnt** and **Py-3-Ant**) from non-luminous α-diketone precursors (**PyDK** and **Py-3-DK**) upon photoirradiation in solution and in film (Scheme 1).

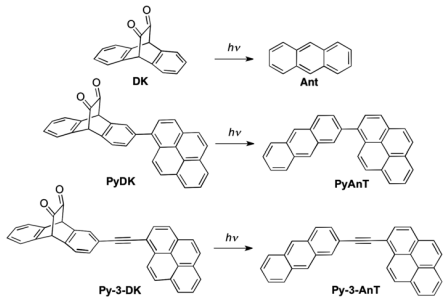

Scheme 1 Photoconversion from α-diketone to pyrenylanthracenes.

PyAnt can be prepared by Suzuki–Miyaura coupling of 2-bromoanthracene (**1**) and pyreneboronic acid, however the yield is only 3% due to its low solubility. **Py-3-Ant** can also be prepared by Sonogashira coupling from **1** and 1-ethynylpyrene in 12% yield, but the purification using silica gel column chromatography was difficult because of its low solubility and close R_f values with byproducts. To solve the solubility problem, the precursors **PyDK** and **Py-3-DK** were prepared as shown in Scheme 2. 2-Bromoanthracene **1** was reacted with vinylene carbonate by the Diels–Alder reaction to give adduct **2** in 76% yield. This compound **2** was coupled with pyreneboronic acid by Suzuki–Miyaura coupling to give adduct **3a** in 51% yield. The obtained adduct **3a** was hydrolyzed to give diol compound **4a** in 74% yield, followed by Swern oxidation to give **PyDK** in 14% yield. **Py-3-DK** was also prepared using 2-ethynylpyrene as shown in Scheme 2.

The UV-vis absorption and fluorescence spectra of **PyAnt** and **PyDK** in toluene are shown in Fig. 1. **PyAnt** has an absorption

[a] *Graduate School of Materials Science, Nara Institute of Science and Technology, Ikoma 630-0192, Japan. E-mail: hyamada@ms.naist.jp*
[b] *Department of Chemistry and Biology, Graduate School of Science and Engineering, Ehime University, Matsuyama 790-8577, Japan*
[c] *CREST, JST, Chiyoda-ku 102-0076, Japan*

† Electronic supplementary information (ESI) available. See DOI: 10.1039/c3cc40827b

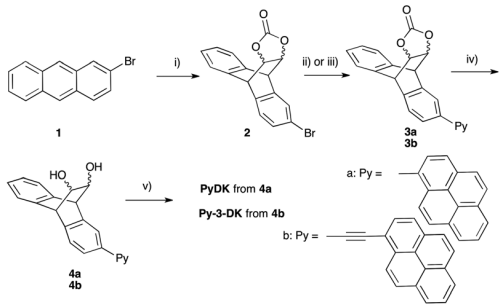

Reagents and conditions: (i) vinylene carbonate, xylene, autoclave, 180 °C, 3 d, 76%; (ii) for **3a**, pyreneboronic acid, $Pd(PPh_3)_4$, Na_2CO_3, 1,4-dioxane, reflux, 18 h, 51%; (iii) for **3b,** 2-ethynylpyrene, CuI, Et_3N, $Pd(PPh_3)_4$, toluene, reflux, 18 h, 34%; (iv) K_2CO_3, THF, methanol, H_2O, rt, overnight, 74% for **4a** and 61% for **4b**; (v) TFAA, dry-DMSO, *N*,*N*-(iso-pro)$_2$EtN, dry-CH_2Cl_2, 1.5 h, 14% for **PyDK** and 60% for **Py-3-DK**.

Scheme 2 Syntheses of **PyDK** and **Py-3-DK**.

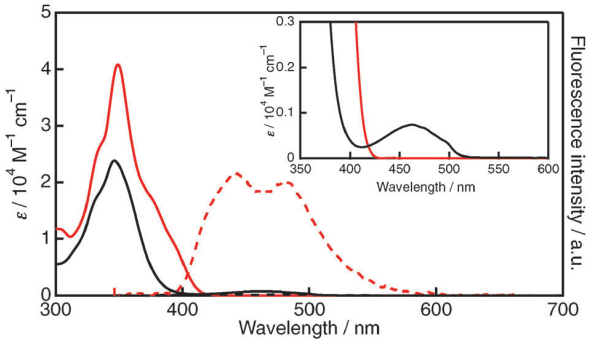

Fig. 1 The absorption (solid lines) and fluorescence (dashed lines) spectra of **PyDK** (black) and **PyAnt** (red) in toluene; excited at 380 nm.

peak at 349 nm ($\varepsilon = 4.50 \times 10^4$ M^{-1} cm^{-1}) with shoulders at both sides in toluene. The emission peaks were observed at 443 and 478 nm with the fluorescence quantum yield (Φ_f) of 0.86 in toluene. The fluorescence peak (443 nm) of **PyAnt** showed a red-shift of 68 nm from the parent pyrene due to the through-bond interaction between pyrene and anthracene moieties. The absorption spectra were similar in toluene, CH_2Cl_2, benzonitrile, and DMSO, but the fluorescence of **PyAnt** showed solvatochromic shifts as shown in Table 1 and ESI,† Fig. S1. The fluorescence peaks (λ_{em}) exhibited bathochromic shifts upon increasing the polarity of the solvents: λ_{em} = 443 nm (Φ_f = 0.86) in toluene, 486 nm (0.92) in CH_2Cl_2, 486 nm (0.99) in PhCN, and 496 nm (0.91) in DMSO. These results correspond well with the known superposition of a nonpolar locally excited (LE) and a strongly polar charge transfer (CT) contribution of substituted pyrene compounds.[11] The fluorescence lifetimes (τ_f) were also measured (Table 1 and ESI,† Fig. S2). Since the rotary motion around the C–C linkage between pyrene and anthracene is possible, **PyAnt** showed bi-exponential decays in CH_2Cl_2, PhCN, and DMSO.

PyDK has the absorption peak of the pyrene moiety at 348 nm ($\varepsilon = 2.71 \times 10^4$ M^{-1} cm^{-1}) in toluene and the absorption of the diketone moiety at 461 nm ($\varepsilon = 7.40 \times 10^2$ M^{-1} cm^{-1}). The absorption at 461 nm is similar to the absorption of non-substituted **DK** (ESI,† Fig. S3) but absorption of **PyDK** at 461 nm is slightly larger than that of **DK** due to the overlap of CT-like absorption from the pyrene moiety to the carbonyl moiety, as predicted by TD-DFT calculations (ESI,† Fig. S4). **PyDK** was non-fluorescent with excitation at 380 and 460 nm due to the quenching of the excited state of pyrene by the diketone moiety (Fig. 1 and ESI,† Fig. S5).

A similar tendency was observed for **Py-3-Ant** and **Py-3-DK**. The UV-vis absorption spectrum of **Py-3-Ant** showed four peaks at 308, 365, 393 and 418 nm in toluene (ESI,† Fig. S3 and S6). Due to the triple bonds between pyrene and anthracene moieties, the π-conjugation of **Py-3-Ant** expanded more than that of **PyAnt**, which resulted in a red-shift of the absorption spectra. Fluorescence spectra of **Py-3-Ant** also showed the solvent effects: λ_{em} = 426, 450 and 482 nm in toluene (Φ_f = 0.90); 485 nm in CH_2Cl_2 (0.92); 488 nm (0.94) in PhCN: 497 nm (0.95) in DMSO. The fluorescence lifetimes (τ_f) were also measured (Table 1 and ESI,† Fig. S7). **Py-3-Ant** showed single-exponential decays due to the rigid linkage with a triple bond.

To investigate the photocleavage reaction of **PyDK**, the photoconversion was monitored using ^{1}H NMR spectroscopy under an argon atmosphere (ESI,† Fig. S8). **PyDK** was placed in degassed $CDCl_3$ and irradiated at 470 nm with a xenon light source through a monochromater (14.9 mW cm^{-2}). During the photoconversion, the singlet peaks at 5.1 and 5.2 ppm due to bridge-head protons of **PyDK** gradually decreased while peaks of peri-positions of **PyAnt** increased at 8.5 ppm. After 25 min the photoconversion completed without giving any by-products. The ^{1}H NMR spectrum at 25 min was identical to the spectrum of **PyAnt**, directly prepared by Suzuki–Miyaura coupling of **1** and pyreneboronic acid. The photoreaction of **Py-3-DK** to **Py-3-Ant** also proceeded successfully (ESI,† Fig. S8).

Table 1 Absorption and fluorescence peaks (λ_{abs} and λ_{flu}), fluorescence quantum yields (Φ_f), and fluorescence lifetimes (τ_f) of **PyAnt** and **Py-3-Ant** in various solvents[a]

Compounds	Solvents	ε^a	λ_{abs}/nm	$\lambda_{flu}{}^a$/nm	$\Phi_f{}^b$	$\tau_f{}^c$/ns (A)	χ^2
PyAnt	Toluene	2.38	349	443, 478	0.86	4.22	1.64
	CH_2Cl_2	8.93	348	486	0.92	4.26 (0.46) 6.71 (0.54)	1.33
	PhCN	25.2	352	486	0.99	4.79 (0.85) 8.78 (0.15)	1.39
	DMSO	46.5	351	496	0.91	4.47 (0.61) 7.69 (0.39)	1.11
Py-3-Ant	Toluene	2.38	308, 365, 393, 418	426, 450, 482	0.90	1.98 (0.99) 6.74 (0.01)	1.68
	CH_2Cl_2	8.93	306, 364, 391, 416	485	0.92	2.85	1.52
	PhCN	25.2	310, 366, 397, 420	488	0.94	2.96	1.14
	DMSO	46.5	308, 367, 397, 421	497	0.95	3.56 (0.92) 5.59 (0.08)	1.40

[a] Dielectric constant. [b] λ_{flu} and Φ_f were measured by excitation at 380 nm. [c] τ_f was measured by excitation at 366 nm.

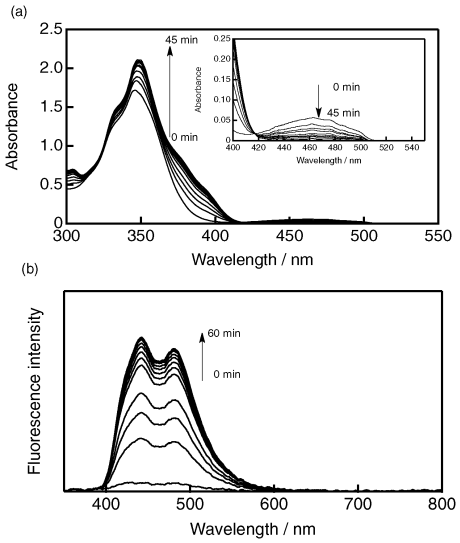

Fig. 2 The change in (a) absorption spectra (5.6×10^{-5} M) and (b) fluorescence spectra (4.4×10^{-5} M) during photolysis (λ_{ex} = 370 nm) of **PyDK** in toluene.

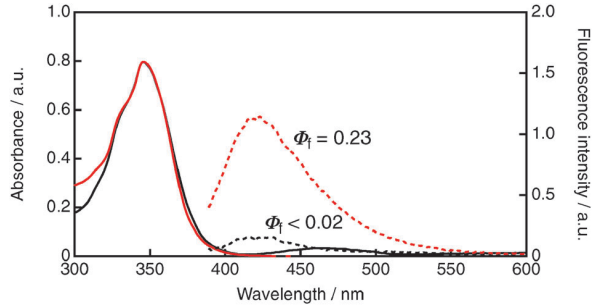

Fig. 3 Absorption and emission spectra of **PyDK** (black) and **PyAnt** (red) in the PMMA film; excited at 380 nm.

The change in UV-vis absorption spectra during the photolysis of **PyDK** was monitored. When **PyDK** was irradiated at 468 nm (1.86 mW cm^{-2}), decarbonylation occurred giving the corresponding **PyAnt** (ESI,† Fig. S9). The relative quantum yield of the photoconversion reaction of **PyDK** excited at 468 nm was 0.29, compared to the absolute quantum yield of **DK** (0.37). The photoreactions of **PyDK** were also performed by excitation at π–π* absorption of pyrene moieties (370 nm, $<$0.88 mW cm^{-2}), monitored by the spectral change of the absorption and fluorescence in toluene (Fig. 2). During the irradiation, the blue fluorescence increased, since **PyDK** was not fluorescent while **PyAnt** was strongly fluorescent. The same phenomenon was also observed for **Py-3-DK** and **Py-3-Ant** and the relative quantum yield of the photoconversion reaction of **Py-3-DK** was 0.27 (ESI,† Fig. S9 and S10).

Finally we have performed the photoconversion of **PyDK** and **Pt-3-DK** in the PMMA film, as shown in Fig. 3 and ESI,† Fig. S11. After photoirradiation over >390 nm for 10 min, the Φ_f of **Py-Ant** was increased to 0.23. For the **PyDK** film fluorescence was also observed around 420 nm with Φ_f less than 0.02, which belonged to **Py-Ant** generated during the measurement. This result indicates that **PyDK** in film is highly sensitive to the light and the photoconversion from **PyDK** to **Py-Ant** occurred during the measurement. The Φ_f of the PMMA film of **Py-3-Ant** prepared by this photoconversion was 0.11.

We have succeeded in preparing **PyDK** and **Py-3-DK** as latent fluorophores which can be effectively converted to highly blue-fluorescent **PyAnt** and **Py-3-Ant** by photoirradiation in solution and in film. The one-way convertible precursors of highly-fluorescent fluorophores will be promising for various applications in the areas of microanalysis and memory media.

The authors thank Ms Mika Yamamura and Ms Yuriko Nishiyama for the measurement of mass spectra and Mr Yasuo Okajima for the fluorescence lifetimes measurement. The authors also thank Mr Leigh McDowell for checking the English in the manuscript. This work was partly supported by Grants-in-Aid (No. 22350083 to H.Y.) and the Green Photonics Project in NAIST sponsored by the Ministry of Education, Culture, Sports, Science and Technology, MEXT, Japan.

Notes and references

1 W. E. Moerner, *J. Phys. Chem. B*, 2002, **106**, 910–927.
2 M. Vendrell, D. Zhai, J. C. Er and Y.-T. Chang, *Chem. Rev.*, 2012, **112**, 4391–4420.
3 S. Kawata and Y. Kawata, *Chem. Rev.*, 2000, **100**, 1777–1788.
4 M. Irie, T. Fukaminato, T. Sasaki, N. Tamai and T. Kawai, *Nature*, 2002, **420**, 759–760.
5 P. Dedecker, J. Hotta, C. Flors, M. Sliwa, H. Uji-i, M. B. J. Roeffaers, R. Ando, H. Mizuno, A. Miyawaki and J. Hofkens, *J. Am. Chem. Soc.*, 2007, **129**, 16132–16141.
6 S. W. Hell, *Science*, 2007, **316**, 1153–1158.
7 V. N. Belov, C. A. Wurm, V. P. Boyarskiy, S. Jakobs and S. W. Hell, *Angew. Chem., Int. Ed.*, 2010, **49**, 3520–3523.
8 E. Betzig, G. H. Patterson, R. Sougrat, O. W. Lindwasser, S. Olenych, J. S. Bonifacino, M. W. Davidson, J. Lippincott-Schwartz and H. F. Hess, *Science*, 2006, **313**, 1642–1645.
9 S. T. Hess, T. P. K. Girirajan and M. D. Mason, *Biophys. J.*, 2006, **91**, 4258–4272.
10 M. J. Rust, M. Bates and X. Zhuang, *Nat. Methods*, 2006, **3**, 793–796.
11 W. Weigel, W. Rettig, M. Dekhtyar, C. Modrakowski, M. Beinhoff and A. D. Schlüter, *J. Phys. Chem. A*, 2003, **107**, 5941–5947; S.-W. Yang, A. Elangovan, K.-C. Hwang and T.-I. Ho, *J. Phys. Chem. B*, 2005, **109**, 16628–16635; M. Baumgarten, L. Gherghel, J. Friedrich, M. Jurczok and W. Rettig, *J. Phys. Chem. A*, 2000, **104**, 1130–1140.
12 J. Strating, B. Zwanenburg, A. Wagenaar and A. C. Udding, *Tetrahedron Lett.*, 1969, **10**, 125–128.
13 H. Uno, Y. Yamashita, M. Kikuchi, H. Watanabe, H. Yamada, T. Okujima, T. Ogawa and N. Ono, *Tetrahedron Lett.*, 2005, **46**, 1981–1983; H. Yamada, Y. Yamashita, M. Kikuchi, H. Watanabe, T. Okujima, H. Uno, T. Ogawa, K. Ohara and N. Ono, *Chem.–Eur. J.*, 2005, **11**, 6212–6220; T. Aotake, S. Ikeda, D. Kuzuhara, S. Mori, T. Okujima, H. Uno and H. Yamada, *Eur. J. Org. Chem.*, 2012, 1723–1729.
14 A. Masumoto, Y. Yamashita, S. Go, T. Kikuchi, H. Yamada, T. Okujima, N. Ono and H. Uno, *Jpn. J. Appl. Phys.*, 2009, **48**, 051505; H. Yamada, C. Ohashi, T. Aotake, S. Katsuta, Y. Honsho, H. Kawano, T. Okujima, H. Uno, N. Ono, S. Seki and K. Nakayama, *Chem. Commun.*, 2012, **48**, 11136–11138.
15 Y. Zhao, R. Mondal and D. C. Neckers, *J. Org. Chem.*, 2008, **73**, 5506–5513; S. Katsuta, H. Yamada, T. Okujima and H. Uno, *Tetrahedron Lett.*, 2010, **51**, 1397–1400.
16 R. Mondal, C. Tönshoff, D. Khon, D. C. Neckers and H. F. Bettinger, *J. Am. Chem. Soc.*, 2009, **131**, 14281–14289; R. Mondal, R. M. Adhikari, B. K. Shah and D. C. Neckers, *Org. Lett.*, 2007, **9**, 2505–2508; C. Tönshoff and H. F. Bettinger, *Angew. Chem., Int. Ed.*, 2010, **49**, 4125–4128.
17 T. Aotake, Y. Yamashita, T. Okujima, N. Shirasawa, Y. Jo, S. Fujimori, H. Uno, N. Ono and H. Yamada, *Tetrahedron Lett.*, 2013, DOI: 10.1016/j.tetlet.2013.01.014.
18 H. Yamada, D. Kuzuhara, K. Ohkubo, T. Takahashi, T. Okujima, H. Uno, N. Ono and S. Fukuzumi, *J. Mater. Chem.*, 2010, **20**, 3011–3024.

Tetrahedron Letters 54 (2013) 1790–1793

Contents lists available at SciVerse ScienceDirect

Tetrahedron Letters

journal homepage: www.elsevier.com/locate/tetlet

Photochemical synthesis of naphthacene and its derivatives for irreversible photo-responsive fluorescent molecules

Tatsuya Aotake [a], Yuko Yamashita [b], Tetsuo Okujima [b], Nobuhiko Shirasawa [c], Yukari Jo [c], Shigeo Fujimori [c], Hidemitsu Uno [b], Noboru Ono [b], Hiroko Yamada [a,d,*]

[a] Graduate School of Materials Science, Nara Institute of Science and Technology, Ikoma 630-0192, Japan
[b] Department of Chemistry and Biology, Graduate School of Science and Engineering, Ehime University, Matsuyama 790-8577, Japan
[c] Electronic and Imaging Materials Research Laboratories, Toray Industries, Inc., 3-2-1 Sonoyama, Ohtsu 520-0842, Japan
[d] CREST, JST, Chiyoda-ku 102-0075, Japan

ARTICLE INFO

Article history:
Received 20 November 2012
Revised 28 December 2012
Accepted 7 January 2013
Available online 12 January 2013

Keywords:
Naphthacene
Photoconversion
Fluorescent
Photoprecursor

ABSTRACT

Highly fluorescent naphthacene derivatives and their photoconvertible precursors were synthesized for irreversibly photo-responsive fluorescent molecules. The fluorescence quantum yields (Φ_f) of the precursors were less than 0.02, and the precursors can be converted to the highly fluorescent naphthacene derivatives (Φ_f = 0.67–0.70) quantitatively by photo-irradiation.

Organic semiconducting molecules are very attractive for new device materials such as organic light emitting diodes (OLEDs), organic field-effect transistors (OFETs), and organic photovoltaic cells (OPVCs). Acenes and their derivatives are classic fluorescent materials and can be used to fabricate OLEDs.[1] In this context aryl-substituted acenes have been reported to improve the fluorescence quantum yields effectively.[2] In many cases, however, these acenes are insoluble in common organic solvents due to their high crystallinity. To solve such problems, the soluble precursors with thermally or photochemically removable leaving groups have been synthesized.[3–5] The photochemical conversion of an α-diketone precursor into anthracene with the production of two CO molecules has been known for a long time.[6] This reaction has recently been applied to the photochemical synthesis of pentacene and larger acences,[7,8] which had been difficult to synthesize due to their air-instability and low solubility in common organic solvents. The methodology was also applied to the solution process to make OFET devices without using vacuum deposition.[9]

Now we found this reaction is useful for the synthesis of highly fluorescent materials in situ from non-fluorescent compounds upon photoirradiation. Some photochromic molecules have been proposed for photo-responsive fluorescent molecules.[10,11] However, in many cases these photochromic molecules undergo thermally or photochemically reversible reactions. As a result, the reacted molecules could be returned to the starting compounds. For the application of bioimaging and read-only memories, an irreversible system is desirable. Herein we report the synthesis and spectroscopic properties of highly fluorescent naphthacene derivatives, **1b** and **1c** (Scheme 1), and their quantitative photochemical generation from their non-fluorescent α-diketone precursors (**2b**, and **2c**), proposing irreversibly photo-responsive fluorescent molecules.

The synthesis of the substituted naphthacenes **1b** and **1c** is shown in Scheme 2. 1,1′-Biphenyl-4-yllithium, which was prepared from 4-phenyl-bromobenzenene and *n*-BuLi, was reacted

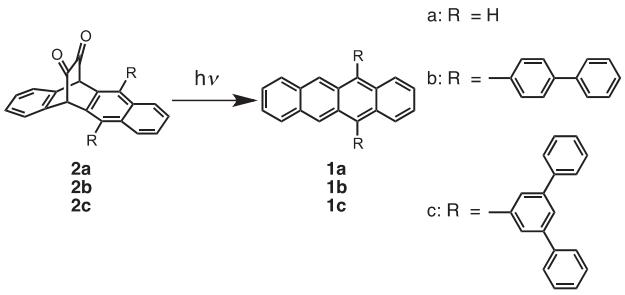

Scheme 1. Photochemical conversions of naphthacenediketones.

* Corresponding author. Tel.: +81 743 72 6041; fax: +81 743 72 6042.
E-mail address: hyamada@ms.naist.jp (H. Yamada).

0040-4039/$ - see front matter © 2013 Elsevier Ltd. All rights reserved.
http://dx.doi.org/10.1016/j.tetlet.2013.01.014

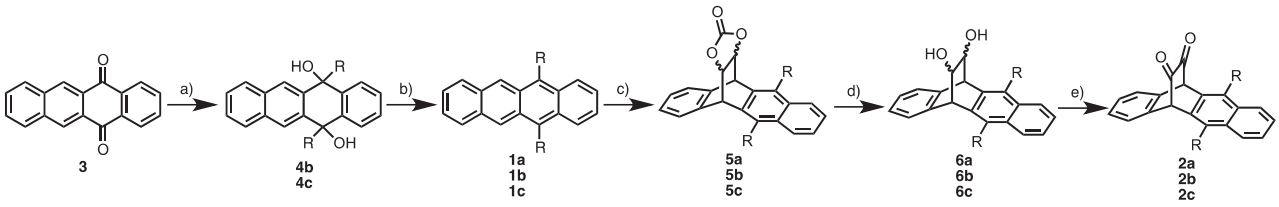

Scheme 2. Reagents and conditions: (a) 1,1′-biphenyl-4-yllithium for **4b** and 3,5-diphenylphenyllithium for **4c**, dry-toluene, dry-Et_2O, −45 °C, 5 h; **4b**: 52%; **4c**: 29%; (b) $SnCl_2$, concd HCl, reflux, 2 h; **1b**: 95%; **1c**: 87%; (c) vinylene carbonate, xylene, in autoclave, 180 °C, 3 days; **5a**: 95%; **5b**: 92%; **5c**: 78%; (d) 4 M NaOH aq, 1,4-dioxane, reflux, 2 h; **6a**: 95%; **6b**: 83%; **6c**: 72%; (e) dry-DMSO, TFAA, DIPEA, dry-CH_2Cl_2, −60 °C, 1.5 h; **2a**: 69%; **2b**: 85%; **2c**; 82%.

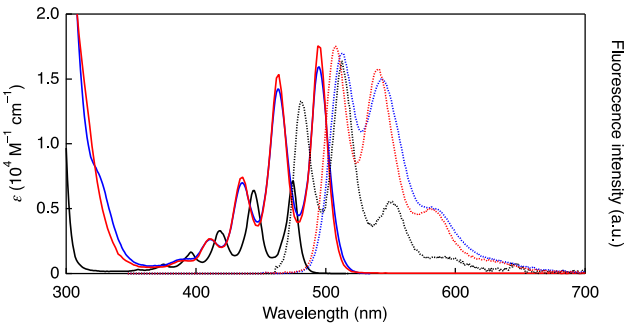

Figure 1. Absorption spectra (solid lines) and fluorescence spectra (dotted lines) of **1a** (black), **1b** (blue), and **1c** (red) in toluene.

with 5,12-naphthacenequinone (**3**) to afford **4b** in 52% yield. The compound **4b** was reacted with $SnCl_2$ and concd HCl in refluxing THF to give naphthacene **1b** in 95% yield. Similarly **4c** was prepared by the reaction of **3** and 3,5-diphenylphenyllithium, which was prepared from 1-iodo-3,5-diphenylbenzene,[12,13] in 29% yield, and then converted to **1c** in 87% yield. The synthesis of α-diketone precursors **2a**–**c** is also shown in Scheme 2. The Diels–Alder reaction of naphthacenes **1a**–**c** with vinylene carbonate quantitatively gave **5a**–**c**, respectively. Their hydrolysis followed by Swern oxidation gave α-diketone compounds **2a**–**c**. The solubility of **1a**, **1b**, and **1c** in toluene were 0.15, 0.81, and 5.2 mg/mL, respectively, and the solubility of the precursors **2a**, **2b**, and **2c** were much improved to 17, 15, and >23 mg/mL, respectively.

Absorption and fluorescence spectra of naphthacenes **1a**–**c** in toluene are summarized in Figure 1 and Table 1. The absorption maxima of **1b** and **1c** in toluene were red-shifted by 20 nm in comparison with those of **1a**. Fluorescence peaks of **1b** (511 nm) and **1c** (506 nm) are red-shifted by 30 and 25 nm from that of **1a** (481 nm). The Stokes shifts of **1a**–**c** are 6, 16, and 12 nm, respectively, as shown in Table 1. The absolute fluorescence quantum yields of naphthacenes were 0.67 for **1b** and 0.70 for **1c**, which are more than 5 times larger than that of **1a** (Φ_f = 0.12). The fluorescence lifetimes (τ_f) of **1b** and **1c** were 9.4 and 9.6 ns, respectively, and are 2.5 times longer than that of **1a** (τ_f = 3.9 ns) (Fig. S1). These phenomena are similar to the relationship between naphthacene (**1a**), 5,12-diphenylnaphthacene, and 5,6,11,12-tetraphenylnaphthacene (ruburene). The Φ_f's of **1a**, diphenylnaphthacene and ruburene were 0.12, 0.85, and 0.98, respectively and their fluorescence lifetimes in benzene or toluene were reported as 4.2, 15.2, and 16 ns, respectively.[14] The fluorescence spectra of **1a**–**c** were also measured as shown in Figure S2. The quantum yields of **1a**–**c** in solid state were <0.01, 0.03, and 0.11, respectively. The bulky substituents seemed to disturb the stacking of the compounds in solid state.

The electrochemical properties of naphthacenes were investigated by cyclic voltammetry (CV) in anhydrous dichloromethane (Fig. 2 and Table 1). Reversible oxidation peaks were observed for **1a** (0.51 V vs Fc/Fc^+), **1b** (0.44 V), and **1c** (0.47 V), and the reduction potential observed for **1b** (−2.10 V) and **1c** (−2.09 V). The HOMO levels or ionization potentials (IP) were calculated by the known equation $IP = E^{ox}_{onset} + 4.80$.[15] The HOMO of **1b** (5.17 eV) and **1c** (5.20 eV) are lower than non-substituted naphthacene **1a** by 0.06 and 0.03, respectively. The calculated HOMO energy levels relative to naphthacene **1a** are also summarized in Table 1 (Fig. S3).[16]

The UV–vis absorption spectra of α-diketone precursors **2a**, **2b,** and **2c** in toluene are shown in Figure 3. The absorption spectra show n–π* absorption of α-diketone moiety at 468 nm.

The absolute fluorescence quantum yield (Φ_f) of **2a** was not detected. The Φ_f of **2b** and **2c** were 0.016 and 0.017, respectively, in the beginning of the measurement, but Φ_f's were increased gradually at every measurement. These results imply that the precursors immediately reacted to release CO molecules when they were excited for the measurement of fluorescence quantum yield (λ_{ex} = 462 nm), and fluorescence from the generated acenes were gradually observed depending on the irradiation period.

To investigate the photoreaction of the compounds **2a**–**c** in detail, the photoreactions were monitored by ^1H NMR spectroscopy (Fig. 4). α-Diketone precursor **2b** was placed in degassed $CDCl_3$ and irradiated with blue LED (λ = 470 nm, 25 W/m^2) under nitrogen atmosphere. During the photoreaction, the singlet peak of

Table 1
Optical and electrochemical characterization of naphthacenes

	λ_{abs}[a] (nm) (log ε)	λ_{em}[a] (nm)	Φ_f	τ_f (ns)	$E^{ox}_{1/2}$ (V)[b]	E^{ox}_{onset} (V)[b]	$E^{red}_{1/2}$ (V)[b]	$HOMO_{exp}$ (eV)[c]	$HOMO_{cal}$ (eV)[d]	$LUMO_{exp}$ (eV)[e]	$LUMO_{cal}$ (eV)[d]	E_g (eV)[f]
1a	396 (3.22), 419 (3.52), 445 (3.81), 475 (3.85)	481, 512, 551	0.12	3.9	0.51	0.43	–	−5.23	−4.86	−2.66[f]	−2.08	2.57
1b	411 (3.42), 436 (3.84), 463 (4.15), 495 (4.20)	511, 541, 583	0.67	9.4	0.44	0.37	−2.10	−5.17	−4.76	−2.75	−2.04	2.42
1c	410 (3.43), 436 (3.87), 464 (4.19), 494 (4.24)	506, 539, 589	0.70	9.6	0.47	0.40	−2.09	−5.20	−4.77	−2.77	−2.05	2.43

[a] Recorded in toluene at room temperature.
[b] The values were obtained by cyclic voltammetry. V versus Fc/Fc^+. See Supplementary data for experimental details.
[c] The values were obtained by ionization potentials in toluene.
[d] The values were calculated at the B3LYP/6-31G(d) levels.
[e] The values were obtained from HOMO levels and E_g.
[f] The values were obtained from the edge of the absorption spectra in toluene.

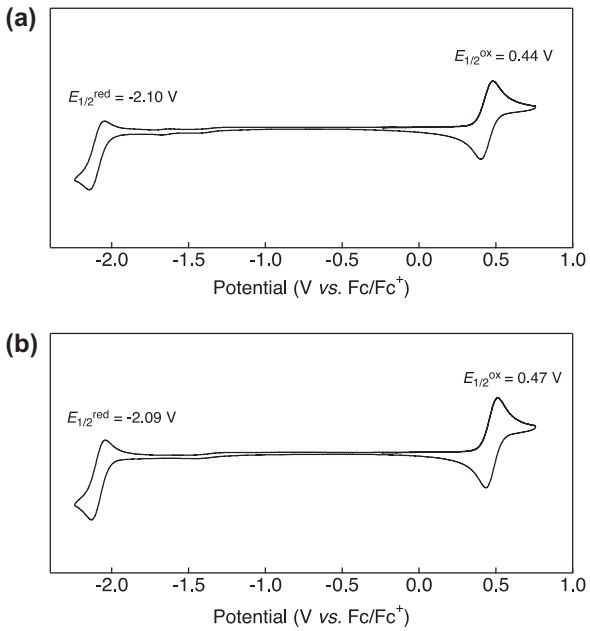

Figure 2. Cyclic voltammograms of **1b** (a) and **1c**; (b) in 0.1 M $TBAPF_6$ in acetonitrile. Scan rate 0.1 V/s. [Naphthacene] = 0.1 mM. WE: glassy carbon, CE: Pt, RE: $Ag/AgNO_3$.

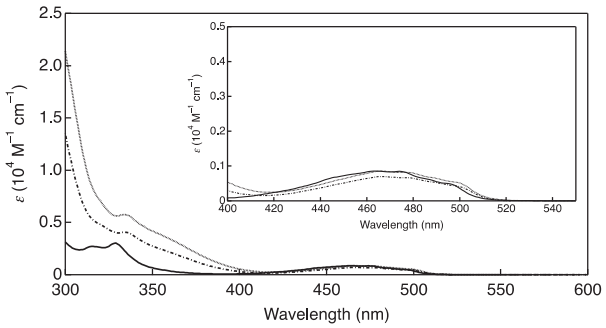

Figure 3. Absorption spectra of α-diketone **2a** (black line), **2b** (gray line), **2c** (dotted line).

bridgehead protons at 5.2 ppm gradually decreased while singlet peak due to peri-position of **1b** increased at 8.4 ppm. These results suggested the photoreaction form **2b** to **1b** proceeded clearly. The photoconversion of α-diketone precursor **2c** to the naphthacene **1c** gave similar results (Fig. S4).

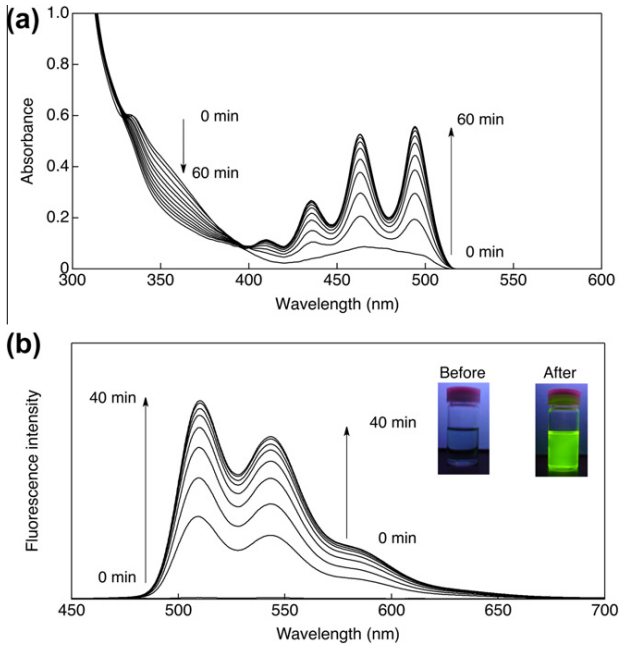

Figure 5. (a) The UV–vis absorption spectra change of **2b** upon photoirradiation in toluene (1.02×10^{-4} M) under argon atmosphere (λ_{ex} = 468 nm); (b) the fluorescence spectra change of **2b** upon photoirradiation in toluene (3.48×10^{-5} M) under argon atmosphere (λ_{ex} = 468 nm).

The change of UV–vis spectra during the photoreaction of **2b** in toluene under argon atmosphere is shown in Figure 5a. Before irradiation, only the broad n–π* peak at 465 nm was observed. During the irradiation, the new peaks at 436, 463, and 495 nm assigned to **1b** increased. The absorbance of naphthacene became constant after 60 min irradiation. Judging from the observation of the isosbestic points at 334 and 390 nm, the photoreaction proceeded directly. Similarly, α-diketone precursors **2a** and **2c** were converted to **1a** and **1c** as shown in Figure S5. The change of the fluorescence spectra of **2b** during the photoirradiation is shown in Figure 5b. The colorless fluorescence of the solution gradually changed to light green. Fluorescence intensity of **2b** increases significantly with no change of the emission maxima position. After irradiation for 40 min, the fluorescence intensity stayed constant and the reaction seemed to be finished. The similar change was observed for **2c**, as shown in Figure S6.

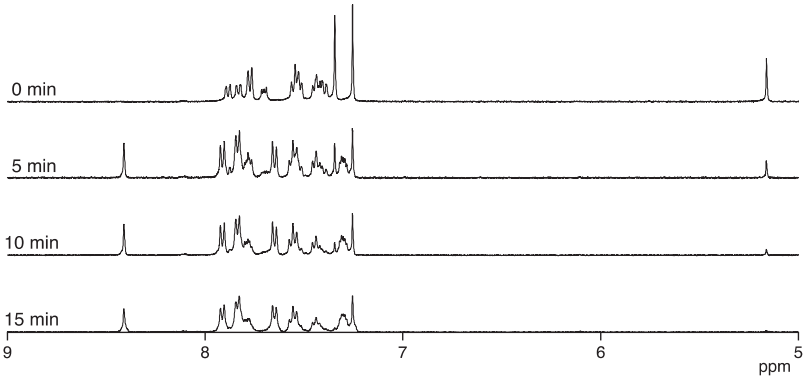

Figure 4. ^1H NMR spectra during the photoreaction of **2b** in $CDCl_3$ under nitrogen atmosphere.

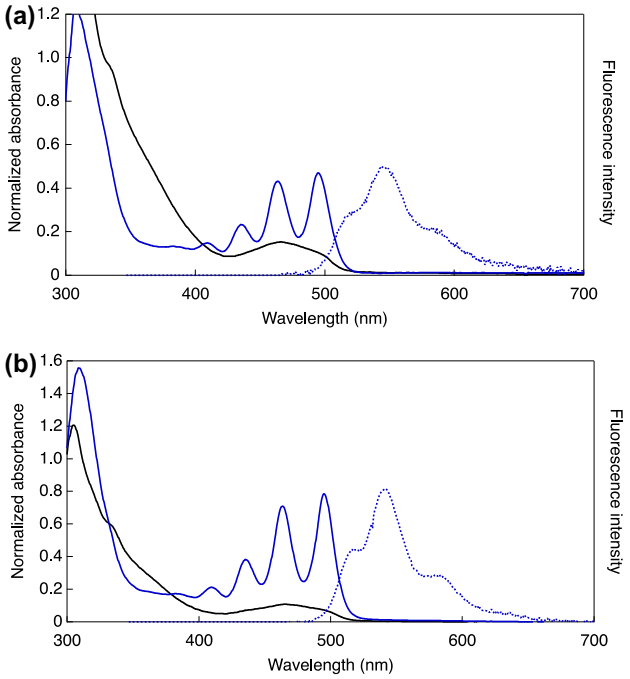

Figure 6. UV–vis absorption (solid lines) and fluorescence (dotted lines) spectra of (a) **1b** (blue) and **2b** (black); and (b) **1c** (blue) and **2c** (black) in PMMA films (λ_{ex} = 435 nm).

The photoconversion reaction was also performed in a PMMA film. PMMA (470 mg) was dissolved in toluene (10 mL), and the residue was filtered off after overnight stirring. 150 μL of PMMA solution and 50 μL of CH_2Cl_2 solution of the precursor (5 mg/mL) were mixed. The mixture was spin-coated on a glass plate and the film was irradiated for 1 h using a 375 W metal-halide lamp over 390 nm under vacuum. The experimental detail is described in the Supplementary data. The UV–vis spectra before and after photoirradiation are shown in Figure 6. Before irradiation, a typical n–π* absorption was observed at 470 nm. After irradiation, the peaks at 435, 463, and 494 nm appeared, similar to those in toluene solution. The fluorescence of **1b** in the PMMA film was also observed which indicated the compound **2b** was fully converted to **1b** and the obtained acene compounds are dispersed in the PMMA film without stacking. Similar results were obtained for the photoconversion from **2c** to **1c** in PMMA film and the fluorescence quantum yields of **1b** and **1c** were 0.33 and 0.34, respectively, in the PMMA films.

In conclusions, we have succeeded in preparing the highly fluorescent naphthacenes **1b** and **1c** and their precursors **2b** and **2c**. The non-fluorescent precursors can be easily converted to highly fluorescent naphthacenes (Φ_f = 0.67–0.70) by photo irradiation in solution. This conversion can also be possible in PMMA matrix. These new materials can be applicable in the field of OLED and memory media as printable fluorescent materials.

Acknowledgments

We thank Division of Synthesis and Analysis, Department of Molecular Science, Integrated Center for Sciences (INCS), Ehime University for its help in using mass and NMR spectrometer. We also thank Venture Business Laboratory, Ehime University, for its help in using TOF-MS. This work was partially supported by Grants-in-Aid (No. 22350083 to H.Y.) and the Green Photonics Project in NAIST sponsored by the Ministry of Education, Culture, Sports, Science and Technology, MEXT, Japan, and Adaptable and Seamless Technology Transfer Program through Target-driven R&D (A-STEP) (No. AS2111283D to S.F. and H.Y.) sponsored by Japan Science and Technology Agency.

Supplementary data

Supplementary data (synthetic detail, characterization, fluorescence decay curves, and spectral change of absorption and fluorescence during the photolysis in solution) associated with this article can be found, in the online version, at http://dx.doi.org/10.1016/j.tetlet.2013.01.014.

References and notes

1. Anthony, J. E. *Chem. Rev.* **2006**, *106*, 5028–5048.
2. (a) Danel, K.; Huang, T.-H.; Lin, J. T.; Tao, Y.-T.; Chuen, C.-H. *Chem. Mater.* **2002**, *14*, 3860–3865; (b) Odom, S. A.; Parkin, S. R.; Anthony, J. E. *Org. Lett.* **2003**, *5*, 4245–4248.
3. (a) Brown, A. R.; Pomp, A.; de Leeuw, D. M.; Klaassen, D. B. M.; Havinga, E. E.; Herwig, P.; Müllen, K. *J. Appl. Phys.* **1996**, *79*, 2136–2138; (b) Herwig, P. T.; Müllen, K. *Adv. Mater.* **1999**, *11*, 480–483.
4. (a) Afzali, A.; Dimitrakopoulos, C. D.; Breen, T. L. *J. Am. Chem. Soc.* **2002**, *124*, 8812–8813; (b) Afzali, A.; Dimitrakopoulos, C. D.; Graham, T. O. *Adv. Mater.* **2003**, *15*, 2066–2069; (c) Weidkamp, K. P.; Afzali, A.; Tromp, R. M.; Hamers, R. J. *J. Am. Chem. Soc.* **2004**, *126*, 12740–12741.
5. (a) Chen, K.-Y.; Hsieh, H.-H.; Wu, C.-C.; Hwang, J.-J.; Chow, T. J. *Chem. Commun.* **2007**, 1065–1067; (b) Chuang, T.-H.; Hsieh, H.-H.; Chen, C.-K.; Wu, C.-C.; Lin, C.-C.; Chou, P.-T.; Chao, T.-H.; Chow, T. J. *Org. Lett.* **2008**, *10*, 2869–2872; (c) Watanabe, M.; Chang, Y. J.; Liu, S.-W.; Chao, T.-H.; Goto, K.; Islam, M. M.; Yuan, C.-H.; Tao, Y.-T.; Shinmyozu, T.; Chow, T. J. *Nat. Chem.* **2012**, *4*, 574–578.
6. Strating, J.; Zwanenburg, B.; Wagenaar, A.; Udding, A. C. *Tetrahedron Lett.* **1969**, *10*, 125–128.
7. (a) Uno, H.; Yamashita, Y.; Kikuchi, M.; Watanabe, H.; Yamada, H.; Okujima, T.; Ogawa, T.; Ono, N. *Tetrahedron Lett.* **2005**, *46*, 1981–1983; (b) Yamada, H.; Yamashita, Y.; Kikuchi, M.; Watanabe, H.; Okujima, T.; Uno, H.; Ogawa, T.; Ohara, K.; Ono, N. *Chem. Eur. J.* **2005**, *11*, 6212–6220; (c) Zhao, Y.; Mondal, R.; Neckers, D. C. *J. Org. Chem.* **2008**, *73*, 5506–5513; (d) Katsuta, S.; Yamada, H.; Okujima, T.; Uno, H. *Tetrahedron Lett.* **2010**, *51*, 1397–1400; (e) Tönshoff, C.; Bettinger, H. F. *Chem. Eur. J.* **2012**, *18*, 1789–1799.
8. (a) Mondal, R.; Shah, B. K.; Neckers, D. C. *J. Am. Chem. Soc.* **2006**, *128*, 9612–9613; (b) Mondal, R.; Adhikari, R. M.; Shah, B. K.; Neckers, D. C. *Org. Lett.* **2007**, *9*, 2505–2508; (c) Mondal, R.; Tönshoff, C.; Khon, D.; Neckers, D. C.; Bettinger, H. F. *J. Am. Chem. Soc.* **2009**, *131*, 14281–14289; (d) Tönshoff, C.; Bettinger, H. F. *Angew. Chem., Int. Ed.* **2010**, *49*, 4125–4128.
9. (a) Masumoto, A.; Yamashita, Y.; Go, S.; Kikuchi, T.; Yamada, H.; Okujima, T.; Ono, N.; Uno, H. *Jpn. J. Appl. Phys.* **2009**, *48*, 051505-5; (b) Yamada, H.; Ohashi, C.; Aotake, T.; Katsuta, S.; Honsho, Y.; Kawano, H.; Okujima, T.; Uno, H.; Ono, N.; Seki, S.; Nakayama, K. *Chem. Commun.* **2012**, *48*, 11136–11138.
10. Irie, M.; Fukaminato, T.; Sasaki, T.; Tamai, N.; Kawai, T. *Nature* **2002**, *420*, 759–760.
11. Deniz, E.; Sortino, S.; Raymo, F. M. *J. Phys. Chem. Lett.* **2010**, *1*, 1690–1693.
12. Garden, S. J.; Torres, J.; Ferreira, A. A.; Silva, R. B.; Pinto, A. C. *Tetrahedron Lett.* **1997**, *38*, 1501–1504.
13. Heitman, L. H.; Narlawar, R.; de Vries, H.; Willemsen, M. N.; Wolfram, D.; Brussee, J.; IJzerman, A. P. *J. Med. Chem.* **2009**, *52*, 2036–2042.
14. (a) Löhmannströben, H.-G. *Appl. Phys. B* **1988**, *47*, 195–199; (b) Burgdorff, C.; Lircher, T.; Löhmannströben, H.-G. *Spectrochim. Acta A.* **1988**, *44*, 1137–1141; (c) Bayrakçeron, F. *J. Lumin.* **1992**, *54*, 29; (d) Burdett, J. J.; Müller, A. M.; Gosztola, D.; Bardeen, C. J. *J. Chem. Phys.* **2010**, *133*, 144506-1–144506-12.
15. Pommerehne, J.; Vestweber, H.; Guss, W.; Mahrt, R. F.; Bässler, H.; Porsch, M.; Daub, J. *Adv. Mater.* **1995**, *7*, 551–554.
16. Frisch, M. J.; Trucks, G. W.; Schlegel, H. B.; Scuseria, G. E.; Robb, M. A.; Cheeseman, J. R.; Scalmani, G.; Barone, V.; Mennucci, B.; Petersson, G. A.; Nakatsuji, H.; Caricato, M.; Li, X.; Hratchian, H. P.; Izmaylov, A. F.; Bloino, J.; Zheng, G.; Sonnenberg, J. L.; Hada, M.; Ehara, M.; Toyota, K.; Fukuda, R.; Hasegawa, J.; Ishida, M.; Nakajima, T.; Honda, Y.; Kitao, O.; Nakai, H.; Vreven, T., ; Montgomery, J. A., Jr.; Peralta, J. E.; Ogliaro, F.; Bearpark, M.; Heyd, J. J.; Brothers, E.; Kudin, K. N.; Staroverov, V. N.; Kobayashi, R.; Normand, J.; Raghavachari, K.; Rendell, A.; Burant, J. C.; Iyengar, S. S.; Tomasi, J.; Cossi, M.; Rega, N.; Millam, J. M.; Klene, M.; Knox, J. E.; Cross, J. B.; Bakken, V.; Adamo, C.; Jaramillo, J.; Gomperts, R.; Stratmann, R. E.; Yazyev, O.; Austin, A. J.; Cammi, R.; Pomelli, C.; Ochterski, J. W.; Martin, R. L.; Morokuma, K.; Zakrzewski, V. G.; Voth, G. A.; Salvador, P.; Dannenberg, J. J.; Dapprich, S.; Daniels, A. D.; Farkas, Ö.; Foresman, J. B.; Ortiz, J. V.; Cioslowski, J.; Fox, D. J. GAUSSIAN *09 Re-Vision A.2*; GAUSSIAN: Wallingford, CT, 2009.

ChemComm

RSC Publishing

COMMUNICATION

View Article Online
View Journal | View Issue

Cite this: *Chem. Commun.*, 2013, **49**, 11638

Received 13th August 2013,
Accepted 17th October 2013

DOI: 10.1039/c3cc46178e

www.rsc.org/chemcomm

Solution-processed anthradithiophene–PCBM p–n junction photovoltaic cells fabricated by using the photoprecursor method†

Hiroko Yamada,*[ab] Yuji Yamaguchi,[c] Ryuta Katoh,[d] Takao Motoyama,[c] Tatsuya Aotake,[a] Daiki Kuzuhara,[a] Mitsuharu Suzuki,[a] Tetsuo Okujima,[d] Hidemitsu Uno,[d] Naoki Aratani[a] and Ken-ichi Nakayama*[bc]

P–n junction solar cells based on anthradithiophene (ADT) as a p-type semiconductor were fabricated by using the photoprecursor method in which an α-diketone-type precursor was spin-coated and then transformed to ADT *in situ* by photoirradiation. Combination with $PC_{71}BM$ as an n-layer material led to 1.54% photoconversion efficiency.

Solution-processable organic semiconductors are expected to enable the fabrication of low-cost, large-area electronic devices by simple deposition techniques.[1] Along these lines, a variety of soluble low band gap polymers[2] and molecular materials[3] have been developed in order to achieve cost-effective, high-performance organic solar cells. High photoconversion efficiencies (PCEs) of over 8% have already been realized with these materials in bulk-heterojunction-type devices.[2,3]

Besides bulk heterojunction cells, it has been shown that organic solar cells in a multilayer structure, especially the p–i–n structure, can also afford high PCEs.[4] An advantage associated with the multilayer configuration is that one can have more precise control over the morphology and material distribution within the active layer, which would contribute to, for example, improving the electrode–organic interface properties and decreasing the leak current. However, solution deposition processes are typically not suitable for making layer-by-layer structures, and more costly vacuum deposition is commonly employed. The precursor method has recently been the focus of attention in order to resolve this issue and achieve layer-by-layer structures by solution deposition. In this context, thermally convertible precursors have been developed to employ intact acenes,[5,6] phthalocyanines,[7] benzoporphyrins,[8] oligothiophenes,[9] diketopyrrolopyrroles,[10] quinacridones[11] and indigos[12] in solution-processed devices to take advantage of their favourable photoelectronic properties.[13] This approach has also been applied to polymer-based devices.[14]

Several groups including us have reported on photoconvertible precursors of acenes which can be converted to the corresponding acenes in solution or thin films quantitatively.[6,15,16] In addition, it has been demonstrated that acene-based thin films prepared by the photoprecursor approach can be used in electronic devices; *e.g.*, a hole mobility of 0.86 $cm^2\ V^{-1}\ s^{-1}$ was obtained in a top-contact-type thin-film transistor (TFT) based on pentacene (**PEN**) photogenerated *in situ* from the corresponding α-diketone-type precursor (**PDK**, Scheme 1).[17] Here, the photoconversion of α-diketone derivatives can proceed at room temperature or lower, though higher device performance sometimes results when gentle heating (<100 °C) is applied during the reaction. This unnecessity of intense heating is highly beneficial in that organic devices can be fabricated on thermolabile substrates.

Recent progress in the search for new organic semiconductors has shown that thiophene-based molecular compounds, especially fused-thiophene aromatics, often afford superior device performances owing to their favourable intermolecular interactions in nanocrystalline films, such as van der Waals interactions, π–π stacking, and sulfur–sulfur contact.[18] One of the representative compounds in this class is anthradithiophene (**ADT**, Scheme 1), which possesses a similar electronic structure to that of **PEN**.[19] In this communication, we report the synthesis, characterization, and photoreaction of **ADT-DK**, the α-diketone-type photoprecursor of **ADT**. In addition, p–n junction organic photovoltaic (OPV) devices based on **ADT** as a p-layer material were fabricated by the photoprecursor method by using **ADT-DK** as a precursor. [6,6]-Phenyl-C_{61}- or C_{71}-butyric acid methyl ester ($PC_{61}BM$ or $PC_{71}BM$) was employed as an n-layer material, and the performance of the resulting devices was evaluated in comparison with **PEN**–PCBM devices. The obtained results show high potential of **ADT** as a p-layer material to be used in OPV devices fabricated by using the photoprecursor approach.

The parent **ADT** was prepared as a *syn–anti* isomeric mixture following the previously reported procedure.[19a] The precursor **ADT-DK** was prepared from the parent **ADT** in three steps as shown

[a] *Graduate School of Materials Science, Nara Institute of Science and Technology, 8916-5, Ikoma, Nara 630-0192, Japan. E-mail: hyamada@ms.naist.jp; Fax: +81-743-72-6042; Tel: +81-743-72-6041*
[b] *CREST, JST, Chiyoda-Ku, Tokyo 102-0075, Japan*
[c] *Department of Organic Device Engineering, Graduate School of Science and Engineering, Yamagata University, Yonezawa 992-8510, Japan. E-mail: nakayama@yz.yamagata-u.ac.jp; Fax: +81-238-26-3713*
[d] *Graduate School of Science and Engineering, Ehime University, Matsuyama 790-8577, Japan*

† Electronic supplementary information (ESI) available. CCDC 955408. For ESI and crystallographic data in CIF or other electronic format see DOI: 10.1039/c3cc46178e

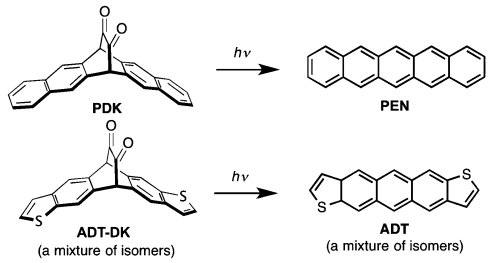

Scheme 1 Photoreaction of the precursors to acenes.

in Scheme 2: (1) a Diels–Alder reaction of **ADT** with vinylene carbonate at 180 °C for 3 days to give **1** in 81% yield; (2) deprotection under basic conditions to give diol **2** in 74% yield; (3) Swern oxidation of **2** to give **ADT-DK** in 81% yield. The compounds were characterized by ^{1}H and ^{13}C NMR and mass spectrometry. The structure of **ADT-DK** was also confirmed by single-crystal X-ray analysis (ESI,† Fig. S1).‡ The *syn–anti* isomers of **ADT-DK** are randomly distributed at a 50 : 50 ratio in crystals.

The UV–vis absorption spectra of **ADT** and **ADT-DK** are shown in ESI,† Fig. S2. **ADT-DK** shows a broad absorption at around 460 nm, which can be attributed to the n–π* absorption of the diketone moiety. The photoreaction of **ADT-DK** to **ADT** was monitored by the change in UV–vis absorption (ESI,† Fig. S2). A toluene solution of **ADT-DK** (0.2 mg in 10 ml) was bubbled with argon, and the solution was irradiated by a 500 W xenon lamp through a monochromator (λ_{ex} = 468 nm, 14.9 mW cm^{-2}). The reaction finished in 17.5 min in this case. The photoreaction of **ADT-DK** was also performed in a spin-coated thin film, and the complete conversion to **ADT** was confirmed by IR spectra (ESI,† Fig. S3); namely, the C=O stretching band at 1730 cm^{-1} disappeared after irradiation by a blue LED lamp for 30 min in a glove box. The ionization potential of the thus obtained **ADT** film was determined to be 5.1 eV by photoelectron spectroscopy (ESI,† Fig. S4). This value is comparable with that obtained for a thin film of directly deposited anthra(2,3-*b*:6,7-*b*′)dithiophene (*anti*-**ADT**).[19b]

Solution-processed p–n junction devices based on photogenerated acene and $PC_{61}BM$ were typically fabricated as follows (Fig. 1): After spin-coating of PEDOT:PSS on ITO, **PDK** or **ADT-DK** in $CHCl_3$ (5 mg ml^{-1}) was spin-coated at 800 rpm for 30 s then irradiated by a blue LED at rt for 30 min. On top of that, $PC_{61}BM$ in $CHCl_3$ (10 mg ml^{-1}) was spin-coated at 800 rpm for 30 s, then Ca (10 nm) and Al (80 nm) were sequentially deposited. This process affords devices with a structure described as [ITO/PEDOT:PSS (30 nm)/Acene (40 nm)/$PC_{61}BM$ (40 nm)/Ca (10 nm)/Al (80 nm)].

The photovoltaic performance of the obtained devices is summarized in Fig. 2 and Table 1. The device based on **PEN** and $PC_{61}BM$ showed a PCE of 0.25% (short circuit current density, J_{sc} = 0.80 mA cm^{-2}; open circuit voltage, V_{oc} = 0.52 V; fill factor, FF = 0.59). By replacing **PEN** with **ADT**, the PCE increased by approximately three times to 0.74% (J_{sc} = 1.91 mA cm^{-2}, V_{oc} = 0.61 V and FF = 0.64). Employment of $PC_{71}BM$ instead of $PC_{61}BM$ led to a considerably higher J_{sc} value,[18] resulting in an even higher PCE of 1.54% (J_{sc} = 3.46 mA cm^{-2}; V_{oc} = 0.67 V; FF = 0.66). In this case again, the **ADT**-based device showed a PCE approximately three times higher than that of the **PEN**-based counterpart (PCE = 0.44, J_{sc} = 1.56 mA cm^{-2}; V_{oc} = 0.53 V; FF = 0.53).

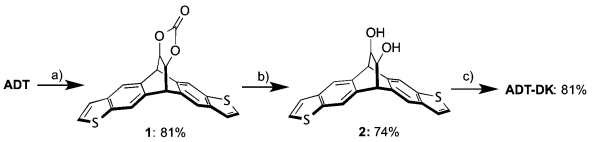

Scheme 2 Synthesis of **ADT-DK**. Reagents and conditions: (a) vinylene carbonate, xylenes, autoclave, 180 °C, 3 days; (b) 4 M NaOH, THF, reflux, 2 h; (c) TFAA, DMSO, DIPEA, dry-CH_2Cl_2, −60 °C, 1.5 h.

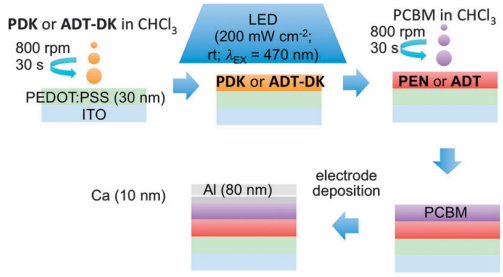

Fig. 1 Schematic diagram of fabrication of p–n junction OPV devices.

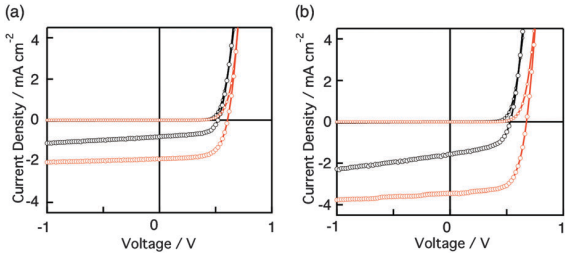

Fig. 2 (a) *I–V* curves of **PEN**–$PC_{61}BM$ (black lines) and **ADT**–$PC_{61}BM$ (red lines) devices; (b) *I–V* curves of **PEN**–$PC_{71}BM$ (10 mg ml^{-1}) (black lines) and **ADT**–$PC_{71}BM$ (red lines) devices; larger circles: under AM 1.5G illumination; smaller circles: in the dark.

To evaluate the influence of n-layer thickness, a few **ADT**–$PC_{71}BM$ devices were additionally prepared using $PC_{71}BM$ solutions of different concentrations from 5 to 20 mg ml^{-1}, which correspond to the resulting film thickness of 13–116 nm. (The film thicknesses are summarized in Table S1 in ESI†) The best performance was achieved at 10 mg ml^{-1} concentration (40 nm film thickness). When the $PC_{71}BM$ film is thicker, J_{sc} decreased because of the higher resistance of the film. With a thinner $PC_{71}BM$ film, V_{oc} decreased because of the higher leak current.

The incident photon-to-current conversion efficiency (IPCE) curves and the UV–vis spectra of the acene–PCBM (10 mg ml^{-1}) devices are shown in Fig. 3. By using $PC_{71}BM$, the absorbance of the multilayer films in the visible region increased by 1.5 to 2 times compared to the cases when $PC_{61}BM$ was used.[20] Furthermore, the **ADT** device showed

Table 1 Performance of the acene–PCBM p–n junction OPV devices

Acene	PCBM/ mg ml^{-1}	J_{sc}/ mA cm^{-2}	V_{oc}/ V	FF	PCE/ %	R_s/ ohm cm^{-2}	R_p/ ohm cm^{-2}
PEN	$PC_{61}BM$(10)	0.80	0.52	0.59	0.25	57	2416
ADT	$PC_{61}BM$(10)	1.91	0.61	0.64	0.74	31	5052
PEN	$PC_{71}BM$(10)	1.56	0.53	0.53	0.44	45	1015
ADT	$PC_{71}BM$(5)	2.08	0.49	0.53	0.53	42	888
ADT	$PC_{71}BM$(10)	3.46	0.67	0.66	1.54	24	13 336
ADT	$PC_{71}BM$(15)	2.49	0.66	0.58	0.95	69	2522
ADT	$PC_{71}BM$(20)	1.82	0.64	0.48	0.56	194	3116

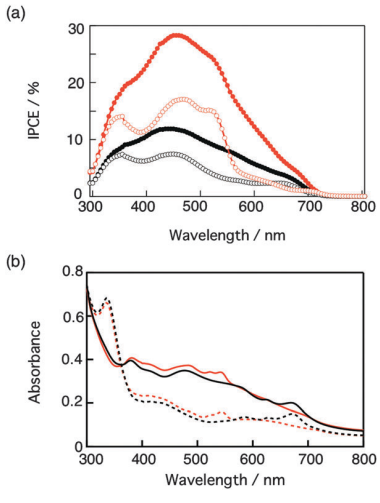

Fig. 3 (a) IPCE curves of [ITO/PEDOT:PSS/acene/PCBM/Ca/Al] and (b) absorption spectra of the same active layer films on ITO/PEDOT:PSS without the Ca and Al layers: **PEN**/$PC_{61}BM$ (black open circles in (a); the black broken line in (b)); **ADT**/$PC_{61}BM$ (red open circles in (a); the black red line in (b)); **PEN**/$PC_{71}BM$ (black closed circles in (a); the black solid line in (b)); **ADT**/$PC_{71}BM$ (red closed circles in (a); the red solid line in (b)). The concentration of PCBM solutions is 10 mg ml^{-1}.

higher performance than the **PEN** device in each case, although the absorption abilities are comparable to each other.

The slightly higher V_{oc} of the **ADT** device is attributed to the deeper HOMO level of **ADT** (5.1 eV) compared to **PEN** (5.0 eV). The photocurrent in reverse voltage (Fig. 2) was nearly constant in the **ADT** device, whereas it increased in the **PEN** device with increasing reverse voltage, which is reflected in the higher FF, lower series resistance (R_s), and higher parallel resistance (R_p) in the **ADT** device. This difference indicates that the p-layer based on **ADT** has a higher charge extraction ability; *i.e.*, higher charge mobility. To check the film structures of **PEN** and **ADT** prepared by photoconversion, X-ray diffraction patterns of the films were measured (ESI,† Fig. S5). For the **PEN** film, a peak corresponding to a *d*-space of 15.1 Å was observed, suggesting the edge-on arrangement of **PEN** molecules.[21] On the other hand, the **ADT** film gave a featureless trace without any recognizable peaks. This implies that the randomly oriented **ADT** film is more suitable for charge extraction in the device, compared to the **PEN**-based film with the edge-on arrangement having less overlap of π-orbitals along the vertical direction.[22]

Bulk heterojunction devices with acenes as p-type and $PC_{61}BM$ as n-type materials were also evaluated; however, the PCE values were less than 0.1% with significantly low J_{sc} values. Considering the high crystallinity of **PEN** and **ADT**, the well-mixed i-layers might not be formed in combination with $PC_{61}BM$.

In summary, we were successful in preparing p–n heterojunction solar cells based on **ADT** and PCBM *via* the photoprecursor method for the first time. The PCE of the best performed **ADT**–$PC_{71}BM$ device is 1.54%, which is a significant improvement from the 0.25% PCE obtained with our prototype **PEN**–$PC_{61}BM$ device prepared by the same method. The results clearly demonstrate that the photoprecursor method makes hardly soluble organic semiconductors such as **ADT** compatible with solution-based deposition techniques. In addition, the photoprecursor approach enables the formation of multilayer structures by solution processes. These achievements pave the way to a widely applicable methodology for the construction of sophisticated multilayer structures (*e.g.*, p–i–n type triple-layer structures) by solution processes. Further research along these lines is underway.

Notes and references

‡ Crystallographic data for **ADT-DK:** $C_{20}H_{10}O_2S_2$, M = 346.42, orthorhombic, space group *Fdd*2 (#43), a = 27.546(11) Å, b = 33.092(13) Å, c = 6.766(3) Å, V = 6156(4) $Å^3$, T = 100 K, Z = 16, R_1 = 0.0448, wR_2 = 0.1028, GOF = 1.086. CCDC 955408 contains the supplementary crystallographic data.

1 (*a*) M. Mas-Torrent and C. Rovira, *Chem. Soc. Rev.*, 2008, **37**, 827; (*b*) J. E. Anthony, *Angew. Chem., Int. Ed.*, 2008, **47**, 452; (*c*) A. R. Murphy and J. M. J. Fréchet, *Chem. Rev.*, 2007, **107**, 1096.
2 (*a*) C. Duan, F. Huang and Y. Cao, *J. Mater. Chem.*, 2012, **22**, 10416; (*b*) H. Zhou and W. You, *Macromolecules*, 2012, **45**, 607; (*c*) P.-L. T. Boudreault, A. Najari and M. Leclerc, *Chem. Mater.*, 2011, **23**, 456; (*d*) C. L. Chochos and S. A. Choulis, *Prog. Polym. Sci.*, 2011, **36**, 1326; (*e*) Y.-J. Cheng, S.-H. Yang and C.-S. Hsu, *Chem. Rev.*, 2009, **109**, 5868; (*f*) J. Chen and Y. Cao, *Acc. Chem. Res.*, 2009, **42**, 1709; (*g*) Y. Liang and L. Yu, *Acc. Chem. Res.*, 2009, **42**, 1227.
3 (*a*) A. Mishra and P. Bauerle, *Angew. Chem., Int. Ed.*, 2012, **51**, 2020; (*b*) Y. Lin, Y. Li and X. Zhan, *Chem. Soc. Rev.*, 2012, **41**, 4245; (*c*) B. Walker, C. Kim and T.-C. Nguyen, *Chem. Mater.*, 2011, **23**, 470; (*d*) F. Würthner and K. Meerholz, *Chem.–Eur. J.*, 2010, **16**, 9366.
4 (*a*) D. Gebeyehu, M. Pfeiffer, B. Maennig, J. Drechsel, A. Werner and K. Leo, *Thin Solid Films*, 2004, **451–452**, 29; (*b*) K. Suemori, T. Miyata, M. Yokoyama and M. Hiramoto, *Appl. Phys. Lett.*, 2005, **86**, 063509; (*c*) Y. Matsuo, Y. Sato, T. Niinomi, I. Soga, H. Tanaka and E. Nakamura, *J. Am. Chem. Soc.*, 2009, **131**, 16048.
5 (*a*) P. T. Herwig and K. Müllen, *Adv. Mater.*, 1999, **11**, 480; (*b*) A. Afzali, C. D. Dimitrakopoulos and T. L. Breen, *J. Am. Chem. Soc.*, 2002, **124**, 8812; (*c*) J. Xiao, H. M. Duong, Y. Liu, W. Shi, L. Ji, G. Li, S. Li, X.-W. Liu, J. Ma, F. Wudl and Q. Zhang, *Angew. Chem., Int. Ed.*, 2012, **51**, 6094.
6 M. Watanabe, K.-Y. Chen, Y. J. Chang and T. J. Chow, *Acc. Chem. Res.*, 2013, **46**, 1606, and references cited therein.
7 (*a*) T. Akiyama, A. Hirao, T. Okujima, H. Yamada, H. Uno and N. Ono, *Heterocycles*, 2007, **74**, 835; (*b*) A. Hirao, T. Akiyama, T. Okujima, H. Yamada, H. Uno, Y. Sakai, S. Aramaki and N. Ono, *Chem. Commun.*, 2008, 4714.
8 S. Ito, T. Murashima, H. Uno and N. Ono, *Chem. Commun.*, 1998, 1661.
9 A. R. Murphy, J. M. J. Fréchet, P. Chang, J. Lee and V. Subramanian, *J. Am. Chem. Soc.*, 2004, **126**, 1596.
10 J. S. Zambounis, Z. Hao and A. Iqbal, *Nature*, 1997, **388**, 131.
11 T. L. Chen, J. J.-A. Chen, L. Catane and B. Ma, *Org. Electron.*, 2011, **12**, 1126.
12 E. D. Głowacki, G. Voss, K. Demirak, M. Havlicek, N. Sünger, A. C. Okur, U. Monkowius, J. Gasiorowski, L. Leonat and N. S. Sariciftci, *Chem. Commun.*, 2013, **49**, 6063.
13 H. Yamada, T. Okujima and N. Ono, *Chem. Commun.*, 2008, 2957.
14 H. Yamada, Y. Yamashita, M. Kikuchi, H. Watanabe, T. Okujima, H. Uno, T. Ogawa, K. Ohara and N. Ono, *Chem.–Eur. J.*, 2005, **11**, 6212.
15 (*a*) J. H. Edwards and W. J. Feast, *Polymer*, 1980, **21**, 595; (*b*) L. H. Nguyen, S. Günes, H. Neugebauer, N. S. Sariciftci, F. Banishoeib, A. Henckens, T. Cleij, L. Lutsen and D. Vanderzande, *Sol. Energy Mater. Sol. Cells*, 2006, **90**, 2815.
16 (*a*) J. Strating, B. Zwanenburg, A. Wagenaar and A. C. Udding, *Tetrahedron Lett.*, 1969, **10**, 125; (*b*) R. Mondal, B. K. Shah and D. C. Neckers, *J. Am. Chem. Soc.*, 2006, **128**, 9612; (*c*) C. Tönshoff and H. F. Bettinger, *Angew. Chem., Int. Ed.*, 2010, **49**, 4125; (*d*) References cited in ref. 13.
17 K. Nakayama, C. Ohashi, Y. Oikawa, T. Motoyama and H. Yamada, *J. Mater. Chem. C*, 2013, **1**, 6244.
18 K. Takimiya, S. Shinamura, I. Osaka and E. Miyazaki, *Adv. Mater.*, 2011, **23**, 4347.
19 (*a*) J. G. Laquindanum, H. E. Katz and A. J. Lovinger, *J. Am. Chem. Soc.*, 1998, **120**, 664; (*b*) M. Nakano, K. Niimi, E. Miyazaki, I. Osaka and K. Takimiya, *J. Org. Chem.*, 2012, **77**, 8099.
20 (*a*) M. M. Wienk, J. M. Kroon, W. J. H. Verhees, J. Knol, J. C. Hummelen, P. A. van Hal and R. A. J. Janssen, *Angew. Chem., Int. Ed.*, 2003, **42**, 3371; (*b*) S. Pfuetzner, J. Meiss, A. Petrich, M. Riede and K. Leo, *Appl. Phys. Lett.*, 2009, **94**, 223307.
21 C. D. Dimitrakopoulos and P. R. L. Malenfant, *Adv. Mater.*, 2002, **14**, 99.
22 Preliminary space charge limited current measurements gave hole mobilities along the vertical direction of 3.41×10^{-4} and 1.06×10^{-4} cm^2 V^{-1} s^{-1} in **ADT** and **PEN**, respectively. See ESI,† Fig. S6.

ChemPubSoc Europe

DOI: 10.1002/chem.201406384

CHEMISTRY
A European Journal
Full Paper

BODIPY Dyes

An Optically and Thermally Switchable Electronic Structure Based on an Anthracene–BODIPY Conjugate**

Tatsuya Aotake,[a] Mitsuharu Suzuki,[a] Kazuaki Tahara,[b] Daiki Kuzuhara,[a] Naoki Aratani,[a] Naoto Tamai,[b] and Hiroko Yamada*[a, c]

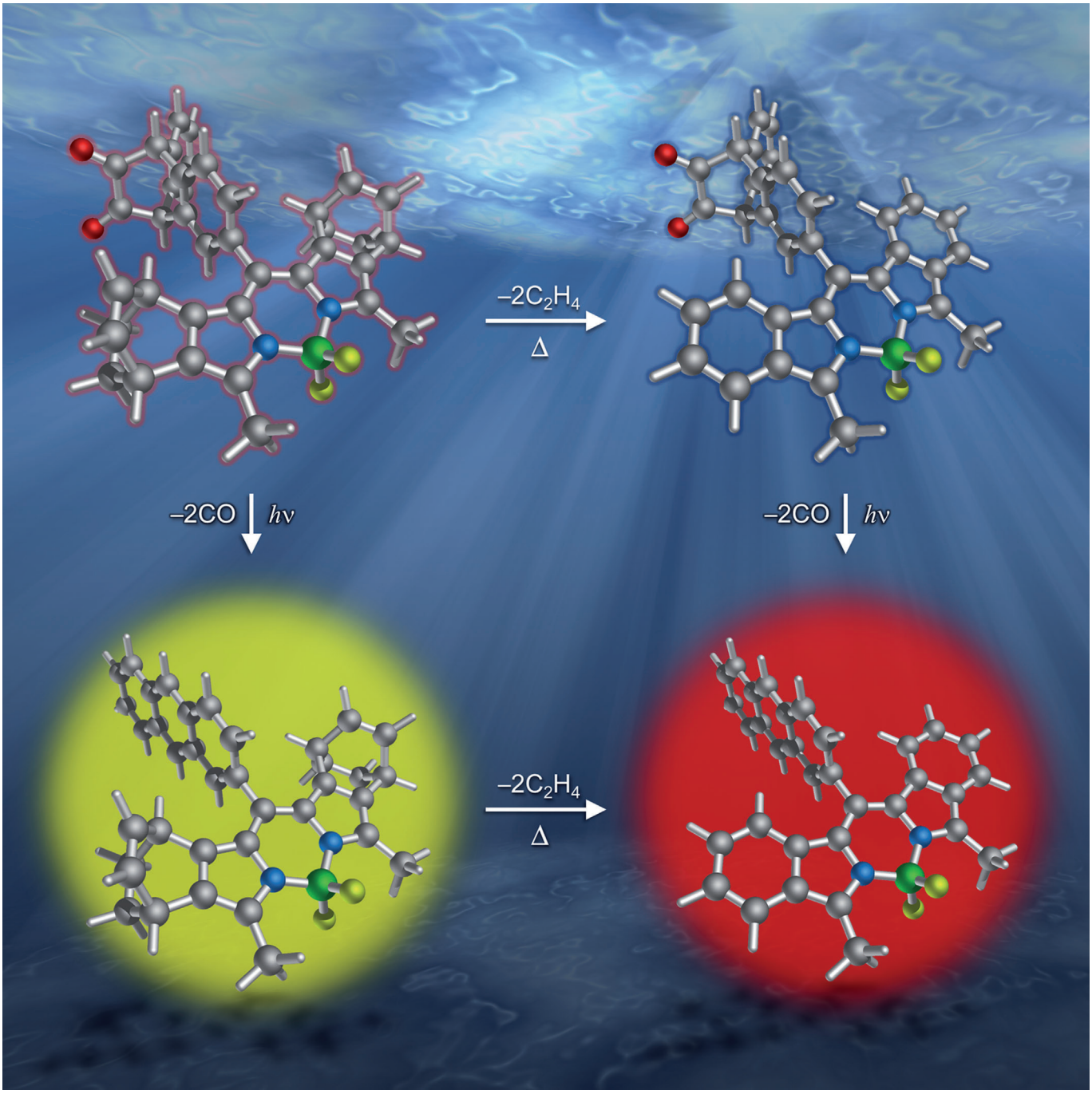

Abstract: An optically and thermally responsive boron dipyrromethene (BODIPY) dye, namely, *meso*-2-(9,10-dihydro-9,10-ethanoanthracene-11,12-dione) (DK)-linked, bicyclo[2.2.2]octadiene (BCOD)-fused BODIPY (**BCOD-DK**), was synthesized. The weakly luminous structure of **BCOD-DK** can be changed quantitatively to that of the strongly fluorescent BODIPY **BCOD-Ant** by optical excitation at the DK unit, which induces double decarbonylation of the DK unit to give an anthracene unit. The solvent effect on the fluorescence properties of **BCOD-DK** suggests that the dramatic change in fluorescence intensity is controlled by intramolecular electron transfer from the BODIPY moiety to the *meso*-DK substituent. **BCOD-DK** is converted to *meso*-**DK** benzene-fused BODIPY (**Benzo-DK**) by heating at 220 °C with 64–70 nm red-shift of absorption and fluorescence peaks without changing the fluorescence quantum yield of $\Phi_F = 0.08$ in dichloromethane. **Benzo-DK** can be converted to strongly fluorescent *meso*-anthracene benzene-fused BODIPY **Benzo-Ant** by optical excitation. Thus, **BCOD-DK** can show four different optical performances simply by irradiation and heating, and hence may be applicable for optical data storage and security data encryption.

Introduction

Stimuli-induced fluorescence switching has received much attention for application in data storage, sensing, and imaging.[1] Specifically, if the induced change is limited to the fluorescence intensity while photoabsorption characteristics are essentially unchanged, the switching phenomenon is intrinsically useful for security data encryption.[2] Boron dipyrromethene (BODIPY) dyes are characterized by large molar absorption coefficients, suitable emission spectral profiles, high fluorescence quantum yields, and excellent photostability.[3] They also have versatile uses in sensors, biolabels, and bioimaging.[4] BODIPYs with π systems extended, for example by aryl substitution or fusion with aromatic rings have attained long-wavelength fluorescence extending into the near-infrared region.[5] In this context, benzo-fused BODIPYs prepared by the retro-Diels–Alder reaction of corresponding bicyclo[2.2.2]octadiene (BCOD)-fused BODIPYs have been reported.[6] This reaction typically proceeds quantitatively around 200 °C and is associated with dramatic changes in optical properties.

The quantitative photochemical formation of anthracenes from α-diketone-type precursors has long been known.[7,8] We and others have recently shown that the α-diketone moiety can serve as a turn-on photoswitching unit of fluorophores.[9] α-Diketone derivatives are nonluminescent owing to efficient quenching of excited states, while the photoinduced decarbonylation reaction leads to recovery of the intrinsic fluorescence associated with the fluorophore. However, these fluorescence switching systems have a problem to be solved: the overlap of the excitation wavelengths to trigger the structural change and to monitor the fluorescence. Excitation of the precursor only to monitor the fluorescence is difficult, because simultaneous decarbonylation occurs during the fluorescence measurement. Therefore, the selective excitation of the fluorophore is difficult.

To separate the switching function and fluorescence monitoring,[10] we designed 9,10-dihydro-9,10-ethanoanthracene-11,12-dione (DK)–BODIPY compound **BCOD-DK**, in which a diketone (DK) is linked at the *meso* position and BCOD substituents are fused at the β positions of BODIPY. Since the DK and BCOD substituents are bulky, the BODIPY plane and phenyl ring of DK are expected to show little electronic interaction.[11] Since the singlet excited state of the BODIPY moiety lies below that of the DK moiety,[12] excitation of the BODIPY moiety induces the fluorescence of BODIPY but not photoconversion of DK, and **BCOD-DK** is photostable during the fluorescence measurements. Moreover, because DK is a good electron acceptor, photoinduced electron transfer from BODIPY to DK can quench the fluorescence of BODIPY in **BCOD-DK** (Scheme 1).[13] Furthermore, because there is little interaction between the DK and BODIPY parts, the absorption and fluorescence wavelength of the BODIPY is not changed by the photoconversion. This behavior is useful for security systems.

Herein, we report weakly fluorescent BODIPY **BCOD-DK**, which can be converted to the corresponding highly fluorescent BODIPY **BCOD-Ant** by photoirradiation. On photoconversion, little change in absorption and fluorescence peaks in the

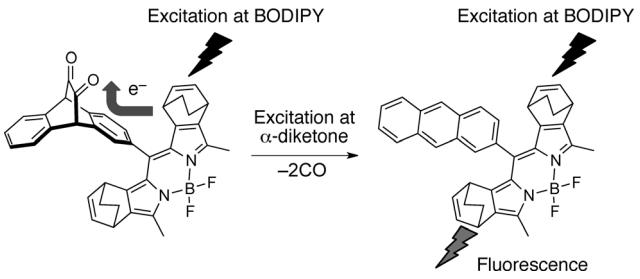

Scheme 1. Mechanism of fluorescence control based on intramolecular electron transfer.

[a] *T. Aotake, Dr. M. Suzuki, Dr. D. Kuzuhara, Prof. Dr. N. Aratani, Prof. Dr. H. Yamada*
Graduate School of Materials Science
Nara Institute of Science and Technology
Ikoma 630-0192 (Japan)
E-mail: hyamada@ms.naist.jp

[b] *K. Tahara, Prof. Dr. N. Tamai*
Department of Chemistry, Kwansei Gakuin University
2-1 Gakuen, Sanda, Hyogo 669-1337 (Japan)

[c] *Prof. Dr. H. Yamada*
CREST, Japan Science and Technology Agency JST
4-1-8, Honcho, Kawaguchi, Saitama 102-0075 (Japan)

[**] *BODIPY: boron dipyrromethene.*

Supporting information for this article is available on the WWW under http://dx.doi.org/10.1002/chem.201406384.

visible range is expected, but a dramatic change in fluorescence intensity could occur. Furthermore, **BCOD-DK** and **BCOD-Ant** can be converted to benzene-fused BODIPYs **Benzo-DK** and **Benzo-Ant**, respectively, simply by heating. These thermal conversions result in redshifts of the absorption and fluorescence spectra without changing the fluorescence quantum yields. Thus, four states are available from **BCOD-DK** simply by photoirradiation and/or heating (Scheme 2). Studies

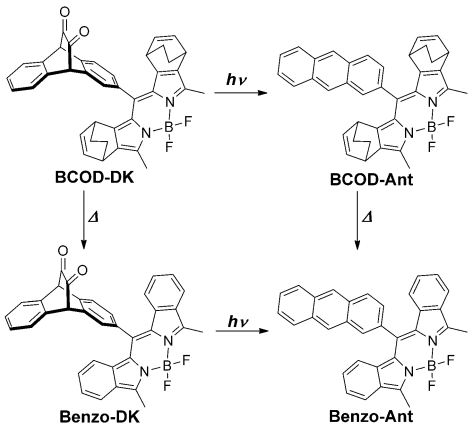

Scheme 2. Thermal and photochemical conversions of BODIPYs.

on the solvent effect indicated that fluorescence quenching in the DK-substituted derivatives is due to the electron transfer from the BODIPY moiety to the α-diketone unit. Thus, **BCOD-DK** can show four different optical performances simply by irradiation and heating, and thus will be applicable for optical data storage and security data encryption.

Results and Discussion

The preparation of **BCOD-DK** is shown in Scheme 3. Formylanthracene **1**[14] underwent a Diels–Alder reaction with vinylene carbonate to give adduct **2** as a mixture of stereoisomers in 78% yield. Isoindole **3** was prepared according to the literature.[6] Compound **4** was synthesized in 55% yield by trifluoroacetic acid (TFA)-catalyzed condensation between **2** and **3**, followed by oxidation with 2,3-dichloro-5,6-dicyanobenzoquinone (DDQ) and then treatment with BF_3·OEt_2 and *N*,*N*-diisopropylethylamine. Compound **4** was hydrolyzed to give diol **5** in 79% yield, oxidation of which by a Swern reaction gave **BCOD-DK** in 30% yield.

Crystallization of **BCOD-DK** from dichloromethane/hexane gave prism-shaped orange crystals suitable for single-crystal X-ray diffraction. The structure is shown in Figure 1 and the crystallographic data are summarized in Table S1 (Supporting Information). The BCOD unit was treated as a disordered structure of the bicyclo[2,2,2]octadiene moiety. The BODIPY core is substantially planar. The dihedral angle between the BODIPY core and DK unit is 57.9°, and the C5–C24 bond length is 1.487(4) Å. The dihedral angle and bond length suggest that the electronic interaction between the two units is rather

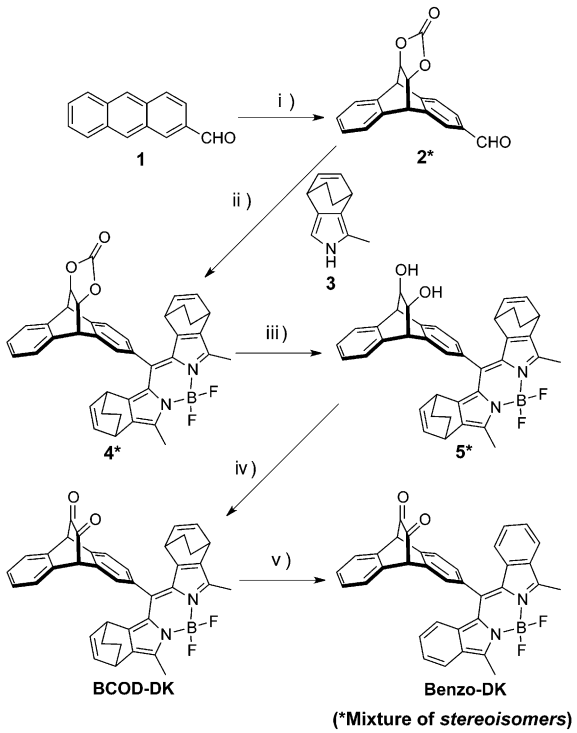

Scheme 3. Reagents and conditions: i) vinylene carbonate, xylenes, autoclave, 160 °C, 3 d, 78%; ii) TFA, dry dichloromethane, 3 h; DDQ, 20 min; *N*,*N*-diisopropylethylamine, BF_3·OEt_2, 30 min, 55%; iii) K_2CO_3, THF, methanol, water, 79%; iv) trifluoroacetic anhydride, dry DMSO, dry dichloromethane, 2 h; *N*,*N*-diisopropylethylamine, 1 h, 30%; v) 220 °C, quantitative.

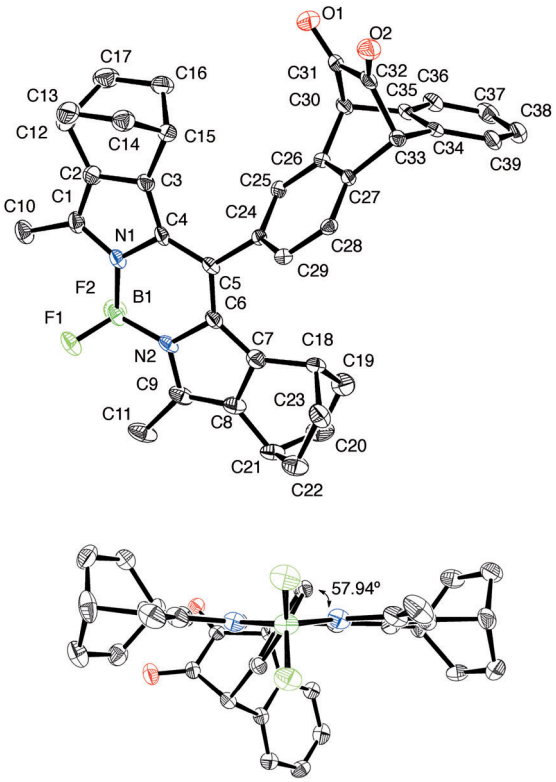

Figure 1. ORTEP of the X-ray structure of **BCOD-DK**. Solvent molecules and hydrogen atoms are omitted for clarity. Ellipsoids are drawn at 50% probability.

small, and thus state-to-state electronic and/or excitonic analysis should be possible.

Thermogravimetric analysis of **BCOD-DK** was performed to investigate its thermal conversion properties (Figure 2). **BCOD-DK** exhibited mass loss starting at 127 °C and ending at 208 °C. This demonstrates that the BCOD-fused precursor was smoothly converted to the corresponding benzo-fused BODIPY by heating. Therefore, a bulk sample of **BCOD-DK** was heated at 220 °C to form **Benzo-DK**. Quantitative conversion was confirmed by ^{1}H NMR spectroscopy (Supporting Information, Figure S1).

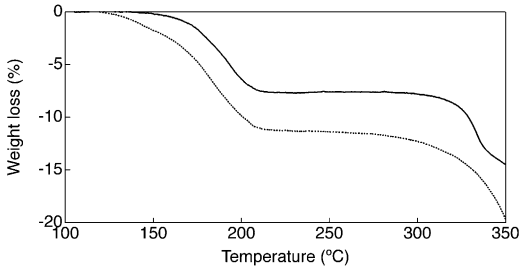

Figure 2. Thermogravimetric analysis of **BCOD-DK** (solid line) and **BCOD-Ant** (dotted line). Scan rate: 5 °C min^{-1}.

The photoconversion of the DK moiety to an anthracene moiety was performed with a metal-halide lamp through a UV cutoff filter under an argon atmosphere. Figure 3 shows the change in ^{1}H NMR spectra during the photoreaction of **BCOD-DK** in $CDCl_3$. The peaks at 5.04–5.18 ppm assigned to H^a and $H^{a'}$ of the diketone moiety gradually decreased, while the peaks at 8.51–8.60 ppm assigned to the *peri* protons H^b and $H^{b'}$ of **BCOD-Ant** increased. After 60 min, the photoreaction finished without giving any byproducts. The same measurement was performed for **Benzo-DK** in $CDCl_3$ (Supporting Information, Figure S2). During the photoreaction, the peaks at 5.07 and 5.24 ppm decreased while the peaks at 8.66 and 8.51 ppm increased, indicating the formation of **Benzo-Ant**. These results revealed that **BCOD-DK** and **Benzo-DK** were quantitatively converted to the corresponding **BCOD-Ant** and **Benzo-Ant**, respectively, on photoirradiation. Finally, thermogravimetric analysis of **BCOD-Ant** was carried out (Figure 2). The mass loss associated with the transition from **BCOD-Ant** to **Benzo-Ant** started at 149 °C and finished at 207 °C. Thus, we can completely control the four different optical performances of these BODIPYs solely by irradiation and heating.

The UV/Vis absorption and fluorescence spectra of the BODIPYs in dichloromethane are shown in Figure 4 and Table 1. The UV/Vis absorption spectrum of **BCOD-DK** shows a peak at 534 nm associated with a shoulder at 500 nm,

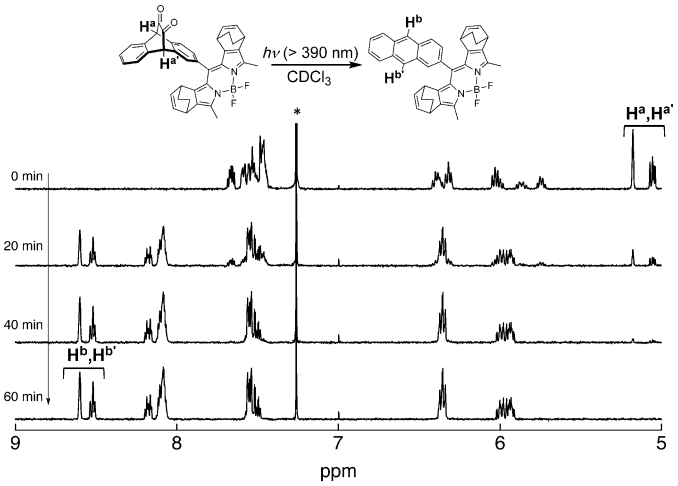

Figure 3. Changes in ^{1}H NMR spectra during photolysis of **BCOD-DK** in $CDCl_3$ under an argon atmosphere. The reaction was monitored at 0, 20, 40 and 60 min. $\lambda_{EX} > 390$ nm. The solvent peak is marked with an asterisk.

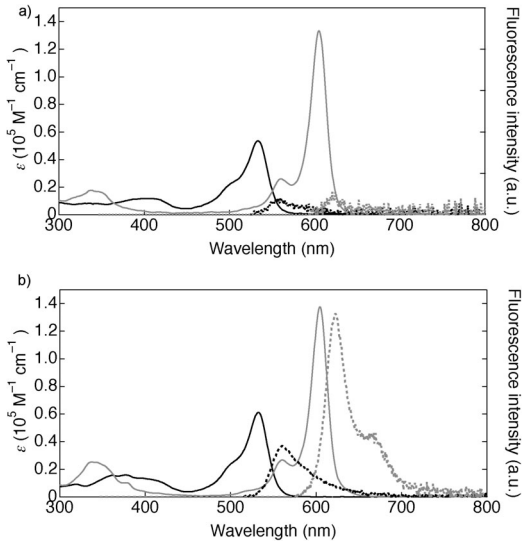

Figure 4. UV/Vis absorption (solid line) and fluorescence (dotted line) spectra in dichloromethane. a) **BCOD-DK** (black) and **Benzo-DK** (gray). b) **BCOD-Ant** (black) and **Benzo-Ant** (gray).

Table 1. UV/Vis absorption peaks λ_{abs}, fluorescence peaks λ_F, quantum yields Φ_F, and redox potentials E_{ox} and E_{red} of BODIPY dyes.

Dye	λ_{abs} [nm] (lg ε)		λ_F [nm] (Φ_F)[a]		E_{ox}[d] [V]	E_{red}[d] [V]
	CH_2Cl_2	Toluene	CH_2Cl_2	Acetonitrile		
BCOD-DK	534 (4.73)	560 (0.79)[b]	560 (0.08)[b]	553 (0.08)[b]	+0.65	−1.60, −1.76
Benzo-DK	560 (4.41) 605 (5.13)	623 (0.84)[c]	624 (0.08)[c]	617 (0.08)[c]	+0.32	−1.60, −1.72
BCOD-Ant	534 (4.78)	565 (0.73)[b]	560 (0.61)[b]	556 (0.61)[b]	+0.65	−1.69
Benzo-Ant	560 (4.422) 605 (5.12)	626 (0.90)[c]	622 (0.90)[c]	615 (0.83)[c]	+0.29	−1.69

[a] Measured on an Absolute PL Quantum Yield Measurement System C9920-02. [b] Excited at 500 nm. [c] Excited at 562 nm. [d] Potentials were measured by CV in 0.1 M nBu$_4$NPF$_6$/dichloromethane. The values (vs. Fc/Fc$^+$) were obtained by cyclic voltammetry. Scan rate: 0.1 Vs^{-1}, [BODIPY] = 0.1 mM. Working electrode: glassy carbon, counter electrode: Pt, reference electrode: Ag/$AgNO_3$.

while **Benzo-DK** shows an absorption peak at 605 nm with a shoulder at 560 nm. The 71 nm redshift for **Benzo-DK** relative to **BCOD-DK** is caused by the π expansion of the BODIPY moiety. **BCOD-Ant** and **Benzo-Ant** show similar UV/Vis absorption spectra to **BCOD-DK** and **Benzo-DK**, respectively, and this indicates little through-bond electronic interaction between the *meso*-anthryl part and the BODIPY framework. The absorption coefficient for the n–π* transition of the diketone moiety is about 1000 $M^{-1}cm^{-1}$, which is 60 times lower than that of the peak maximum of the BODIPY moiety; therefore, the typical n–π* absorption peaks around 460 nm cannot be observed for **BCOD-DK** and **Benzo-DK**. The fluorescence spectra in dichloromethane showed different trends to the absorption spectra. Whereas **BCOD-DK** emitted only weakly at 560 nm with a fluorescence quantum yield Φ_F of 0.08, **BCOD-Ant** had a Φ_F value of 0.61 at the same wavelength. Similarly, **Benzo-DK** emitted at 624 nm with a low Φ_F of 0.08, whereas the Φ_F value of **Benzo-Ant** reached 0.90 at 622 nm. Thus, the fluorescence wavelengths are almost the same before and after the photoreaction, whereas fluorescence quantum yields are drastically increased on photoinduced activation associated with the decarbonylative aromatization.

The fluorescence properties of BODIPYs were also measured in toluene and acetonitrile (Table 1 and Supporting Information, Figure S3). The fluorescence spectra of **BCOD-Ant** and **Benzo-Ant** exhibited small blueshifts on increasing the solvent polarity. However, the fluorescence properties of **BCOD-DK** and **Benzo-DK** were dramatically different. The Φ_F values of **BCOD-DK** and **Benzo-DK** were as low as 0.08 in dichloromethane, but in nonpolar toluene they were 0.79 for **BCOD-DK** and 0.84 for **Benzo-DK**. In aprotic, high-polarity acetonitrile, the Φ_F values of **BCOD-DK** and **Benzo-DK** were 0.08, as in dichloromethane. To confirm the correlation between the fluorescence quantum yields and solvent polarity, Φ_F values of **BCOD-DK** and **Benzo-DK** were measured in toluene/dichloromethane mixtures to change the solvent polarity systematically. The Φ_F values of **BCOD-DK** and **Benzo-DK** decreased gradually with increasing fraction of dichloromethane (Figure 5 and Supporting Information, Table S2). The dielectric constants ε of the solvent mixtures were calculated by means of the ratio of the two solvents. The Φ_F values are constant above $\varepsilon = 8$ for **BCOD-DK** and above $\varepsilon = 5$ for **Benzo-DK**. Thus the Φ_F values in dichloromethane and in acetonitrile are almost the same. This solvent effect suggested that it was fluorescence quenching owing to an intramolecular electron-transfer process.[10]

The fluorescence lifetimes τ_F of BODIPYs were measured by femtosecond laser flash photolysis in each solvent with excitation at 365 nm (Supporting Information, Figures S4–S7 and Table 2). The τ_F values of **BCOD-Ant** were determined to be 5.59 ns in toluene, 5.87 ns in dichloromethane, and 5.96 ns in acetonitrile. Because of the

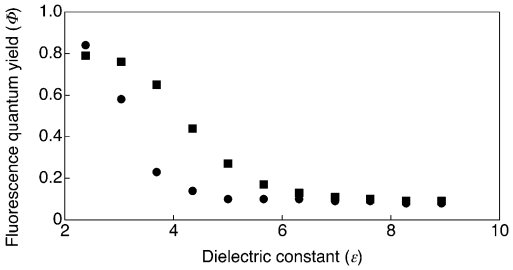

Figure 5. Correlation between Φ_F and ε for **BCOD-DK** (■) and **Benzo-DK** (●).

effect of the solvent relaxation, τ_F becomes longer in more polar solvents. The τ_F values of **Benzo-Ant** showed a similar tendency: 5.68 (toluene), 6.29 (dichloromethane), and 6.41 ns (acetonitrile). The values for **BCOD-DK** and **Benzo-DK** in toluene were 6.29 and 6.17 ns, respectively, analyzed by single-exponential decay similarly to the anthracene adducts. On the other hand, the τ_F values in dichloromethane and acetonitrile were analyzed by double-exponential curves. The shorter τ_F of **BCOD-DK** was 0.59 ns in dichloromethane and acetonitrile, and those of **Benzo-DK** were 0.50 ns in dichloromethane and 0.54 ns in acetonitrile. The longer components of **BCOD-DK** and **Benzo-DK** were 6.35 and 5.46 ns in dichloromethane and 6.71 and 5.63 ns in acetonitrile. The longer lifetimes were assigned to **BCOD-Ant** and **Benzo-Ant** generated by irradiation during the measurement.

The electrochemical properties of the BODIPY dyes were investigated by cyclic voltammetry (CV) in dichloromethane containing 0.1 M nBu$_4$NPF$_6$ as supporting electrolyte. The results are summarized in Table 1 and Figure S8 (Supporting Information). The one-electron oxidation potentials [$E_{ox}^{1/2}$ vs. ferrocene/ferrocenium (Fc/Fc$^+$)] of **BCOD-DK**, **Benzo-DK**, **BCOD-Ant**, and **Benzo-Ant** were 0.65, 0.32, 0.62, and 0.29 V, respectively. The $E_{ox}^{1/2}$ values of **BCOD-DK** and **BCOD-Ant** were similar to each other, and **BCOD-DK** showed a slightly higher $E_{ox}^{1/2}$ value of 0.03 V. **Benzo-DK** and **Benzo-Ant** showed a similar trend to the BCOD pair. Thus, the first oxidation occurred at the BODIPY moiety and π expansion lowered the oxidation potential from 0.65 to 0.32 and 0.62 to 0.29 V for **BCOD-BODIPY**s and **Benzo-BODIPY**s, respectively. Each of **BCOD-Ant** and **Benzo-Ant** showed one reduction peak at −1.69 V, whereas **BCOD-DK** and **Benzo-DK** showed two reversible reduction waves: −1.60 and −1.76 V for **BCOD-DK** and −1.60 and −1.72 V for **Benzo-**

Table 2. Fluorescence lifetimes in various solvents.

Toluene/CH_2Cl_2	ε	τ_F[a] [ns] (A) [χ^2]			
		BCOD-DK[b]	**Benzo-DK**[c]	**BCOD-Ant**[b]	**Benzo-Ant**[c]
100/0	2.38	6.29 [1.44]	6.17 [1.49]	5.59 [1.52]	5.68 [1.36]
90/10	3.03	–	4.65 [1.90]	–	–
80/20	3.69	5.81 [1.40]	–	–	–
70/30	4.35	4.20 [1.46]	–	–	–
0/100	8.93	0.59 (0.79), 6.35 (0.21) [1.36]	0.50 (0.53), 5.46 (0.47) [1.13]	5.87 [1.51]	6.29 [1.51]
–[d]	35.9	0.59 (0.92), 6.71 (0.08) [1.36]	0.54 (0.64), 5.63 (0.36) [1.24]	5.96 [1.37]	6.41 [1.59]

[a] Excited at 365 nm; A:propotion of the components. [b] Monitored at 560 nm. [c] Monitored at 624 nm. [d] Acetonitrile.

DK. The first reduction potentials of **BCOD-DK** and **Benzo-DK** were shifted to the cathodic side compared to those of **BCOD-Ant** and **Benzo-Ant**. The first reductions of **BCOD-DK** and **Benzo-DK** were assigned to the reduction of diketone moieties.

To elucidate the fluorescence quenching mechanism of **BCOD-DK** and **Benzo-DK**, the energy level of the charge-separated (CS) state (BODIPY$^{\bullet+}$-DK$^{\bullet-}$) was determined from the redox potential.[15] The driving forces $-\Delta G_{CR}$ for the intramolecular charge-recombination processes from the anion radical of the diketone moiety (DK$^{\bullet-}$) to the cation radical of the BODIPY moiety (BODIPY$^{\bullet+}$) were calculated by using Equations (1) and (2), in which e is the elementary charge, E_{ox}(BOD$^{\bullet+}$/BOD) the oxidation potential of BODIPY moieties in dichloromethane, E_{red}(DK/DK$^{\bullet-}$) the reduction potential of DK moieties in dichloromethane, ε_s and ε_r are the static dielectric constants of the solvent used for estimating energy level and measuring the redox potential, respectively, and R^+ and R^- the radii of BODIPY and DK moieties, respectively.

$$-\Delta G_{CR} = [E_{ox}(\mathrm{BOD}^{\bullet+}/\mathrm{BOD}) - E_{red}(\mathrm{DK}/\mathrm{DK}^{\bullet-})] + \Delta G_S \quad (1)$$

$$\Delta G_S = e^2/(4\pi e_0)[(1/(2R^+) + 1/(2R^-) - (1/R_{cc})(1/\varepsilon_s) - [1/(2R^+) + 1/(2R^-)(1/\varepsilon_r)] \quad (2)$$

The molecular structures were estimated from the optimized geometries obtained by DFT calculations (Figure S9 in the Supporting Information), whereby R_{cc} is the center-to-center distance between BODIPY and DK moieties and R^+ and R^- are the radii of cation and anion radicals, respectively: $R^+ = 3.4$ Å for the BCOD-fused BODIPY, $R^+ = 5.4$ Å (maximum) for benzo-fused BODIPY, $R^- = 1.5$ Å for the diketone, 7.7 Å for **BCOD-DK**, and $R_{cc} = 7.0$ Å for **Benzo-DK**. The driving forces $-\Delta G_{CS}$ for the intramolecular CS processes from the BODIPY unit to the diketone moiety were determined by using Equation (3) in which ΔE_{0-0}(BODIPY) is the energy of the singlet excited-state of the BODIPY moiety (^{1}BODIPY*).

$$-\Delta G_{CS} = \Delta E_{0-0}(\mathrm{BODIPY}) - (-\Delta G_{CR}) \quad (3)$$

The energy levels of ^{1}BODIPY* were calculated from the absorption and fluorescence spectra of **BCOD-Ant** and **Benzo-Ant**. In the case of **BCOD-DK**, the ^{1}BODIPY* level (2.27 eV) was higher than the CS state (2.04 eV) in dichloromethane (Figure 6). Thus, electron transfer from the BODIPY moiety to the DK moiety occurs to give the CS state in dichloromethane. This electron transfer causes the lower fluorescence intensity ($\Phi_F = 0.08$) of **BCOD-DK** in dichloromethane. However, the energy level of the CS state in toluene is raised because of the smaller ε value in Equation (1). Since the energy was calculated to be 3.60 eV in toluene, the CS level of **BCOD-DK** in toluene is higher than the ^{1}BODIPY* level and fluorescence was observed. Although the Born equation does not give correct values for ΔG_S in nonpolar solvents such as toluene because of the overestimation of the polarity, the values of $-\Delta G_{CR}$ were estimated

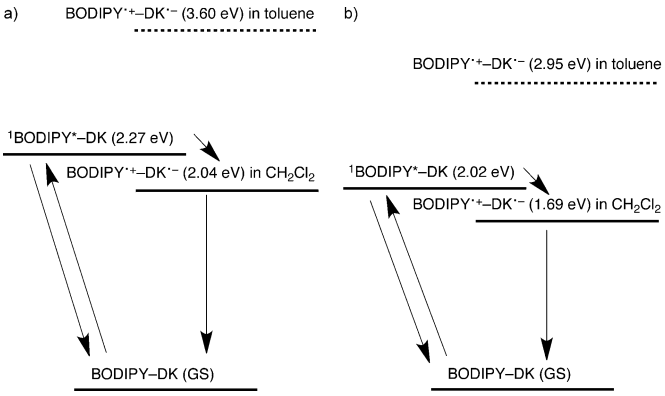

Figure 6. Energy diagrams of a) **BCOD-DK** and b) **Benzo-DK** in dichloromethane.

tentatively. A similar phenomenon was observed for **Benzo-DK** for the same reason. The CS level of **Benzo-DK** was estimated to be 1.71 and 3.25 eV in dichloromethane and toluene, respectively, and the value in toluene is also higher than that of the singlet excited state of benzo-fused BODIPY. Thus, the fluorescence of **Benzo-DK** was not quenched in toluene. In addition, the energy difference between the CS level and singlet excited state for **Benzo-DK** in dichloromethane is larger than that of **BCOD-DK**; therefore, fluorescence quenching was effectively induced by the increase in solvent polarity.

To investigate the decay process of the excited state, femtosecond transient absorption spectra were measured for each BODIPY in toluene, dichloromethane, and acetonitrile (Figures S12–S15 and Table S4 in the Supporting Information). When **BCOD-Ant** was irradiated at 500 nm, it showed clear bleaching of the ground state at 480–650 nm, while a new absorption band appeared around 450 nm. This new absorption band corresponded to the excited singlet state of BODIPY.[16] Decay to the ground state occurred with a lifetime of 6.3 ns in toluene. **BCOD-DK** showed a similar bleaching and decay profile (6.9 ns) to **BCOD-Ant** in toluene on irradiation at 450 nm. In contrast, the decay time shortened to 248 ps (dichloromethane) and 351 ps (acetonitrile), which agreed with the fluorescence lifetime of **BCOD-DK**. However, after irradiation only the singlet excited state of BODIPY was observed, and no other transient species, such as the radical cation of BODIPY, were detected (Supporting Information, Figure S16).[17] Transient absorption measurements were also performed with **Benzo-Ant** and **Benzo-DK** in each solvent. In both cases, laser irradiation caused bleaching of the ground state of the BODIPY moiety around 600 nm and a broad rise at higher energy. The decay time of **Benzo-Ant** was 4.8 ns, while those of **Benzo-DK** were 3.6 ns (toluene), 80 ps (dichloromethane), and 101 ps (acetonitrile), respectively. Near-infrared (NIR) transient absorption spectra were also measured, but evidence for the radical cation of the BODIPY moiety was not observed (Supporting Information Figure S17). This is probably because back electron transfer from BODIPY$^{\bullet+}$-DK$^{\bullet-}$ is faster than intramolecular electron transfer from ^{1}BODIPY* to DK.[18]

Conclusion

Photochemical generation of the highly-fluorescent BODIPYs **BCOD-Ant** and **Benzo-Ant** from the weakly fluorescent BODIPYs **BCOD-DK** and **Benzo-DK** has been achieved. The optical properties dramatically changed before and after the conversion of DK to anthracene, whereas the intrinsic color of BODIPY was only slightly altered by photoactivation. BODIPYs with a DK moiety showed lower fluorescence quantum yields Φ_F in dichloromethane and acetonitrile. The Φ_F values increased in a nonpolar solvent such as toluene. The dramatic solvent dependency of Φ_F and fluorescence lifetimes suggested intramolecular electron transfer from the BODIPY moiety to diketone moiety.

Experimental Section

Materials

Commercially available reagents and solvents for syntheses were of reagent grade and used without further purification. TLC and gravity column chromatography were performed on Art. 5554 (Merck KGaA) plates and silica gel 60N (Kanto Chemical), respectively. For spectral measurements, spectral-grade toluene, dichloromethane, methanol, and acetonitrile were purchased from Nacalai Tesque. The dichloromethane used for CV measurements was distilled from CaH_2.

Synthesis

13-Oxo-9,10,11,15-tetrahydro-9,10-epidioxoloanthracene-3-carbaldehyde (2): A solution of 2-formylanthracene **1** (0.10 g, 0.49 mmol) and vinylene carbonate (0.50 mL, 7.90 mmol) in xylenes (10 mL) was mixed at 160 °C in an autoclave for 3 d. After removal of the solvent in vacuo, the residue was purified by silica-gel column chromatography with chloroform and recrystallization from $CHCl_3$/hexane to give **2** as a mixture of two stereoisomers as white powder. Yield: 78% (0.11 g, 0.38 mmol); ^{1}H NMR ($CDCl_3$, 400 MHz): δ = 9.99 (s, 1H, CHO), 7.92 (s, 1H), 7.79 (dt, J = 4.0, 7.2 Hz, 1H), 7.57 (d, 1H, J = 7.8 Hz), 7.42 (m, 2H), 7.30 (m, 2H), 4.95 (t, J = 1.6 Hz, 1H), 4.92 (t, J = 1.6 Hz, 1H), 4.83 (m, 2H); ^{13}C NMR ($CDCl_3$, 100 MHz): δ = 191.59, 191.33, 153.76, 153.72, 144.44, 143.30, 138.94, 137.62, 136.94, 136.38, 136.02, 135.84, 135.54, 135.00, 130.46, 130.22, 138.30, 128.24, 128.14, 128.09, 127.34, 126.93, 126.86, 126.81, 126.38, 125.91, 125.87, 125.81, 76.00, 75.96, 75.79, 75.66, 48.02, 47.96, 47.63, 47.63; MS (ESI): *m/z*: 315 $[M+Na]^+$; HRMS (ESI) found: *m/z* 315.06338; calcd for $C_{18}H_{12}NaO_4$: 315.06333 $[M+Na]^+$.

Compound 4: Six drops of TFA were added to a solution of isoindole **3** (0.31 g, 1.9 mmol) and **2** (0.265 g, 0.91 mmol) in dry dichloromethane (98 mL) under an argon atmosphere. The mixture was stirred for 3 h in the dark. DDQ (0.45 g, 2.0 mmol) was added, and the mixture was stirred for an additional 20 min. After addition of *N,N*-diisopropylethylamine (3.0 mL) and BF_3·OEt_2 (3.0 mL), the mixture was stirred for 30 min. The reaction mixture was poured into water and extracted with dichloromethane. The organic layer was washed with water and brine, dried over sodium sulfate, and concentrated under reduced pressure. The residue was purified by silica-gel column chromatography with chloroform. Recrystallization from chloroform/methanol gave **4** as a mixture of eight stereoisomers as an orange powder. Yield: 55% (0.32 g, 0.50 mmol); ^{1}H NMR ($CDCl_3$, 400 MHz, mixture of stereoisomers): δ = 7.68–7.65 (m, 1H), 7.60–7.43 (m, 6H), 6.41–5.98 (m, 3H), 5.90–5.72 (m, 1H), 5.05–4.78 (m, 2H), 3.83–3.77 (m, 2H), 2.80–2.10 (m, 2H), 2.48 (s, 3H), 2.44 (s, 3H), 1.59–0.86 (m, 8H); the ^{13}C NMR spectrum ($CDCl_3$, 100 MHz) was measured, but the number of peaks did not match because of the presence of isomers; MS (ESI): *m/z*: 660 $[M+Na]^+$; HRMS (ESI) found: *m/z* 660.24868; calcd for $C_{40}H_{33}B_1F_2N_2NaO_3$: 660.24863 $[M+Na]^+$.

Compound 5: Potassium carbonate (3.00 g) was added to a solution of **4** (0.27 g, 0.42 mmol) in THF (16 mL), methanol (16 mL), and water (8.1 mL). The solution was stirred overnight at room temperature. The reaction mixture was quenched with water and extracted with chloroform. The organic layer was washed with water and brine, dried over sodium sulfate, and concentrated under reduced pressure. The residue was purified by column chromatography on silica gel with ethyl acetate/chloroform (1/4) to give **5** as a mixture of eight stereoisomers as orange powder. Yield: 79% (0.20 g, 0.33 mmol); ^{1}H NMR (CD_2Cl_2, 400 MHz): δ = 7.43–7.20 (m, 4H), 7.19–7.06 (m, 3H), 6.37–6.19 (m, 2H), 6.11–5.68 (m, 2H), 4.48–4.35 (m, 2H), 4.08–3.94 (m, 2H), 3.76–3.69 (m, 2H), 2.62–2.20 (m, 8H), 1.41–0.63 (m, 8H); ^{13}C NMR spectrum (CD_2Cl_2, 100 MHz) was measured, but the number of peaks did not match because of the presence of isomers; MS (ESI): *m/z* 634 $[M+Na]^+$; HRMS (ESI) found: *m/z* 634.26933; calcd for $C_{39}H_{35}B_1F_2N_2NaO_2$: 634.26937 $[M+Na]^+$.

BCOD-DK: Under an argon atmosphere, dry DMSO (1.0 mL, 14 mmol) and dry dichloromethane (8.5 mL) were cooled to −60 °C. Trifluoroacetic anhydride (0.5 mmol, 3.5 mmol) was added dropwise over 5 min. After the solution was stirred for 10 min, **5** (0.15 g, 0.33 mmol) in dry dichloromethane (5.0 mL) was added dropwise over 10 min. After the solution was stirred for 2 h, *N,N*-diisopropylethyamine (2.0 mL, 12 mmol) was added over 5 min. The solution was stirred for 60 min and left to warm to room temperature. The reaction was quenched with water. The organic layer was washed with water, 1 M HCl, and brine, dried over sodium sulfate, and concentrated under reduced pressure. The residue was purified by silica-gel column chromatography with dichloromethane. Recrystallization from dichloromethane/hexane gave **BCOD-DK** as a mixture of four stereoisomers as an orange powder. Yield: 30% (0.045 g, 0.074 mmol); ^{1}H NMR ($CDCl_3$, 400 MHz, mixture of stereoisomers): δ = 7.69–7.43 (m, 7H), 6.42–5.72 (m, 2H), 5.18–5.04 (m, 2H), 3.83–3.76 (m, 2H), 2.53 (s, 3H), 2.51 (s, 3H), 2.47–2.10 (m, 2H), 1.44–0.88 (m, 8H); ^{13}C NMR spectrum ($CDCl_3$, 100 MHz) was measured, but the number of peaks did not match because of the presence of isomers: δ = 183.38, 183.35, 183.29, 183.17, 183.13, 150.36, 150.30, 149.81, 148.50, 148.48, 148.03, 148.00, 147.98, 147.89, 138.73, 138.70, 138.34, 138.25, 138.23, 136.96, 136.93, 136.36, 136.33, 136.28, 136.14, 136.12, 136.09, 136.06, 135.97, 135.95, 135.90, 135.88, 135.36, 135.32, 135.22, 134.52, 134.49, 134.47, 134.43, 134.40, 134.37, 133.69, 133.63, 133.60, 133.54, 133.52, 133.46, 133.39, 130.38, 129.99, 129.86, 129.81, 129.78, 129.76, 129.67, 127.78, 127.41, 127.35, 127.21, 127.16, 127.10, 127.03, 126.61, 126.39, 126.36, 126.32, 126.30, 126.19, 126.12, 126.06, 59.93, 59.89, 59.87, 59.85, 59.82, 35.43, 35.41, 35.35, 35.32, 35.13, 35.10, 35.07, 32.87, 32.79, 32.77, 26.43, 26.36, 26.32, 26.30, 26.27, 25.99, 25.96, 25.89, 25.82, 25.78, 25.72, 12.61, 12.58, 12.56 ppm; MS (ESI): *m/z* 662 $[M+Na]^+$; HRMS (ESI) found: *m/z* 662.26420; calcd for $C_{40}H_{35}B_1F_2N_2NaO_3$: 662.26428 $[M+Na]^+$.

Benzo-DK: **BCOD-DK** was heated to 220 °C in the solid phase under vacuum for 1 h. After cooling to room temperature, **Benzo-DK** was obtained quantitatively as a blue solid. ^{1}H NMR ($CDCl_3$, 400 MHz): δ = 7.78 (d, 1H, J = 7.5 Hz), 7.68–7.57 (m, 5H), 7.53–7.46 (m, 3H), 7.13 (t, J = 6.9 Hz, 1H), 7.00 (m, 2H), 6.70 (t, J = 6.9 MHz, 1H), 6.02 (d, J = 8.4 Hz, 1H), 5.81 (d, J = 8.4 Hz, 1H), 5.24 (s, 1H), 5.07 (s, 1H), 2.97 (s, 3H), 2.95 (s, 3H); ^{13}C NMR ($CDCl_3$, 100 MHz):

δ = 183.49, 183.29, 151.50, 150.62, 136.53, 136.46, 136.31, 134.59, 134.52, 133.69, 133.43, 132.85, 130.68, 130.46, 130.25, 129.84, 129.76, 129.40, 128.65, 127.41, 127.39, 126.59, 126.54, 124.52, 124.26, 124.21, 123.72, 122.23, 122.16, 120.60, 120.53, 60.03, 59.84, 12.47, 12.47 ppm; MS (ESI): *m/z* 606 $[M+Na+MeOH]^+$; HRMS (ESI) found: *m/z* 606.20153; calcd for $C_{36}H_{27}B_1F_2N_2NaO_3$:606.20168 $[M+Na+MeOH]^+$.

BCOD-Ant: Photoirradiation of **BCOD-DK** was performed at 390 nm in an NMR tube under an argon atmosphere and monitored by ^{1}H NMR spectroscopy. After removal of the solvent, **BCOD-Ant** was obtained as a mixture of four stereoisomers as an orange powder. ^{1}H NMR ($CDCl_3$, 400 MHz): δ = 8.60 (s, 1H), 8.52 (t, *J* = 6.0 Hz, 1H), 8.18 (m, 1H), 8.12–8.07 (m, 3H), 7.57–7.49 (m, 3H), 6.36 (m 2H), 6.02–5.92 (m, 2H), 3.82 (m, 2H), 2.69 (m, 2H), 2.56 (s, 6H), 1.40–1.32 (m, 4H), 1.18–1.09 (m, 4H); ^{13}C NMR ($CDCl_3$, 100 MHz): δ = 150.41, 150.33, 150.26, 147.66, 147.64, 147.60, 147.57, 139.05, 138.33, 138.29, 138.24, 135.81, 133.94, 133.88, 132.35, 132.28, 132.26, 132.24, 131.70, 131.59, 131.43, 131.18, 131.15, 131.13, 130.58, 130.53, 130.50, 128.96, 128.63, 128.35, 128.27, 128.24, 128.20, 128.07, 127.54, 127.47, 127.07, 127.02, 126.96, 126.72, 126.58, 126.56, 126.42, 126.13, 126.13, 126.04, 35.42, 35.39, 32.89, 26.50, 26.45, 26.43, 26.38, 25.96, 25.92, 25.87, 25.83, 12.62 ppm (some peaks were missing due to overlap); MS (ESI): *m/z* 574 $[M+Na]^+$; HRMS (ESI) found: *m/z* 574.24803; calcd for $C_{37}H_{31}B_1F_2N_2Na$: 574.24824 $[M+Na]^+$.

Benzo-Ant: Photoirradiation of **Benzo-DK** was performed at 390 nm in an NMR tube under argon atmosphere and monitored by ^{1}H NMR spectroscopy. After removal of the solvent, **Benzo-Ant** was obtained as blue solid. ^{1}H NMR ($CDCl_3$, 400 MHz): δ = 8.66 (s, 1H), 8.51 (s 1H), 8.32 (d, *J* = 8.8 Hz, 1H), 8.23 (s, 1H), 8.13 (d, *J* = 8.4 Hz, 1H), 8.06 (d, *J* = 8.8 Hz, 1H), 7.66 (d, *J* = 8.0 Hz, 2H), 7.60–7.52 (m, 3H), 7.05 (t, *J* = 8.0 Hz, 2H), 6.84 (t, *J* = 7.6 Hz, 2H), 6.22 (d, *J* = 8.0 Hz, 2H), 3.00 (s, 6H); ^{13}C NMR ($CDCl_3$, 100 MHz): δ = 150.51, 134.62, 133.84, 132.38, 132.20. 131.68, 131.24, 131.18, 130.56, 129.68, 128.85, 128.64, 128.24, 128.23, 127.16, 126.69, 126.36, 126.10, 126.02, 124.84, 123.79, 121.97, 121.24, 12.51; MS (ESI): *m/z* 518 $[M+Na]^+$; HRMS (ESI) found: *m/z* 518.18645; calcd for $C_{33}H_{23}B_1F_2N_2Na$: 518.18564 $[M+Na]^+$.

General methods

^{1}H and ^{13}C NMR spectra were recorded with a JEOL JNM-ECX 400 spectrometer at ambient temperature by using TMS as internal standard. Mass spectra were measured on a JEOL JMS-700 spectrometer. Thermogravimetric analyses were carried out by using an SII Nanotechnology DSC/TG-DTA 6200.

Optical spectroscopy

UV/Vis spectra were measured with a JASCO UV/Vis/NIR spectrophotometer V-570. Fluorescence quantum yields were measured on an Absolute PL Quantum Yield Measurement System C9920-02 (Hamamatsu Photonics). The fluorescence decays were measured by using a C4780 picosecond fluorescence lifetime measurement device (Hamamatsu Photonics). A Mira Model 900-F & Pulse Switch femtosecond pulse laser was used, and the excitation light wavelength was 365 nm from a Coherent Verdi V-5 Nd:YVO4 laser.

Photochemical reactions

Photochemical reactions were carried out in an NMR tube irradiated by a metal-halide lamp (Nippon P. I. PCS-UMX375RC, 375 W) through a UV cutoff filter (390 nm) under an argon atmosphere and monitored with a JNM-ECX 400 spectrometer.

Cyclic voltammetry

CV measurements were conducted in a solution of 0.1 M nBu$_4$NPF$_6$ in dry dichloromethane or acetonitrile at a scan rate of 100 mV s^{-1} at room temperature in an argon-filled cell. A glassy carbon electrode and a Pt wire were used as working and counter electrode, respectively. An Ag/Ag^+ electrode was used as a reference electrode, which was normalized with the half-wave potential of the Fc/Fc^+ redox couple.

X-ray crystallography

Single-crystal X-ray diffraction data were collected at 90 K on a Bruker APEX II X-Ray diffractometer equipped with a large-area CCD detector by using graphite-monochromated $Mo_{K\alpha}$ radiation (λ = 0.71073 Å). The structure was solved by direct method (SHELXS-97) and refined with SHELX-97.[19] CCDC 1012964 contains the supplementary crystallographic data for this paper. These data can be obtained free of charge from The Cambridge Crystallographic Data Centre via www.ccdc.cam.ac.uk/data_request/cif.

Laser flash photolysis

Transient absorption spectra were measured by femtosecond pump–probe experiments. Samples were exited at 500 or 605 nm by using an optical parametric amplifier (TOPAS, Light Conversion Ltd.) with an amplified mode-locked Ti:sapphire laser (Spitfire and Tsunami, Spectra-Physics). Excitation intensity was 30–70 μW with a repetition rate of 0.5 kHz, obtained by using a chopper (MODEL 3501, New Focus Inc.). Absorption transients were probed by delayed pulses of a femtosecond white-light continuum generated by focusing fundamental laser pulse into a D_2O cell (for visible region) or a sapphire plate (for NIR region) and detected by a polychromator–CCD combination (Spectra Pro-275 and Spec-10, Acton Research Co. and Princeton Instruments) for the visible region or a polychromator–InGaAs combination (Spectra Pro-2150 and OMA V, Acton Research Co. and Princeton Instruments) for NIR region. The temporal resolution was 100 fs.

Theoretical calculations

The geometries of **BCOD-DK** and **Benzo-DK** were fully optimized by DFT. The functional and basis set used in the DFT calculations were the Becke's three-parameter hybrid functional combined with the Lee–Yang–Parr correlation functional (B3LYP)[20] and the 6-31G(d) basis set,[21] respectively. Equilibrium geometries were verified by frequency calculations in which no imaginary frequency was found. All calculations were carried out with the Gaussian 09 suite of programs.[22]

Acknowledgements

The authors thank Ms. Y. Nishikawa and Ms. Y. Nishiyama for the measurement of mass spectra, Mr. Y. Okajima for the fluorescence lifetime measurements, Mr. F. Asanoma for two-dimensional NMR measurement, and Dr. K. Yoza of Bruker AXS for his help in refinement of the crystal structure. T.A. sincerely appreciates the financial support from the Japan Society for the Promotion of Science. This work was partly supported by Grants-in Aid (No. 25288092 to H.Y.), the Green Photonics Project in NAIST, and the program for promoting the enhance-

ment of research universities in NAIST supported by MEXT and JSPS Grant-in-Aid for Scientific Research (No. 26105004 to H.Y.).

Keywords: dyes/pigments · electron transfer · fluorescence · molecular switches · photochemistry

[1] a) M. Irie, T. Fukaminato, T. Sasaki, N. Tamai, T. Kawai, *Nature* **2002**, *420*, 759 – 760; b) E. Betzig, G. H. Patterson, R. Sougrat, O. W. Lindwasser, S. Olenych, J. S. Bonifacino, M. W. Davidson, J. Lippincott-Schwartz, H. F. Hess, *Science* **2006**, *313*, 1642 – 1645; c) M. Bates, B. Huang, G. T. Dempsey, X. Zhuang, *Science* **2007**, *317*, 1749 – 1753; d) C. Yun, J. You, J. Kim, J. Huh, E. Kim, *J. Photochem. Photobiol. C* **2009**, *10*, 111 – 129.

[2] a) H. H. Pham, I. Gourevich, J. K. Oh, J. E. N. Jonkman, E. Kumacheva, *Adv. Mater.* **2004**, *16*, 516 – 520; b) G. Jiang, S. Wang, W. Yuan, Z. Zhao, A. Duan, C. Xu, L. Jiang, Y. Song, D. Zhu, *Eur. J. Org. Chem.* **2007**, 2064 – 2067; c) J. W. Chung, S.-J. Yoon, S.-J. Lim, B.-K. An, S. Y. Park, *Angew. Chem. Int. Ed.* **2009**, *48*, 7030 – 7034; *Angew. Chem.* **2009**, *121*, 7164 – 7168; d) M. – J. Teng, X.-R. Jia, S. Yang, X.-F. Chen, Y. Wei, *Adv. Mater.* **2012**, *24*, 1255 – 1261; e) H. Sun, S. Liu, W. Lin, K. Y. Zhang, W. Lv, X. Huang, F. Huo, H. Yang, G. Jenkins, Q. Zhao, W. Huang, *Nat. Commun.* **2014**, *5*, 3601; f) X. Zhu, R. Liu, Y. Li, H. Huang, Q. Wang, D. Wang, X. Zhu, S. Liu, H. Zhu, *Chem. Commun.* **2014**, *50*, 12951 – 12954; g) S. Mukherjee, P. Thilagar, *Chem. Eur. J.* **2014**, *20*, 9052 – 9062.

[3] G. Ulrich, R. Ziessel, A. Harriman, *Angew. Chem. Int. Ed.* **2008**, *47*, 1184 – 1201; *Angew. Chem.* **2008**, *120*, 1202 – 1219.

[4] a) N. Boens, V. Leen, W. Dehaen, *Chem. Soc. Rev.* **2012**, *41*, 1130 – 1172; b) C. N. Baki, E. U. Akkaya, *J. Org. Chem.* **2001**, *66*, 1512 – 1513; c) W. Qin, M. Baruah, W. M. De Borggraeve, N. Boens, *J. Photochem. Photobiol. A* **2006**, *183*, 190 – 197; d) Y. Urano, D. Asanuma, Y. Hama, Y. Koyama, T. Barrett, M. Kamiya, T. Nagano, T. Watanabe, A. Hasegawa, P. L. Choyke, H. Kobayashi, *Nat. Med.* **2009**, *15*, 104 – 109; e) D. P. Kennedy, C. M. Kormos, S. C. Burdette, *J. Am. Chem. Soc.* **2009**, *131*, 8578 – 8586; f) Y. Ni, J. Wu, *Org. Biomol. Chem.* **2014**, *12*, 3774 – 3791; g) M. J. Hall, L. T. Allen, D. F. O'Shea, *Org. Biomol. Chem.* **2006**, *4*, 776 – 780; h) X. Peng, J. Du, J. Fan, J. Wang, Y. Wu, J. Zhao, S. Sun, T. Xu, *J. Am. Chem. Soc.* **2007**, *129*, 1500 – 1501; i) B. Wang, P. Li, F. Yu, J. Chen, Z. Qu, K. Han, *Chem. Commun.* **2013**, *49*, 5790 – 5792.

[5] a) A. B. Descalzo, H.-J. Xu, Z.-L. Xue, K. Hoffmann, Z. Shen, M. G. Weller, X.-Z. You, K. Rurack, *Org. Lett.* **2008**, *10*, 1581 – 1584; b) K. Umezawa, Y. Nakamura, H. Makino, D. Citterio, K. Suzuki, *J. Am. Chem. Soc.* **2008**, *130*, 1550 – 1551; c) G. Ulrich, S. Goeb, A. De Nicola, P. Retailleau, R. Ziessel, *J. Org. Chem.* **2011**, *76*, 4489 – 4505; d) S. G. Awuah, J. Polreis, V. Biradar, Y. You, *Org. Lett.* **2011**, *13*, 3884 – 3887; e) L. Zeng, C. Jiao, X. Huang, K.-W. Huang, W.-S. Chin, J. Wu, *Org. Lett.* **2011**, *13*, 6026 – 6029; f) Y. Hayashi, N. Obata, M. Tamaru, S. Yamaguchi, Y. Matsuo, A. Saeki, S. Seki, Y. Kureishi, S. Saito, S. Yamaguchi, H. Shinokubo, *Org. Lett.* **2012**, *14*, 866 – 869; g) T. Sarma, P. K. Panda, J. Setsune, *Chem. Commun.* **2013**, *49*, 9806 – 9808; h) Y. Ni, W. Zeng, K.-W. Huang, J. Wu, *Chem. Commun.* **2013**, *49*, 1217 – 1219.

[6] a) M. Wada, S. Ito, H. Uno, T. Murashima, N. Ono, T. Urano, Y. Urano, *Tetrahedron Lett.* **2001**, *42*, 6711 – 6713; b) Z. Shen, H. Röhr, K. Rurack, H. Uno, M. Spieles, B. Schulz, G. Reck, N. Ono, *Chem. Eur. J.* **2004**, *10*, 4853 – 4871; c) T. Okujima, Y. Tomimori, J. Nakamura, H. Yamada, H. Uno, N. Ono, *Tetrahedron* **2010**, *66*, 6895 – 6900; d) M. Nakamura, M. Kitatsuka, K. Takahashi, T. Nagata, S. Mori, D. Kuzuhara, T. Okujima, H. Yamada, T. Nakae, H. Uno, *Org. Biomol. Chem.* **2014**, *12*, 1309 – 1317.

[7] J. Strating, B. Zwanenburg, A. Wagenaar, A. C. Udding, *Tetrahedron Lett.* **1969**, *10*, 125 – 128.

[8] M. Suzuki, T. Aotake, Y. Yamaguchi, N. Noguchi, H. Nakano, K. Nakayama, H. Yamada, *J. Photochem. Photobiol. C* **2014**, *18*, 50 – 70.

[9] a) T. Aotake, H. Tanimoto, H. Hotta, D. Kuzuhara, T. Okujima, H. Uno, H. Yamada, *Chem. Commun.* **2013**, *49*, 3661 – 3663; b) T. Aotake, Y. Yamashita, T. Okujima, N. Shirasawa, Y. Jo, S. Fujimori, H. Uno, N. Ono, H. Yamada, *Tetrahedron Lett.* **2013**, *54*, 1790 – 1793; c) P. Peng, C. Wang, Z. Shi, V. K. Johns, L. Ma, J. Oyer, A. Copik, R. Igarashi, Y. Liao, *Org. Biomol. Chem.* **2013**, *11*, 6671 – 6674; d) E. R. Thapaliya, S. Swaminathan, B. Captain, F. M. Raymo, *J. Am. Chem. Soc.* **2014**, *136*, 13798 – 13804.

[10] a) M. W. Holman, R. Liu, L. Zang, P. Yan, S. A. DiBenedetto, R. D. Bowers, D. M. Adams, *J. Am. Chem. Soc.* **2004**, *126*, 16126 – 16133; b) T. Fukaminato, T. Doi, N. Tamaoki, K. Okuno, Y. Ishibashi, H. Miyasaka, M. Irie, *J. Am. Chem. Soc.* **2011**, *133*, 4984 – 4990; c) H. Sun, X. Dong, S. Liu, Q. Zhao, X. Mou, H. Y. Yang, W. Huang, *J. Phys. Chem. C* **2011**, *115*, 19947 – 19954.

[11] a) H. L. Kee, C. Kirmaier, L. Yu, P. Thamyongkit, W. J. Youngblood, M. E. Calder, L. Ramos, B. C. Noll, D. F. Bocian, W. R. Scheidt, R. R. Birge, J. S. Lindsey, D. Holten, *J. Phys. Chem. B* **2005**, *109*, 20433 – 20443; b) E. Bahaidarah, A. Harriman, P. Stachelek, S. Rihn, E. Heyer, R. Ziessel, *Photochem. Photobiol. Sci.* **2014**, *13*, 1397 – 1401.

[12] R. Mondal, A. N. Okhrimenko, B. K. Shah, D. C. Neckers, *J. Phys. Chem. B* **2008**, *112*, 11 – 15.

[13] a) H. Yamada, D. Kuzuhara, K. Ohkubo, T. Takahashi, T. Okujima, H. Uno, N. Ono, S. Fukuzumi, *J. Mater. Chem.* **2010**, *20*, 3011 – 3024; b) T. Aotake, S. Ikeda, D. Kuzuhara, S. Mori, T. Okujima, H. Uno, H. Yamada, *Eur. J. Org. Chem.* **2012**, 1723 – 1729.

[14] J. Dauselt, J. Zhao, M. Kind, R. Binder, A. Bashir, A. Terfort, M. Zharnikov, *J. Phys. Chem. C* **2011**, *115*, 2841 – 2854.

[15] M. Fujitsuka, O. Ito, H. Imahori, K. Yamada, H. Yamada, Y. Sakata, *Chem. Lett.* **1999**, *28*, 721 – 722.

[16] a) A. Harriman, J. P. Rostron, M. Cesario, G. Ulrich, R. Ziessel, *J. Phys. Chem. A* **2006**, *110*, 7994 – 8002; b) G. Duvanel, N. Banerji, E. Vauthey, *J. Phys. Chem. A* **2007**, *111*, 5361 – 5369.

[17] G. Jones II, S. Kumar, O. Klueva, D. Pacheco, *J. Phys. Chem. A* **2003**, *107*, 8429 – 8434.

[18] For examples: a) T. Asahi, M. Ohkohchi, R. Matsusaka, N. Mataga, R. P. Zhang, A. Osuka, K. Maruyama, *J. Am. Chem. Soc.* **1993**, *115*, 5665 – 5674; b) M. Kanematsu, P. Naumov, T. Kojima, S. Fukuzumi, *Chem. Eur. J.* **2011**, *17*, 12372 – 12384.

[19] G. M. Sheldrick, *Acta. Crystallogr. Sect. A* **2008**, *64*, 112 – 122.

[20] a) A. D. Becke, *J. Chem. Phys.* **1993**, *98*, 5648 – 5652; b) C. Lee, W. Yang, R. G. Parr, *Phys. Rev. B* **1988**, *37*, 785 – 789.

[21] a) W. J. Hehre, R. Ditchfield, J. A. Pople, *J. Chem. Phys.* **1972**, *56*, 2257 – 2261; b) P. C. Hariharan, J. A. Pople, *Theoret. Chimica Acta* **1973**, *28*, 213 – 222.

[22] Gaussian 09, Revision D.01, M. J. Frisch, G. W. Trucks, H. B. Schlegel, G. E. Scuseria, M. A. Robb, J. R. Cheeseman, G. Scalmani, V. Barone, B. Mennucci, G. A. Petersson, H. Nakatsuji, M. Caricato, X. Li, H. P. Hratchian, A. F. Izmaylov, J. Bloino, G. Zheng, J. L. Sonnenberg, M. Hada, M. Ehara, K. Toyota, R. Fukuda, J. Hasegawa, M. Ishida, T. Nakajima, Y. Honda, O. Kitao, H. Nakai, T. Vreven, J. A. Montgomery, Jr., J. E. Peralta, F. Ogliaro, M. Bearpark, J. J. Heyd, E. Brothers, K. N. Kudin, V. N. Staroverov, R. Kobayashi, J. Normand, K. Raghavachari, A. Rendell, J. C. Burant, S. S. Iyengar, J. Tomasi, M. Cossi, N. Rega, J. M. Millam, M. Klene, J. E. Knox, J. B. Cross, V. Bakken, C. Adamo, J. Jaramillo, R. Gomperts, R. E. Stratmann, O. Yazyev, A. J. Austin, R. Cammi, C. Pomelli, J. W. Ochterski, R. L. Martin, K. Morokuma, V. G. Zakrzewski, G. A. Voth, P. Salvador, J. J. Dannenberg, S. Dapprich, A. D. Daniels, Ö. Farkas, J. B. Foresman, J. V. Ortiz, J. Cioslowski, D. J. Fox, Gaussian, Inc., Wallingford CT, **2009**.

Received: December 8, 2014
Published online on ■■ ■■, 0000

FULL PAPER

BODIPY Dyes

*T. Aotake, M. Suzuki, K. Tahara, D. Kuzuhara, N. Aratani, N. Tamai, H. Yamada**

■■ – ■■

An Optically and Thermally Switchable Electronic Structure Based on an Anthracene–BODIPY Conjugate

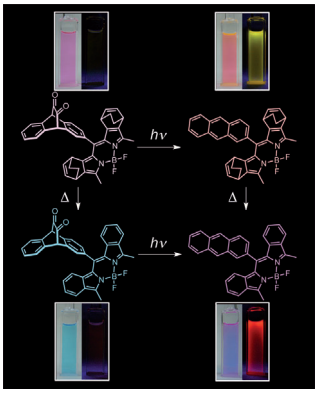

Four-way switch: An optically and thermally switchable BODIPY dye was designed and synthesized (see figure). Separate photoexcitation for structure change and fluorescence monitoring was achieved by means of fluorescence quenching based on an intramolecular electron-transfer mechanism. As the absorption characteristic can be switched by thermal activation, the construction of a completely irreversible multifluorescence switching system is possible.

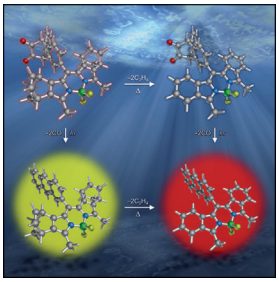

Switchable Anthracene–BODIPY Dyes

A completely irreversible multifluorescence switching system is possible by a stepwise structural change of BODIPY through optical excitation and/or heating. For more details, see the Full Paper by H. Yamada et al. on page ■■ ff.

ChemComm

Chemical Communications
www.rsc.org/chemcomm

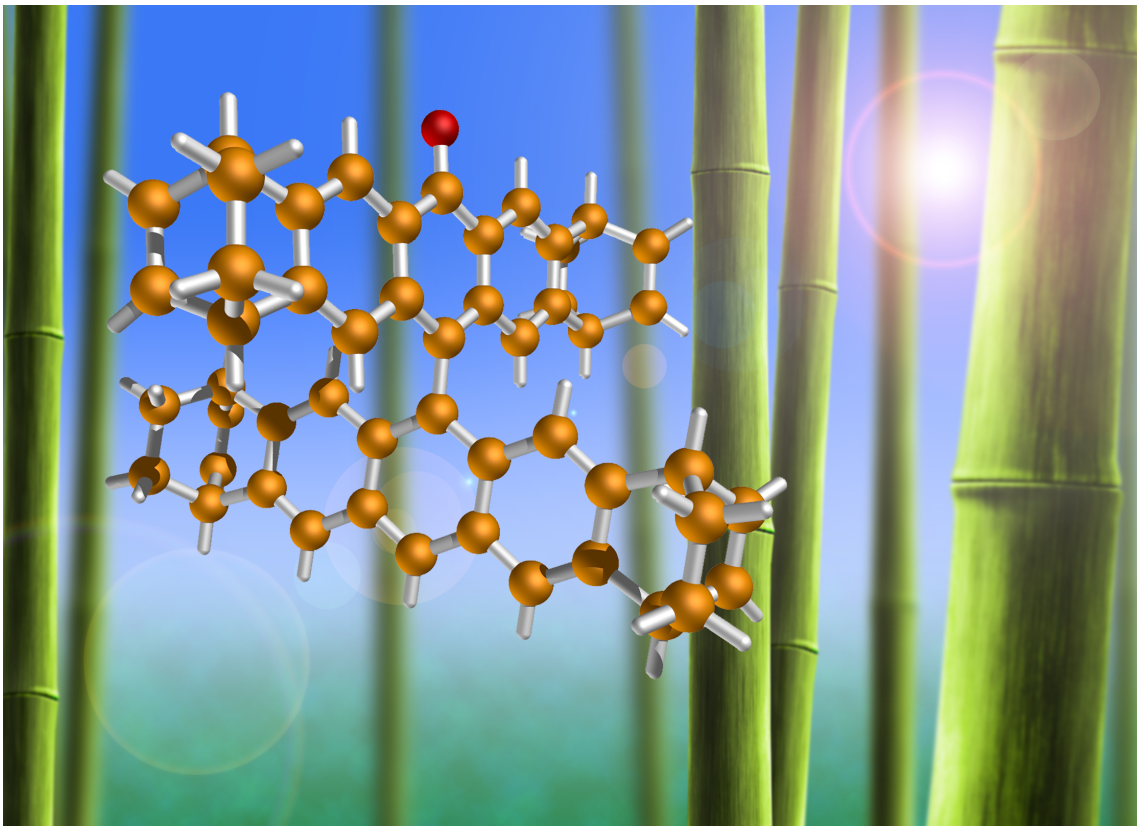

9,9′-Anthryl-anthroxyl radicals: strategic stabilization of highly reactive phenoxyl radicals

ChemComm

COMMUNICATION

View Article Online
View Journal

Cite this: DOI: 10.1039/c4cc10104a

Received 18th December 2014,
Accepted 27th January 2015

DOI: 10.1039/c4cc10104a

www.rsc.org/chemcomm

9,9′-Anthryl-anthroxyl radicals: strategic stabilization of highly reactive phenoxyl radicals†

Tatsuya Aotake,[a] Mitsuharu Suzuki,[a] Naoki Aratani,[a] Junpei Yuasa,[a] Daiki Kuzuhara,[a] Hironobu Hayashi,[a] Haruyuki Nakano,[b] Tsuyoshi Kawai,[a] Jishan Wu*[c] and Hiroko Yamada*[ad]

Stable 9,9′-anthryl-anthroxyl radicals were synthesized and isolated, and the structures were fully characterized by single crystal X-ray diffraction analysis and ESR measurement. The resonance structure and steric protection of the peripheral positions and the most reactive 9-position of anthracene prolong the half-life of the radical in solution to 11 days.

Phenoxyl radical,[1] which is one of the highly reactive radicals, is observed in biological processes as a tyrosyl radical related to electron transfer, hydrogen atom transfer and proton-coupled electron transfer.[2] It formally contains resonance structure, as shown in Scheme 1, in which the carbon atom at the 4-position is also reactive. The stabilization has been achieved by substitution with bulky *ortho*-substituents,[3] coordination to metal ions[4] or π-conjugation expansion.[5]

During the synthetic investigation of molecular graphene nano-ribbons (GNRs),[6] we found the formation of a stable anthroxyl radical. The preparation of 9,9′-anthryl-anthr-10-oxy radical (**1**), an example of a π-expanded phenoxyl radical, was reported by Singer *et al.* in 1971, where **1** was obtained by the oxidation of 9,9′-bianthryl by molecular oxygen, but only the hyperfine coupling constants (hfccs) and *g*-value were reported without an ESR spectrum.[7] Here, we will report the synthesis and characterization of stable radical **1**, including the direct comparison of **1** and 10-hydroxy-9,9′-anthrylanthracene (**1-H**),

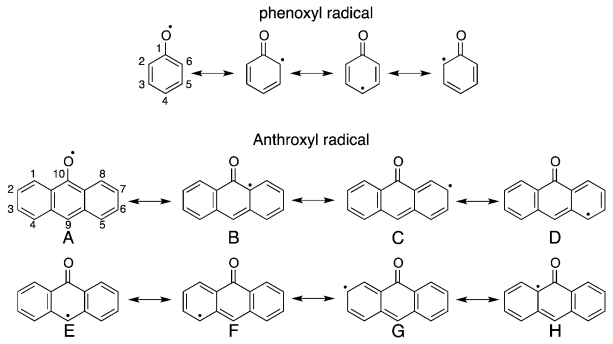

Scheme 1 Resonance structures of phenoxyl radical and anthroxyl radical.

using the X-ray single crystal structure analysis of the co-crystal of **1** and **1-H**. We have also prepared tetrabicyclo[2.2.2]octadiene (BCOD)-fused 9,9′-anthryl-anthr-10-oxy radical derivative **2** as a more stabilized radical species under ambient conditions. The stability of the compound **2** was attained by two factors. One is the expansion of the π-structure as same as radical **1**: the expansion of the phenyl skeleton expanded to anthracene, resulting in the gain of two aromatic stabilization energies as shown in Scheme 1, the other is *ortho* substitution of bulky substituents at periphery and the most reactive 9-position. Thus the radical **2** is stable enough to be purified over a conventional silica gel column.

The synthetic route of **1** and **2** is shown in Scheme 2. Bisanthracene quinones **3** and **4** were prepared according to the literature.[8,9] Hydride reduction of **3** and **4** using lithium aluminium hydride (LAH) and 6 N HCl produced monoketones **5** and **6**, respectively. The monoketones were used in the following reaction without purification because of the instability under ambient conditions. The radicals **1** and **2** were obtained by the treatment of monoketones with pyridine *N*-oxide and $FeSO_4 \cdot 7H_2O$ in 15% and 19% yield in 2 steps, respectively. The products were identified by mass spectrum measurement (Fig. S1–S3, ESI†), single crystal X-ray diffraction analysis and ESR spectroscopy.

[a] *Graduate School of Materials Science, Nara Institute of Science and Technology (NAIST), 8916-5 Takayama-cho, Ikoma 630-0192, Japan. E-mail: hyamada@ms.naist.jp*
[b] *Department of Chemistry, Graduate School of Sciences, Kyushu University, Fukuoka 812-8581, Japan*
[c] *National University of Singapore, 3 Science Drive 3, 117543, Singapore. E-mail: chmwuj@nus.edu.sg*
[d] *CREST, Japan Science and Technology Agency (JST) 4-1-8 Honcho, Kawaguchi, Saitama 332-0012, Japan*

† Electronic supplementary information (ESI) available: Synthetic details, X-ray crystal structural analysis, DFT calculations, time profiles of UV-vis absorption spectra, and thermal analysis. CCDC 1021762 (**1**), 1021763 (**1** and **1-H**), and 1021764 (**2**). For ESI and crystallographic data in CIF or other electronic format see DOI: 10.1039/c4cc10104a

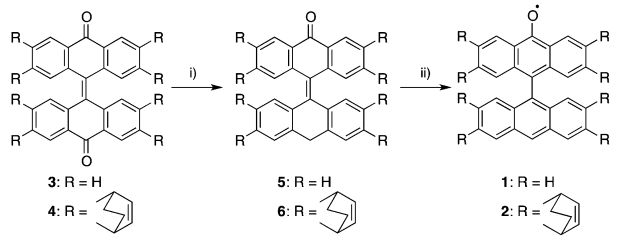

Scheme 2 Syntheses of **1** and **2**: (i) lithium aluminium hydride (LAH), dry THF, then 6 N HCl, reflux; (ii) $FeSO_4{\cdot}7H_2O$, pyridine-*N*-oxide, pyridine, piperidine, 100 °C.

The single crystals were obtained by diffusion crystallization with chloroform/methanol for **1**, and the crystallographic data is summarized in Fig. 1, Fig. S4 and S5 and Tables S1–S3, ESI.† The radical **1** gave two types of crystals in one batch: a brown needle type and brown plate type. The needle-shaped crystal is the pure crystal of **1**, as shown in Fig. 1a and b. The crystal data was solved as a disordered structure due to the position of an oxy-radical unit. The dihedral angle between two-anthracene units is 70.1(2)°. The bond length at C8–C8′ is 1.492(3) Å, indicating a single bond. This is different from a stable 2,6-di-*tert*-butyl-4-(4′-nitrophenyl)phenoxyl (^{t}BuNPArO$^\bullet$) radical with an aryl–aryl bond length of 1.4754 Å and an aryl–aryl

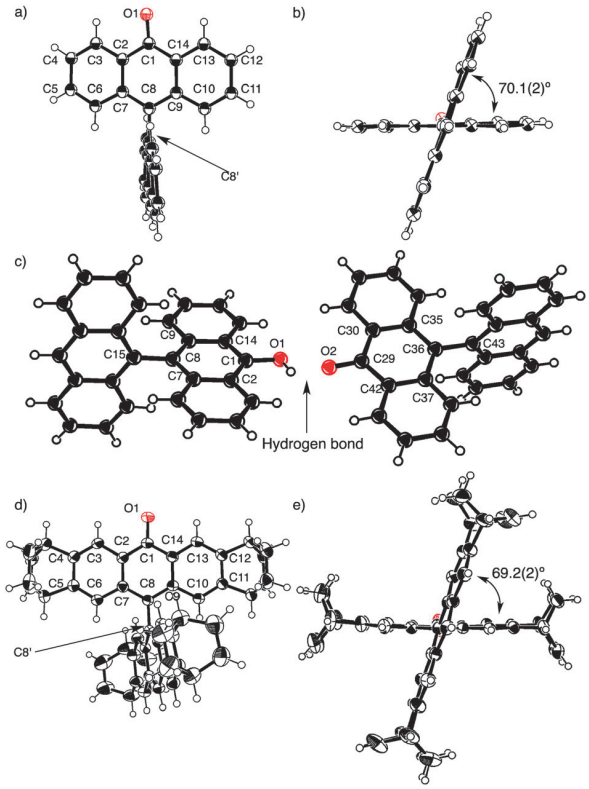

Fig. 1 Crystal structures of (a) top view; and (b) side view of **1**; (c) co-crystal with **1** and anthroxyl anthracene (**1-H**); (d) top view; and (e) side view of **2**. Solvent molecules are omitted for clarity. Thermal ellipsoids represent 50% probability.

torsion angle of 17.5°, where the spin density expanded the whole molecule.[5b] The crystal with the plate-shape contains 10-hydroxy-9,9′-anthyrylanthracene (**1-H**) and the radical **1** as a pair *via* [O–H···O$^\bullet$] hydrogen bonding (Fig. 1c, Fig. S4 and S5, ESI†) in the co-crystal. The compound **1-H** was obtained from **1** *in situ* during the crystallization. The bond length of O1–C1 of **1-H** is 1.364(3) Å, which confirms to a normal phenoxyl bond. The C–C bond lengths of **1-H** are those of typical aromatic C–C bonds and the bond length of C8–C15 for **1-H** is 1.496(3) Å. Thus, **1-H** in the co-crystal is 9,9′-anthryl-10-anthranol. The bond length of O2–C29 of **1** is 1.247(3) Å, which is 0.12 Å shorter than that of O1–C1 of **1-H**. The bond lengths of C29–C42, C29–C30, C35–C36, and C36–C37 are 1.457(3), 1.464(4), 1.425(3), and 1.425(7) Å, respectively, assigned to single bonds and the central ring next to O2 is not aromatic. The bond length of C36–C43 for **1** is 1.492(3) Å. The bond lengths of **1** suggest that the resonant structure E in Scheme 1 mainly contributes to the structure of radical **1**. The radical spin density should be higher at the 9-position and the steric protection of the most reactive carbon atom is effective in stabilizing the phenoxyl type radicals. The two anthryl units are orthogonal to each other with the mutual angles of 87.4(3)° for **1** and 89.1(3)° for **1-H**. The crystal structure of **2** shows a similar result to the needle-shaped crystal of **1** (Fig. 1d and e).[10] The crystal data was solved as a disordered structure due to the position of the oxy-radical unit. The two anthracene units are cross-shaped and the dihedral angle is 69.2(2)°. The C8–C8′ bond length that connects two anthracene skeletons is 1.498(3) Å. A co-crystal of **2** and **2-H** was not obtained.

The electronic structures of **1** and **2** were investigated by electron spin resonance (ESR) measurement. The ESR spectra of **1** and **2** in toluene are shown in Fig. 2, together with the simulation pattern. The signals of **1** are attributed to four positions in the anthroxyl skeleton, and the simulated hfccs are 0.90 (2H), 3.28 (2H), 0.90 (2H) and 3.28 G (2H). The *g*-value is 2.0023, which corresponds to a general organic free radical compound. The line width of the ESR spectrum of **2** was wider than that of **1** and the spectrum was hardly changed even by varying the temperature. The signals of **2** are ascribed to the two positions in the skeleton. The simulated hfccs are 1.00 (2H) and 2.80 G (2H) and the *g*-value is 2.0024. According to the spin density calculation (Fig. 2c and d), both **1** and **2** have the highest spin densities on C8 substituted with anthryl or the derivative (for numbering, see Fig. 1). This result suggests that the resonant structure E in Scheme 1 is also the main structure for **1** and **2** in solution. The anthryl groups are substantially orthogonal to the phenoxyl skeleton, contributing as steric protection to the radical. Density functional theory (DFT) calculations at the B3LYP/6-31G(d) level were conducted to provide further understanding of SOMO.[11] Computed spin densities showed that the unpaired electrons were delocalized on the anthroxyl skeleton for each compound rather than the substituent-acenes (Fig. S7, ESI†).

The UV-vis absorption spectra of **1** and **2** recorded in toluene are shown in Fig. 3a and Table 1. Each solution displayed a dark yellow color. The UV-vis absorption spectrum of **1** shows

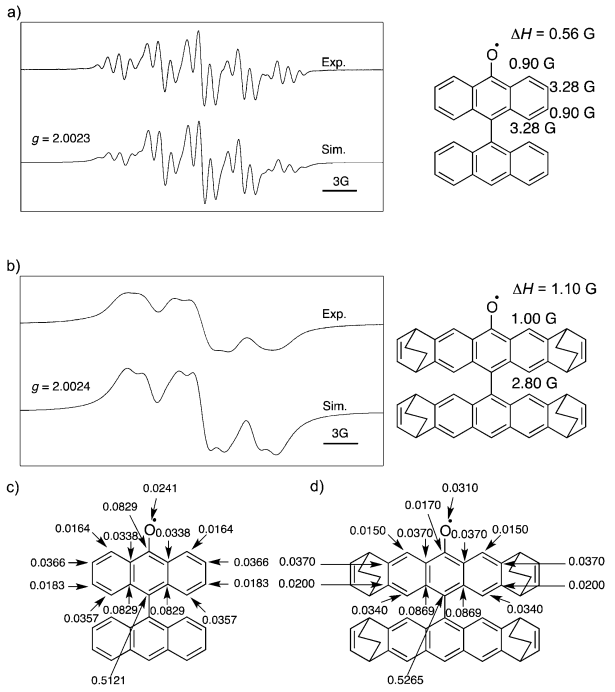

Fig. 2 ESR spectra and simulations of (a) **1** in toluene (1.6×10^{-2} mM) at 183 K and (b) **2** in toluene (2.7×10^{-2} mM) at 183 K. Spin density of (c) **1**; and (d) **2** computed at the B3LYP/6-31G(d) level.

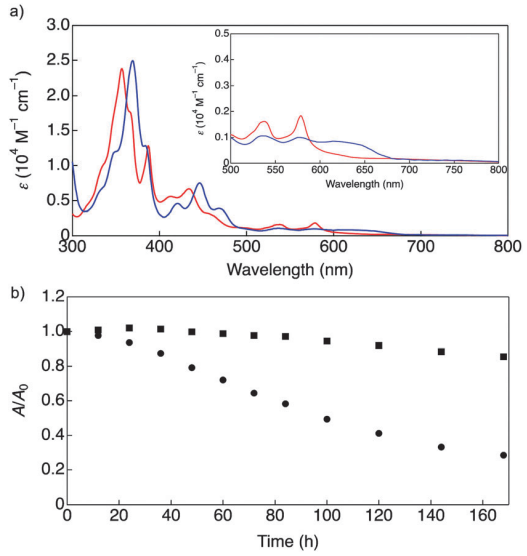

Fig. 3 (a) UV-vis absorption spectra of **1** (red line) and **2** (blue line) in toluene. (b) Decay profiles of UV-vis absorption spectra of (a) **1** (● 357 nm) and (b) **2** (■ 369 nm).

the major absorption at 357 (ε = 23 900 M^{-1} cm^{-1}) and 387 nm (ε = 12 900 M^{-1} cm^{-1}) and the minor absorption broadened to 800 nm with a maxima at 413 (ε = 5590 M^{-1} cm^{-1}), 434 (ε = 6660 M^{-1} cm^{-1}), 537 (ε = 1620 M^{-1} cm^{-1}) and 578 nm (ε = 1830 M^{-1} cm^{-1}). Because the UV-vis absorption spectrum of 9,9′-bianthryl is up to 400 nm,[12] the absorption wavelength is

Table 1 Summary of optical and electrochemical properties of radicals

Compd.	λ_{abs} [a] (nm)	E_{ox} [b] (V)	E_{red} [b] (V)
1	357, 387, 413, 434, 537, 578	0.55	−0.77
2	369, 384, 421, 446, 537, 576, 615	0.25, 0.91	−0.94

[a] In toluene. [b] The values were obtained by cyclic voltammetry. V *vs.* Fc/Fc^+.

red-shifted by the contribution of SOMO, as shown by the TD-DFT calculations (Fig. S8, ESI†). The BCOD-fused compound **2** displays an absorption spectrum with the red-shifted major absorption at 369 (ε = 25 000 M^{-1} cm^{-1}) and 384 (ε = 12 800 M^{-1} cm^{-1}) nm, and with the minor absorption broader and spread to 800 nm compared to those of **1**. The photo-stability of the radical in toluene was checked by UV-vis absorption spectral change. The solution was kept in room light under air and the temporal spectral change was measured, as shown in Fig. 3b, Fig. S9 and S10, ESI.† The peak-top (357 nm) of the absorbance of **1** is gradually decreased and the half life ($\tau_{1/2}$) is calculated to be 92 h. In contrast, $\tau_{1/2}$ of **2** was significantly longer than that of **1** and was estimated to be 274 h (11.4 d). The stability was improved about 3 times by inserting the BCOD moieties.

The electrochemical properties of the radicals were studied by cyclic voltammetry (CV) in dry dichloromethane containing 0.1 M tetra-*n*-butylammonium hexafluorophosphate ($n$$Bu_4NPF_6$) as a supporting electrolyte. The results are summarized in Table 1 and Fig. S11, ESI.† The one-electron reduction potentials ($E_{red}^{1/2}$ *vs.* Fc/Fc^+) of **1** and **2** are at −0.77 V and −0.94 V, respectively. The radical **1** shows one oxidation potential at 0.55 V (*vs.* Fc/Fc^+), whereas **2** shows two reversible oxidation waves at 0.25 and 0.91 V (*vs.* Fc/Fc^+). In comparison with **1**, the first oxidation and reduction potentials of compound **2** are shifted to the negative side. It is considered that the SOMO energy level of **2** rises by receiving the electric effect of σ–π hyperconjugation of BCOD-units to the anthracene moiety.[13] From CV and DFT calculations, the stability of **2** against electrochemical oxidation is predicted to be lower than that of **1**. The surrounding structures of the C8 position of **1** and **2** are similar in crystals due to the similarity of the angles of two anthryl planes and the C8–C8′ distances. However, the better stability of **2** in solution suggests the restricted freedom of rotation on the C8–C8′ axis for **2** compared to that for **1** owing to the BCOD substituents at the edge of the anthracene unit, thus restricting the reactivity of C8 to give a quinoid structure (Fig. S12, ESI†).

In conclusion, we were successful in preparing and characterizing stable 9,9′-anthryl-anthroxyl radicals.[14] The result of X-ray structural analysis, ESR spectra and DFT calculations suggested the highest spin density of radical **1** localized at the 9-position due to the resonance and the stabilization of the phenoxyl radical achieved by protection of the most reactive position with an anthryl group. The peripheral BCOD-substituents influenced the energy levels of SOMOs to be raised by σ–π hyperconjugation to encourage the electrochemical oxidation and the absorption spectrum to be red-shifted. Furthermore, the stability of radical **2** in solution was improved owing to the steric hindrance of the BCOD-moiety to restrict the

rotation around the C8–C8′ axis. Finally, we have tried to prepare 6,6′-penthryl-penthroxy radical (**7**) from **2** by a retro-Diels–Alder reaction.[8,15] Although the formation of a pentacene dimer was detected,[16] the ESR measurement of the product was not successful at present because the life-time of the product is much shorter than that of **1**.

The authors thank Ms Yoshiko Nishikawa in NAIST for the measurement of mass spectra, Mr Fumio Asanoma in NAIST for the measurement of ESR spectra, Mr Shouhei Katao in NAIST for the measurement of single-crystal structure analysis. This work was partly supported by Grants-in Aid (No. 22350083 and 26105004 to H.Y. and No. 26288038 to N.A.), the Green Photonics Project in NAIST and the program for promoting the enhancement of research universities in NAIST supported by MEXT. J.W. acknowledges financial support from Singapore MOE Tier 2 grant (MOE2014-T2-1-080).

Notes and references

1 R. Pummerer and F. Frankfurter, *Chem. Ber.*, 1914, **47**, 1472.
2 (*a*) R. W. Kreilick and S. I. Weissman, *J. Am. Chem. Soc.*, 1962, **84**, 306; (*b*) H.-J. Krüger, *Angew. Chem., Int. Ed.*, 1999, **38**, 627; (*c*) S. Itoh, M. Taki and S. Fukuzumi, *Coord. Chem. Rev.*, 2000, **198**, 3; (*d*) C. T. Lyons and T. D. P. Stack, *Coord. Chem. Rev.*, 2013, **257**, 528.
3 (*a*) E. Müller, A. Schick and K. Scheffler, *Chem. Ber.*, 1959, **92**, 474; (*b*) E. R. Altwicker, *Chem. Rev.*, 1967, **67**, 475; (*c*) V. W. Manner, T. F. Markle, J. H. Freudenthal, J. P. Roth and J. M. Mayer, *Chem. Commun.*, 2008, 256; (*d*) J. M. Wittman, R. Hayoun, W. Kaminsky, M. K. Coggins and J. M. Mayer, *J. Am. Chem. Soc.*, 2013, **135**, 12956.
4 (*a*) A. Sokolowski, J. Müller, T. Weyhermüller, R. Schnepf, P. Hildebrandt, K. Hildenbrand, E. Bothe and K. Wieghardt, *J. Am. Chem. Soc.*, 1997, **119**, 8889; (*b*) A. Philibert, F. Thomas, C. Philouze, S. Hamman, E. Saint-Aman and J.-L. Pierre, *Chem. – Eur. J.*, 2003, **9**, 3803; (*c*) Y. Shimazaki, S. Huth, S. Karasawa, S. Hirota, Y. Naruta and O. Yamauchi, *Inorg. Chem.*, 2004, **43**, 7816.
5 (*a*) C. Xie, P. M. Lahti and C. George, *Org. Lett.*, 2000, **2**, 3417; (*b*) T. R. Porter, W. Kaminsky and J. M. Mayer, *J. Org. Chem.*, 2014, **79**, 9451.
6 (*a*) J. Cai, P. Ruffieux, R. Jaafar, M. Bieri, T. Braun, S. Blankenburg, M. Muoth, A. P. Seitsonen, M. Saleh, X. Feng, K. Müllen and R. Fasel, *Nature*, 2010, **466**, 470; (*b*) L. Chen, Y. Hernandez, X. Feng and K. Müllen, *Angew. Chem., Int. Ed.*, 2012, **51**, 7640; (*c*) A. Konishi, Y. Hirao, K. Matsumoto, H. Kurata, R. Kishi, Y. Shigeta, M. Nakano, K. Tokunaga, K. Kamada and T. Kubo, *J. Am. Chem. Soc.*, 2013, **135**, 1430.
7 L. S. Singer, I. C. Lewis, T. Richerzhagen and G. Vincow, *J. Phys. Chem.*, 1971, **75**, 290.
8 K. Tanaka, N. Aratani, D. Kuzuhara, S. Sakamoto, T. Okujima, N. Ono, H. Uno and H. Yamada, *RSC Adv.*, 2013, **3**, 15310.
9 (*a*) S. M. Arabei and T. A. Pavich, *J. Appl. Spectrosc.*, 2000, **67**, 236; (*b*) X. Zhang, J. Li, H. Qu, C. Chi and J. Wu, *Org. Lett.*, 2010, **12**, 3946.
10 The single crystals of **2** from chloroform/methanol also gave crystal of **2**, but not co-crystal like **1** and **1H** (Fig. S6 and Table S4, ESI†). CCDC number is 1042904.
11 M. J. Frisch, *et al.*, *Gaussian 09, Revision D.01*, see the ESI† for details.
12 P. Natarajan and M. Schmittel, *J. Org. Chem.*, 2013, **78**, 10383.
13 (*a*) K. Komatsu, H. Akamatsu, Y. Jinbu and K. Okamoto, *J. Am. Chem. Soc.*, 1988, **110**, 633; (*b*) A. Matsuura, T. Nishinaga and K. Komatsu, *J. Am. Chem. Soc.*, 2000, **122**, 10007.
14 Whilst this work was under consideration, the following manuscript was published: Y. Hirao, T. Saito and T. Kubo, *Angew. Chem., Int. Ed.*, 2015, **54**, 2402.
15 (*a*) S. Ito, T. Murashima, N. Ono and H. Uno, *Chem. Commun.*, 1998, 1661; (*b*) H. Yamada, T. Okujima and N. Ono, *Chem. Commun.*, 2008, 2957.
16 The weight loss in thermogravimetric analysis of **2** (Fig. S13, ESI†) starts at 200 °C and ends around 300 °C, but soon the weight loss started again. The preparation of radical **7** was tried by heating by microwave in ethyleneglycol at 300 °C for 5 min under argon atmosphere. After the quick filtration, the precipitate was suggested to have pentacene dimer unit by APCI-mass measurement (Fig. S14, ESI†).

